ISSN 2542-1565

Vol. 14 2021 No. 02

GEOGRAPHY ENVIRONMENT SUSTAINABILITY

«The journal GEOGRAPHY, ENVIRONMENT, SUSTAINABILITY was founded in 2008 by Russian Geographical Society, the Lomonosov Moscow State University Geography Department, and the Russian Academy of Sciences Institute of Geography. Since that time the journal publishes **4 issues per year**, containing original research papers and reviews. The journal issues are open source and distributed through subscriptions, library exchanges of leading universities, and via the website through the world»

FOUNDERS OF THE JOURNAL: Russian Geographical Society, Faculty of Geography, Lomonosov Moscow State University and Institute of Geography of the Russian Academy of Sciences

The journal is published with financial support of the Russian Geographical Society.

The journal is registered in Federal service on supervision of observance of the legislation in sphere of mass communications and protection of a cultural heritage. The certificate of registration: ПИ № ФС77-67752, 2016, December 21.

PUBLISHER
Russian Geographical Society
Moscow, 109012 Russia
Novaya ploshchad, 10, korp. 2
Phone 8-800-700-18-45
E-mail: press@rgo.ru
www.rgo.ru/en

EDITORIAL OFFICE
Lomonosov Moscow State University
Moscow 119991 Russia
Leninskie Gory, 1,
Faculty of Geography, 1806a
Phone 7-495-9391552
Fax 7-495-9391552
E-mail: ges-journal@geogr.msu.ru
www.ges.rgo.ru

DESIGN
Layout designer: Tereshkin Anton
Moscow, 115088,
26 Simonovsky Val str., bldg. One
Phone: +7 (903) 108-04-44
E-mail: smile.tai@gmail.com

DOI prefix: 10.24057

Format A4 (210x297mm)

"GEOGRAPHY, ENVIRONMENT, SUSTAINABILITY" is the only original English-language journal in the field of geography and environmental sciences published in Russia. It is supposed to be an outlet from the Russian-speaking countries to Europe and an inlet from Europe to the Russian-speaking countries regarding environmental and Earth sciences, geography and sustainability. The main sections of the journal are the theory of geography and ecology, the theory of sustainable development, use of natural resources, natural resources assessment, global and regional changes of environment and climate, social-economical geography, ecological regional planning, sustainable regional development, applied aspects of geography and ecology, geoinformatics and ecological cartography, ecological problems of oil and gas sector, nature conservations, health and environment, and education for sustainable development.

OPEN ACCESS POLICY. "GEOGRAPHY, ENVIRONMENT, SUSTAINABILITY" is an open access journal. All articles are made freely available to readers immediately upon publication. Our open access policy is in accordance with the Budapest Open Access Initiative (BOAI) definition - it means that articles have free availability on the public internet, permitting any users to read, download, copy, distribute, print, search, or link to the full texts of these articles, crawl them for indexing, pass them as data to software, or use them for any other lawful purpose, without financial, legal, or technical barriers other than those inseparable from gaining access to the internet itself.

Date of publication: July 1st, 2021.

© Russian Geographical Society, 2021

EDITORIAL BOARD

EDITORS-IN-CHIEF:

Kasimov Nikolay S.
Lomonosov Moscow State University,
Faculty of Geography, Russia

Kotlyakov Vladimir M.
Russian Academy of Sciences
Institute of Geography, Russia

DEPUTY EDITORS-IN-CHIEF:

Solomina Olga N. - Russian Academy of Sciences, Institute of Geography, Russia
Tikunov Vladimir S. - Lomonosov Moscow State University, Faculty of Geography, Russia

Vandermotten Christian - Université Libre de Bruxelles Belgium
Chalov Sergei R. - (Secretary-General) Lomonosov Moscow State University, Faculty of Geography, Russia

Alexeeva Nina N. - Lomonosov Moscow State University, Faculty of Geography, Russia
Baklanov Alexander - World Meteorological Organization, Switzerland
Baklanov Petr Ya. - Russian Academy of Sciences, Pacific Institute of Geography, Russia
Chubarova Natalya E. - Lomonosov Moscow State University, Faculty of Geography, Russia
De Maeyer Philippe - Ghent University, Department of Geography, Belgium
Dobrolubov Sergey A. - Lomonosov Moscow State University, Faculty of Geography, Russia
Ferjan J. Ormeling - University of Amsterdam, Amsterdam, Netherlands
Sven Fuchs - University of Natural Resources and Life Sciences
Haigh Martin - Oxford Brookes University, Department of Social Sciences, UK
Golosov Valentin N. - Lomonosov Moscow State University, Faculty of Geography, Russia
Gulev Sergey K. - Russian Academy of Sciences, Institute of Oceanology, Russia
Guo Huadong - Chinese Academy of Sciences, Institute of Remote Sensing and Digital Earth, China
Jarsjö Jerker - Stockholm University, Department of Physical Geography and Quaternary Geography, Sweden
Jeffrey A. Nittrouer - Rice University, Houston, USA
Ivanov Vladimir V. - Arctic and Antarctic Research Institute, Russia
Karthe Daniel - German-Mongolian Institute for Resources and Technology, Germany
Kolosov Vladimir A. - Russian Academy of Sciences, Institute of Geography, Russia
Kosheleva Natalia E. - Lomonosov Moscow State University, Faculty of Geography, Russia

Konečný Milan - Masaryk University, Faculty of Science, Czech Republic
Kroonenberg Salomon - Delft University of Technology, Department of Applied Earth Sciences, The Netherlands
Kulmala Markku - University of Helsinki, Division of Atmospheric Sciences, Finland
Olchev Alexander V. - Lomonosov Moscow State University, Faculty of Geography, Russia
Malkhazova Svetlana M. - Lomonosov Moscow State University, Faculty of Geography, Russia
Meadows Michael E. - University of Cape Town, Department of Environmental and Geographical Sciences South Africa
Nefedova Tatyana G. - Russian Academy of Sciences, Institute of Geography, Russia
O'Loughlin John - University of Colorado at Boulder, Institute of Behavioral Sciences, USA
Paula Santana - University of Coimbra, Portugal
Pedroli Bas - Wageningen University, The Netherlands
Pilyasov Alexander N. - Institute of Regional Consulting, Moscow, Russia
Radovanovic Milan - Serbian Academy of Sciences and Arts, Geographical Institute "Jovan Cvijić", Serbia
Sokratov Sergei A. - Lomonosov Moscow State University, Faculty of Geography, Russia
Tishkov Arkady A. - Russian Academy of Sciences, Institute of Geography, Russia
Wuyi Wang - Chinese Academy of Sciences, Institute of Geographical Sciences and Natural Resources Research, China
Zilitinkevich Sergey S. - Finnish Meteorological Institute, Finland

EDITORIAL OFFICE

ASSOCIATE EDITOR

Maslakov Alexey A.
Lomonosov Moscow State University,
Faculty of Geography, Russia

ASSISTANT EDITOR

Grishchenko Mikhail Yu.
Lomonosov Moscow State University,
Faculty of Geography, Russia

PROOF-READER

Troshko Maria M.
Lomonosov Moscow State University,
Faculty of Geography, Russia

CONTENTS

Disclaimer:

The information and opinions presented in the Journal reflect the views of the authors and not of the Journal or its Editorial Board or the Publisher. The GES Journal has used its best endeavors to ensure that the information is correct and current at the time of publication.

Endpoint levels of biological organization are highlighted: cellular and molecular (green); individual (without color); population, community, and ecosystem (yellow).

Supplementary Table 1. Total arsenic effective concentrations (EC_x) and the properties of soils under study

Study	SO	Soil properties			Species	EP	TD	As_{total} (mg kg^{-1})		
		pH	CEC ($cmol_+ kg^{-1}$)	OM (%)				EC_{10}	EC_{25}	EC_{50}
Invertebrates: Worms										
Bustos et al. (2015)	Chile	5.7-7.6	NA	0.7-4.9	*Eisenia fetida*	CQ	28	**8**	**14**	**22**
Microorganisms										
Nordgren et al. (1986)	Sweden	3.5-5.0a	NA	NA	Native microbes	FG	NAP	-	-	200
Wang et al. (2020)	China	4.6-8.2	8.1-22	0.5-5.3	Native microbes	ACP K_a	<1	20	-	184
						ACP V_{max}	<1	49	-	438
						ALP K_a	<1	42	-	378
						ALP V_{max}	<1	36	-	327
						BG K_a	<1	29	-	259
						BG V_{max}	<1	41	-	369
						DHA K_a	<1	30	-	266
						DHA V_{max}	<1	32	-	285
						Mean		35	-	313
						Microbe mean		**35**	**-**	**257**

CEC: cation exchange capacity; EP: endpoint; NA: not available; NAP: not applicable (field observations); native microbes: biological response is attributed to several soil microorganism taxa (i.e., archaea, bacteria, actinomycete, algae, fungi, and protozoa); OM: organic matter; SO: soil origin; TD: test duration (days).
ACP K_a: acid phosphatase catalytic efficiency; ACP V_{max}: acid phosphatase maximum reaction rate; ALP K_a: alkaline phosphatase catalytic efficiency; ALP V_{max}: alkaline phosphatase maximum reaction rate; BG K_a: β-glucosidase catalytic efficiency; BG V_{max}: β-glucosidase maximum reaction rate; CQ: cocoon quantity; DHA K_a: dehydrogenase catalytic efficiency; DHA V_{max}: dehydrogenase maximum reaction rate; FG: functional groups. [a]Estimate based on illustrations.

Supplementary Table 2. Total copper effective concentrations (EC_x) and the properties of soils under study

Study	SO	Soil properties			Species	EP	TD	Cu_{total} (mg kg^{-1})		
		pH	CEC ($cmol_+ kg^{-1}$)	OM (%)				EC_{10}	EC_{25}	EC_{50}
Plants										
Hamels et al. (2014)	Sweden	5.0-6.1	9-16	12.1	*Hordeum vulgare* (Barley)	SH DW	14	-	-	1260
Kolbas et al. (2014)	France	7.0-7.5	3.1-19	1.5-7.8	*Helianthus annuus* (Sunflower)	CC	28	151	-	759
						ChlTot	28	138	-	691
						EL	28	912	-	-
						LA	28	282	-	954
						R DW	28	155	-	677
						SH DW	28	323	-	717
						TLA	28	395	-	-
						WC	28	620	-	-
						Mean		372	-	760
Verdejo et al. (2015)	Chile	5.7-7.6	NA	0.7-5.8	*Lolium perenne* (Perennial ryegrass)	R L	21	500	765	1031
						SH L	21	327	735	1144
						Mean		414	750	1088

Verdejo et al. (2016)	Chile	5.7-7.6	NA	0.7-5.8	*Lactuca sativa* (Lettuce)	SH L	21	445	955	1805
Mondaca et al. (2017)	Chile	5.7-7.6	NA	0.7-5.8	*Avena sativa* (Oat)	SH DW	21	607	900	1230
						SH L	21	908	1328	1802
						R DW	62	363	593	853
						SH DW	62	454	616	798
						SH L	62	569	720	889
						Mean		580	831	1114
					Brassica rapa (Turnip)	SH DW	21	161	298	452
						SH L	21	197	352	526
						R L	42	412	598	809
						SH DW	42	254	372	506
						SH L	42	245	419	616
						SPQ	42	297	383	480
						Mean		261	404	565
Plants										
Kolbas et al. (2018)	France	5.9-7.2	2.7-3.2	1.2-1.5	*Helianthus annuus* (Sunflower)	ChlTot	28	51	-	329
						R DW	28	74	-	203
						SH DW	28	166	-	333
						SH L	28	355	-	407
						TAC	28	23	-	301
						TLA	28	201	-	335
						Mean		145	-	318
						Plant mean		**369**	**735**	**987**
Invertebrates										
a. Nematodes										
Naveed et al. (2014)	Denmark	5.9-6.6	NA	3.3-6.0	Native nematodes	ACE R	NAP	275[c]	-	-
						S-W D	NAP	400[c]	-	-
						Mean		**338**	-	-
b. Springtails										
Scott-Fordsmand et al. (2000a)	Denmark	6.1-7.1	10-13	3.9-5.5	*Folsomia fimetaria*	FPZ	NAP	643	-	-
						JQ	21	2463[d]	-	-
Liu et al. (2018)	China	7.2	18	3.2	*Folsomia candida*	FPZ	NAP	31	-	153
						BL	28	68	-	-
						JQ	28	21	-	135
						SV	28	355	-	1560
						Mean		148	-	848
					Folsomia quadrioulata	FPZ	NAP	52	-	258
					Sinella curviseta	BL	28	880	-	-
						JQ	28	26	-	174
						SV	28	645	-	3089
						Mean		517	-	1632
						Springtail mean		**278**	-	**723**

c. Worms										
Scott-Fordsmand et al. (2000b)	Denmark	6.5-7.0	NA	NA	*Eisenia fetida*	CQ	21	248	-	517
						NRRT	21	69	-	163
						Mean		159	-	340
Van Zwieten et al. (2004)	Australia	6.6-6.9	NA	3.3-12	*Eisenia fetida*	AT	2	-	-	131[a]
Maraldo et al. (2006)	Denmark	NA	NA	NA	*Enchytraeus crypticus*	JQ	14	99	-	439
Konečný et al. (2014)	Zambia	5.1-6.9	3.5-15	1.7-15	*Enchytraeus crypticus*	JQ	28	-	-	351
Naveed et al. (2014)	Denmark	5.9-6.6	NA	3.3-6.0	Native earthworms	FPZ	NAP	110	-	-
Delgadillo et al. (2017)	Chile	5.7-8.3	NA	0.7-10	*Eisenia fetida*	AT	2	-	-	213
Mirmonsef et al. (2017)	Denmark	NA	NA	NA	*Aporrectodea tuberculata*	CQ	21	-	-	220
							42	-	-	220[d]
							63	-	-	450[d]
						Worm mean		**123**	**-**	**282**
Microorganisms										
Baath et al. (1991)	Sweden	NA	NA	NA	Native microbes	SIR + ATP	<1	-	-	2500[d]
Sauvé (2006)	Denmark	6.0-7.1	NA	3.7-5.1	Native microbes	SOM D	NAP	154	193[b]	285
Arthur et al. (2012)	Denmark	6.1-6.6	NA	2.7-5.1	Native microbes	DHA	<1	-	-	542
						FDA	<1	-	-	521
						Mean		-	-	532
Naveed et al. (2014)	Denmark	5.9-6.6	NA	3.3-6.0	Native microbes	DHA	NA	350[c]	-	-
						FDA	NA	800	-	-
						Mean		575	-	-
						Microbe mean		**365**	**-**	**408**
a. Archaea/Bacteria										
Mertens et al. (2010)	Denmark	5.2-5.9	6.7	3.6	AOA and AOB	PNR	4	-	-	2060[d]
Naveed et al. (2014)	Denmark	5.9-6.6	NA	3.3-6.0	Native bacteria	ACE R	NAP	170	-	-
						S-W D	NAP	170	-	-
						Mean		**170**	**-**	**-**
b. Fungi										
Naveed et al. (2014)	Denmark	5.9-6.6	NA	3.3-6.0	Native fungi	ACE R	NAP	800	-	-
						S-W D	NAP	2370	-	-
						Mean		**1585**	**-**	**-**
Soil properties										
Naveed et al. (2014)	Denmark	5.9-6.6	NA	3.3-6.0	Physical properties	AP	NAP	320	-	-
						SWR	NAP	275	-	-
						GD	NAP	200[c]	-	-
						R-R α	NAP	260[c]	-	-
						R-R β	NAP	170[c]	-	-
						TPO	NAP	320[c]	-	-
						Mean		275	-	-
					Chemical properties	OC	NAP	290[c]	-	-
						TN	NAP	470	-	-
						TP	NAP	225	-	-
						Mean		348	-	-
					Soil properties mean			**311**	**-**	**-**

CEC: cation exchange capacity; EP: endpoint; NA: not available; NAP: not applicable (field observations); native microbes: biological response is attributed to several soil microorganism taxa (i.e., archaea, bacteria, actinomycete, algae, fungi, and protozoa); OM: organic matter; SO: soil origin; TD: test duration (days).
ACE R: ACE richness; AOA and AOB: ammonia-oxidizing archaea and ammonia-oxidizing bacteria community; AP: air permeability; AT: avoidance test; BL: body length; SWR: Soil water retention; CC: carotenoid content; Chl*a*/Chl*b*: chlorophyll a/chlorophyll b ratio; ChlTot: total chlorophyll content; CQ: cocoon quantity; DHA: dehydrogenase activity; EL: epicotyl length; FDA: fluorescein diacetate hydrolysis; FPZ: field population size; GD: gas diffusivity; JQ: juvenile quantity; LA: leaf asymmetry; LL: leaf length; NRRT: neutral-red retention time; OC: organic carbon; PC: plant cover; PNR: potential nitrification rate; R DW: root dry weight; R L: root length; R-R α: soil pore size distribution (Rosin-Rammler α); R-R β: soil pore size distribution (Rosin-Rammler β); SH DW: shoot dry weight; SH L: shoot length; SIR + ATP: substrate induced respiration and ATP content; SO: soil origin; SOM D: soil organic matter decomposition; SPQ: seeds pods quantity; SR: species richness; SV: survival; S-W D: Shannon-Wiener diversity index; TAC: total antioxidant capacity; TLA: total leaf area; TN: total nitrogen; TP: total phosphorus; TPO: total porosity; WC: water content.
[a]Mean value for several soils. [b]EC_{20} instead of EC_{25}. (not included in the mean). [c]Estimate based on illustrations. [d]Not considered for mean calculation.

Supplementary Table 3. Extractable, soluble, and free copper ion effective concentrations (EC_x)

Study	Species	EP	TD	Extractant	$Cu_{extractable}$ (mg kg^{-1})	$Cu_{soluble}$ (µg L^{-1})			pCu^{2+}		
					EC_{50}	EC_{10}	EC_{25}	EC_{50}	EC_{10}	EC_{25}	EC_{50}
Plants											
Hamels et al. (2014)	*Hordeum vulgare* (Barley)	SH DW	14	0.0155 M Cohex, SSR: NA	**50**	-	-	-	-	-	-
				1 M NH_4NO_3, SSR: 1/2.5	**8.9**	-	-	-	-	-	-
				0.05 M EDTA, SSR: 1/2.5	**930**	-	-	-	-	-	-
				0.001 M $CaCl_2$, SSR: 1/10	-	-	-	**390**	-	-	-
				C_{DGT}	-	-	-	**40**	-	-	-
Kolbas et al. (2014)	*Helianthus annuus* (Sunflower)	CC	28	Pore water	-	114	-	571	7.3	-	6.6
		Chl*a*/Chl*b*	28	Pore water	-	-	-	-	7.3	-	6.6
		ChlTot	28	Pore water	-	104	-	524	7.4	-	6.7
		EL	28	Pore water	-	728	-	-	-	-	-
		LA	28	Pore water	-	-	-	-	6.7	-	5.7
		LL	28	Pore water	-	-	-	-	6.5	-	-
		R DW	28	Pore water	-	118	-	590	7.3	-	6.5
		SH DW	28	Pore water	-	261	-	607	7.0	-	5.2
		SH L	28	Pore water	-	-	-	608	-	-	-
		TLA	28	Pore water	-	312	-	-	-	-	6.9
		WC	28	Pore water	-	538	-	-	-	-	6,4
		Mean			-	311	-	580	7.1	-	6.3
Kolbas et al. (2018)	*Helianthus annuus* (Sunflower)	R DW	28	Pore water	-	-	-	290	-	-	-
		SH DW	28	Pore water	-	-	-	432	-	-	-
		Mean			-	-	-	361	-	-	-
Lillo-Robles et al. (2020)	Several species	PC	180	0.1 M KNO_3, SSR: 1/2.5	-	376	448	532	7.3	6.8	6.1
		SH DW	180	0.1 M KNO_3, SSR: 1/2.5	-	184	304	444	8.0	7.2	6.3
		SR	180	0.1 M KNO_3, SSR: 1/2.5	-	240	440	640	7.2	6.3	5.3
		Mean			-	**267**	**397**	**539**	**7.5**	**6.8**	**5.9**
		Plant mean		**Pore water**	-	-	-	471	-	-	-
Invertebrates: Worms											
Konečný et al. (2014)	*Enchytraeus crypticus*	JQ	28	0.05 M EDTA, SSR: 1/2.5 (recalculated from SSR: 1/10)	**398**	-	-	-	-	-	-
Microorganisms											
Aponte et al. (2021)	Native microbes	ARY	<1	NA M DTPA, SSR: NA	**139**	-	-	-	-	-	-

EP: endpoint; TD: test duration (days); SSR: soil/solution ratio. CC: carotenoid content; C_{DGT}: diffusive gradients in thin films measured concentration; native microbes: biological response is attributed to several soil microorganism taxa (i.e., archaea, bacteria, actinomycete, algae, fungi, and protozoa).
ARY: arylsulfatase activity; Chl_a/Chl_b: chlorophyll a/chlorophyll b ratio; ChlTot: total chlorophyll content; EL: epicotyl length; JQ: juvenile quantity; LA: leaf asymmetry; LL: leaf length; NA: not available; PC: plant cover; R DW: root dry weight; SH DW: shoot dry weight; SH L: shoot length; SR: species richness; TLA: total leaf area; WC: water content.
Lillo-Robles et al. (2020): various Chilean field-collected soils with pH 4.9-7.1 and 0.9-8.0% organic matter. This study demonstrates the impact of a single pollutant on biological responses.
Aponte et al. (2021): various Chilean field-collected soils with pH 4.7-5.9 and 1.0-2.8% organic matter. This study demonstrates the impact of a single pollutant on biological responses.

Supplementary Table 4. Total nickel effective concentrations (EC_x) and the properties of soils under study

Study	SO	Soil properties			Species	EP	TD	Ni_{total} (mg kg^{-1})	
		pH	CEC ($cmol_+$ kg^{-1})	OM (%)				EC_{25}	EC_{50}
Plants									
Dan et al. (2008)	Canada	5.7-6.9	5.0-63	6.0-28	*Avena sativa* (Oat)	SH DW	28-70	1727[a]	-
Cioccio et al. (2017)	Canada	4.6-6.1	23-54	9.6-25	*Avena sativa* (Oat)	AY	NA	-	1270
		NA	NA	NA	*Glycine max* (Soybean)	AY	NA	-	1590
Gopalapillai et al. (2018)	Canada	5.5-7.4	9.7-49	3.6-18	*Avena sativa* (Oat)	SH DW	NA	-	2269[a]
						Plant mean		**1727**	**1710**

CEC: cation exchange capacity; EP: endpoint; OM: organic matter; NA: not available; SO: soil origin; TD: test duration (days). AY: Agronomic yield. SH DW: Shoot dry weight; R DW: Root dry weight. [a] Mean value for several soils.

Supplementary Table 5. Extractable, soluble, and free nickel ion effective concentrations (EC_x)

Study	Species	EP	TD	Extractant	$Ni_{extractable}$ (mg kg^{-1})		$Ni_{soluble}$ (µg L^{-1})	pNi^{2+}
					EC_{25}	EC_{50}	EC_{25}	EC_{50}
Plants								
Kukier and Chaney (2004)	*Avena sativa* (Oat)	SH DW	42	0.01 M $Sr(NO_3)_2$, SSR: 1/4	-	-	5.7	-
	Beta vulgaris (Red beet)	SH DW	42	0.01 M $Sr(NO_3)_2$, SSR: 1/4	-	-	6.4	-
	Beta vulgaris var. cicla (Swiss chard)	SH DW	42	0.01 M $Sr(NO_3)_2$, SSR: 1/4	-	-	6.2	-
	Glycine max (Soybean)	SH DW	42	0.01 M $Sr(NO_3)_2$, SSR: 1/4	-	-	4.6	-
	Hordeum vulgare (Barley)	SH DW	42	0.01 M $Sr(NO_3)_2$, SSR: 1/4	-	-	15	-
	Lolium perenne (Perennial ryegrass)	SH DW	42	0.01 M $Sr(NO_3)_2$, SSR: 1/4	-	-	20	-
	Phaseolus vulgaris (Bean)	SH DW	42	0.01 M $Sr(NO_3)_2$, SSR: 1/4	-	-	3.5	-
	Raphanus sativus (Radish)	R DW	31	0.01 M $Sr(NO_3)_2$, SSR: 1/4	-	-	6.0	-
		SH DW	31	0.01 M $Sr(NO_3)_2$, SSR: 1/4	-	-	7.2	-
		Mean			-	-	6.6	-
	Solanum lycopersicum (Tomato)	SH DW	42	0.01 M $Sr(NO_3)_2$, SSR: 1/4	-	-	6.6	-
	Triticum aestivum (Wheat)	SH DW	42	0.01 M $Sr(NO_3)_2$, SSR: 1/4	-	-	22	-
	Zea mays (Corn)	SH DW	42	0.01 M $Sr(NO_3)_2$, SSR: 1/4	-	-	6.8	-
Dan et al. (2008)	*Avena sativa* (Oat)	SH DW	28-70	0.2 M $C_2H_2O_4$ + $(NH_4)_2C_2O_4$, SSR: 1/20	**465**[a]	-	-	-
Gopalapillai et al. (2018)	*Avena sativa* (Oat)	SH DW	NA	0.2 M $C_2H_2O_4$ + $(NH_4)_2C_2O_4$, SSR: 1/20	-	**607**[a]	-	-
				Pore water	-	-	-	**6.8**[a]
		Plant mean		**0.01 M $Sr(NO_3)_2$, SSR: 1/4**	-	-	**9.3**	-

EP: endpoint; TD: test duration (days); SSR: soil/solution ratio. SH DW: shoot dry weight; R DW: root dry weight. [a] Mean value for several soils. Kukier and Chaney (2004): Canadian field-collected soil artificially adjusted to pH 5.2-7.8 by adding $CaCO_3$ and $MgCO_3$; contains 17% of organic matter. The study demonstrates the impact of a single pollutant on biological responses.

Supplementary Table 6. Total lead effective concentrations (EC_x) and the properties of soils under study

Study	SO	Soil properties			Species	EP	TD	Pb_{total} (mg kg^{-1})	
		pH	CEC ($cmol_+$ kg^{-1})	OM (%)				EC_{10}	EC_{50}
Invertebrates									
a. Mites									
Luo et al. (2015)	Netherlands	3.2-6.8	1.8-21	3.8-13	*Platynothrus peltifer*	JQ	84	**658**	**696**
b. Worms									
Hui et al. (2009)	Finland	NA	NA	NA	Native enchytraeids	SV	33	-	11,030[a]
Luo et al. (2014b)	Netherlands	3.2-6.8	1.8-21	3.8-13	*Eisenia andrei*	SV	28	-	1603
						JQ	56	1377	1482
						Mean		1377	1543
Luo et al. (2014a)	Netherlands	3.2-6.8	1.8-21	3.8-13	*Enchytraeus crypticus*	SV	21	-	638
						JQ	21	583	645
						Mean		583	642
						Worm mean		**980**	**1092**
Microorganisms									
Vanhala and Ahtiainen (1994)	Finland	3.1-4.8	NA	NA	Native microbes	ATP	NAP	-	68,700
						RR	<1	-	25,000
						Mean		-	**46,850**

CEC: cation exchange capacity; EP: endpoint; NA: not available; NAP: not applicable (field observations); native microbes: biological response is attributed to several soil microorganism taxa (i.e., archaea, bacteria, actinomycete, algae, fungi, and protozoa); OM: organic matter; SO: soil origin; TD: test duration (days).
ATP: ATP content; JQ: Juvenile quantity; RR: Respiration rate; SV: Survival. [a] Not considered for mean calculation.

Supplementary Table 7. Extractable and soluble lead effective concentrations (EC_x)

Study	Species	EP	TD	Extractant	$Pb_{extractable}$ (mg kg^{-1})		$Pb_{soluble}$ (µg L^{-1})	
					EC_{10}	EC_{50}	EC_{10}	EC_{50}
Invertebrates								
a. Mites								
Luo et al. (2015)	*Platynothrus peltifer*	JQ	84	Water, SSR: 1/5	**2.2**	**5.5**	-	-
				0.01 M $CaCl_2$, SSR: 1/5	**7.2**	**49**	-	-
				Pore water	-	-	**3040**	**6418**
b. Worms								
Luo et al. (2014b)	*Eisenia andrei*	SV	28	Water, SSR: 1/5	-	5.5	-	-
				0.01 M $CaCl_2$, SSR: 1/5	-	98	-	-
				Pore water	-	-	-	5100
		JQ	56	Water, SSR: 1/5	0.4	0.5	-	-
				0.01 M $CaCl_2$, SSR: 1/5	0.4	2.2	-	-
				Pore water	-	-	99,000	130,000
		Mean		Water, SSR: 1/5	0.4	3.0	-	-
				0.01 M $CaCl_2$, SSR: 1/5	0.4	50	-	-
				Pore water	-	-	99,000	67,550
Luo et al. (2014a)	*Enchytraeus crypticus*	SV	21	Water, SSR: 1/5	-	1.5	-	-
				0.01 M $CaCl_2$, SSR: 1/5	-	8.5	-	-
				Pore water	-	-	-	643

Luo et al. (2014a)	*Enchytraeus crypticus*	JQ	21	Water, SSR: 1/5	0.4	0.5	-	-
				0.01 M $CaCl_2$, SSR: 1/5	1.3	1.6	-	-
				Pore water	-	-	119	126
		Mean		Water, SSR: 1/5	0.4	1.0	-	-
				0.01 M $CaCl_2$, SSR: 1/5	1.3	5.1	-	-
				Pore water	-	-	119	385
		Worm mean		**Water, SSR: 1/5**	**0.4**	**2.0**	**-**	**-**
				0.01 M $CaCl_2$, SSR: 1/5	**0.9**	**28**	**-**	**-**
				Pore water	**-**	**-**	**49,560**	**33,967**

EP: endpoint; TD: test duration (days); SSR: soil/solution ratio. JQ: juvenile quantity; SV: survival.

Supplementary Table 8. Total zinc effective concentrations (EC_x) and the properties of soils under study

Study	SO	Soil properties			Species	EP	TD	Zn_{total} (mg kg^{-1})	
		pH	CEC ($cmol_+$ kg^{-1})	OM (%)				EC_{10}	EC_{50}
Plants									
De Knecht et al. (1998)	Netherlands	NA	NA	NA	*Trifolium pratense* (Red clover)	SH FW	24	-	347
Smolders et al. (2002)	Belgium	5.5-6.1	17-21	6.0-13	*Triticum aestivum* (Wheat)	SH DW	21	217	1215
Beyer et al. (2011)	United States	3.8-4.8	NA	NA	Wild shrubs and vines	PC	NAP	-	1350
						SR	NAP	-	4287[a]
					Wild trees	PC	NAP	-	1740
						SD	NAP	-	2740[b]
					Wild trees, shrubs, and vines	PC	NAP	-	2060
						Mean		-	2359
Beyer et al. (2013)	United States	3.6-4.2	14-16	8.0-13	*Acer rubrum* (Red maple)	L FW	126	-	160
						R FW	126	-	180
						Mean		-	170
					Betula populifolia (Gray birch)	L FW	119	-	110
						R FW	119	-	110
						Mean		-	110
					Glycine max (Soybean)	L FW	28	-	160
						R FW	28	-	250
						Mean		-	205
					Pinus strobus (Eastern white pine)	L FW	126	-	970
						R FW	126	-	880
						Mean		-	925
					Quercus prinus (Chestnut oak)	L FW	84	-	340
						R FW	84	-	220
						Mean		-	280
					Quercus rubra (Northern red oak)	L FW	77	-	180
						R FW	77	-	170
						Mean		-	175
Hamels et al. (2014)	Belgium/France	4.8-7.6	1.0-69	1.7-40	*Hordeum vulgare* (Barley)	SH DW	14	-	9820[a]
						Plant mean		**217**	**1561**

Invertebrates									
Spurgeon et al. (2005)	United Kingdom	3.7-7.1	NA	NA	Decomposer community	OM R	6	-	**979**
a. Springtails									
Mertens and Smolders (2013)	Belgium / United Kingdom	NA	NA	NA	*Folsomia candida*	R	NA	**507**	-
b. Worms									
Spurgeon and Hopkin (1995)	United Kingdom	5.5-7.4	NA	9.4-27	*Eisenia fetida*	CQ	21	-	3605
						W	21	-	22,371[d]
Posthuma and Notenboom (1996)	Netherlands	5.5	NA	1.9-6.4	*Eisenia andrei*	CQ	21	-	2553
					Enchytraeus crypticus	JQ	28	-	205
Spurgeon and Hopkin (1996)	United Kingdom	5.5-7.4	NA	9.4-27	*Eisenia fetida*	W	35	-	3120
						SM	56	-	1860
						CQ	84	-	637
						CQ	140	-	4950[d]
						CQ	NA	-	3600[d]
						Mean		-	1872
Nahmani and Lavelle (2002)	France	NA	NA	NA	*Aporrectodea caliginosa*	FPZ	NAP	-	2000[c]
Spurgeon et al. (2005)	United Kingdom	NA	NA	NA	*Lumbricus rubellus*	CQ	70	-	3236
						NRRT	70	-	645
						GE	70	-	616
						Mean		-	1499
		5.4-7.4	NA	NA	Native earthworms	S-W D	NAP	-	1737
Mertens and Smolders (2013)	Belgium / United Kingdom	NA	NA	NA	*Eisenia fetida*	R	NA	924[a]	-
						Worm mean		**924**	**1912**
Microorganisms									
Vanhala and Ahtiainen (1994)	Finland	4.3-7.2	NA	NA	Native microbes	ATP	NAP	-	1550
						RR	<1	-	4000
						Mean		**-**	**2775**
a. Bacteria									
Broos et al. (2004)	United Kingdom	5.2-5.7	2.5-4.7	NA	*Rhizobium leguminosarum* bv. *trifolii*	N_{dff}	32	-	602
Broos et al. (2004)	United Kingdom	5.2-5.7	2.5-4.7	NA	*Rhizobium leguminosarum* bv. *trifolii*	MPN	149	-	204
						Bacteria mean		-	**403**

CEC: cation exchange capacity; decomposer community: biological response is attributed to several soil organism taxa (i.e., earthworms, isopods, microbes, mites, mollusks, myriapods and springtails); EP: endpoint; NA: not available; NAP: not applicable (field observations); native microbes: biological response is attributed to several soil microorganism taxa (i.e., archaea, bacteria, actinomycete, algae, fungi, and protozoa); OM: organic matter; SO: soil origin; TD: test duration (days).
AS: arylsulfatase stability; ATP: ATP content; CQ: cocoon quantity; EA: enzymatic activity of arylsulfatase, β-glucosidase, invertase, phosphatase, protease and urease; ES: enzymatic stability of arylsulfatase, β-glucosidase, invertase, phosphatase, protease and urease; FPZ: field population size; GE: gene expression (*mt-2*); JQ: juvenile quantity; L FW: leaf fresh weight; MPN: most probable number; N_{dff}: symbiotic nitrogen fixation; NRRT: neutral-red retention time; OM R: organic material removal (feeding); PC: plant cover; PS: protease stability; R FW: root fresh weight; R: reproduction (not detailed); RR: respiration rate; SD: seedling density; SH DW: shoot dry weight; SH FW: shoot fresh weight ; SM: sexual maturity; SR: species richness; S-W D: Shannon-Wiener diversity index; US: urease stability; W: weight. [a] Mean value for several soils. [b] EC_{90} instead of EC_{50} (not included in the mean). [c] EC_{100} instead of EC_{50} (not included in the mean). [d] Not considered for mean calculation.

Supplementary Table 9. Extractable, soluble, and free zinc ion effective concentrations (EC_x)

Study	Species	EP	TD	Extractant	$Zn_{extractable}$ (mg kg^{-1})	$Zn_{soluble}$ (µg L^{-1})		pZn^{2+}	
					EC_{50}	EC_{10}	EC_{50}	EC_{10}	EC_{50}
Plants									
De Knecht et al. (1998)	*Trifolium pratense* (Red clover)	SH FW	24	0.01 $CaCl_2$, SSR: NA	**121**	-	-	-	-
Smolders et al. (2002)	*Triticum aestivum* (Wheat)	SH DW	21	Pore water	-	**400**	**6900**	-	-
				C_{DGT}	-	150	4410	-	-
Nolan et al. (2005)	*Triticum aestivum* (Wheat)	SH DW	16	Pore water	-	-	-	**3.9**	**3.4**
Beyer et al. (2011)	Wild shrubs and vines	PC	NAP	0.01 M $Sr(NO_3)_2$, SSR: 1/4	71	-	-	-	-
		SR	NAP	0.01 M $Sr(NO_3)_2$, SSR: 1/4	186[a]	-	-	-	-
	Wild trees	SD	NAP	0.01 M $Sr(NO_3)_2$, SSR: 1/4	133[b]	-	-	-	-
	Wild trees, shrubs, and vines	PC	NAP	0.01 M $Sr(NO_3)_2$, SSR: 1/4	102	-	-	-	-
		Mean			120	-	-	-	-
Beyer et al. (2013)	*Acer rubrum* (Red maple)	L FW	126	0.01 M $Sr(NO_3)_2$, SSR: 1/4	28	-	-	-	-
				Mehlich 3, SSR: NA	48	-	-	-	-
		R FW	126	0.01 M $Sr(NO_3)_2$, SSR: 1/4	28	-	-	-	-
				Mehlich 3, SSR: NA	56	-	-	-	-
		Mean		0.01 M $Sr(NO_3)_2$, SSR: 1/4	28	-	-	-	-
				Mehlich 3, SSR: NA	52	-	-	-	-
	Betula populifolia (Gray birch)	L FW	119	0.01 M $Sr(NO_3)_2$, SSR: 1/4	19	-	-	-	-
				Mehlich 3, SSR: NA	32	-	-	-	-
		R FW	119	0.01 M $Sr(NO_3)_2$, SSR: 1/4	18	-	-	-	-
				Mehlich 3, SSR: NA	35	-	-	-	-
		Mean		0.01 M $Sr(NO_3)_2$, SSR: 1/4	19	-	-	-	-
				Mehlich 3, SSR: NA	34	-	-	-	-
	Glycine max (Soybean)	L FW	28	0.01 M $Sr(NO_3)_2$, SSR: 1/4	27	-	-	-	-
				Mehlich 3, SSR: NA	48	-	-	-	-
		R FW	28	0.01 M $Sr(NO_3)_2$, SSR: 1/4	36	-	-	-	-
				Mehlich 3, SSR: NA	76	-	-	-	-
		Mean		0.01 M $Sr(NO_3)_2$, SSR: 1/4	32	-	-	-	-
				Mehlich 3, SSR: NA	62	-	-	-	-
Plants									
Beyer et al. (2013)	*Pinus strobus* (Eastern white pine)	L FW	126	0.01 M $Sr(NO_3)_2$, SSR: 1/4	160	-	-	-	-
				Mehlich 3, SSR: NA	300	-	-	-	-
		R FW	126	0.01 M $Sr(NO_3)_2$, SSR: 1/4	156	-	-	-	-
				Mehlich 3, SSR: NA	270	-	-	-	-
		Mean		0.01 M $Sr(NO_3)_2$, SSR: 1/4	158	-	-	-	-
				Mehlich 3, SSR: NA	285	-	-	-	-
	Quercus prinus (Chestnut oak)	L FW	84	0.01 M $Sr(NO_3)_2$, SSR: 1/4	59	-	-	-	-
				Mehlich 3, SSR: NA	100	-	-	-	-
		R FW	84	0.01 M $Sr(NO_3)_2$, SSR: 1/4	40	-	-	-	-
				Mehlich 3, SSR: NA	68	-	-	-	-
		Mean		0.01 M $Sr(NO_3)_2$, SSR: 1/4	50	-	-	-	-
				Mehlich 3, SSR: NA	84	-	-	-	-

Beyer et al. (2013)	*Quercus rubra* (Northern red oak)	L FW	77	0.01 M $Sr(NO_3)_2$, SSR: 1/4	29	-	-	-	-
				Mehlich 3, SSR: NA	52	-	-	-	-
		R FW	77	0.01 M $Sr(NO_3)_2$, SSR: 1/4	27	-	-	-	-
				Mehlich 3, SSR: NA	50	-	-	-	-
		Mean		0.01 M $Sr(NO_3)_2$, SSR: 1/4	28	-	-	-	-
				Mehlich 3, SSR: NA	51	-	-	-	-
Hamels et al. (2014)	*Hordeum vulgare* (Barley)	SH DW	14	0.0155 M Cohex, SSR: NA	**327**[a]	-	-	-	-
				1 M NH_4NO_3, SSR: 1/2.5	**145**[a]	-	-	-	-
				0.05 M EDTA, SSR: 1/2.5	**3798**[a]	-	-	-	-
				0.001 M $CaCl_2$, SSR: 1/10	-	-	**2388**[a]	-	-
				C_{DGT}	-	-	2770[a]	-	-
		Plant mean		**0.01 M $Sr(NO_3)_2$, SSR: 1/4**	**62**	-	-	-	-
				Mehlich 3, SSR: NA	**95**	-	-	-	-
				C_{DGT}	-	-	**3590**	-	-
Invertebrates: Worms									
Spurgeon and Hopkin (1995)	*Eisenia fetida*	CQ	21	Water, SSR: 1/13 to 1/17	**21**	-	-	-	-
Posthuma and Notenboom (1996)	*Eisenia andrei*	CQ	21	0.01 M $CaCl_2$, SSR: 1/10	183	-	-	-	-
				Pore water	-	-	41,000	-	-
	Enchytraeus crypticus	JQ	28	0.01 M $CaCl_2$, SSR: 1/10	6.8	-		-	-
				Pore water	-	-	1270	-	-
		Worm mean		**0.01 M $CaCl_2$, SSR: 1/10**	**95**	-	-	-	-
				Pore water	-	-	**21,135**	-	-
Microorganisms									
Lessard et al. (2014b)	Native microbes	EA	<1	0.01 M KNO_3, SSR: 1/2	-	-	5254	-	-
				ASV: 0.01 M KNO_3, SSR: 1/2	-	-	4740	-	-
		ES	1	0.01 M KNO_3, SSR: 1/2	-	-	10,808	-	-
				ASV: 0.01 M KNO_3, SSR: 1/2	-	-	14,221	-	-
		Mean		0.01 M KNO_3, SSR: 1/2	-	-	**8031**	-	-
				ASV: 0.01 M KNO_3, SSR: 1/2	-	-	9481	-	-
Lessard et al. (2014a)	Native microbes	AS	11	ASV: 0.01 M KNO_3, SSR: 1/2	-	-	455	-	-
		PS	11	ASV: 0.01 M KNO_3, SSR: 1/2	-	-	359	-	-
		US	11	ASV: 0.01 M KNO_3, SSR: 1/2	-	-	387	-	-
		Mean			-	-	400	-	-
		Microbe mean		**ASV: 0.01 M KNO_3, SSR: 1/2**	-	-	**4940**	-	-

ASV: measured by square wave anodic stripping voltammetry; C_{DGT}: Diffusive gradients in thin films measured concentration. EP: endpoint; NA: not available; NAP: not applicable (field observations); TD: test duration (days); SSR: soil/solution ratio. AS: arylsulfatase stability; CQ: cocoon quantity; EA: enzymatic activity of arylsulfatase, β-glucosidase, invertase, phosphatase, protease and urease; ES: enzymatic stability of arylsulfatase, β-glucosidase, invertase, phosphatase, protease and urease; JQ: juvenile quantity; L FW: leaf fresh weight; PC: plant cover; PS: protease stability; R FW: root fresh weight; SD: seedling density; SH DW: shoot dry weigh; SH FW: shoot fresh weight; SR: species richness; US: urease stability.
[a] Mean value for several soils. [b] EC_{90} instead of EC_{50}.
Lessard et al. (2014a): various Canadian field-collected soils. The study demonstrates the impact of a single pollutant on biological responses.
Lessard et al. (2014b): various Canadian various field-collected soils with pH 3.3-7.1, CEC 15-247 $cmol_+ kg^{-1}$, and 1.6-70.3% organic matter. The study demonstrates the impact of a single pollutant on biological responses.
Nolan et al. (2005): various Australian and United States field-collected soils, with pH 3.6-8.1 and 0.2-20% of organic matter. The study, however, does not demonstrate the impact of a single pollutant on biological responses.

Check for updates

CC BY

RESEARCH PAPER

SEASONAL MONITORING OF CHLOROPHYLL-A WITH LANDSAT 8 OLI IN THE MADURA STRAIT, PASURUAN, EAST JAVA, INDONESIA

Arief Darmawan[1*], Endang Yuli Herawati[1], Millati Azkiya[2], Rizka Nur Cahyani[2], Siti Hasanah Aryani[2], Fradaningtyas[2], Citra Anjani Hardiyanti[2], Retno Suminar Mey Dwiyanti[2]

[1]Lecturer of Dept. Aquatic Resource Management, Faculty of Fisheries and Marine Science, Univ. Brawijaya, Jl. Veteran, 65145, Malang, Indonesia

[2]Student of Dept. Aquatic Resource Management, Faculty of Fisheries and Marine Science, Univ. Brawijaya, Jl. Veteran, 65145, Malang, Indonesia

***Corresponding author:** ariefdarma@ub.ac.id

Received: November 4th, 2020 / Accepted: May 25th, 2021 / Published: July 1st, 2021

https://DOI-10.24057/2071-9388-2020-199

ABSTRACT. Chlorophyll-a (Chl-a) is a type of pigment is most common and predominant in all oxygen-evolving photosynthetic organisms such as higher plants, red and green algae. The concentrations of high chlorophyll-a (Chl-a) in coastal waters tend to be lower offshore due to land through river water runoff. The Madura Strait is one of the Indonesian basins that is widely used for fisheries activity, which directly impacts and puts quite high pressure on the aquatic resources. In addition, the development of urban areas and changes of land use in the hinterland areas of East Java Province due to increasing population are also intensive. The objectives of this research were: (1) to map the distribution of chlorophyll-a, its concentration and dynamics in the Madura Strait near the Pasuruan coastal area using remote sensing for both dry and rainy seasons, (2) figure out the influence of rivers or other oceanographic factors that may occur, and (3) calculate the accuracy of the estimation compared to the field data. The Landsat 8 OLI imagery was used to determine the concentration of Chl-a and analyze its seasonal spatial distribution pattern. The results show that (1) spatial distribution of chlorophyll-a (Chl-a), its concentration and dynamics in the Madura Strait waters near the Pasuruan coastal area varies between dry and rainy months or seasons, (2) input from rivers, waves, tidal level, and eddy circulation constitute the oceanographic parameters that influence the spatial distribution pattern of chlorophyll-a (Chl-a) in the Madura Strait waters near the Pasuruan coastal area, and (3) validation of the estimated Chl-a concentrations from Landsat 8 OLI using field data has shown RMSE value of 0.49.

KEYWORDS: Chlorophyll-a, Landsat 8, remote sensing, spatial distribution, Madura

CITATION: Arief Darmawan, Endang Yuli Herawati, Millati Azkiya, Rizka Nur Cahyani, Siti Hasanah Aryani, Fradaningtyas, Citra Anjani Hardiyanti, Retno Suminar Mey Dwiyanti (2021). Seasonal Monitoring Of Chlorophyll-A With Landsat 8 Oli In The Madura Strait, Pasuruan, East Java, Indonesia (2020). Geography, Environment, Sustainability, Vol.14, No 2, p. 22-29
https://DOI-10.24057/2071-9388-2020-199

ACKNOWLEDGMENTS: The authors would like to acknowledge the University of Brawijaya for research funding (Professor and Doctor Research Grant Program: No:35/2020) and the supporting team: Muhammad Bayu Krisnahadi and Wahyudi Arif.

Conflict of interests: The authors reported no potential conflict of interest.

INTRODUCTION

Chlorophyll-a (Chl-a) is a type of pigment is most common and predominant in all oxygen-evolving photosynthetic organisms such as higher plants, red and green algae. It is best at absorbing wavelength between 400-450 nm and 650-700 nm range of the electromagnetic spectrum (Ibrahim 2016). Chlorophyll-a is also present in aquatic organisms such as phytoplankton and algae. It enables them to use energy from the sunlight to convert carbon dioxide into complex organic molecules, such as sugar or protein (Suther & Rissik 2009). Due to the chlorophyll-a property of phytoplankton that allows them to absorb certain wavelengths of the electromagnetic spectrum, their concentration in water can be estimated using remote sensing data from a satellite that is equipped with a sensor system sensitive to these particular wavelengths. The concentration as identified and estimated from remote sensing can be used as a proxy that reflects the amount of phytoplankton. Moreover, estimates of the chlorophyll-a concentrations can be used to estimate the primary productivity of waters.

Meanwhile, the concentrations of chlorophyll-a (Chl-a) in coastal waters tend to be lower offshore due to the land through river water runoff. However, in several places in the sea, chlorophyll-a concentrations were still found entirely high. This is caused by the presence of a

water mass circulation which allows trapping of some nutrients from other places (Paramitha et al. 2014). As a result, monitoring of the dynamics, distribution add and concentration of chlorophyll-a through satellite imagery can be used in coastal zone management and aquatic resource management as well.

The Madura Strait is one of the Indonesian basins that widely used for fisheries activity, which directly impacts and puts quite high pressure on the aquatic resources. In addition, in the hinterland areas of East Java Province, the development of urban areas and changes of land use due to increasing population are also intensive. Because of that, it is suspected that there are many pollutants and land erosion products that are carried out by the rivers into the Madura Strait. There are many rivers that flow into the Madura Strait such as the Brantas River (including Porong and Kali Mas) in Sidoarjo Regency, Kali Jagir (Wonokromo) in Surabaya City, Gembong, Rejoso, Petung, and Porangan Rivers in Pasuruan etc. The Sidoarjo-Surabaya City rivers are part of the Brantas Watershed which begins from Mount Arjuno – Welirang. Meanwhile, the Rejoso River and many other rivers in Pasuruan are part of the Welang-Rejoso Watershed, which starts from the Bromo – Tengger mountains. As a consequence, those rivers that flow to the Madura Strait from Sidoarjo, Surabaya add or Pasuruan already pass through different landscapes and are affected by various human activities as they flow miles away from their wellsprings. On the other hand, the Madura Strait is also connected to the Java Sea and the Bali Strait, which makes it very complex in terms of fisheries and oceanography. From both these perspectives, it is important to study chlorophyll-a concentration, which reflects phytoplankton and their dynamics in the Madura Strait.

In general, objectives of this research were: (1) to map the distribution of chlorophyll-a, its concentration and dynamic in the Madura Strait near the Pasuruan coastal area using remote sensing for both dry and rainy seasons, (2) figure out the influence of rivers or other oceanographic parameters that may occur, and (3) calculate the accuracy of the estimation compared to the field data.

The research used spectral indices obtained from satellite remote sensing imagery for mapping of Chl-a in the Madura Strait waters. We used an equation developed by Bhirawa and Djaelani (2015), which only requires the values of reflectance for Band 4 and Band 5 of Landsat 8 OLI rather than the algorithm used by Watanabe et al. (2018) and Yadav et al. (2019). Results from the equation were validated with in situ data to determine the accuracy of the Chl-a estimation from the Landsat 8 OLI data.

MATERIALS AND METHODS

The study area was located in the Madura Strait waters, to the north of Pasuruan City and Pasuruan District, East Java, Indonesia (Fig. 1). As the main data source, we used the Landsat 8 OLI path: 118 row: 65 from May 2019 to September 2020 (from http://earthexplorer.usgs.gov). Moreover, to verify the estimation from the Landsat imagery analysis, field data on chlorophyll-a (Chl-a) were obtained from three sampling locations in (1) the Nguling, (2) Lekok, and (3) near Kraton coastal area with JFE Model AAQ 1183s-IP, which is a water quality profiler or a device to measure water quality. The field measurements with the water quality profiler were conducted on 16 August 2020, on the same day and nearly at the same time with the scene center of the Landsat 8 OLI image as it was crossing the research area at 9:35 am. With one water quality profiler available and a small boat to reach the area, we were only able to measure at 3 sampling locations. Besides that, we also obtained the data on currents direction and rainfall data from BMKG (The Indonesian Meteorological, Climatological and Geophysical Agency) along with the data on rivers and streams from the RBI Map/ topographic map of BIG (The Indonesian Bureau of Geospatial Information).

Within the Landsat 8 OLI image processing, we determined Top of Atmosphere (TOA) reflectance from the planetary spectral reflectance with correction for solar angle using an equation expressed as:

$$\rho\lambda' = M\rho * Qcal + A\rho \quad (1)$$

$$\rho\lambda = (\rho\lambda'/\cos(\theta SZ)) = (\rho\lambda'/\sin(\theta SE)) \quad (2)$$

where: ρλ' is TOA planetary spectral reflectance (unitless), Mρ is reflectance multiplicative scaling factor for the band (taken from the metadata), Aρ is reflectance additive scaling factor for the band (also taken from the metadata) and Qcal is Level 1pixel value in Digital Number (DN). Moreover, ρλ is TOA planetary spectral reflectance with correction for solar angle (unitless), θSE is local sun elevation angle, the scene center sun elevation angle in degrees is provided in the metadata, and θSZ is local solar zenith angle (USGS 2019). Chl-a was estimated from the Landsat 8 OLI images using the equation adapted from Bhirawa and Djaelani (2015), which was developed to observe water quality using Landsat 7 ETM. The equation is as follow:

$$\text{Chl a} = 0.9889\,(\text{ETM3/ETM4}) - 0.3619$$
$$\rightarrow \text{Chl a} = 0.9889\,(\text{Rs4/Rs5}) - 0.3619 \quad (3)$$

where: ETM3 and ETM4 is the TOA reflectance of Band 3 and Band 4 of Landsat 7, respectively. Meanwhile, Rs 4 and Rs5 is the TOA reflectance of Band 4 and Band 5 of Landsat 8 OLI. ETM3 and ETM4 are equal to Rs 4 and 5 in Landsat 8 OLI. The image processing was conducted with Quantum GIS 3.10 Coruna on Windows 10 - 64 bit.

Validation of the Chl-a estimation from the Landsat 8 OLI data was performed using RMSE (Root Mean Square Error) with the equation as follows:

Where ŷi, ŷn are predicted values, yi, yn are observed values and n is the number of observations.

$$RMSE = \sqrt{\sum_{i=1}^{n} \frac{(\hat{y}_i - y_i)^2}{n}} \quad (4)$$

RESULTS

The concentrations of Chl-a, obtained from the analysis of the Landsat 8 OLI imagery path: 118 row: 65 acquired from May 2019 to September 2020 using equation (3), are presented in Table 1 and Table 2. From the two tables, it can be clearly observed observed that Chl-a concentration in each sampling location was dynamic and was characterized by a certain pattern. The concentration of Chl-a was at the lowest level during rainy months such as November, December, January. Meanwhile, during dry months such as June, July, and August, the Chl-a concentration was higher than during the rainy months. The detailed dynamics of Chl-a concentration are presented in Figure 2.

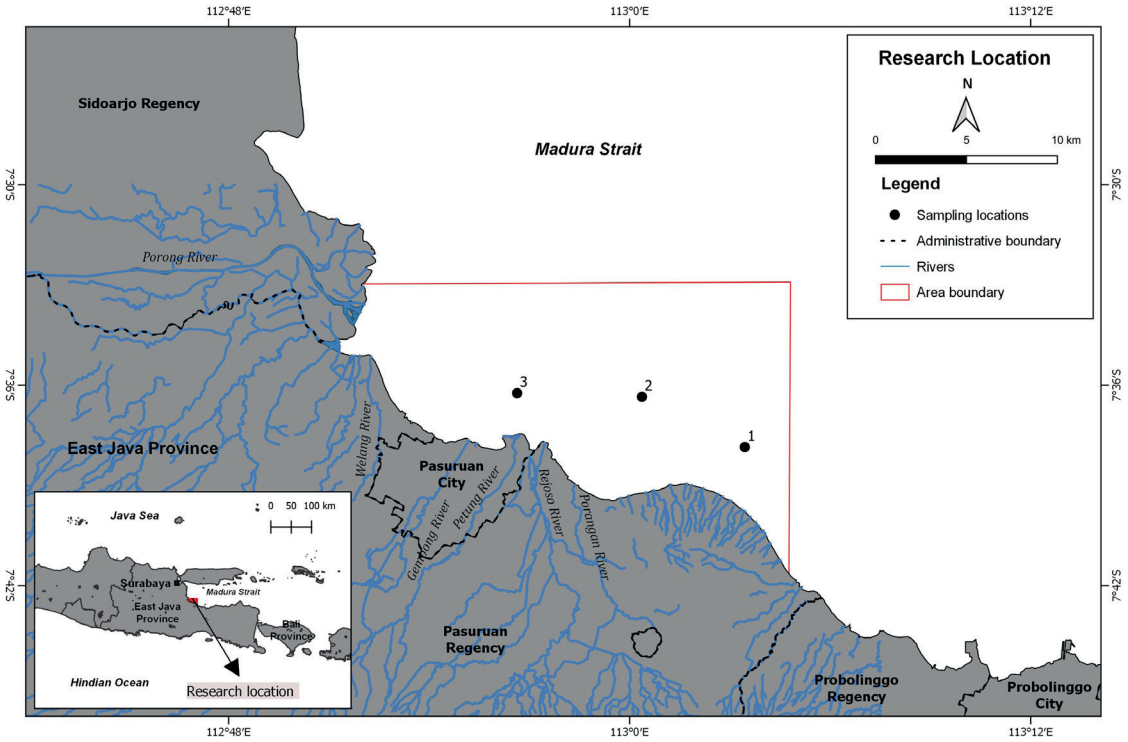

Fig. 1. Research location in the Madura Strait, Pasuruan

May 2019 – September 2020Furthermore, according to Figure 2, Nguling was characterized by the highest average Chl-a concentration compared to two other locations, while Lekok had the lowest average Chl-a concentration among others. From a spatial perspective, during the period from May 2019 to September 2020, the distribution of Chl-a was also dynamic as represented in Figure 3.

In several locations the concentration of Chl-a was high (represented by red color), in other locations it was low (represented by green color). For example, in the Madura Strait waters close to the Porong River mouth, the average concentrations were higher for the entire period except October 2019 and May 2020. From a spatial point of view, the existing rivers that end up in the Pasuruan coastal area where it directly connects to the Madura Strait influenced the concentration of Chl-a respectively as they transport nutrients from the hinterland to the Madura Straits. Unfortunately, Landsat 8 imagery for February 2020 could not be obtained and analyzed because the high clouds cover.

DISCUSSION

Dynamics and spatial distribution patterns of Chl-a

According to Figure 4, the Madura Straits waters near the Pasuruan coastal area have 4 seasonal patterns of Chl-a distribution. The first distribution pattern is represented by the figures where a high concentration of Chl-a is observed near the Porong River mouth and spreads to the area around Nguling waters (sampling location 1). An example of this distribution pattern can be seen on 26 May 2019, which is shown in Figure 4 (a), as well as on 15 September 2019 and 16 August 2020. The second distribution pattern was observed on 01 October 2019 and is given in Figure 4 (b). It is marked by an almost uniform Chl-a concentration in the waters of the Madura Strait close to the Pasuruan coastal area. Compared to the first distribution pattern of the Chl-a concentration, the second distribution pattern shows almost a reverse situation.

Table 1. Chlorophyll-a concentration in each sampling location from May 2019 to December 2019 according to Landsat 8 OLI

Chl-a (µg/L) or mg/m^3										
No	Location	May-19	Jun-19	Jul-19	Aug-19	Sep-19	Oct-19	Nov-19	Dec-19	Average
1	Nguling	2.379	1.742	2.037	2.232	1.487	1.266	1.360	1.042	1.693
2	Lekok	1.643	1.640	1.652	1.407	1.272	1.045	1.233	0.998	1.361
3	Kraton	2.125	1.988	2.133	2.116	1.174	1.465	1.757	0.861	1.702

Table 2. Chlorophyll-a concentration in each sampling location from January 2020 to September 2020 according to Landsat 8 OL

Chl-a (µg/L) or mg/m^3									
No	Location	Jan-20	Mar-20	Apr-20	May-20	Jun-20	Jul-20	Aug-20	Sep-20	Average
1	Nguling	1.230	2.004	1.949	2.814	2.291	2.430	2.678	1.096	2.061
2	Lekok	1.319	1.328	2.015	1.692	2.137	2.302	2.359	1.079	1.779
3	Kraton	1.581	1.768	2.067	1.336	2.139	2.294	2.227	1.316	1.841

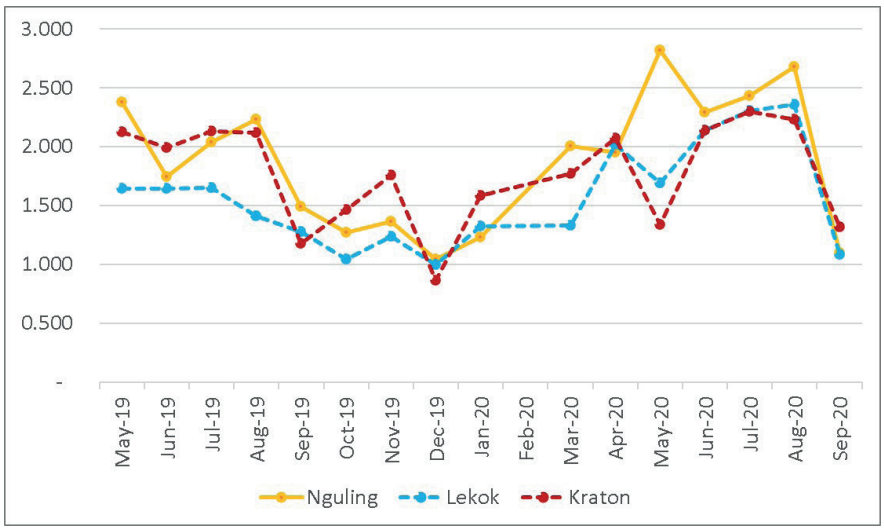

Fig. 2. Chlorophyll-a concentration (mg/m3) from Landsat 8 OLI, May 2019 – September 2020

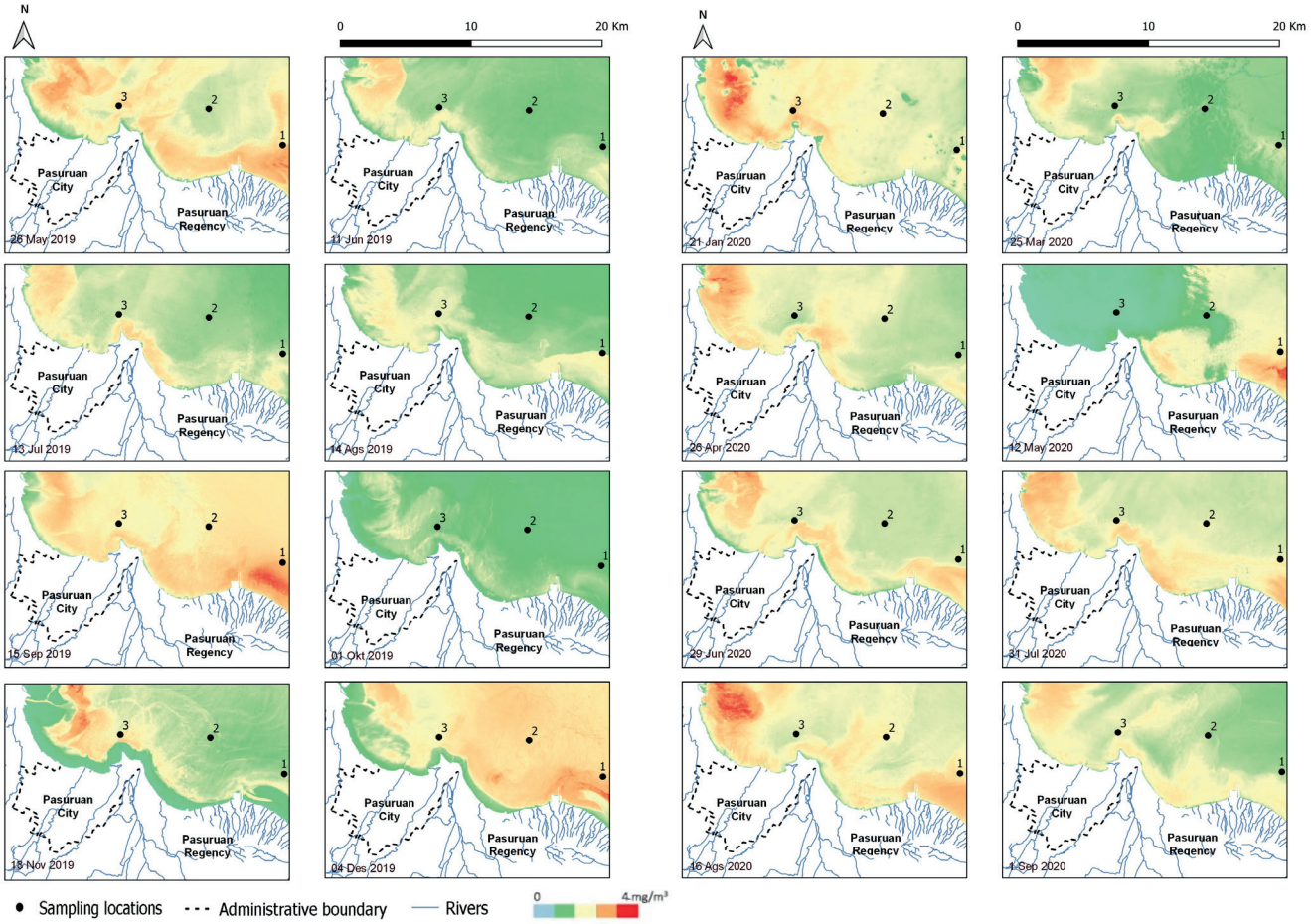

Fig. 3. Chlorophyll -a distribution from Landsat 8 OLI, May 2019 – September 2020

The third distribution pattern, presented in Figure 4 (c), is characterized by a low concentration of Chl-a in the coastal area from near the Porong River mouth to Nguling (sampling location 1). The fourth distribution pattern of Chl-a concentration was observed on 12 May 2020 and is shown in Figure 4 (d). In this case, waters from near the Porong River mouth to Kraton (sampling location 3) are characterized by a lower concentration of Chl-a compared to Nguling waters (sampling location 1). It seems that there was one center of Chl-a concentration located near Nguling (sampling location 1). We could also attribute it to the first distribution pattern (Figure 4 (a)) as it demonstrates the normal spatial distribution of Chl-a in the research location, which can be observed almost in all seasons. For further detail, see Figure 4, where all the Chl-a distribution patterns are presented sequentially.

According to Figure 3 and Figure 4, the concentration of Chl-a in the coastal area was relatively low compared to the offshore waters, which might be caused by the low tide at the moment when the Landsat 8 OLI satellite crossed and captured the waters of the research area. To give evidence of this statement, we analyzed the tide level data with the moon phase as well as the date and time of the Landsat 8 scene center acquisition as presented in Table 3. The data were obtained from the Tide Chart® application on Android® Smartphones and the Landsat 8 OLI metadata. We used the tide

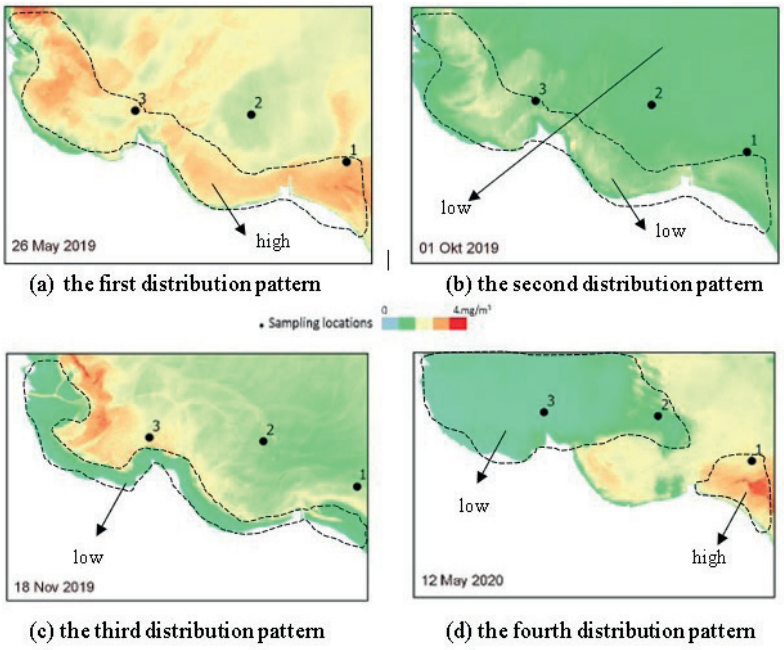

Fig. 4. Spatial distribution pattern of Chl-a concentration in the Madura Strait near Pasuruan coastal area

measurement station located in Surabaya, which was closest to the research area (See map insert in Figure 1). For example, the distribution pattern as presented in Figure 4 (c), or the third pattern, was influenced by the low tide level as seen in Table 3 row number 8. The waters near the coastal area of Pasuruan were receding when the Landsat satellites covered the area. Because of that, we can confidently state that the spatial distribution patterns of Chl-a concentration in the Madura Strait near the Pasuruan coastal area were also influenced by the tidal level. Also, the coastal area of Pasuruan includes a mangrove ecosystem, especially close to Kraton (between the Petung and Rejoso Rivers in Figure 1). In this mangrove ecosystem, tidal cycle or tidal amplitude is particularly important in determining the extent of variation of Chl-a concentration (Nion et al. 2019). Furthermore, according to H.J Ha et al. (2020), during the spring tide (when the high tide occurred at midday) Chl-a decreased during the daytime flood tide. Meanwhile, during the neap tide (when the low tide occurred at midday) Chl-a increased during the early to mid-flood tide.

Table 3. Tides and moon phase from the nearest station (Surabaya)

No	Landsat 8 OLI Date Acquired	Scene Center Time (AM)	Moon phase	Tides (m)
1	26-May-19	9:35:26	Last quarter	1.2
2	11-Jun-19	9:35:33	67% waxing	1.2
3	13-Jul-19	9:35:42	90 % waxing	1.4
4	14-Aug-19	9:35:53	99% waxing	1.6
5	15-Sep-19	9:36:02	97 % waning	1.2
7	01-Oct-19	9:36:07	13 % waxing	0.7
8	18-Nov-19	9:36:05	16 % waning	-0.1
9	04-Dec-19	9:36:04	First quarter	0.1
10	21-Jan-20	9:35:54	9 % waning	0.6
11	25-Mar-20	9:35:32	2 % waxing	1
12	26-Apr-20	9:35:16	12 % waxing	1.4
13	12-May-20	9:35:10	67 % waning	1.3
14	29-Jun-20	9:35:31	67% waxing	1.1
15	31-Jul-20	9:35:42	91 % waxing	1.4
16	16-Aug-20	9:35:47	6% waning	1.3
17	01-Sep-20	9:35:55	99% waxing	1.6

Source: Tide Chart (SeventhGear 2020)

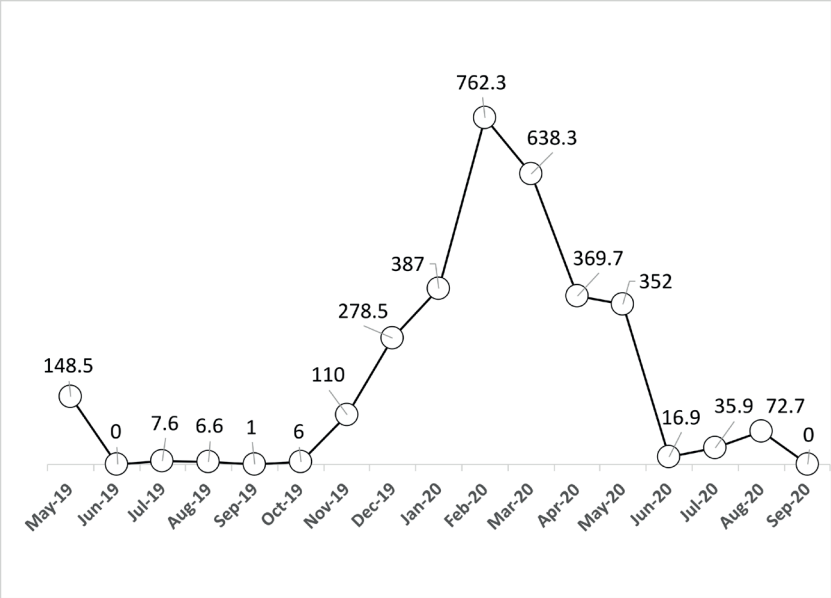

Fig. 5. Monthly total amount of rainfall (mm) recorded at Pasuruan Geophysics Station from May 2019 to September 2020 (Source: BMKG)

Low tide sometimes occurred at midday and vice versa. Research findings by Nion et al. (2019) and H.J Ha et al (2020) are relevant to the situation in the research location.

Meanwhile, according to BMKG data from May 2019 to September 2020, the highest total amount of rainfall in Pasuruan (96945-Pasuruan Geophysics Station) was in February 2020 with about 763.3 mm as represented in Figure 5. The period from June 2019 to October 2019 was characterized by the low intensity of rainfall. Although the intensity of rainfall was not very high from November 2019 to May 2020, there was rainfall occurring and it, of course, affected the discharge of river water. This condition is strengthened by Hidayah et al. (2016), where it was shown that the high chlorophyll-a concentration at the coast was due to the supply of nutrients through river runoff from the land. A similar distribution pattern of Chl-a was observed in the Madura Strait close to the Pasuruan coastal area. In the end, the dynamics, variation, and spatial distribution of Chl-a were affected by this factor too, which is in line with the research of Muhsoni et al. (2009).

We realize that in this study, monthly river discharge data was not obtained remove to precisely connecting the results from remote sensing data analysis and in situ data as it was ready in the research conducted by Siswanto et al. (2014) in the Malaka Strait. The influence of river discharge was also strengthened by the study of Masotti et al. (2018) and Otsuka et al. (2018). We also did not obtain the data on the amount of organic matter (Nitrate and Phosphate) from the river water and it is something that can be added for future research and analysis.

From a wider point of view, the Indonesia archipelago is located in the middle of the tropical region, which has two annual seasons characterized as dry and rainy. These seasons are distinguished by the different patterns of temperature as well as wind and waves direction. During dry months, the direction of waves is from east to west, including the waves in the Madura Strait. Meanwhile, in rainy months such as March, waves direction changes and becomes from west to east (locally called the western season), which is also observed in the Madura Strait. A clear example of that can be seen in the spatial distribution of Chl-a on 12 May 2020 (Figure 3). The total amount of rainfall that month was 352 mm (Figure 5) and waves were coming from the west, which resulted in the concentration and spatial distribution of Chl-a, represented by the third pattern in Figure 4 (c).

Furthermore, during the dry season when waves are directed from east to west (locally called the eastern season), we found that the concentration and spatial distribution of Chl-a corresponded to the first pattern presented in Figure 4 (a), which was observed from May 2019 to September 2019 and from June 2020 to September 2020. Unusual concentration and spatial distribution of Chl-a in the Madura Strait close to the coastal area of Pasuruan were found on 01 October 2019 when the second pattern presented in Figure 4 (b) was observed.

The spatial distribution pattern of Chl-a in the Madura Strait found in this research is also in line with the results of Semedi and Safitri (2014). It was noticed that in September, the season in the Madura Strait starts to change. This change can be observed in the data in Table 1 and Table 2 as well as Figure 2 and Figure 3 for September 2019 and 2020. The concentration of Chl-a surely went down and became less than in August 2019 and August 2020. Overall, the temporal variation pattern shows that marine waters are more turbid on rainy months than on dry months, which is in line with the research of Buditama et al. (2017). Moreover, in the broader geographic view, the distribution of Chl-a according to Taufiqurrahman and Ismail (2020) is associated with the eddy circulation in the Madura Strait. They highlighted that the deep basin under the Madura Strait creates an eddy within the water body, which appears to affect the Chl-a distribution. According to Trinugroho et al. (2019), there is also a seasonal thermal front in the Madura Strait caused by the eddy circulation, which we believe affects the distribution pattern in the waters near the Pasuruan coastal area too.

Another factor related to the dynamics and spatial distribution pattern of Chl-a that still requires further study in the research location is the thermal stratification. Thermal stratification, as mentioned by Blauw et al. (2018), also acts as one of the environmental drivers that can cause Chl-a fluctuation across different time scales and areas.

Concentration of Chl-a, tropic state and validation

Based on the Landsat 8 OLI data, Chl-a concentration in water at all the sampling locations during the period from May 2019 to September 2020, according to Novo et al. (2013), can be categorized as oligotrophic (between 1.17 – 3.24 µg/L) or < 2 µg/L (Hakanson and Blenckner 2008). Furthermore, the average concentration of Chl-a in the research area can also be categorized as medium-high to low according to Lundberg et al. (2005). The medium-high concentration of Chl-a corresponds to the range 2.2 – 3.2 µg/L and the low concentration of Chl-a is around 1.5 – 2.2 µg/L. Only Lekok, and Kraton sampling locations on 4 December 2019 and Nguling and Lekok sampling locations on 1 September 2020 were below the level of oligotrophic (ultraoligotrophic) or could be characterized by a very low concentration of Chl-a according to Lundberg et al. (2005).

As for the comparison of Chl-a derived from Landsat 8 OLI, we conducted in situ measurements on 16 August 2020 at Nguling, Lekok and Kraton. Especially in Lekok, we were lucky to arrive on time and our water quality profiler JFE Model AAQ 1183s-IP was applied close to the scene center time of Landsat 8 OLI, which crossed the area on the same day. The water quality profiler was deployed at 9:31 am, about 4 minutes earlier than the Landsat 8 p118 r65 scene center time, which was at 9:35 am. With near real-time measurement only at one site, we were still able to conduct Chl-a data validation by comparing Chl-a from the Landsat 8 OLI images derived with equation (3) with the data from the water quality profiler at a depth of approximately 10 cm from the surface as presented in Table 4.

Due to the limitation of the research equipment, it was only possible to validate the Chl-a concentrations predicted from Landsat 8 OLI using water quality profiler data obtained on 16 August 2020. From equation (4), we obtained an RMSE value of 0.491741. Low RMSE indicates that variation of the values obtained from an estimation/forecast is close to the variation in the observed values. In other words, the smaller is the RMSE value, the closer the predicted values are to the observed ones. Compared with the previous works by Muhsoni et al. (2008) and Nuriya et al. (2010), who have reached RMSE of 1.0631 and 0.934663, the results of this research with RMSE of 0.491741 look much better. RMSE equal to 0 means that predicted and observed values match perfectly, so the value obtained in this research is still not sufficient to fulfill the requirement as the target is to reach RMSE of 0.1.

Meanwhile, the following reasons could explain why the RMSE value obtained from this research only reached 0.491741: (1), only at one location water quality profiler was deployed at the same time with the Landsat 8 OLI satellite image. At other locations, the time was about 1 to 2 hours before and after the satellite crossing the research area because it took some time to move from the sampling location at Nguling to Lekok and then to Kraton with the fisherman boat. (2), it was hardest to match the availability of the water quality profiler from the laboratory with the schedule of Landsat 8 OLI crossing the research area and, as a result, we were only able to conduct one in situ measurements in time at sampling location number 2 (Lekok), (3) the equation applied to predict/estimate Chl-a concentration from Landsat 8 OLI was developed by Bhirawa and Djaelani (2015) for closed waters (lake).

Furthermore, we also applied a different atmospheric correction to get the reflectance values from the DN (digital number). Bhirawa and Jaelani (2015) as well as Jaelani et al. (2016) used 6S for their Landsat imagery while this research only used Landsat standard TOA according to USGS (2019). Sriwongsitanon et al. (2011) and Ye et al. (2017) mentioned that the 6S atmospheric correction model proved to have a better effect on the results while using Landsat imagery. Thus, the results of this research could be improved by applying other atmospheric corrections. Meanwhile, Yadav et al. (2019) estimated Chl-a using Landsat 8 by combining the TOA, mid-latitude summer atmospheric model and maritime aerosol model in the module FLAASH of ENVI 5.2 for further validation of the atmospheric correction. On the other hand, Poddar et al. (2019) used four steps to retrieve Chl-a. The steps included obtaining TOA reflectance, determining surface reflectance from TOA reflectance for the two sensors following Moran et al. (1992), and converting it to the corresponding remote sensing reflectance according to Moses et al. (2015), which is then used in the OC^2 algorithm to get Chl-a.

On the other hand, according to Cui et al. (2020), accurate estimation of Chl-a concentration in coastal waters from the ocean color using remote sensing faces challenges due to the optical complexity if compared with clear oceanic waters. Furthermore, Jaelani et al. (2016) also mentioned that the accuracy of the estimated data depends on an accurate atmospheric correction algorithm and algorithms for determining physical parameters. This statement is remove relevant to the conditions of the water in the research area. Somehow, we were facing turbid water at a few centimeters depth from the surface during the use of the water quality profiler as mentioned earlier. Chl-a data derived from Landsat 8 OLI in turbid water probably would be better if the algorithm of Watanabe et al. (2018) was applied or different algorithms were used for the dry and wet season as conducted by Gholizadeh and Melesse (2017). We consider it as parts for improvement in future works.

CONCLUSIONS

According to the analysis: (1) spatial distribution of chlorophyll-a (Chl-a), its concentration and dynamics in the Madura Strait waters near the Pasuruan coastal area varies between dry and rainy months or seasons, (2) input from rivers, waves, tidal level, and eddy circulation constitute the oceanographic parameters that influence the spatial distribution pattern of chlorophyll-a (Chl-a) in the Madura Strait waters near the Pasuruan coastal area, and (3) validation of the estimated Chl-a concentration from Landsat 8 OLI using field data has shown RMSE value of 0.49.

Table 4. Validation of Chl-a concentration predicted from Landsat 8 OLI vs observed from water quality profiler

No	Location	Observed value from Water Quality Profiler 16 Aug 2020 (A)	Predicted value from Landsat 8 OLI 16 Aug 2020 (B)	A-B
1	Nguling	1.29	2.678	-1.388
2	Lekok	3.01	2.359	0.651
3	Kraton	4.44	2.227	2.213
			RMSE	0.491741

REFERENCES

Buditama G., Damayanti A., and Pin T.G. (2017). Identifying Distribution of Chlorophyll-a Concentration Using Landsat 8 OLI on Marine Waters Area of Cirebon. IOP Conf. Series: Earth and Environmental Science, 98, 012-040, DOI:10.1088/1755-1315-98-1-012040.

Bhirawa Jayeng Rangga., Jaelani, and Lalu M. (2015). Comparison of Chlorophyll-a Value Using Landsat and Meris Images in Sentani Lake, Jayapura. Geoid, 11(1),79-84. [in Indonesia]

Blauw A.N. Benincà E., Laane R.W.P.M., Greenwood N., and Huisman J. (2018). Predictability and Environmental Drivers of Chlorophyll Fluctuations Vary Across Different Time Scales and Regions of The North Sea. Progress in Oceanography, 161, 1-18, DOI: 10.1016/2018-01-005.

Cui T.W., Zhang J., Wang K., Wei J.W., Mu B., Ma Y., Zhu J.H., Liu R.J., and Chen X.Y. (2020). Remote Sensing of Chlorophyll a Concentration in Turbid Coastal Waters Based on a Global Optical Water Classification System. ISPRS Journal of Photogrammetry and Remote Sensing, 163, 187-201.

Gholizadeh M.H., and Melesse A.M. (2017). Study on Spatiotemporal Variability of Water Quality Parameters in Florida Bay Using Remote Sensing. J Remote Sensing and GIS, 6, 207, DOI: 10.4172/2469-4134-1000207.

H.J. Ha, Kim H., Kwon Bong-Oh., Khim J.S., and Ha H.K. (2020). Influence of tidal forcing on microphytobenthic resuspension dynamics and sediment fluxes in a disturbed coastal environment. Environment International, 139, 105-743.

Hakanson L., and Blenkckner T. (2008). A Review on Operational Bioindicators for Sustainable Coastal Management-Criteria, Motives and Relationships. Ocean Coast Manag, 51(1), 43-72.

Hidayah G., Wulandari S.Y., and Zainuri M. (2016). Study of the Horizontal Distribution of Chlorophyll-a in the Silugonggo River Mouth Waters, Batangan District, Pati. Jurnal buletin oseanografi marina, 5(1), 52-59. [in Indonesia]

brahim A.E. (2016). Pictured Glossary in Biology. Scientific Research Publishing, Inc., USA, ISBN: 978-1-61896-368-0.

Jaelani L.M., Limehuwey R., Kurniadin N., Pamungkas A., Koenhardono, and E.S., Sulisetyono A. (2016). Estimation of TSS and Chl-a Concentration from Landsat 8-OLI: The Effect of Atmosphere and Retrieval Algoritm. IPTEK, The Journal for Technology and Science, 27(1), 16-23.

Lundberg C., Lonnroth, M., Von Numers, M., and Bonsdorff, E. (2005). A Multivariate Assessment of Coastal Eutrophication. Example from Gulf of Finland, northen Baltic Sea. Mar Pollut Bull, 50(11), 1185 -1196.

Masotti I., Aparicio-Rizzo P., Yevenes M.A., Garreaud R., Belmar Lucy., and Farías L. (2018). The Influence of River Discharge on Nutrient Export and Phytoplankton Biomass Off the Central Chile Coast (33°–37°S): Seasonal Cycle and Interannual Variability. Frontiers in Marine Science, 5 (23), DOI: 10.3389/fmars2018-00423.

Muhsoni F.F., Efendy M., and Triaji H. (2008). Mapping of Fishing Ground Location and Fishery Utilization Status in Madura Strait Waters. Jurnal Fisika FLUX, 6(1), 50-64. [in Indonesia]

Moran M.S., Jackson R.D., Slater P.N., and Teillet P.M. (1992). Evaluation of Simplified Procedures for Retrieval of Land Surface Reflectance Factors from Satellite Sensor Output. Remote Sens. Environ, 41, 169-184, DOI: 10.1016/0034-4257-92-0076-V.

Moses W.J., Bowles J.H., and Corson M.R. (2015). Expected Improvements in the Quantitative Remote Sensing of Optically Complex Waters with the use of an Optically Fast Hyperspectral Spectrometer-a Modeling Study. Sensors, 15, 6152-6173, DOI: 10.3390/s150306152.

Nion S.H., Islam M.S., Hoq E., Kabir H., and Hoque M.M. (2019). Seasonal and Tidal Dynamics of Nutrients and Chlorophyll a Concentration in Water at the Sundarbans Mangrove Ecosystems of Bangladesh. J Ecol and Nat Resour, 3(5). ISSN: 2578-4994.

Novo E.M.L.M, Londe L.R., Barbosa C., Araujo C.A.S., and Renno C.D. (2013). Proposal for a Remote Sensing Trophic State Index Based Upon Thematic Landsat images. Rev. Ambient. Água, 8(3), 65-82.

Nuriya H., Hidayah Z., and Nugraha W.A. (2010). Measurement of Chlorophyll – a With Landsat 7 ETM image processing and Laboratory Test in the West Madura Strait. Jurnal Kelautan, 3(1), 60-65. [in Indonesia].

Otsuka A.Y., Feitosa F.A.N, Montes M.J.F., and Silva A.C. (2018). Influence of Fluvial Discharge on the Dynamics of Chlorophyll-α in the Continental Shelf Adjacent to the Recife Port Basin (Pernambuco-Brazil). Brazilian Journal of Oceanography, 66(1), 91-103, DOI: 10.1590/1679-8759-2018-1-49-106601.

Poddar S., Chacko N., and Swain D. (2019). Estimation of Chlorophyll-a in Northern Coastal Bay of Bengal Using Landsat-8 OLI and Sentinel-2 MSI Sensors. Frontiers in Marine Science, 6 (598), 1-11, DOI: 10.3389/2019-005-98.

Semedi B., and Safitri N.M. (2015). Estimation of Chlorophyll-A Distribution in Madura Strait Waters Using MODIS Satellite Imagery and In Situ Measurements during the Eastern Season. Research Journal of Life Science, 1(2), 117-126. [in Indonesia]

SeventhGear. (2020). Tide Chart, version 2.35 (software). SeventhGear: South Carolina. Available at https://play.google.com/store/apps/details?id=com.SeventhGear.tides

Siswanto E., and Tanaka K. (2014). Phytoplankton Biomass Dynamics in the Strait of Malacca within the Period of the SeaWiFS Full Mission: Seasonal Cycles, Interannual Variations and Decadal-Scale Trends. Remote Sens, 6, 2718-2742, DOI:10.3390/rs6042718.

Sriwongsitanon N., Surakit. K., and Thianpopurug S. (2011). Influence of Atmospheric Correction and Number of Sampling Points on the Accuracy of Water Clarity Assessment Using Remote Sensing Application. Journal of Hydrology, 401, 203-220.

Suther I.M., and Rissik D. (2009). Plankton, A Guide to Their Ecology and Monitoring for Water Quality. CSIRO Publishing: Australia.

Taufiqurrahman E., and Ismail M.F.A. (2020). Distribution of Chlorophyll-a Associated with Eddy Circulation in the Strait of Madura. OLDI, 5(2), 93-103, DOI:10.14203/2020-v5i2-308. [in Indonesia].

Trinugroho T., Satriadi A., and Muslim M. (2019). Distribution of Seasonal Thermal Front in Madura Strait Waters using Single Image Edge Detection. Journal of Marine Research, 8(4), 416-423. [in Indonesia].

Watanabe F., Alcantara E., Rodrigues T., Rotta L., Bernardo N and Imai N. (2018). Remote Sensing of the Chlorophyll-a based on OLI/Landsat-8 and MSI/Sentinel-2A (Barra Bonita reservoir, Brazil). Anais da Academia Brasileira de Ciências, 90(2), 1987-2000, DOI: 10.1590/0001-3765201720170125.

USGS. (2019). Landsat 8 (L8) Data Users Handbook Version 5.0. USGS: South Dakota.

Yadav S., Yamashiki Y, Susaki J., Yamashita Y and Ishikawa K. (2019). Chlorophyll Estimation of Lake Water and Coastal Water Using Landsat-8 and Sentinel -2A Satellite. The international Achieve of the Photogrammetry, Remote Sensing and Spatial Information Sciences, Vol XLII-3/W7.

Ye Haibin., Chen Chuqun., and Yang Chaoyu. (2017). Atmospheric Correction of Landsat 8/OLI Imagery in Turbid Estuarine Waters: A Case Study for the Pearl River Eastuary. IEE Journal of Selected Topics in Applied Earth Observations and Remote Sensing, 10, 252-261.

Check for updates

CC BY

RESEARCH PAPER

DEVELOPING OF AN URBAN ENVIRONMENTAL QUALITY INDICATOR

Jocy A. P. Sousa[1*], Jomil C. A. Sales[2], Darllan C. C. Silva[3], Rita C. F. Silva[1], Roberto W. Lourenço[1]

[1]São Paulo State University (UNESP), Institute of Science and Technology, Sorocaba Campus, 511, 3 March Avenue, P.O. box 18087-180, Sorocaba, São Paulo, Brazil

[2]Sorocaba University (UNISO), Raposo Tavares, km, 92.5 Road, P.O. box 18023-000, Sorocaba, São Paulo State, Brazil

[3]São Paulo State University (UNESP), Registro Campus, 430, Nelson Brihi Badur Avenue, Tupy Village, P.O. box 11900-000, Registro, São Paulo, Brazil

***Corresponding author:** jocy_belem@hotmail.com

Received: December 16th, 2020 / Accepted: May 25th, 2021 / Published: July 1st, 2021

https://DOI-10.24057/2071-9388-2020-210

ABSTRACT. Human intervention on vegetation cover has always had a negative impact on the environment, directly affecting the quality of life in urban areas. Therefore, this study aimed to develop a methodology for the construction of an urban environmental quality indicator (UEQI) that could reflect the environmental quality of urban areas considering the vegetation conditions to which the resident population is exposed. For this, the method sought to integrate data on demographic density (Dd), leaf area index (LAI), normalized difference vegetation index (NDVI), and surface temperature (St). The Mamdani fuzzy inference system was used to generate a rule base containing 108 variations and a defuzzed output with five condition classes, ranging from very bad to excellent. The results showed that the studied area is characterized by a very bad to good UEQI, with most neighbourhoods having poor conditions (64.51%) and only two with good conditions. It was found that in general the studied area has unsatisfactory environmental quality, showing the need for initiatives aimed at urban afforestation in order to improve the quality of life for the studied population. It can be concluded that UEQI proved to be an efficient tool to identify priority areas for the planning and management of vegetation cover in urbanized areas, enabling the improvement of people's living conditions.

KEYWORDS: vegetation indexes, population dynamics, urban areas, fuzzy logic

CITATION: Jocy A. P. Sousa, Jomil C. A. Sales, Darllan C. C. Silva, Rita C. F. Silva, Roberto W. Lourenço (2021). Developing Of An Urban Environmental Quality Indicator. Geography, Environment, Sustainability, Vol.14, No 2, p. 30-41

https://DOI-10.24057/2071-9388-2020-210

ACKNOWLEDGMENTS: This study was carried out with the support of the Coordination for the Improvement of Higher Education Personnel – Brazil (CAPES). Financing code 001.

Conflict of interests: The authors reported no potential conflict of interest.

INTRODUCTION

The dynamics of urbanization and its effects, such as high population density and human pressure on natural areas, result in the hindering of the urban environmental balance, which is manifested mainly in the reduction of vegetation cover (Melazo and Nishiyama 2010; Hartig et al. 2014; Duarte et al. 2017), as many cities have a low amount of vegetation. This reflects, above all, the lack of planning during the expansion of cities and the lack of projects aiming to restore degraded areas or encourage conservation, preservation and maintenance of the vegetation cover.

Understanding how transformations take place in the urban environment is essential for proposing strategies to mitigate the negative consequences of the urbanization process. According to Magalhães et al. (2017) and Bargos and Matias (2012), urban vegetation directly influences the population's quality of life and the maintenance of ecological balance. Such claims are essential for its prioritization in urban planning.

Thus, the analysis of urban quality of life can be performed by combining several factors, both social and environmental. Among them, this article addresses the integration of population data that could show spatial distribution patterns of demography, vegetation and heat flow in a densely occupied urban area using geoprocessing techniques (Shimabukuro et al. 2015) and fuzzy inference system, as proposed by Mamdani (1974).

To carry out studies like this it is necessary to use tools such as geographic information systems (GIS), which Magalhães et al. (2017) classified as of great importance due to its reliability, agility in obtaining data and low cost, as even in small areas, without the support of this geotechnology, the costs for conducting a research can be high. Therefore, the use of spatial analysis tools is essential to assist in the identification and analysis of urban environmental conditions, thus helping to support management and planning programs aiming to maintain and conserve vegetation, especially trees or shrubs.

In this sense, this study aims to present a model that, using GIS, integrates data on demographic density (Dd), leaf area index (LAI), normalized difference vegetation index (NDVI) and surface temperature (St) for the creation of an urban environmental quality indicator (UEQI) applied to study an urban area of a municipality with a high population concentration.

MATERIALS AND METHODS

Study area

The study was carried out in the urbanized area of the municipality of Sorocaba, located in the southeastern part of the state of São Paulo, Brazil, with an estimated population of 671,186 inhabitants and a demographic density of approximately 1,304.18 inhabitants/km2 (Figure 1).

The municipality is highly urbanized and marked by the presence of an important commercial and industrial area (Lopes et al. 2019). It has Argisols, Cambisols, Gleysols and Latosols (Rossi 2017). The vegetation is transitional between the Atlantic Forest and the Cerrado biome and is marked by high forest fragmentation (IBGE 2012; Mello et al. 2014). Both biomes are characterized by rich biodiversity of fauna and flora, being considered worldwide hotspots (Myers et al. 2000).

The climate is Cwa, which is characterized by hot summers and dry winters (Dubreuil et al. 2017; Lopes et al. 2019). The average annual temperature ranges from 14.5°C to 27.5°C. The monthly rainfall for the rainiest period (January) reaches 200 mm, while for the driest period (August) it is 35 mm (CIIAGRO, 2019).

Demographic density (Dd)

Demographic density (Dd) was obtained from values found in the urban and rural census sectors (IBGE 2010; IBGE 2011), which were subsequently adjusted for the population by neighborhoods in the study area.

After obtaining the population of the neighborhoods, the total population was divided by the neighborhood area according to Equation 1.

$$Dd = \frac{Pop}{Csa} \quad (1)$$

Where: *Dd* = Demographic density (inhabitants/ha); *Pop* = Number of inhabitants per census sector; *Csa* = Census sector area.

The values of Dd obtained by census sector area were converted into the centroid of the polygon of each neighborhood using the Feature to Point tool and interpolated using inverse distance weighing (IDW) in the ArcGIS 10.6 software (ESRI 2016).

Obtaining vegetation indexes

The study of vegetation indexes was based on the images of the Landsat 8 bands 4, 5, 10 and 11 with orbit 220/point 76 and a spatial resolution of 30 meters, available free of charge on the United States Geological Survey website (USGS 2018a). The images were taken for August 2018 and January 2019 and were redesigned for the southern hemisphere. The reference is the plane coordinate system SIRGAS 2000 and spindle 23S. For the treatment and processing of images as well as for other modeling, Matlab R2010a (Mathworks 2014) and ArcGIS 10.6 (ESRI 2016) software were used.

The indexes NDVI, LAI and St indexes were obtained for January and August using the bands 4, 5, 10 and 11 of the Landsat 8 satellite.

NDVI is one of the most used indexes for studies on the quality of vegetation cover. The higher is the density of vegetation, the greater is the reflectance in the near-infrared part of the spectrum. The values of NDVI usually range from -1 to 1: the closer to 1, the better is the vegetation condition, and the closer to zero, the worse is the vegetation condition (Gandhi et al. 2015; Santos and Aquino 2015).

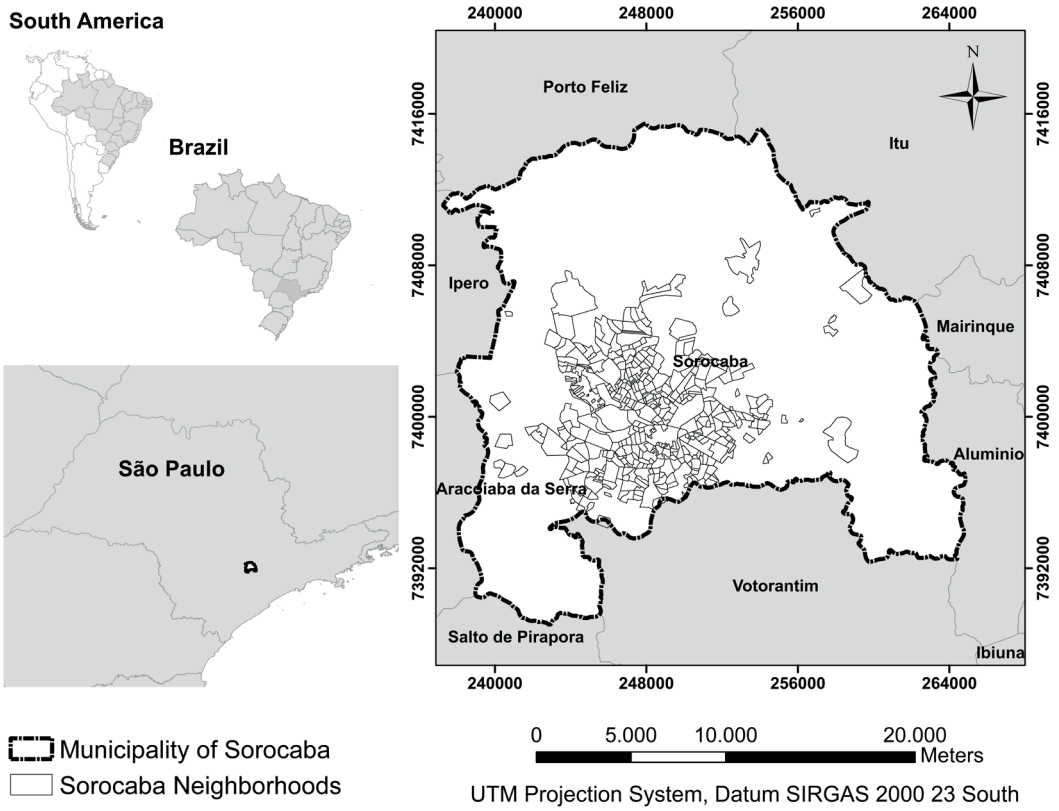

Fig. 1. Location of the Municipality of Sorocaba, São Paulo, Brazil

LAI corresponds to the ratio of leaf area over the land where the vegetation is found. It is an important index to estimate, for example, vegetative development and biomass (Allen et al. 2002; Fernandes et al. 2016).

To calculate NDVI and LAI, the bands 4 and 5 of Landsat 8, previously converted from digital numbers (DN) into reflectance at the top of the atmosphere (TOA), were used according to Equation 2, and later this value was corrected for solar angulation using Equation 3. This conversion was performed using the radiometric coefficients available in the image file metadata. Further details can be found in the LDCM Cal/Val Algorithm Description Document and Landsat 8 Science Users' Handbook available at <http://landsat.usgs.gov/Landsat8_Using_Product.php>.

$$P\lambda' = Mp * Qcal + Ap \quad (2)$$

Where: Pλ'= TOA reflectance without correction of the solar angle; Mρ = Multiplying factor for resizing the band (0.00002); Qcal = Quantified and calibrated pixel value in gray level (DN); Ap = Additive scaling factor specific to the band (-0.1).

$$P\lambda = \frac{P\lambda'}{\mathrm{Cos}(\theta_{SZradian})} \quad (3)$$

Where: Pλ= TOA reflectance with correction of the solar angle; θSZ = Local solar zenith angle, defined as θSZ = 90° – θSE; where θSE = Local solar elevation angle. Its value for August 2018 was 43.36905219 and for January 2019 – 58.8671889; θSZradian = θSZ*(π/180).

After correcting the images, Equation 4 was used to calculate NDVI (Rouse et al. 1973).

$$NDVI = \frac{(NIR - R)}{NIR + R} \quad (4)$$

Where: NDVI = Normalized difference vegetation index; NIR = Planetary reflectance at the top of the atmosphere within the near-infrared range; R = Planetary reflectance at the top of the atmosphere within the red range.

For the calculation of LAI, Equation 5 was used (Allen et al. 2002).

$$LAI = -\frac{Ln\left(\frac{069 - SAVI}{0.59}\right)}{0.91} \quad (5)$$

Where: LAI = leaf area index; SAVI = Soil-adjusted vegetation index.

SAVI is calculated according to Equation 6, proposed by Huete (1988). Its value varies from -1.5 to 1.5. The factor L varies according to the characteristics of the vegetation. However, the value most used in the literature is 0.5, the same as adopted in this study.

$$SAVI = \frac{(1 + L) * (NIR - RED)}{(L + NIR + RED)} \quad (6)$$

Surface temperature (St)

Generally, urban climate presents different micro-meteorological conditions, such as increase of temperature and decrease of humidity, and specific climatic conditions such as heat islands may occur. The surface temperature can be determined through the flow of energy that arrives and leaves a given Earth surface creating an interaction with the atmosphere. The range that allows greater transmission of the energy emitted from the Earth that reaches the sensor in the thermal infrared region of the electromagnetic spectrum is the range 8.0-14.0 μm (Steinke et al. 2010). Thus, to perform the St calculation, the quantized and calibrated values (DN) of the bands 10 and 11 of the Landsat 8 OLI sensor system were converted into spectral radiance at the top of the atmosphere using the radiometric coefficients provided in the metadata of the images files (USGS, 2018a) according to Equation 7.

$$L\lambda = ML * Qcal + AL \quad (7)$$

Where: Lλ = Spectral radiance at the top of the atmosphere (Watts/(m^2*srad*μm)); ML = Multiplying factor of band resizing (0.0003342); Qcal = Quantified and calibrated pixel value in gray level (DN); AL = Additive scaling factor specific to the band (0.10000). Then, the spectral radiance at the top of the atmosphere in bands 10 and 11 was converted into brightness temperature at the top of the atmosphere (satellite temperature) according to Equation 8 (USGS, 2019b).

$$T = K2 / \ln\left(\frac{K1}{L\lambda} + 1\right) - K \quad (8)$$

Where: T = Effective temperature on the satellite in Kelvin (K); K1 = Band 10 or 11 calibration constant; K2 = Band 10 or 11 calibration constant; Lλ = Spectral radiance (Watts/(m^2*srad*μm)); and K = Kelvin temperature constant (273.15).

Finally, S_t is obtained by Equation 9 (Artis and Carnahan 1982).

$$T_S = TM / \left[1 + \left(\frac{\lambda * TM}{C2}\right) * \ln(e)\right] \quad (9)$$

Where: TM = Temperature mean (°C) of bands 10 and 11; λ= Radiation emission wavelength equal 10.89 μm (referring to the average wavelength of the Landsat 8 band 10); c2 = h*c/s= 1.4380*10^{-2} m.K = 14,380 μm. K, where h = Planck constant = 6,626*10^{-34} Js and s = Stefan Boltzmann constant = 1.38*10^{-23}J/K; c = speed of light = 2,998*10^8m/s; = Emissivity from the Earth's surface calculated according to Equation 10 (Sobrino et al. 2004).

$$e = 0.004 * Pv + 0.986 \quad (10)$$

The vegetation proportion (Pv) value is calculated by Equation 11, where NDVImax = 0.5 and NDVImin = 0.2 (Carlson and Ripley 1997; Sobrino et al. 2004).

$$Pv = \left[\frac{(NDVI - NDVImin)}{(NDVI\,max - NDVImin)}\right]^2 \quad (11)$$

After calculating the vegetation indexes and the St, the ArcGIS 10.6 tool Cell Statistics was applied to obtain a matrix image of the means of the two periods, which was used for the preparation of the indicator.

Preparation of the urban environmental quality indicator (UEQI)

The urban environmental quality indicator (UEQI) was quantified from a fuzzy inference system considering the simultaneous treatment of quantitative and qualitative variables.

The indicators used to calculate the UEQI were Dd, NDVI, LAI and St. These indicators were interpreted through linguistic variables, since, when using these linguistic expressions in a fuzzy inference system, it is possible to define sets in which the values are allocated with different degrees of pertinence, this process is called fuzzification. Through this process the main function of the

linguistic variables is to provide an approximate way for the characterization of complex phenomena to be analyzed through conventional mathematical models (Lourenço et al. 2015). In this study, these linguistic variables were expressed by ranges of values found in the literature in pertinence functions of the triangular and trapezoidal type.

Demographic density directly affects the environment and, at the same time, has negative impacts and benefits for both regions with a low population density and regions with a high population density (Campoli and Maclean, 2007).

In this context, Haughton and Hunter (1994) and Chakrabarti (2013) stated that regions with a high demographic density can be considered relevant in the process of achieving sustainable development. This is explained by the large concentration of people, which allows to maximize the use of the installed infrastructure, reduce the relative cost of its implementation and reduce the need for its expansion to peripheral areas as well as the need for travel since the concentration of people favors economic activities such as commerce and service at the local level, and, finally, encourage walking and enable the implementation of public transport systems (Haughton and Hunter 1994; Cioly and Davidson 1998; Jacobs 2000; Campoli and Maclean, 2007).

However, in many cases, these environments that do not interact with nature, since there is an absence of tree-lined streets, which directly impacts the thermal sensitivity of these places, maximizing the use of energy, among other impacts. Therefore, there is a need to use indicators or indexes that can reflect the variables affecting such regions, including temperature and the presence of tree vegetation.

Thus, there is uncertainty about the ideal demographic density, which justifies the process of fuzzification of this variable in the current study. To assist in the process of identifying ranges of values that portray adequate linguistic figures for the construction of the pertinence curve, studies by Del Rio (1990) were used. In their study in the favelas of Rio de Janeiro (RJ), the authors showed that areas with a density equal to or over 1,500 inhabitants/ha have deficiencies in the infrastructure service. Rodrigues (1986) stated that density below 100 inhabitants/ha makes the presence of services unfeasible, while density greater than 1,500 inhabitants/ha generate 'dis-economies'. Mascaró and Yoshinaga (2005) argued that demographic density should be close to 600 inhabitants/ha to sustain infrastructure systems.

In this sense, the value considered ideal for population concentration in this study was Dd equal to 600 inhabitants/ha, while ranges of less than 100 inhabitants/ha and above 1,500 inhabitants/ha were classified as regular Dd, as there are exceptions in regions with densities within these ranges of values that present ideal housing conditions (Figure 2).

The NDVI values found for areas covered by vegetation in tropical regions vary from 0.10 to 0.80 depending on the vegetation architecture, density and humidity, with the highest values associated with a very dense vegetation cover and, normally, around 0.6 for humid forests such as the Atlantic Forest (Parkinson 1997). According to the studies by Chouhan and Rao (2011), NDVI values lower than 0.1 indicate areas where there is no vegetation, values between 0.2 to 0.3 represent pasture areas and shrubs, while values between 0.6 to 0.8 correspond to tropical and temperate forests and indicate the presence of 'living vegetation'. In these studies on NDVI it was noticed that there is uncertainty about the classification of NDVI values, which makes its fuzzification justified.

Given the above, the pertinence curve of NDVI values was plotted (Figure 3), with values lower than 0.1 classified as bad, values between 0.2 and 0.3 classified as regular, values between 0.4 to 0.6 classified as good, and values above 0.6 classified as excellent.

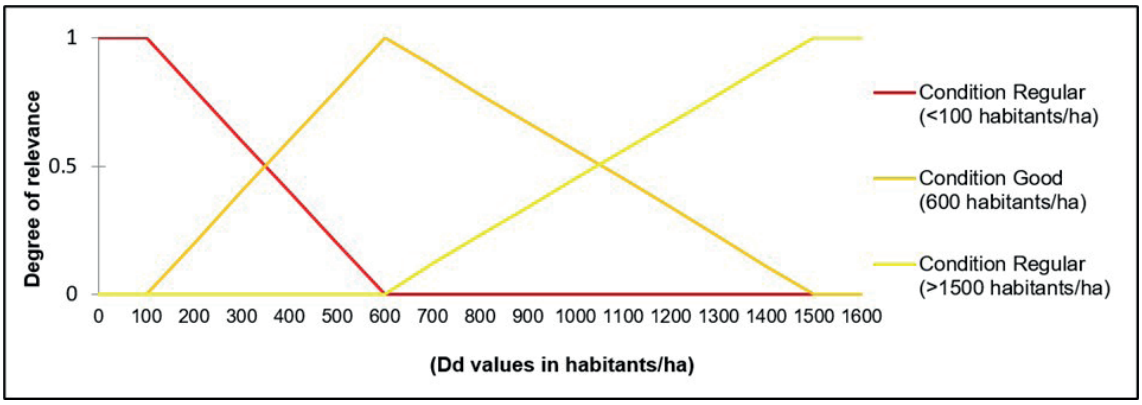

Fig. 2. Relevance function of the input variable Dd

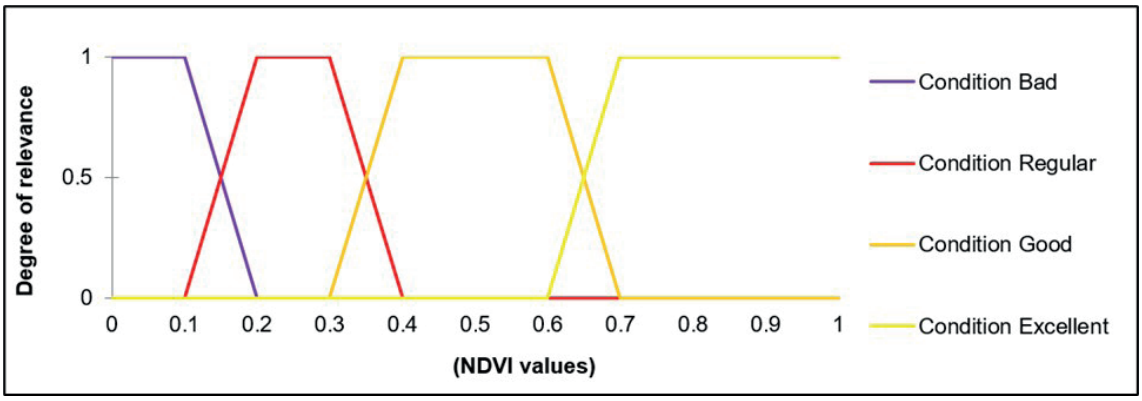

Fig. 3. Relevance function of the input variable NDVI

Regarding the LAI parameter, Garcia et al. (2018) studied the Mata de Santa Genebra in Campinas, SP, Brazil. They studied the interior of the forest and its edges, finding a variation between 0.955 and 3.522 m^2/m^2 in the countryside and 0.741 and 3.120 m^2/m^2 for forest edges. The lower values for forest edges are due to the existence of clearings of different sizes that appear in different periods, resulting from both the extraction and the shallow cut, and also due to the occurrence of specimens decrease due to winds, lightning and fires. Thus, the influence of vegetation density on the LAI values is verified.

For the fuzzification of the values and the construction of the pertinence curve, the following values were adopted: bad = values below 0.5 m^2/m^2, since these values are usually associated with the absence of shrub vegetation at the forest edges; regular = values between 0.7 and 0.9 m^2/m^2, as this interval, in most cases, is associated with border shrub vegetation with greater exposure to anthropic action; and good = values above 1.0 m^2/m^2, which corresponds to the vegetation in the countryside with no clearings and protected from anthropic action (Figure 4).

García (1995) identified in the Madrid region that values close to 25.0°C are considered the ideal comfort temperature for humans, while values below 20.0°C and above 30°C already begin to cause discomfort. Such thermal comfort intervals are consistent with the Brazilian reality, so much so that Gomes and Amorim (2003) used this classification to assess the thermal comfort of public squares in Presidente Prudente (SP). Using the values established by Garcia (1995) the pertinence curve was plotted. Values below 20°C and above 30°C were considered bad and values close to 25°C were considered good (Figure 5).

From the pertinence curves of each variable, a set of rules was established based on the model proposed by Mamdani (1974), which used the knowledge base of linguistic variables (output) for a fuzzy inference system (Table 1).

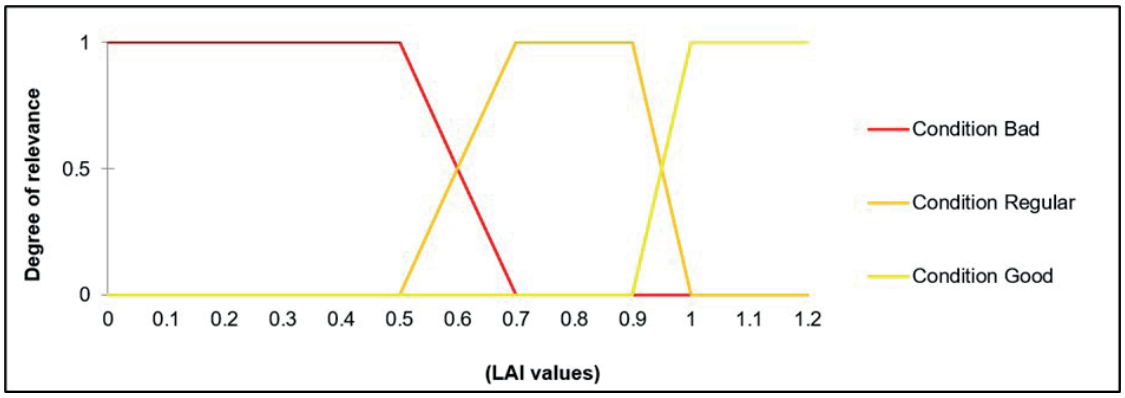

Fig. 4. Relevance function of the input variable LAI

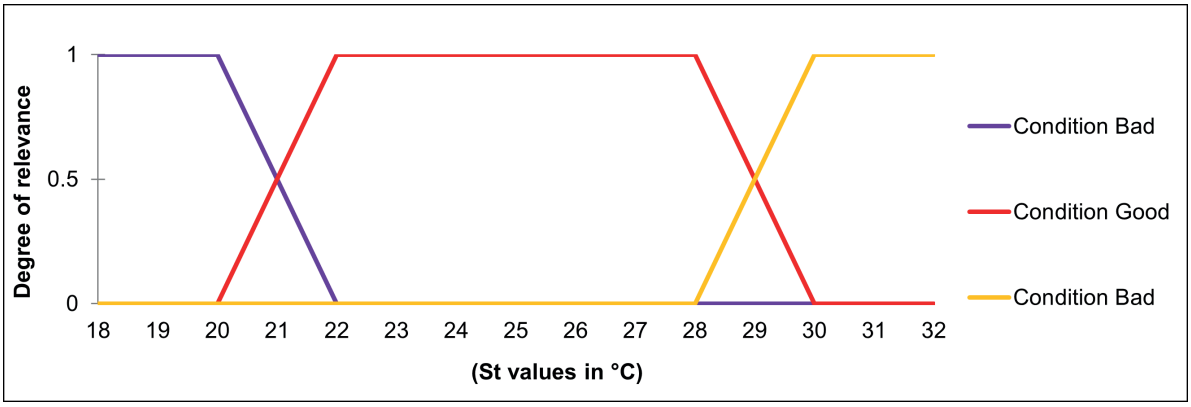

Fig. 5. Relevance function of the input variable St

Table 1. Model rules basis

Rules	Input				Output
	NDVI	LAI	St	Dd	UEQI
1	Condition Bad	Condition Bad	Condition Bad	Condition Regular	Condition Very Bad
2				Condition Good	Condition Bad
3			Condition Good	Condition Regular	Condition Regular
4				Condition Good	Condition Regular
5		Condition Regular	Condition Bad	Condition Regular	Condition Bad
6				Condition Good	Condition Regular

7	Condition Bad	Condition Regular	Condition Good	Condition Regular	Condition Regular
8				Condition Good	Condition Regular
9		Condition Good	Condition Bad	Condition Regular	Condition Regular
10				Condition Good	Condition Regular
11			Condition Good	Condition Regular	Condition Good
12				Condition Good	Condition Good
13	Condition Regular	Condition Bad	Condition Bad	Condition Regular	Condition Very Bad
14				Condition Good	Condition Bad
15			Condition Good	Condition Regular	Condition Regular
16				Condition Good	Condition Regular
17		Condition Regular	Condition Bad	Condition Regular	Condition Bad
18				Condition Good	Condition Regular
19			Condition Good	Condition Regular	Condition Regular
20				Condition Good	Condition Regular
21		Condition Good	Condition Bad	Condition Regular	Condition Regular
22				Condition Good	Condition Regular
23			Condition Good	Condition Regular	Condition Good
24				Condition Good	Condition Good
25	Condition Good	Condition Bad	Condition Bad	Condition Regular	Condition Very Bad
26				Condition Good	Condition Bad
27			Condition Good	Condition Regular	Condition Regular
28				Condition Good	Condition Good
29		Condition Regular	Condition Bad	Condition Regular	Condition Bad
30				Condition Good	Condition Regular
31			Condition Good	Condition Regular	Condition Good
32				Condition Good	Condition Good
33		Condition Good	Condition Bad	Condition Regular	Condition Regular
34				Condition Good	Condition Good
35			Condition Good	Condition Regular	Condition Good
36				Condition Good	Condition Excellent
37	Condition Excellent	Condition Bad	Condition Bad	Condition Regular	Condition Very Bad
38				Condition Good	Condition Bad
39			Condition Good	Condition Regular	Condition Regular
40				Condition Good	Condition Good
41		Condition Regular	Condition Bad	Condition Regular	Condition Bad
42				Condition Good	Condition Regular
43			Condition Good	Condition Regular	Condition Good
44				Condition Good	Condition Good
45		Condition Good	Condition Bad	Condition Regular	Condition Regular
46				Condition Good	Condition Good
47			Condition Good	Condition Regular	Condition Good
48				Condition Good	Condition Excellent

For the output variable (Figure 6), five linguistic variables were used, namely: very bad, bad, regular, good, and excellent (condition). Thus, the UEQI relevance curve was plotted, as shown in Figure 5. UEQI values were classified as very bad (0.0 to 0.2), bad (> 0.2 to 0.4), regular (> 0.4 to 0.5), good (> 0.5 to 0.7), excellent (0.9 to 1.0), giving rise to five output classes from the fuzzy inference system rule basis.

To numerically quantify the UEQI, after establishing the set of rules and the output membership function a conversion method called defuzzification was applied using the center of gravity method (Lourenço et al. 2015). This procedure was carried out using the Matlab R2010a Fuzzy Logic Toolbox module (Mathworks 2014), with output values corresponding to the final numerical values of the UEQI by points (pixels) distributed throughout the study area. Then, the average of the values by neighborhood was extracted, which were geocoded and stored in their respective centroids.

RESULTS

Figure 7 shows Dd (a), NDVI (b), LAI (c) and St (d) for the urban area of the Sorocaba municipality.

Figure 7(a) shows that the highest demographic density is observed in the northernmost, easternmost and westernmost regions of the urbanized area, which may imply a greater impact on wooded areas or an impediment to the creation of these spaces, since the greater concentration of population there

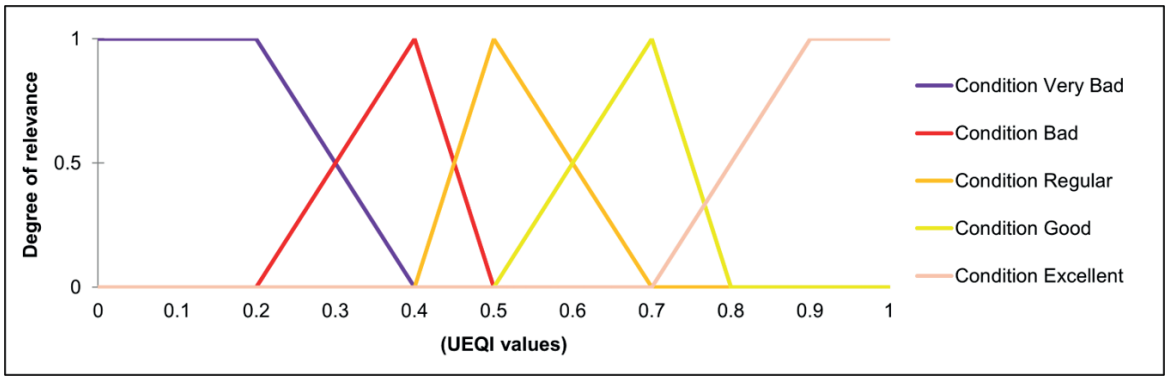

Fig. 6. Output variable membership function (UEQI)

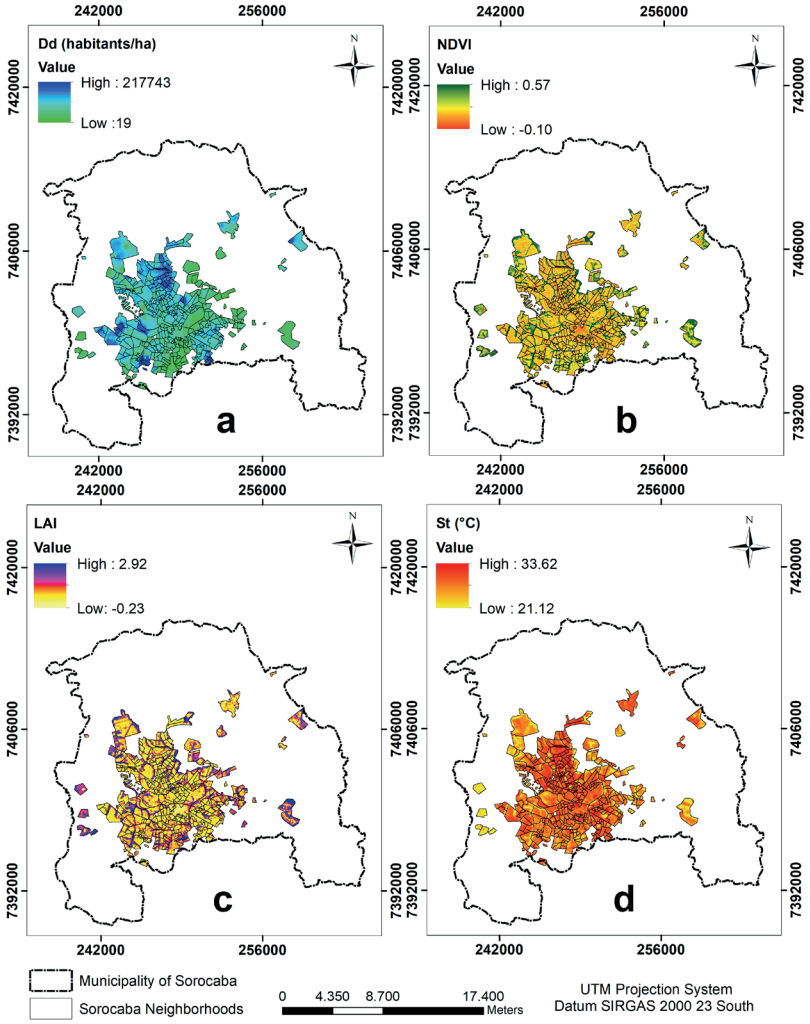

Fig. 7. Dd (a), NDVI (b), LAI (c) and St (d)

demands more services, which has a negative impact the environment, for example, through an increase in impermeable areas.

NDVI for the studied area showed values varying from -0.10 to 0.57 (Figure 7b), with only a few places with values approaching 0.57, since most areas do not have vegetation or, when they have it, vegetation is at a stage of low vegetative vigor. This NDVI analysis made it possible to confirm how compromised the quality of the municipality's vegetation is, especially in the areas of greater urban concentration.

LAI ranged from -0.23 to 2.92 (Figure 7c) with a predominance of negative values, which was expected since it is an urbanized area. In general, this index reflects what has already been verified by NDVI, i.e., vegetation with low health characteristics indicating areas that tend to have higher temperatures, contributing to thermal discomfort. In addition, these indexes make it possible to observe that vegetation in most neighborhoods is isolated as there are no long stretches formed by dense vegetation cover.

For the surface temperature (Figure 7d), it can be seen that the minimum was approximately 21.12°C and the maximum was 33.62°C with higher temperatures corresponding to the urban perimeter. This is justified by the dense urbanization and low vegetation coverage, which lead to differences in atmospheric pressure and retention of particulate material on the surface, contributing to heating and thermal discomfort. This is extremely harmful to the health of the population as it may cause more respiratory problems and allergies in these areas.

Figure 8 shows the UEQI maps, in which the conditions, classified as very bad, bad, regular and good, are presented per pixel and as the average value per neighborhood, respectively. It is important to note that excellent conditions were not found. Table 2 shows the number of neighborhoods for each condition class.

The bad condition of UEQI was prevalent in more than 64% of Sorocaba neighborhoods, almost double the regular condition, which ranked second (34.05%). The very bad condition was present in only four neighborhoods, namely, Jardim Maria do Carmo, Jardim Henrique, Vila Franco, and Vila Porcel. The good condition, on the other hand, had the lowest number (Vivenda do Lago and Portal da Raposo) (Table 2).

Figure 9(b) shows a neighborhood with a very bad condition, Jardim Maria do Carmo, which does not have areas with a representative tree or shrub cover, vegetation is only present alongside roads or in some homes. Moreover, it is marked by the predominance of built areas with a high population density.

DISCUSSION

It can be stated that the isolation of vegetation cover makes it difficult to form an environmental balance and create ecological corridors. According to Bryant (2006), Haaren and Reich (2006) and Hong et al. (2017), corridors are essential to provide ecosystem services such as dispersion and biological migration, buffer zones, and conservation of water resources, in addition to mitigating the effects of high temperatures.

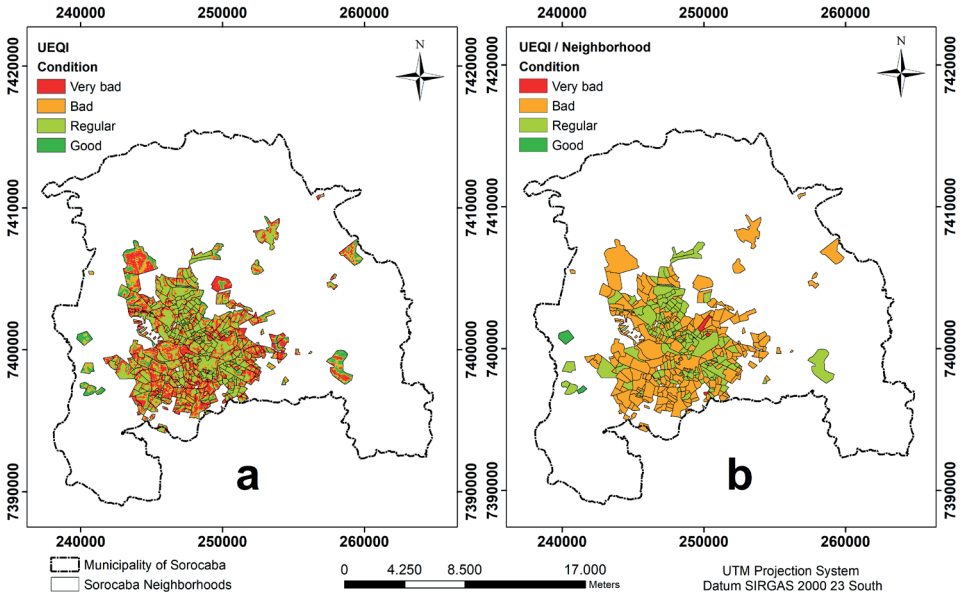

Fig. 8. Distribution of UEQI condition classes

Table 2. Distribution of neighborhoods according to UEQI condition

Condition of UEQI	Total Neighbourhoods	Neighborhoods (%)
Very bad	4	0.96
Bad	269	64.51
Regular	142	34.05
Good	2	0.48
Total	417	100.00

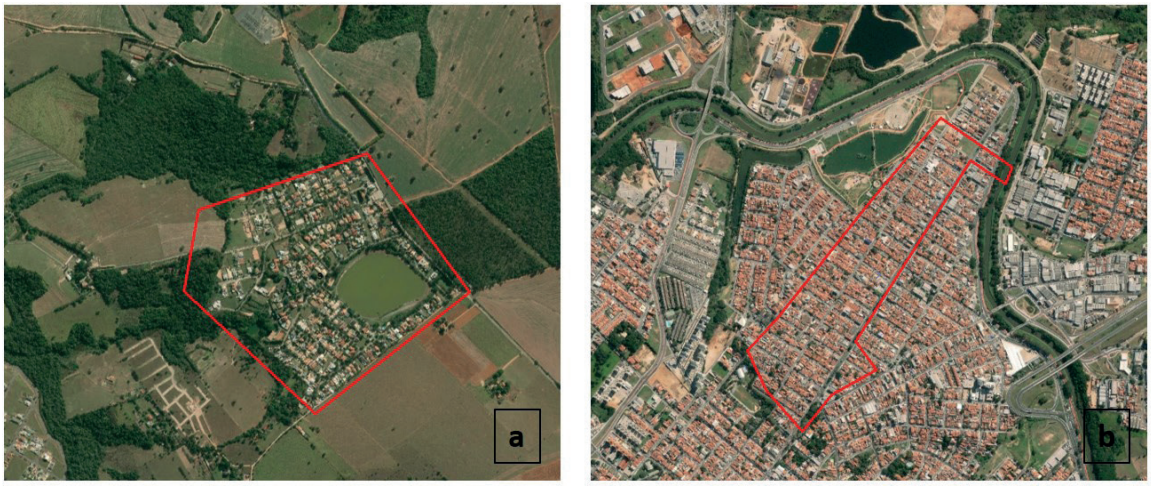

Fig. 9. Neighborhood Vivenda do Lago (a) and Neighborhood Jardim Maria do Carmo (b). Source: Google Earth Pro images, year 2019

The low vegetation cover can also contribute to the formation of heat islands, which are areas with higher temperature than in their surroundings. They are considered as one of the factors responsible for the increase in thermal discomfort, thus contributing to the reduction of the population quality of life and impairment of ecosystem functions (Amorim et al. 2009; Amorim 2017). Barros and Lombardo (2016) suggested detailing the existing relationship between heat islands and problems such as concentration of pollutants and gases in the atmosphere and pointed it out as a factor responsible for morbidity and mortality due to problems in respiratory functions.

According to Amorim et al. (2009) and Amorim (2017), the development of such heat islands is driven by multiple processes including suppression of vegetation, waterproofing of soils, and increase in built area. Amorim (2017) reported that areas covered by vegetation have a greater thermal capacity, that is, they need a greater amount of solar incidence to raise their temperature by 1°C. This is different from urban areas, which are formed by other materials that make that thermal capacity smaller.

In cities, there are areas with little afforestation. In the central region this is due to the urban expansion process and in the peripheral areas – due to the absence of public policies aiming at the implementation and maintenance of this vegetation. However, it should be noted that urban planning must be done seeking to reconcile the demands of urbanization with demands of the environment to reduce the impacts that may be caused (Cruz 2009; Teixeira and Amorim 2011).

Barros and Lombardo (2016), also using NDVI, LAI and St, found that in the city of São Paulo the highest concentration of vegetation were marked by a decrease in the intensity of heat island, therefore making vegetation responsible for mitigating heat in urban areas. These results are similar to the conclusions of this study as areas with the highest concentration of vegetation present a more pleasant temperature. It is worth highlighting places furthest from areas with high urban density, where temperature around 21.12-25°C was observed, which is within the ideal thermal comfort interval.

The resulting UEQI classification is consistent with the reality of the neighborhoods. Figure 9 shows the representation of two neighborhoods, one with conditions characterized as good, which refers to the neighborhood Vivenda do Lago (Figure 9a). This neighborhood is further away from the urban center and is surrounded by tree or shrub vegetation, which contribute to its environmental quality, especially in terms of thermal comfort.

Figure 8 shows that the neighborhoods that presented the worst indicators of urban environmental quality are those characterized by a set of factors that determine this result, such as the absence of dense vegetation cover, high ratio of urbanized areas and presence of areas that may cause some type of soil degradation.

Duarte et al. (2017) stated that the urbanization process enlarges the distance between society and nature as artificial spaces are increasingly created. Often the lack of knowledge of the benefits provided by the vegetation cover restricts its use to only the beautification of cities. However, its benefits go beyond the aesthetic factor, as they present social, ecological and educational functions.

The ecological function of vegetation is in providing well-being to the local population, thus mitigating the negative impacts of the urbanization process, such as thermal discomfort and soil waterproofing. The social function is to provide leisure. Therefore, it is essential that these locations are properly maintained so that they can properly perform their functions (Porto-Gonçalvez 2006; Bargos and Matias, 2011; Bargos and Matias 2012).

As mentioned, there are several factors that contribute to urban quality of life, but the main one is the presence of plant cover given its association with improving the quality of life of the population. Therefore, Souza and Amorim (2016) emphasized the need to allocate areas and financial resources aiming to implement afforestation. However, according to Bargos and Matias (2012), there is a neglect of vegetation, which is not given due importance in the urban planning of cities.

Many studies have reported the positive impacts of urban vegetation, which go beyond improving the microclimate, such as its relationship with the physical and mental health of the population. Among these studies, Lin et al. (2019) focused on a survey conducted in different green spaces and Juan et al. (2017) studied the role of public squares in offering psychological benefits. These authors define them as potential restorer of natural landscapes.

The UEQI analysis has shown that none of the neighborhoods in the municipality of Sorocaba demonstrates ideal conditions that could guarantee a

good environmental harmonization. It confirmed that vegetation cover is not sufficient to provide a pleasant environment to the population, as neighborhoods lack spaces with vegetation, which can contribute to the residents' quality of life. However, it is not just a question of planting flowerbeds and roads but of creating well-wooded squares, restoring degraded areas and creating campaigns encouraging the population to contribute to the maintenance of these areas.

Degraded areas may be subject to ecological restoration, but a feasibility study must be carried out so that appropriate management techniques are adopted to restore the environmental quality of these places, thus providing well-being for the population, scenic beauty and proper environment for fauna and flora, in addition to helping to maintain the quality of water resources. Therefore, given the results, urban planning for the expansion of urban vegetation is recommended in different neighbourhoods of the municipality of Sorocaba, especially in those where UEQI was very bad or bad, as it indicates conditions that can compromise the quality of life of the population.

Studies on environmental quality are essential to understand the problems resulting from the expansion of urbanization since they serve as subsidies for decision-making aiming to mitigate the environmental impacts resulting from anthropic interventions on the urban environment (Estêvez and Nucci 2015). Duarte et al. (2017) reported that it is possible to reconcile urban space with environmental quality as long as there is adequate urban planning and the population is willing to contribute to the insertion of vegetation cover.

There are several methodologies to assess urban environmental quality, such as the ones presented in Ávila and Pancher (2014), Minaki and Amorim (2012), Dias, Gomes and Alkmim (2011) and Nucci (2008). However, most of them aim to characterize factors, different from the point of view proposed in this study, which, in addition to using special analysis tools, adopts a fuzzy inference system to encompass environmental quality.

The methodology applied to elaborate UEQI becomes relevant as it can cover the resident population and small spatial variations disregarding local homogeneity, that is, any changes that occur in the studied variables are included in the modeling of the reproduced scenario, thus enabling results consistent with reality.

Given the above, UEQI becomes an important public management tool since the support of geospatial technology tools for spatial analysis can assist in obtaining data and allow to identify the places where the most urgent interventions are needed, thus improving the conditions in these locations in order to guarantee environmental quality.

The use of population data referring to the last demographic census (2010) was a limiting factor in this research, since such a census is carried out every ten years and, due to the pandemic, it was not carried out in 2020. And these data are particularly important because they provide a population overview of the municipality, serving as the basis for several studies carried out in Brazil.

Temporal analysis of UEQI using data on the demographic density and other variables (St, NDVI and LAI) referring to the year of publication of the demographic census is suggested for future research. In this way, a future projection will be obtained, which can help to identify neighbourhoods that are more conducive to a scenario of suppression of urban vegetation cover or intensification of the heat island phenomenon. This will help to outline more effective urban planning strategies and, consequently, positively affect the quality of urban life.

CONCLUSIONS

The variables used in this research are adequate for the assessment of UEQI, which is evident from the coherence of the information presented since areas without vegetation cover and with the highest demographic density presented the worst conditions and the highest temperatures.

The municipality needs measures that prioritize urban afforestation, such as greater incentives for the recovery of degraded areas and creation of green spaces for leisure. Such measures can be carried out in conjunction with an environmental education project for the population focused on the importance of green areas, as they are essential for improving environmental conditions and, consequently, people's quality of life. It should be noted that the urban center of Sorocaba is old and there has been no urban planning that considers factors that were presented in this study.

It is important to highlight the use of geospatial technology for data analysis as these tools enable using environmental and social variables that are not considered in traditional methods. This contributes significantly to the detailing of certain conditions not usually mapped in traditional models and provides the assessment UEQI which can easily be replicated since all variables can be represented spatially making UEQI an important tool that can be used by the public agencies.

REFERENCES

Allen R., Bastiaanssen W., Wartes R., Tasumi M. and Trezza R. (2002). Surface energy balance algorithms for land (SEBAL), Idaho implementation – Advanced training and user manual, version 1.0. Available at: http://www.posmet.ufv.br/wp-content/uploads/2016/09/MET-479-Waters-et-al-SEBAL.pdf [Accessed 20 Mar. 2019].

Amorim M., Quenol V. and Sant'ana Neto, J. (2009). Características das ilhas de calor em cidades de porte médio: exemplos de Presidente Prudente (Brasil) e Rennes (França), Confins, 7, 116, DOI: 10.4000/confins.6070.

Amorim M. (2017). Detecção Remota de Ilhas de Calor Superficiais: Exemplos de Cidades de Porte Médio e Pequeno do Ambiente Tropical, Brasil. Finisterra, 105, 111-133, DOI: 10.18055/Finis6888.

Artis D.A. and Carnahan W. H. (1982). Survey of emissivity variability in thermography of urban areas. Remote Sensing of Environment, 12, 313-329, DOI: 10.1016/0034-4257(82)90043-8.

Ávila M. and Pancher A. (2015). Estudo das Áreas Verdes Urbanas como Indicador de Qualidade Ambiental no Município de Americana – SP. Rev. Bras. Cartogr., 67(3), 527-544. Available at: http://www.seer.ufu.br/index.php/revistabrasileiracartografia/article/view/44648 [Accessed 2 May 2019].

Bargos D., Matias L. (2011). Áreas Verdes Urbanas: Um Estudo de Revisão e Proposta Conceitual. REVSBAU, 6, 3, 172-188, DOI: 10.5380/revsbau.v6i3.66481.

Bargos D. and Matias L. (2012). Mapeamento e Análise de Áreas Verdes Urbanas em Paulínia (SP): Estudo com a Aplicação de Geotecnologias. Sociedade & Natureza, 1, 143-156, DOI: 10.1590/S1982-45132012000100012.

Barros H. and Lombardo M. (2016). A ilha de calor urbana e o uso e cobertura do solo em São Paulo – SP. GEOUSP (Online), 20(1), 160-177, DOI: 10.11606/issn.2179-0892.geousp.2016.97783.

Bryant M.M. (2006). Urban landscape conservation and the role of ecological greenways at local and metropolitan scales. Landscape and Urban Planning, 76, 23-44, DOI: 10.1016/j.landurbplan.2004.09.029.

Campoli J. and Maclean A. (2007). Visualizing density. Cambridge: Lincoln Institute of Land Policy. Available at: www.lincolninst.edu/publications/books/visualizing-density. [Accessed 16 Mar. 2019].

Carlson T. and Ripley D. (1997). On the relation between NDVI, fractional vegetation cover, and leaf area index. Remote Sensing of Environment, 62, 241-252, DOI: 10.1016/S0034-4257(97)00104-1.

CIIAGRO (2019). Valores mensais de temperatura do município de Sorocaba. São Paulo. Available at: www.ciiagro.sp.gov.br/climasp.html. [Accessed 2 Aug. 2018].

Chakrabarti V. (2013). A coutry of cities: A manifesto for an urban America. New York: Metropolis Books.

Chouhan R. and Rao N. (2011). Vegetation Detection in Multispectral Remote Sensing images: Protective Role-Analysis of Vegetation in 2004 Indian Ocean Tsunami. Geo-Information for disaster management, Turkey. Available at: http://www.isprs.org/proceedings/2011/Gi4DM/PDF/OP37.pdf. [Accessed 13 Mar. 2019].

Cioly C. and Davidson F. (1998). Densidade urbana: um instrumento de planejamento e gestão urbana. Rio de Janeiro: Mauad.

Cruz G. (2009). Clima urbano de Ponta Grossa – PR: uma abordagem da dinâmica climática em cidade média subtropical brasileira. Tese de doutorado, Faculdade de Filosofia, Letras e Ciências Humanas, Universidade de São Paulo, São Paulo.

Del Rio V. (1990). Introdução ao Desenho Urbano no Processo de Planejamento. São Paulo: Pini.

Dias F., Gomes L. and Alkmim J. (2011). Avaliação da Qualidade Ambiental Urbana da Bacia do Ribeirão do Lipa Através de Indicadores, Cuiabá/MT. Sociedade & Natureza, 23(1), 127-147. Available at: http://www.seer.ufu.br/index.php/sociedadenatureza/article/view/11389. [Accessed 12 Oct. 2018

Duarte T., Angeoletto F., Santos J., Leandro D, Bohrer J., Vacchiano M. and Leite L. Papel da Cobertura Vegetal nos Ambientes Urbanos e Sua Influência na Qualidade de Vida nas Cidades. Desenvolvimento em Questão, 40, 175-203, DOI: 10.21527/2237-6453.2017.40.175-203.

Dubreuil V., Fante K., Planchon O. and Sant'anna Neto J. (2017). Les types de climats annuels au Brésil: une application de la classification de Köppen de 1961 à 2015. EchoGéo, 41, 01-27, DOI: 10.4000/echogeo.15017.

ESRI (2016). Environmental Systems Research Institute. ArcGis 10.6.

Estêvez L. and Nucci J. (2015). Questão Ecológica Urbana e a Qualidade Ambiental Urbana the Urban Ecological Issue and the Urban Environmental Quality. Revista Geografar, 10(1), 26-49, DOI: 10.5380/geografar.v10i1.37677.

Fernandes A., Coutinho M., Santos V. and Nascimento C. (2016). Utilização de intervalos de índices de vegetação e temperatura da superfície para detecção de queimadas, Cad. Ciênc. Agrá., 8(2), 30-40. Available at: https://periodicos.ufmg.br/index.php/ccaufmg/article/view/2845 [Accessed 4 May 2018].

Gandhi G., Parthiban S., Thummalu N. and Christy A. (2015). NDVI: Vegetation change detection using remote sensing and GIS–A case study of Vellore district. Procedia Computer Science, 57, 1199-1210, DOI: 10.1016/j.procs.2015.07.415

García F. (1995). Manual de climatologia aplicada: clima, medio ambiente y planificación. Madrid: Editorial síntesis S. A.

Garcia J., Longo R., Penereiro J., Mendes D. and Mantovani P. (2018). Uso de fotografias hemisféricas para avaliação da qualidade ambiental na mata de Santa Genebra, Campinas-SP, Brasil. Ciência Florestal, 28(1), 175-190, DOI: 10.5902/1980509831651

Gomes M. and Amorim M. (2003). Arborização e conforto térmico no espaço urbano: estudo de caso nas praças públicas de Presidente Prudente (SP). Caminhos de Geografia, 7(10), 94-106. Available at: http://www.seer.ufu.br/index.php/caminhosdegeografia [Accessed 22 Sep. 2018].

Haaren C.V. and Reich M. (2006). The German way to greenways and habitat networks. Landscape and Urban Planning, 76, 7-22, DOI: 10.1016/j.landurbplan.2004.09.041

Hartig T., Mitchell R., Vries S. and Frumkin H. (2014). Nature and Health. Annu. Rev. Public Health, 35, 207-228, DOI: 10.1146/annurev-publhealth-032013-182443.

Haughton G. and Hunter C. (1994). Sustainable cities. Regional Policy & Development Series, 7, Londres: Jessica Kingsley Publishers LTDA.

Hong W., Guoa R., Sua M., Tang H., Chenb L. and Hua W. (2017). Sensitivity evaluation and land-use control of urban ecological corridors: A case study of Shenzhen, China. Land use Policy, 62, 316-32, DOI: 10.1016/j.landusepol.2017.01.010.

Huete A. (1988). A soil-adjusted vegetation index (SAVI). Remote Sensing of Environment, 25, 295-309, DOI: 10.1016/0034-4257(88)90106-X.

IBGE (2010). Censo demográfico – 2010. Rio de janeiro. Available at: https://mapas.ibge.gov.br/bases-e-referenciais/bases-cartograficas/malhas-digitais. [Accessed 2 Mar. 2018].

IBGE (2011). Base de informações do Censo Demográfico 2010: Resultados do Universo por setor censitário. Rio de janeiro. Available at: http://www.ibge.gov.br/estatisticas/downloads-estatisticas.html. [Accessed 2 Mar. 2018].

IBGE (2012). Manual técnico da vegetação brasileira. Rio de Janeiro: IBGE. Available at: http://www.ibge.gov.br/busca.html?searchword=manual+t%C3%A9cnico. [Accessed 4 Mar. 2018].

IBGE (2019). IBGE Cidades. Available at: https://cidades.ibge.gov.br/brasil/sp/sorocaba/panorama >. [Accessed 4 Mar. 2018].

Jacobs J. (2000). Morte e Vida das Grandes Cidades. 1ª ed. São Paulo: Martins Fontes.

Juan C., Subiza-Pérez M. and Vozmediano L. (2017). Restoration and the City: The Role of Public Urban Squares. Frontiers in Psychology, 8, 1-13, DOI: 10.3389/fpsyg.2017.02093.

Lin W., Chen Q., Jiang M., Zhang X., Liu Z., Tao J., Wu L., Xu S., Kang Y. and Zeng Q. (2019). The effect of green space behaviour and per capita area in small urban green spaces on psychophysiological responses. Landscape and Urban Planning. 192, 1-15, DOI: 10.1016/j.landurbplan.2019.103637.

Lopes E., Sales J., Souza J., Sousa J., Matias M., and Lourenço R. (2019). Evaluation of flood risk in Sorocaba – Brazil, using fuzzy logic and geotechnology. Braz. J. of Develop., 5(2), 1422-1434. Available at: http://www.brjd.com.br/index.php/BRJD/article/view/1119 [Acessed 20 Jun. 2018].

Lourenço R., Silva D., Martins A., Sales J., Roveda S., and Roveda J. (2015). Use of fuzzy systems in the elaboration of an anthropic pressure indicator to evaluate the remaining forest fragments. Environmental Earth Sciences, 73, 1-8, DOI: 10.1007/s12665-015-4253-6.

Magalhães I., Carvalho Junior O. and Santos A. (2017). Análise Comparativa entre Técnicas de Sensoriamento Remoto para Mensuração da Vegetação Urbana no Município de Alegre, ES. Revista Cerrados, 15(1), 156-177, DOI: 10.22238/rc24482692v15n12017p156a177.

Mamdani E. (1974). Application of Fuzzy Algorithms for Control of Simple Dynamic Plant. Proceedings of the IEE Control and Science, 121, 298-316, DOI: 10.1049/piee.1974.0328.

Mascaró J. and Yoshinaga M. (2005). Infraestrutura Urbana. (1° ed.) Porto Alegre: Masquatro Editora.

MathWorks (2014). O MathWorks, Fuzzy Logic Toolbox ™ Guia do usuário. © Copyright 1995–2014 de The MathWorks Inc.

Melazo G., and Nishiyama L. (2010). Mapeamento da Cobertura Arbóreo-Arbustiva em Quatro Bairros da Cidade de Uberlândia- MG. REVSBAU, 5(2), 52-66, DOI: 10.5380/revsbau.v5i2.66272.

Mello K., Petri L., Leite E. and Toppa R. (2014). Cenários Ambientais para o Ordenamento Territorial de Áreas de Preservação Permanente no Município de Sorocaba, SP. Revista Árvore, 38(2), 309-317, DOI: 10.1590/S0100-67622014000200011.

Minaki C. and Amorim M. (2012). Análise da Qualidade Ambiental Urbana. Mercator, 11(24), 229-251. Available at: http://www.mercator.ufc.br/mercator/article/view/648. [Accessed 12 Jan. 2019.

Myers N., Mittermeier R., Mittermeier C, Fonseca G. and Kent J. (2000). Biodiversity hotspots for conservation priorities. Nature, 403, 853-858, DOI: 10.1038/35002501.

Nucci J. (2008). Qualidade ambiental e adensamento urbano: um estudo de ecologia e planejamento da paisagem aplicado ao distrito de Santa Cecília (MSP). 2 ed. Curitiba: O Autor.

Parkinson C. (1997). Earth from above; Using Color-Coded Satellite Images to Examine the Global Environment. California: University Sciences Books.

Porto-Gonçalvez C. (2006). A globalização da natureza e a natureza da globalização. Rio de Janeiro, Civilização Brasileira.

Rodrigues F. (1986). Desenho Urbano, cabeça, campo e prancheta. São Paulo: Projeto Editores.

Rossi M. (2017). Mapa pedológico do Estado de São Paulo: revisado e ampliado. 1 mapa em graus. Escala: 1: 250000. Available at: http://datageo.ambiente.sp.gov.br/. [Accessed 14 Dec. 2018].

Rouse J., Haas R., Schell J., and Deering D. (1973). Monitoring vegetation systems in the Great Plains with ERT. In: NASA Earth Resources Techonology Satellite, I Symposium Proceedings. Washington: NASA, 309-317.

Santos F., and Aquino C. (2015). Análise da Dinâmica do Índice de Vegetação por Diferença Normalizada (NDVI), dos Aspectos Econômicos e suas Relações com a Desertificação/Degradação Ambiental em Castelo do Piauí, Piauí, Brasil. Revista Electrónica de Investigação e Desenvolvimento, 4, 1-17. Available at: https://revistas.uece.br/index.php/CCiT/. [Accessed 5 Mar. 2019].

Shimabukuro Y., Maeda E. and Formaggio A. (2009). Sensoriamento Remoto e Sistemas de Informações Geográficas aplicados ao estudo dos recursos agronômicos e florestais. Revista Ceres, 56 (4), 399-409. Available at: http://www.ceres.ufv.br/ojs/index.php/ceres/article/view/3443/1344. [Accessed 3 Jun. 2019].

Sobrino J., Jiménez-Muñoz J. and Paolini L. (2004). Land surface temperature retrieval from LANDSAT TM 5. Remote Sensing of Environment, 90, 434-440, DOI: 10.1016/j.rse.2004.02.003.

Souza M. and Amorim M. (2016). Qualidade Ambiental em Áreas Verdes Públicas na Periferia de Presidente Prudente (SP): Os Exemplos dos Bairros Humberto Salvador e Morada do Sol. Caminhos de Geografia, 17(57), 59-73, DOI: 10.14393/RCG175704.

Steinke V., Steinke E. and Saito C. (2010). Estimativa da temperatura de superfície em áreas urbanas em processo de consolidação: reflexões e experimento em Planaltina-DF. Revista Brasileira de Climatologia, 6, 37-56, DOI: 10.5380/abclima.v6i0.25604.

Teixeira D. and Amorim M. (2011). Estudo do Clima Urbano a Partir da Análise da Temperatura da Superfície em Piracicaba-SP. Geografia Ambiental e da Saúde. Available at: www2.fct.unesp.br/semanas/geografia/2011/2011-urbana/Danielle%20Frasca.pdf. [Accessed 22 Mar. 2019].

USGS (2019a). Earth explorer. Available at: https://earthexplorer.usgs.gov/. [Accessed 8 Feb. 2019].

USGS (2019b). Data and Tools. Available at: https://landsat.usgs.gov/using-usgs-landsat-8-product. [Accessed 8 Feb. 2019].

Check for updates

CC BY

RESEARCH PAPER

STATE AND NON-STATE CROSS-BORDER COOPERATION BETWEEN NORTH KARELIA AND ITS (UN)FAMILIAR RUSSIAN NEIGHBORS

Henrik D. Nielsen[1*]

[1]University of Eastern Finland, Department of Geographical and Historical Studies, Yliopistokatu 2, FI-80100 Joensuu, Finland

***Corresponding author:** henrik.nielsen@uef.fi

Received: December 17th, 2020 / Accepted: May 25th, 2021 / Published: July 1st, 2021

https://DOI-10.24057/2071-9388-2020-211

ABSTRACT. Russia has often been seen in a negative light and as a difficult place for foreigners to operate, both currently and in the past. To a large extent, this is also true for Finland, which has fought several wars against its eastern neighbor and whose border with Russia has been closed for years. However, Finland, and in particular North Karelia, also has a long history of cross-border cooperation with Russian partners.

This paper seeks to analyze why North Karelian governmental and NGO actors choose to engage in cross-border cooperation with Russian counterparts and explain why they have been so successful.

The answers are sought via a historical review of the relationship between Finland and Russia, in particular the role and importance of Karelia as a source of both conflict and consolidation. Furthermore, semi-structured interviews with Finnish cross-border cooperation actors are utilized in the analysis. The theoretical approach is grounded in (un)familiarity, which is used to explain the pull-push effects of the border.

In conclusion, it was found that the Finnish actors harbor a historical feeling of connectedness and nostalgia towards the Karelian area which pulls them across the border. Because of the proximity they see cross-border cooperation as a natural extension of their work. Finally, the success is connected to the increased familiarity and close personal relations that have been build up over the years.

KEYWORDS: cross-border cooperation, Finnish-Russian relations, Karelia, perception, (un)familiarity

CITATION: Henrik D. Nielsen (2021). State And Non-State Cross-Border Cooperation Between North Karelia And Its (Un)Familiar Russian Neighbors. Geography, Environment, Sustainability, Vol.14, No 2, p. 42-49 https://DOI-10.24057/2071-9388-2020-211

ACKNOWLEDGMENTS: The paper is part of the EuroCORECODE Collaborative Research Project «Unfamiliarity as signs of European times: scrutinizing historical representations of otherness and contemporary daily practices in border regions». Supported by Academy of Finland [grant number 137403]; European Science Foundation [grant number 09-EuroCORECODE-FP-009].

Conflict of interests: The authors reported no potential conflict of interest.

INTRODUCTION

When the Soviet Union collapsed in 1991, the expectations that Russia would transform from its communist-inspired system and adopt a Western understanding of capitalism and democracy were high. Despite making enormous changes, Russia was not even given until the end of the decade before it was labeled a failed and corrupt country led by the mafia (Shleifer and Treisman 2005; Jakobson 1998). While the election of Putin in 2000 brought about a short-lived optimism (Shleifer and Treisman 2005), the negative perception has proven to be quite durable (Nielsen 2019). Some opine that the negative perception is a stigma Russia has had for centuries and that it reflects the country's history (Paul 2001; Rutland and Kazantsev 2016). Whether the negative perception of Russia is a century-old legacy, a Western media construction, or something else is as such irrelevant, yet it is real. So real that it has been a concern for Russian President Putin, who has tried to change the negative perception (Feklyunina 2008).

As a former part of Russia and its neighbor, Finland holds many of the negative narratives that are connected to Russia. In 2017 Finland celebrated its 100th anniversary of independence after breaking with Russia. In that context, I was approached by a Danish journalist who wanted to hear about the Finnish perception of Russia. Although it was not said explicitly, it was clear she expected, perhaps even wanted, me to say that Finns have a negative opinion of Russia, yet to do so would be too simplistic. While the view of Russia in the general media in Finland does hold an overwhelmingly negative tone (Jerman 2004; Laine 2013; Németh 2015), Etzold and Haukkala (2011) have concluded that Finland actually has a much better relationship with Russia, including more and closer ties, than Denmark, Sweden, and their common neighbor Norway. This has led the country to become somewhat of a mediator or gateway for Europe into Russia and vice-versa (Dominguez and Mercier-Suissa 2015; Rytövuoi-Apunen 2008a). Yet how has Finland managed to develop a good working relationship with Russia when it, in general, is very difficult to establish genuine and lasting cross-border activity (O'Dowd 2002; Klatt 2017), especially in an atmosphere dominated by the negative perception towards Russia?

The aim of this paper is twofold: to uncover why Finnish North Karelian local government and NGOs seek cross-border

cooperation (CBC) with their Russian neighbors, and also to offer a perspective on why their CBC has been successful. The questions are answered via a historical review of the Finnish-Russian relationship and interviews with Finnish CBC actors. Throughout the paper, the concept of (un)familiarity is used to analyze the data.

MATERIALS AND METHODS

The data consists of a short historical review on the Finnish relationship with Russia, and particularly the role of Karelia as both a source of conflict and bonding. Because of the special relationship, North Karelia has often been the starting point for Finnish-Russia research (See Ahponen 2011; Laurén 2012; Scott 2013; Nielsen 2019). Not only does North Karelia border Russia, but it also borders the Russian Republic of Karelia with whom it shares a long history and culture (Scott 2013). In addition, a series of semi-structured interviews with Finnish actors have been analyzed on a micro-level using the concept of (un)familiarity.

A total of 11 different actors were identified which in the end amounted to eight interviews. All the interviews were conducted face-to-face, except for two that due to COVID-19 had to be done online. The actors represent different branches of local government, both Joensuu city and the North Karelian council (two interviews), NGOs (five), and higher education institute (one interview). The interviews were structured around four themes creating a natural flow. The themes were Background, Current projects, Experience, and Influence of perceptions, with (un) familiarity embedded in all the themes. Kvale and Brinkmann (2015) compare interviewing to mining, where the interviewer tries to chip away at the information to get to the essence. Following their idea, these interviews have been conducted by starting with broad themes and as the interview progressed the questions became more specific. The questions have therefore varied depending on the information provided by the interviewee.

Conceptualizing (un)familiarity

Earlier (un)familiarity was primarily used to explain why some people crossed borders, whiles others did not within the areas of tourism and shopping (Dann 1981; Timothy 1995; Timothy and Butler 1995). The focus was on the so-called push and pull factors. Since Spierings and Van der Velde (2008) developed their model 'Bandwidth of (un)familiarity', its usage has grown steadily (See e.g., Spierings and Van der Velde 2008; Izotov and Laine 2012; Klatt 2014; Németh 2015; Nielsen 2019). Although the foundation in these studies is built on Spierings and Van der Velde's (2008) theocratization, there have been different adaptations (see e.g., Spierings and Van der Velde 2013; Andersen 2013; Szytniewski and Spierings 2014; Nielsen 2019; Zotova and Gritsenko 2020). Today the usage has expanded to include analysis of cross-border issues within areas such as labor movement, perception, identity, and representation of otherness, including what encourages and discourages mobility across state borders. Yet, much of it is still structured around push-pull, which are the factors that push and pulls us towards the other side of the border e.g., financial gain and adventure, and 'Keep-Repel' factors which discourage us from crossing e.g., language and different legal systems (Spierings and Van der Velde's 2008; 2013).

For a cross-border interaction to occur, the other side of the border cannot be too unfamiliar, nor can it be too familiar as it will weaken the reason for crossing. This means that an unfamiliar place can have just as much of an attraction as a familiar place, but exactly where the line goes is based on the individual and how much familiarity and unfamiliarity (s)he is willing to accept (Spierings and Van der Velde's 2008; 2013). Van der Velde and Naerssen (2015) have expanded the model by adding a threshold. The threshold functions as a gateway, a mental border that needs to be overcome before even contemplating crossing the physical border.

As mentioned earlier, there are different interpretations of (un)familiarity and, while agreeing with Spierings and van der Velde, this paper uses Nielsen's (2019) multi-dimensional division of (un)familiarity into knowledge, experience, and cultural and physical proximity. A similar division has been done by Hu and Ritchie (1993) and Szytniewski and Spierings (2014), although the latter has a fourth dimension, self-assessment, which is not used here. This study will utilize the ideas of push-pull and keep-repel to determine what drives CBC between North Karelia and its neighbors, and what could possibly hinder it. Furthermore, the division of (un)familiarity into knowledge, experience and proximity will provide further dept into the push-pull factors and also help determine the key to the success.

RESULTS

Finland between a rock and a hard place

Like the Danish journalist, some people will undoubtedly think that hatred towards Russia would be embedded in Finns considering Finland was under Russian rule for 100 years until independence in 1917, and later fought two wars against the Soviet Union to keep the independence. On the surface, the signs of resentment are there. The coat of arms of Finland is one example, it dates back to the 16th century when Finland was a part of Sweden and features a lion tramping on a curved saber, a symbol of the wars against Russia. Other similar symbols of the struggle against the eastern neighbor are found in the North and South Karelian coats of arms, in which the western (Finnish) sword faces the eastern (Russian) saber (see fig. 1).

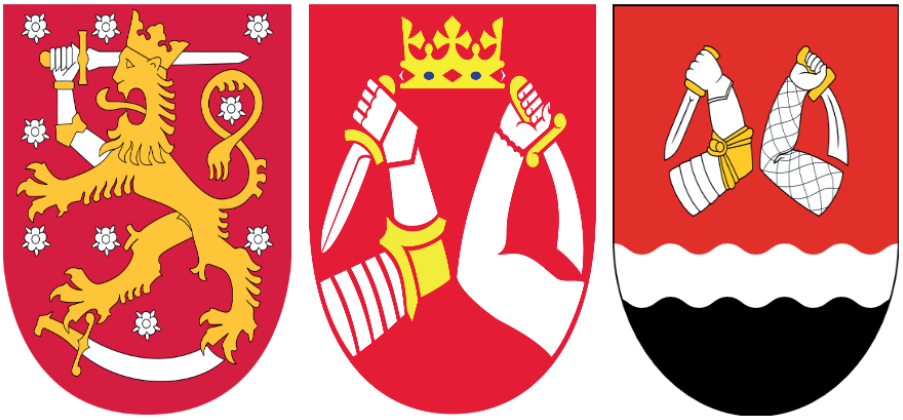

Fig. 1. The Finnish (left), North Karelian (middle) and South Karelian (right) coat of arms

Yet, the perception of Russia in Finland is not straightforward. Point in case, the coat of arms originates from when Finland was under Swedish rule. It was commissioned for King Gustaf Vasa's sarcophagus thus it is a symbol of the Swedish King's fight against Russia and not the Finn's. Later his son, Johan III (King of Sweden and Grand Duke of Finland), used it as the Grand Duchy of Finland's coat of arms as it symbolized the war which he, like his father, fought against Russia (Meinander 2020). With few alterations, Finland has kept the coat of arms and made it their own, thus boasted the argument that Finland, partly, inherent Russophobia from Sweden (Paasi 1996). In addition, both the North and South Karelian coats of arms are just as much symbols of how Finnish Karelia, and all of Finland in general, was in between Sweden and Russia, as they are symbols of being anti-Russian. So, while these images could be used to illustrate Finland's tensions with Russia, it is not the whole story.

Finland has often been described as between East and West in both political and geographical terms (Paasi 1996; Moisio 1998; Browning and Lehti 2007; Rytövuori-Apunen 2008a). Since the 13th century, before there even was a Finnish nation, the area was a battleground for wars between Sweden and the Slavic city-state of Novgorod, and around a century later the first demarcation between the two rivals was placed in the nowadays Finnish territory (Eskelinen 2011; Scott 2013), though it fluctuated until Finland gained independence in 1917. As WWII developed, Finland was once again between two great powers, the Soviet Union and Germany (Vehviläinen 2002), and during the Cold War Finland had to balance between the East and the West, a geopolitical limbo which to a certain extent still exists today (Rytövuori-Apunen 2008a).

When Russia annexed the Crimean Peninsula in 2014, it stirred up public debate in Finland as the country was caught between supporting the sanctions adopted by the EU and continuing to develop its relationship with Russia. Talks of NATO membership surfaced again, yet they were brushed aside on the count of being too damaging for the Finnish-Russian relationship (Åtland 2016). Instead of pushing Russia away, Finland started, and succeeded, a strong lobbying work to keep the Finnish-Russian projects, funded via the European Neighbourhood Instrument, off the EU sanction list so they could continue (Koch and Vainikka 2019). The rising tension between the EU and Russia did in some cases hindering local CBC, yet the Finnish-Russian CBC managed to flourish despite the tense situation (Sebentsov 2020; Palomowski and Federov 2020). The strength of the Finnish-Russia relationship was further emphasized by the fact that the annexation did not influence the general public's concern as to whether Finland is threatened by Russia. Minister for Foreign Trade at the time, Alexander Stubb, said Finland had no reason to be afraid of Russia: "Russia has been our neighbor for a long time. We have been a part of Russia, and have had our difficulties with Russia in course of our history. Sometimes things go really well and other times things are worse. Just now we are going through a difficult phase.[1]

Instead of fearing Russian aggression, the Finnish government was more concerned about the economic situation resulting from the EU sanction.[2] This pragmatic approach has characterized the relationship and is confirmed by the former Finnish President J.K. Paasikivi's famous words «There is nothing we can do about geography» (Raivo 2000).

Having to carve out a space for themselves has impacted the Finnish national identity in many ways. While there is a consensus that Russia plays an important role as 'the other' in the Finnish state and identity building (Paasi 1996; 1997; 1999; Harle and Moisio 2000; Laine 2015), it is often overlooked that the first steps towards an independent state and a national identity were taken with help from and under Russian rule, partly in opposition to the dominant Swedish culture (Paasi 1996; Wassholm 2014). It was not until the turn of the 20th century, and following Finnish independence, that Russia became 'the other' and hatred towards them began building in Finland reaching its highest peak in the interwar period (Paasi 1996; Harle and Moisio (2000). Despite the enmity towards Russia, there was a certain level of self-censorship in Finland in the years between independence and WWII, which meant such feelings were not directly expressed in the media but instead conveyed in codes (Kangas 2007). Post-WWII, the relationship was based on the 1948 Agreement of Friendship, Cooperation and Mutual Assistance (Laine 2014), which laid out the rules for cross-border interaction and gave the Soviet Union a certain level of soft power over Finland (Rytövuori-Apunen 2008a) that led to a continuation of the censorship. The agreement also moved Finland in geopolitical terms. Though officially declaring themselves neutral, it has been argued that Finland shifted from being a part of the western block pre-WWII, to the eastern bloc post-WWII (Paasi 1999)."

Karelia in the Finnish narrative

Border areas are often located away from the political power centers of a country where the attitudes and policies concerning the border are created. Yet, they are experienced and lived in the border areas, creating multiple discourses on the role of the border (Paasi 1999; Nielsen 2020).

Karelia is no exception, it is located away from the political centers in both Finland and Russia, and the border is much more ubiquitous in everyday life. However, before venturing further into Karelia and its meaning, it is imperative to clarify what and where Karelia is. Many areas hold the name Karelia: White Karelia, East Karelia, Ladoga Karelia, etc. and Karelia to a Finn means something else than to a Russian. Russians will most often relate Karelia to the Republic of Karelia. The Finns conceptualization, and the one used here, includes North and South Karelia located in Finland as well as the adjacent areas of the Karelian Isthmus, belonging to Leningrad Oblast, and the south-west part of the Republic of Karelia, sometimes known as Border Karelia (See fig. 2). The remaining part of the Republic of Karelia, especially in a historical context, is sometimes referred to by Finns as East Karelia. The cultural composition in the area is likewise complex to define. Scott (2013, 81) describes it as a «mosaic» border

[1]YLE News article: Ukrainian crisis has not increased Finns' fear of Russia. Available at: https://yle.fi/uutiset/osasto/news/ukrainian_crisis_has_not_increased_finns_fear_of_russia/7150925 (Accessed 18 March 2021)

[2] YLE News articles: Ukrainian crisis has not increased Finns' fear of Russia. Available at: https://yle.fi/uutiset/osasto/news/ukrainian_crisis_has_not_increased_finns_fear_of_russia/7150925 and: Niinistö looks for understanding over Finland's Russia stance. Available at: https://yle.fi/uutiset/osasto/news/niinisto_looks_for_understanding_over_finlands_russia_stance/7155797 (Accessed 18 March 2021)

landscape that from 1809 until now has experienced periods with Russification, Finnishization, conflict, Sovietization, and «New Karelianism» which all have left their trace.

Despite the mosaic, Karelia holds an important role in the Finnish consciousness due to the folklore Kalevala – the national epic of Finland – which takes place in Karelia and East Karelia and is central in the creation of the Finnish identity (Anderson 1983; Scott 2013; Meinander 2020).

The blurred lines between Finland and Russia continued post Finnish independence as the exact location of the Finnish-Russian border remained unsolved. Late in the 19th century, the idea of a Greater Finland had started to gain a foothold, and it continued after Finnish independence. In the spring of 1919, the Finnish politician Santeri Alkio echoed the idea, which was earlier expressed by amongst others General Mannerheim (Kirby 1975) and supported by other politicians: "The concept of the Finnish state includes the union of East Karelia and the Olonets region with Finland, and this has been publicly proclaimed many times over the past few years... The aim of our endeavors is to free East Karelia... we Finns demand that the birthplace of the Kalevala must be united with the rest of Finland. (Kirby 1975, 249)"

Even after the Peace of Tartu in 1920, which officially settled the location of the border, the dream of a Greater Finland lived on. As a result of the treaty, a number of Finnish-speakers stayed on the Russian side, which helped to keep the idea alive and led to tension in the following couple of years (Paasi 1999). Its support, however, quickly diminished post-WWII (Paasi 1996; Meinander 2020). During WWII, Finland fought two wars (Winter War 1939-1940 and Continuation War 1941-1944) against the Soviet Union, which resulted in the Soviet Union annexing almost 10% of Finland, including the Karelian Isthmus and Border Karelia (See figure 2.) (Eskelinen 2011). The loss of territory played, and still plays, an important role in the Finnish consciousness – especially the ceded territory that was a part of Karelia due to its historical and cultural importance. In order to cope with the loss «the Karelians preserved their lost landscapes and homes in their collective memory, their literature, collective action and myths» (Paasi 1999). Today there is a certain familiar strangeness with the Russian part of Karelia that originates from conflicting memories and feelings of nostalgia, enmity, and fear (Scott 2013).

In many regions of the world, the situation in border areas is determined by the geopolitics of memory. Cultivating certain representations, they distinguish key periods of common history with neighboring countries or regions. A negative interpretation of such periods helps to oppose an identity under construction to the identity dominating on the other side of the boundary, to deepen a new cleavage, while a positive attitude forges the feelings of solidarity or reconciliation with the neighbor (Kolossov 2011).

The Finnish part of Karelia is filled with both resentment and hope, as well as nostalgia towards its neighboring area. More recent CBC has been focused on the promotion of local culture and preservation of historical heritage to help mend the gap (Sebentsov 2020; Palmowski and Federov 2020). Oksa (1999) has described Karelia as a bridge between Finland and Russia, yet a more nuanced and fitting border metaphor is that of 'suture' coined by Salter (2012). The suture represents a wound that, despite being healed, has left a noticeable scar both on the body and in the mind.

Fig. 2. Map of Karelia

Involvement of North Karelian Actors with Russian counterparts

In 1992 the Neighborhood Area Cooperation framework was put in place to structure the CBC that lasted until Finland became an EU member in 1995. The change from national to supranational framework also meant that the funding, which is instrumental for most CBCs, changed from Finnish to EU.

Most of the CBC actors have been involved with Russia ever since the Soviet Union collapsed and Russia started to open to the west. As one respondent formulated, we started CBC «as soon as Russia started to be Russia again» (North Karelia Chamber of Commerce). 'Russia being Russia' is as interesting a phrase as it is elusive. Yet what it does convey is that the Soviet Union, or at least the system that was in place during the existence of the Soviet Union, the Agreement of Friendship, Cooperation and Mutual Assistance, which dictated the cross-border interaction, was a threshold that hindered CBC. Russia becoming Russia again, also indicates a perception of Russia returning to normal, which makes it more familiar. While some venture further into Russia in search of CBC, most of the respondents mainly have an interest in the neighboring area. Sometimes the reason is practical and relates to infrastructure, but there are also historical and national memory aspects that create a sense of imaginary community.

To archive a good neighborhood relation and cooperation, it is important to face each other, be orientated towards one another.[1]The Soviet Union was important for Finland in many ways, Finland was also important for the Soviet Union, and later Russia, as a gateway to western Europe and subsequently the EU: "Within the European Union, Finland will always work, in its own interest, for good relations with Russia… Finland's views on Russia are listened to in Brussels. Such a rational view of Russian interests is gaining ground in Moscow… (Jacobson 1998, 153)."

More recently, Finland's role as a mediator between Russia and the EU has diminished, yet the relationship remains friendly. On the local level, the case of North Karelia and its adjacent Russian neighbor is a case of mutual interest. Both regions are peripheral within their respective states (Scott 2013), so the border easily becomes an opportunity that helps to open the neighborhood from a peripheral to more central «…it [CBC] is significant for us, as we are located here at the Eastern border» (North Karelian Regional Council). The Russian wish to engage is reflected in their eagerness to participate in CBC. Most of the local government and the NGO involved in CBC say it has been easy for them to find Russian partners to work with, often they come by themselves which indicates they are facing North Karelia. From the Finnish perspective, the naturalness in which they approach CBC shows that they are also facing Russia, meaning we have a face-to-face situation which according to Henrikson (2011) is essential to create the best possible CBC. Besides changing their peripheral status, the North Karelian actors appear to have a deeper underlining reason to engage in the CBC, a reason that is bound to the Republic of Karelia and its historical ties to Finland (Ahponen 2011). Besides an almost romantic reminisces regarding some of the towns build by Finns when the area was a part of Finland, there is a general sense of connectedness and familiarity with the landscape including a heartfelt feeling towards the area: «We have always had Karelia in our hearts» (Joensuu Diabetes Association).

For both the local government and NGOs it is natural to stretch across the border as they agree that neighborhood is important. In fact, what has driven the CBC has been a sense of naturalness, seeing past the border and perceiving the other as any other neighbor. In this sense, the border can be described by using the concept of intermestic (Lowenthal 1999). Intermestic, a contraction of international and domestic, means the CBC actors comprehend the border and the adjacent area as not entirely international nor national but somewhere in between which is very fitting for this case. Karelia is intermestic for Finns and at the same time, it is also familiar yet unfamiliar, familiar in a historical sense but unfamiliar in a more modern perspective. While some expressed that there were differences in work approaches, it was still «natural» to engage in CBC because of the proximity in both culture and distance (Karelia University of Applied Sciences). The Joensuu Scouts has even received special permission from the central office to act on their own when it comes to CBC with Russia. Normally all international engagements need to go through their central office but in this case, an exception has been made because Russia from the North Karelian view is not necessarily international, but intermestic: «We don't do international work but cooperation with a neighboring area» (Joensuu Scouts Association).

Although borders, physical as well as mental, do pose a threshold for CBC, Koch and Vainikka (2019) argue that it has not been enough to discourage CBC between Finnish and Russian actors. However, it does not mean thresholds are not experienced. Considering O'Dowd (2002) and Zimmerbauer's (2011) conceptualization of borders as layered and manifested in different areas of society, respondents said they experienced boundaries in social, legal, political, and cultural areas, in the form of language, different legal systems, governance, and traditions. They also believed that while the encountered borders most likely keep some from participating in CBC, it is part of the learning process. In fact, most of these hindrances diminish with time as younger generations with better language skills join, and legal systems and traditions are learned on both sides, a process some of the actors help to push. «It is normal for us to have Russian students that do internships in Finnish companies and then use those skills in Russia when interacting with Finnish companies» (Karela University of Applied Sciences). One barrier appears to be constant though, the centralized rules, which include applying for visas, something that is not and cannot be regulated or determined by the CBC partners but relies on what is being agreed at the national, and sometimes supranational level. It has been argued that for Finland, CBC with Russia has more potential but also includes more risks than with other neighbors (Eskelinen 2011). This is also the perception here, thus, knowing your partner becomes more important «…especially with Russia, familiarity is an important element as there have always been more risks connected to Russian co-operation compared to Germany for example» (Joensuu City, Youth Department).

[1]Alafuzoff, Georgij; Blom, Anders; Kurvinen, Mihail; Pyykönen, Juha; Luoma-aho, Vilma & Tsetsura, Katerina (2020) Govorit Moskva – Moskova puhuu: Venäjän strategisen vietinnän erityispiirteet. Valtioneuvoston selvitys- ja tutkimustoiminnan julkaisusarja. Availeble at https://julkaisut.valtioneuvosto.fi/bitstream/handle/10024/162201/VNTEAS_2020_16.pdf?sequence=1&isAllowed=y

One of the risks is concerning the management of funds. There have been cases when spending money on the Russian side has raised some concerns as to whether it was spent according to the plan. It is not only because of corruption concerns but because of different perception and cultural practices in handling a budget that needs to be reached across, like how to get handwritten receipts in Russian accepted by the EU. There is a consensus that it is important to understand both culture and history of the partner country as the devil is in the detail. What may seem strange at first can often be explained by knowing the cultural habits and history and, consequently, allow to avoid misunderstanding. Thus, the actors underline that the better grasp they have of each other's (and their common) history, the greater are the chances of developing fruitful CBC. Several actors also expressed that they often use the same partners for different projects, underlining good personal relations as well. It has been argued that Finland's proximity and common history have afforded them a certain level of familiarity with Russia (Rytövuoi-Apunen 2008b). Yet, living with a closed border for years has eroded, or at least frozen this familiarity in time, thus, it is not a current understanding of Russia, but an understanding of how Russia used to be. Several actors expressed that Russia and the Russian way is unfamiliar to many, the North Karelia Chamber of Commerce also stated that their reason for engaging in CBC is «…to lower the step into Russia a little bit» (North Karelia Chamber of Commerce).

As Koch and Vainikka (2019) aptly stated, there is a high level of trust between Finnish CBC actors and their Russian counterparts, that is detached from the mediated perception of Russia and geopolitical tension. Nonetheless, the trust is not instant but builds up over time and goes both ways. The building of trust is also connected to the increase in knowledge and experience, as it is how it can be earned. In addition to the concerns mentioned earlier, several described Russians as apprehensive and slow to open up at first but when the trust is established, it does not wither easily. The trust, however, is aimed at individuals and does not necessarily extend to the Russian system/government who is described as difficult and tends to halt CBC. In here lies a paradox, while the Russian government sometimes is considered as a hindrance for CBC «…the Moscow end is as stiff as an iron bar» (Joensuu city, youth department), several Finnish actors describe themselves as «stiff» in comparisons to their local Russian partners.

CONCLUSION

Although the history between Finland and Russia has been the root for tension between the two, Finns have been «… on the whole remarkably free of resentments or hang-ups in their attitude towards Russia – self-confident without vindictiveness». (Jakobson 1998: 153). The negative portrayal of Russia both within and outside of Finland has not been enough to deter the CBC, neither have the traumatic Winter War and Continuation War. This has also been the case here. None of the CBC actors expressed historical or current negative images of Russia as having any significant effect on their interests in CBC or on the actual cooperation. The fact that both sides are facing each other is a sign that they are not too unfamiliar with each other. Despite being unfamiliar with such elements as legal systems, procedures, language, etc., which possibly keeps some potential actors from CBC and complicate things, it is still deemed to be worth it due to the potential and historical familiarity. Consequently, the threshold for CBC has not been as high as one could expect, and it is seen in the naturalness in which the North Karelian actors approach it.

The modern Finnish national identity is largely created in opposition to Russia and is partly based on the memories of the wars between the two, still, the mental borders that normally follows in the slipstream (Andersen and Prokkola 2018) have not established themselves as firmly as they could have. The CBC actors do report unfamiliar factors caused by the long period of separation, and it does add to the unfamiliarity, but on the other hand, the familiarity through historical remembrance and sense of connectedness to the Russian side function as a counterbalance, making CBC neither too familiar nor too unfamiliar. This also means that there are several reasons why the local government and NGOs choose to participate in CBC with their Russian neighbor. With the close proximity as well as felt cultural and historical connection to the other side, the Republic of Karelia in particular has a distinct strong pull effect and helps to suture the gap created by decades of the hermetically closed border, transforming the international border into an intermestic one. Most see CBC as a natural extension of their neighborhood cooperation that just happens to cross an international border. It also appears that the local Russian partners see a similar potential in expanding their neighborhood across the border, but without further research on the Russian side this has yet to be confirmed. While there might be a national interest in using these CBCs to exercise soft power, it does not seem to be a factor for the local CBC practitioners.

The key to a successful CBC lies in familiarity. Besides the physical and cultural proximity, there is a certain knowledge about Russia which is important. Although it has been suggested that the generic Finnish understanding of Russia is outdated (Laine 2015), unfamiliarity has not had a deterrent effect, more the opposite. Unfamiliarity is often what pulls us across the border as seen in other studies (See e.g. Nielsen 2019). In that context, an open mind and willingness to learn are embedded in the unfamiliarity pull. After the initial contact, experience and a better knowledge have grown and that is what has ensured the continuation of the success. While the actors concur that the beginning was difficult, they also say that once the tires were established, the increase in knowledge and experience keeps the actors (from both sides) interested in continuing and expanding on the CBC. That means the increase in familiarity, not just with Russia but also with the project partners, helps to ensure the success of CBC. It does not need to be a complete familiarity, but enough to know and respect that things are done differently and that your own approach may not work on the other side. Logically, the novelty of unfamiliarity will eventually wear off, thus the question remains whether Russia will ever become too familiar or the continuance of growth in knowledge and experience will keep the actors interested.

REFERENCES

Åtland K. (2016). North European security after the Ukraine conflict. Defense & Security Analysis, 32(2), 163-176, DOI: 10.1080/14751798.2.

Ahponen P. (2011). Miserable or Golden Karelia? Interpreting a cross-border excursion of students from Finland to Russia. Journal of Borderlands Studies, (26)2, 145-159, DOI: 10.1080/08865655.2011.641324.

Andersen D. and Prokkola E. (2018). Heritage as bordering: heritage making, ontological struggles and the politics of memory in the Croatian and Finnish borderlands. Journal of Borderlands Studies, DOI: 10.1080/08865655.2018.1555052.

Andersen D. (2013). Exploring the concept of (un)familiarity: (un)familiarity in border practices and identity-formation at the Slovenian-Croatian border on Istria. European Planning Studies, 21(1), 42-57, DOI: 10.1080/09654313.2012.716238.

Anderson B. (1983). Imagined Communities. Reflections on the Origin and Spread of Nationalism. London: Verso.

Boesen E. and Schnuer G. (2017). Dwelling in (un)familiarity – examples from the Luxembourg-German borderlands. In E. Boesen and G. Schnuer, eds., European borderlands: living with barriers and bridges. Oxon: Routledge, 144-158.

Browning C. and Lehti M. (2007). Beyond East–West: Marginality and National Dignity in Finnish Identity Construction. Nationalities Papers, 35 (4), 691-716, DOI: 10.1080/00905990701475103.

Dominguez N. and Mercier-Suissa C. (2015). Investir dans un pays tremplin L'implantation d'une PME Française en Finlande pour aborder la Russie. Revue d'études comparatives Est-Ouest, 46(3), 183-210.

Eskelinen H. (2011). Different neighbours: interaction and cooperation at Finland's western and eastern borders. In D. Wastl-Walter ed. The Ashgate research companion to border studies, Farnham: Ashgate, 569-583.

Etzold T. and Haukkala H. (2011). Is there a Nordic Russia Policy? Swedish, Finnish and Danish Relations with Russia in the Context of the European Union. Journal of Contemporary European Studies, 19(2), 249-260, DOI: 10.1080/14782804.2011.580913.

Feklyunina V. (2008). Battle for Perceptions: Projecting Russia in the West. Europe-Asia Studies, 60(4), 605-629, DOI: 10.1080/09668130801999888.

Harle V. and Moisio S. (2000). Missä on suomi? Kansallisen identiteettipolitiikan historia ja geopolitiikka. Tampere: Vastapaino.

Henrikson A. (2011). Border regions as neighbourhoods. In D. Wastl-Walter ed., The Ashgate research companion to border studies. Farnham: Ashgate, 85-102.

Hu Y. and Ritchie, B. (1993). Measuring destination attractiveness: A contextual approach. Journal of Travel Research, 32, 25-34, DOI: 10.1177/004728759303200204.

Izotov, A. and Laine, J. (2012). Constructing (Un) familiarity: Role of Tourism in Identity and Region Building at the Finnish–Russian Border. European Planning Studies, 21(1), 93-111, DOI: 10.1080/09654313.2012.716241.

Jakobson M. (1998). Finland in the new Europe. Westport: Praeger Publishers.

Jerman H. (2004). Russians as Presented in TV documentaries. The Global Review of Ethnopolitics, 3(2), 79-88, DOI: 10.1080/14718800408405168.

Kangas A. (2007). The Beast, the Knight, and the Political Fact in Here: Fiction and Non-Fictional in Finnish Political Imaginary on Russia. In M. Lehtimäki, S. Leisti and M. Rytkönen eds., Real Stories, Imagined Realities: Fictionality and Non-fictionality in Literary Constructs and Historical Contexts. Tampere: Tampere University Press, 272-285.

Kirby D. ed. (1975). Finland and Russia 1808–1920 From Autonomy to Independence – a selection of documents. London: The Macmillan Press Ltd.

Klatt M. (2014). (Un) familiarity? Labor related cross-border mobility in Sønderjylland/Schleswig since Denmark joined the EC in 1973. Journal of Borderlands Studies, 29(3), 353-373, DOI: 10.1080/08865655.2014.938968.

Klatt M. (2017). Dybøl 2014 – constructing familiarity by remembrance? In E. Boesen and G. Schnuer eds., European borderlands: living with barriers and bridges. Oxon: Routledge, 30-46.

Koch K. and Vainikka V. (2019). The geopolitical production of trust discourses in Finland: perspectives from the Finnish-Russian border. Journal of Borderlands Studies, 34(5), 807-827, DOI: 10.1080/08865655.2019.1646152.

Kolossov V. (2011). Post-Soviet boundaries: territoriality, identity, security, circulation. In D. Wastl-Walter ed. (2011) The Ashgate research companion to border studies. Farnham: Ashgate, 171-194.

Kvale S. and Brinkmann S. (2015). Interview – det kvantitative forskningsinterview som håndværk. København: Hans Reitzels Forlag.

Laine J. (2013). New Civic Neighborhood – cross-border cooperation and civic society engagement at the Finnish-Russian border. Doctoral dissertation, University of Eastern Finland, Joensuu.

Laine J. (2014). Opportunities and challenges of non-state dialogue across the Finnish-Russian border. Annales Scientia Politica, 3(1), 4-14.

Laine J. (2015). No news is good news? Making the Finnish public image of Russia. GeoJournal, 80(1), 93-122, DOI: 10.1007/s10708-014-9539-9.

Laurén K. (2012). Fear in Border Narratives: Perspective of the Finnish-Russia Border. Folklore. Electronic Journal of Folklore, 52, 39-62, DOI: 10.7592/FEJF2012.52.lauren.

Lowenthal A. (1999). United States-Latin American Relations at the Century's Turn: Managing the «Intermestic» Agenda. In A. Fishlow and J. Jones eds. The United States and the Americas: A Twenty-First Century View. W.W. Norton and Company: New York, 109-136.

Meinander H. (2020). A history of Finland. Oxford University Press: New York.

Michelsen K. and Kuisma M. (1992). Nationalism and industrial development in Finland. Business and Economic History, 21, 343-353, Available at: https://www.jstor.org/stable/23703237 [Accessed 17 May 2021].

Moisio S. (1998). Finland, geopolitical image of threat and post-cold war confusion. Geopolitics, 3(3), 104-124, DOI: 10.1080/14650049808407630.

Németh A. (2015). Watching the Other Across the Border: Representations of Russia and Estonia on Finnish National Television. Journal of Borderlands Studies, 30(1), 37-52, DOI: 10.1080/08865655.2015.1030187.

Nielsen H. (2019). Encountering (un) familiar Russia: thresholds and perceptions when crossing the border. Journal of Borderlands Studies, DOI: 10.1080/08865655.2019.1621765.

Nielsen H. (2020). Perception of danger in the southern Arizona borderlands. Fennia – International Journal of Geography, 198(1-2), 74-90, DOI: 10.11143/fennia.87338.

Oksa J. (1999). The changing border and the many images of Karelia. In H. Eskelinen, I. Liikanen and J. Oksa eds., Curtains of Iron and Gold. Reconstructing Borders and Scales of Interaction. Aldershot: Ashgate, 285-296.

O'Dowd L. (2002). The Changing Significance of European Borders. Regional & Federal Studies, 12(4), 13-36, DOI: 10.1080/714004774.

Paasi A. (1996). Territories, boundaries and consciousness: the changing geographies of the Finnish-Russian border. Chichester: John Wiley & Sons.

Paasi A. (1997). Geographical perspectives on Finnish national identity. GeoJournal, 43(1), 41-50.

Paasi A. (1999). Boundaries as social practice and discourse: the Finnish-Russian border. Regional Studies, 33(7), 669-680, DOI: 10.1080/00343409950078701.

Palmowski T. and Fedorov G. (2020). The potential for development of Russian-Polish cross-border region. Geography, Environment, Sustainability, 13(1), 21-28, DOI: 10.24057/2071-9388-2019-70.

Paul M. (2001). Western Negative Perception of Russia: «The cold war mentality» over -five hundred years. International Social Science Review, 76(3/4), 103-121.

Raivo P. (2000). 'This is where they fought' Finnish war landscapes as a national heritage. In T. Ashplant, G. Dawson, M. Roper eds., The politics of war memory and commemoration. London: Routledge, 145-164.

Rutland P. and Kazantsev A. (2016). The limits of Russia's 'soft power'. Journal of Political Power, 9(3), 395-413, DOI: 10.1080/2158379X.2016.1232287.

Rytövuoi-Apunen H. (2008a). Revisiting the problem of trust in Finnish-Russian relations. In H. Rytövuoi-Apunen ed., Russia forever? Towards pragmatism in Finnish/Russian relations. Gummerus Printing: Vaajakoski, 121-166.

Rytövuoi-Apunen H. (2008b). Introduction: continuity and change of Finnish/Russian relations in the context of institutional, practical and habitual modes of knowing. In H. Rytövuoi-Apunen ed Russia forever? Towards pragmatism in Finnish/Russian relations. Gummerus Printing: Vaajakoski, 9-26.

Salter M. (2012). Theory of the /: The Suture and Critical Border Studies. Geopolitics, 17, 734-755, DOI: 10.1080/14650045.2012.660580.

Scott J. (2013). Constructing Familiarity in Finnish–Russian Karelia: Shifting Uses of History and the Re-Interpretation of Regions. European Planning Studies, 21(1), 75-92, DOI: 10.1080/09654313.2012.716240.

Sebentsov A. (2020). Cross-border cooperation on the EU-Russian borders: results of the program approach. Geography, Environment, Sustainability, 13(1), 74-83, DOI: 10.24057/2071-9388-2019-136.

Shleifer, A. and Treisman, D. (2005). A normal country: Russia after communism. Journal of Economic Perspectives, 19(1), 151-174, DOI: 10.1257/0895330053147949.

Spierings B. and Van der Velde M. (2008). Shopping, borders and unfamiliarity: Consumer mobility in Europe. Tijdschrift voor Economische en Sociale Geografie, 99(4), 497-505, DOI: 10.1111/j.1467-9663.2008.00484.x.

Spierings B. and Van der Velde M. (2013). Cross-Border Differences and Unfamiliarity: Shopping Mobility in the Dutch-German Rhine-Waal Euroregion. European Planning Studies, 21(1), 5-23, DOI: 10.1080/09654313.2012.716236.

Szytniewski B. and Spierings B. (2014). Encounters with Others: Implications of (Un)familiarity for Daily Life in Borderlands. Journal of Borderlands Studies, 29(3), 339-351, DOI: 10.1080/08865655.2014.938971.

Van der Velde, M. and van Naerssen, T. (2015). The Thresholds to Mobility Disentangled. In M. van der Velde and T. van Naerssen eds., Mobility and Migration Choices: Thresholds to Crossing Borders. Ashgate: Farnham, 3-14, DOI: 10.4324/9781315595740.

Vehviläinen O. (2002). Finland in the Second World War: between Germany and Russia, Hampshire: Palgrave, DOI: 10.1057/9781403919748.

Wassholm J. (2014). Svenskt, finskt och ryskt – Nationens, språkets och historiens dimensioner hos E.G. Ehrström 1808-1835. Svenska Litteratursällskapet i Finland: Helsingfors.

Zimmerbauer K. (2011). Conceptualizing Borders in Cross-Border Regions: Case Studies of the Barents and Ireland – Wales Supranational Regions. Journal of Borderlands Studies, 26 (2), 211-229, DOI: 10.1080/08865655.2011.641322.

Zotova M. and Gritsenko A. (2020). Neighbourhood and perceptions in small cities on different Russian borders. Geography, Environment, Sustainability, 13(1), 64-73, DOI: 10.24057/2071-9388-2019-124.

Check for updates

CC BY

RESEARCH PAPER

THE PHENOMENON OF *EMILIANIA HUXLEYI* IN ASPECTS OF GLOBAL CLIMATE AND THE ECOLOGY OF THE WORLD OCEAN

Dmitry V. Pozdnyakov[1,2], Natalia V. Gnatiuk[1*], Richard Davy[3], Leonid P. Bobylev[1]

[1]Nansen International Environmental and Remote Sensing Centre, 14th Line 7, Vasilievsky Island, St. Petersburg, 199034, Russia

[2]St. Petersburg State University, 7/9 Universitetskaya nab., St. Petersburg, 199034, Russia

[3]Nansen Environmental and Remote Sensing Center, Thormøhlens gate 47, Bergen, N-5006, Norway

***Corresponding author:** natalia.gnatiuk@niersc.spb.ru, d.pozdnyakov@spbu.ru

Received: December 22th, 2020 / Accepted: May 25th, 2021 / Published: July 1st, 2021

https://DOI-10.24057/2071-9388-2020-214

ABSTRACT. *Emiliania huxleyi* (Lohmann) evolved from the genus *Gephyrocapsa* Kamptner (Prymneosiophyceae) of the coccolithophore family Naëlaerhadaceae. Over the past 100 thousand years *E. huxleyi* has acquired the status of the most ecologically predominant coccolithophore due to its remarkable adaptability to a variety of environmental conditions and interspecific competitiveness. *E. huxleyi* plays an important role in both the marine carbon system and carbon cycling between the atmosphere and ocean due to its ability to produce organic and inorganic carbon as well as to form massive blooms throughout the world ocean. This study examines both older information and recent findings to shed light on the current tendencies in the two-way interactions between *E. huxleyi* blooms and the immediate and global environment under conditions of climate change. The assembled knowledge has emerged from laboratory and mesocosm instrumental investigations, retrievals of satellite remote sensing data, machine learning/statistical analyses, and numerical simulations. Special attention is given to both the quantitative data reported over the last two decades on such interactions, and the only very recently appearing mid-term projections of *E. huxleyi* bloom dynamics across the world ocean. These blooms strongly affect the atmosphere and ocean carbon cycles. They reduce CO_2 fluxes from by ~50% to ~150% as is documented for the North Atlantic, and on the global scale release particulate inorganic carbon as calcium calcite in the amounts assessed at 0.4 to 4.8 PgC/yr. At the same time, they are also sensitive to the atmospheric and oceanic state. This results in *E. huxleyi* blooms having an increased impact on the environment in response to ongoing global warming.

KEYWORDS: coccolithophores, *Emiliania huxleyi*, cell morphology, genetic diversity, physiology, blooms, environment and forward and feedback interactions, climate change and future scenarios

CITATION: Dmitry V. Pozdnyakov, Natalia V. Gnatiuk, Richard Davy, Leonid P. Bobylev (2021). The Phenomenon Of Emiliania Huxleyi In Aspects Of Global Climate And The Ecology Of The World Ocean. Geography, Environment, Sustainability, Vol.14, No 2, p. 50-62
https://DOI-10.24057/2071-9388-2020-214

ACKNOWLEDGMENTS: We acknowledge with gratitude that this work was funded by Saint Petersburg State University, project N 75295423 (i.bashmachnikov@spbu.ru).

Conflict of interests: The authors reported no potential conflict of interest.

INTRODUCTION

A coccolithophore *Emiliania huxleyi* (Lohmann) W. W. Hay et H. P. Mohler (Prymneosiophyceae) is known as the most productive calcifying organism on Earth (Paasche 2002; Tyrrell and Young 2009). This alga is found to be an important player in the processes that form the marine carbon system and the CO_2 partitioning between the atmosphere and the uppermost layer of the ocean. Furthermore, *E. huxleyi* contribute to marine sulphur cycles by producing a precursor of dimethylsulphide (DMS), the latter being a precursor for the generation of maritime aerosol. These properties are particularly consequential as *E. huxleyi* is able to form extensive and intensive blooms throughout the world ocean. This gives *E. huxleyi* an important role in marine biogeochemistry, marine ecology and the climate system.

This explains much of the interest in this algal species that has made it one of the best-studied marine organisms, not least due to the ease of growing *E. huxleyi* under laboratory conditions. To date, several reviews on *E. huxleyi* have been published covering a wide range of issues related to this alga (Paasche 2002; Rost and Riebesell 2004; Tyrrell and Merico 2004).

The present review was prompted by many new studies that have appeared since then. These recent works have shed more light on, amongst other things, cell morphology and intracellular biochemistry, including the intrinsic mechanisms of calcification in conjunction with organic matter production. The growing data from satellite observations that began in 1997–1998 enabled regional and worldwide quantitative assessments of the interannual dynamics of bloom extent; the associated

production of particulate inorganic carbon; elevations in dissolved CO_2; and the enhancement of CO_2 partial pressure over *E. huxleyi* bloom areas. New insights have been reported on the two-way interactions between these algae communities and the environment in the context of increasing atmospheric CO_2 concentrations, global warming, and ocean acidification.

Spaceborne data have also contributed to a better (but still incomplete) understanding of the environmental forcing factors that determine the onset, duration, and intensity of *E. huxleyi* blooms. There have also been tentative quantitative assessments of how bloom dynamics may change in the future in response to ongoing climate change.

No single review is able to cover all aspects of the knowledge that has emerged on *E. huxleyi*. In this manuscript we chose to concentrate on the ecology of this alga and its influence on the atmosphere and ocean, as well as the vice versa influence on this alga of the changing climatic conditions of the recent past and near future. Nonetheless, our review explores some «old knowledge», since the basic accomplishments in *E. huxleyi*-related research continue to be fundamental for our understanding of the phenomena related to this remarkable marine organism.

A HISTORIC OVERVIEW OF ORIGIN AND DEVELOPMENT

The coccolithophore family Naëlaerhadaceae has been the most plentiful taxon of coccolithophore communities (Raffi et al. 2006) for the last 20 million years, with *Gephyrocapsa oceanica* Kamptner being predominant. Some 270.000 years ago a new species, *Emiliania huxleyi*, evolved and has become differentiated from the older *G. oceanica* (Thierstein et al. 1977). Some 200.000 years after this differentiation *E. huxleyi* has replaced G. oceanica as the most ecologically prominent coccolithophore. This is due to its phenomenal ability for adaptation to a wide range of environmental conditions and a remarkable interspecific competitiveness. Presently, the cell number of *E. huxleyi* in coccolithophore communities across the world ocean accounts for 30% to 50%, and up to 100% at subpolar latitudes (Mohan et al. 2008).

CELL MORPHOLOGY

Like all coccolithophores, *E. huxleyi* is characterized by the haplodiplontic and heteromorphic life cycle encompassing diploid and haploid phases (Green et al. 1996; Frada et al. 2012). The former incorporates both a coccolith-bearing non-motile phase (formation of calcified cells), and a non-calcified non-motile phase (formation of naked cells). The haploid phase is a non-calcified biflagellated one (formation, presumably because of mutation, of organic scales bound to the plasmalemma). Growing diploid populations eventually transform into a haploid cell stage (Read et al. 2013). In the diploid phase, *E. huxleyi* cells bearing calcified coccoliths often form extensive blooms.

Diploid cells of *E. huxleyi* are composed of an inner organic-rich matter covered by interlocking calcium carbonate scales/coccoliths forming an exoskeleton, whose morphology largely reflects the genetic variability of the gene. *E. huxleyi* has three well-characterized calcification morphotypes: A, B, and C. (Paasche 2002). There are additional morphological variations within each coccolith morphotype. A and B are the two major coccolith morphotypes of *E. huxleyi*. Additionally, the types B/C, R, and corona are recognized (Hagino et al. 2011).

E. huxleyi morphotypes are distinctly ecotypes. They are responsive to such environmental drivers as water temperature, salinity, light and nutrient availability that together determine their biogeography (Rigual-Hernandez et al. 2020). As Krumhardt et al. (2017) reviewed, morphotype A is a widespread «warm water» type inhabiting waters from the subtropics to subpolar. It predominates in the North Atlantic south of 60°N, south of the South Subtropical Front but north of the Subantarctic Front, and in subtropical gyres. Morphotypes B/C and C (which are generally classified as B/C morphotype) are a «cold-water» type native to high latitudes (North Atlantic at latitudes >60°N and south of the Subantarctic Front) as well as in upwelling oceanic regions. They are tolerant to high pCO_2, and are less calcified than morphotype A. There is also an over-calcified group of *E. huxleyi* composed of A-over-calcified and morphotype R. Morphotype R is found in coastal New Zealand and a few other productive coastal waters, whereas A-over-calcified inhabits parts of the Southern Ocean (Poulton et al. 2011). The mass of coccoliths of Type A, overcalcified A, and B do not differ systematically, and hence there is no systematic relationship between relative abundance of a morphotype and the overall calcite production of *E. huxleyi* (Johnsen and Bollmann 2020).

Synthesized intracellularly, coccoliths are eventually extruded to the cell surface until a complete coccosphere covering is formed. Normally, *E. huxleyi* build up a complete single layer (10-15 coccoliths are needed to form a complete coccosphere (Paasche 2002)), but under strained conditions, ene overproduces coccoliths to form a multi-layer cover up to 4 layers thick, made up of over one hundred coccoliths (Balch et al. 1993). Eventually, the excessively overlaid cell becomes unstable and begins losing some upper-layer coccoliths into the surrounding water well before the end of the life cycle when the cell becomes totally naked. The mechanism of coccolith formation and extrusion out of the cell's body is not yet fully understood (Brownlee et al. 2015).

Moreover, even the role of coccoliths still remains uncertain as many possible options have been envisaged (Müller 2019). In terms of the ecologically biotic function, *E. huxleyi* cells might have evolved coccoliths to protect them from grazing by zooplankton (although this is contested by Strom et al. (2020)), as well as to reduce the risk of penetration of viruses and bacteria into the cell. It has also been conjected that, by increasing the cell's weight, the coccoliths raise the rate of diurnal downward movements of cells within the euphotic zone and thus elevate the rate of nutrient uptake by the cell due to its more intense washing. In light of the well-established resistance of *E. huxleyi* to photoinhibition, it appears possible that its carbonate cover protects the cell against very high light intensities by dissipating impinging light (Johnsen and Bollmann 2020). Also, a cellular biochemical aspect may be involved through the carbon concentration mechanism for photosynthesis, phosphorus metabolism (avoidance of intracellular precipitation and detoxication), and the maintenance of a balance between high external and low intracellular Ca concentration (Vargas et al. 2007). In any case, the diversity of coccolith morphology makes it likely that coccoliths have evolved to perform a range of functions.

The remarkable omnipresence of *E. huxleyi* in the world ocean is explained by versatile ecotypes/strains of this alga arising from genetic variability and genomic organization. All *E. huxleyi* morphospecies have a common «core-genome» incorporating the genes responsible for

vital functioning of the cell and defining to a major degree the fundamental features of the species. This core genome is complemented with some specific genes distributed between strains that condition the environmental fitness of *E. huxleyi* strains/ecotypes. As such, a pan-genome ensures the phenomenon of ecological competitiveness/cosmopolitism of this alga (Read et al. 2013; von Dassow et al. 2015), and ostensibly implies that such a high degree of genetic diversity translates into a spectrum of ecological functions (Iglesias-Rodriguez et al. 2006).

This genetic flexibility is the key to the ecological success of *E. huxleyi*. It imparts the ability to endure high radiance levels and low metal (especially Fe) availability (Miller et al. 1991); tolerate nutrient (nitrogen) paucity (Kaffes et al. 2010); possess efficient phosphate uptake and an organically bound phosphate scavenging system (Riegman et al. 2000); and provides immunity to grazing by some microzooplankton species (Merico et al. 2004). These capacities are further complemented by the ability of *E. huxleyi* to grow in marine environments with a wide range of water temperature, salinity, vertical mixing/stratification, and extremely high and low (even under-ice) illumination conditions (Balch et al. 2014; Silkin 2017; Nissen et al. 2018; Kondrik et al. 2019).

CELL intracellular biochemistry related to calcification

Two basic biochemical reactions of photosynthesis and calcification (eq. 1) occur in *E. huxleyi* cells:

$$\begin{aligned} 6CO_2 + 12H_2O &\rightarrow C_6H_{12}O_6 + 6O_6 + H_2O \\ Ca^{2+} + 2HCO_3^- &\rightarrow CaCO_3 + CO_2 + H_2O \end{aligned} \quad (1)$$

Investigation of intracellular calcification indicated that the conditioning role in this process is played by the expression of the *AEL1, CAX3* and *ATPVc'/c* genes (Mackinder et al. 2011). Both reactions proceed within their own compartments that are spatially separated. Nonetheless, there is energetic coupling of the two reactions. It has been claimed that this coupling is unidirectional: that the calcification reaction takes up energy from photosynthesis as both reactions proceed during day-time. Unlike some other coccolithophores (*e.g., Coccolithus braarudii* (K. R. Gaarder) K. Baumann, M. Cachao, J. R. Young and M. Geisen in the diploid phase), the photosynthesis reaction in *E. huxleyi* cells does not necessarily need the intracellular CO_2 and\or protons produced by calcification [the latter for conversion of $2HCO^-_3$ to CO_2] (Brownlee and Taylor 2004; Walker et al. 2018). Moreover, it is shown that calcification – an energy demanding process for a cell - plays photoprotective roles when the cell is exposed to excessively high solar radiation (Xu and Gao 2012).

Thus, CO_2 for photosynthesis is principally of external origin, similarly to $2HCO^-_3$ (Balch et al. 2014). CO_2 is transported into the cell by diffusion from ambient water, which in turn comes from the dissolution of atmospheric CO_2 into water:

$$CO_2 + H_2O \leftrightarrow H_2CO_3 \leftrightarrow 2HCO_3^- + H^+ \leftrightarrow CO_3^{2-} + 2H^+ \quad (2)$$

Although the bulk calcification process (i.e., precipitation of $CaCO_3$ from Ca^{2+} and CO_3^{2-}) is well-established, the intricate intracellular transport routes remain unclear. Thus, it is presently assumed that most likely Ca^{2+} enters the cell via Ca^{2+} permeable channels in the plasma membrane (Brownlee and Taylor 2004) with further accumulation in the Golgi. This question of how the transport routes work is of fundamental importance because it determines the kinetic rate of the entire process. So, while it remains unanswered, so too do questions about the associated cellular machinery at a more intimate level. Meanwhile, the precise understanding of Ca^{2+} homeostasis is important for a more precise prediction of the world ocean response to increasing global atmospheric CO_2 concentrations, especially in light of the fact that calcification triggers the expression of specific genes within the pan-genome that regulate metabolic processes in response to environmental conditions (Section 3).

Biochemical role in carbon cycling and emissions of organo-phosphorus compounds and methane: machinery and consequences

The flow of atmospheric CO_2 into the surface ocean is determined by the fixation of dissolved CO_2 via photosynthesis (Eq. 1), followed by the downward transport of particulate organic carbon (the so-called carbon pump). The absorption of atmospheric CO_2 into the ocean can be further enhanced by the drawdown of sea water alkalinity i.e., the number of negative ions formed through dissociation of carbonic acid (Eq. 2) due to the removal of HCO^-_3 from surface water. This latter process is hugely important within *E. huxleyi* blooms due to the production of $CaCO_3$ via calcification i.e., subsequent settling of coccoliths (calcite) down into the deep sea (known as the carbonate pump). At the same time, the CO_2 produced during calcification permeates through the membrane, goes out into the surrounding water, and replenishes the pool of dissolved CO_2 within the euphotic zone (Rost and Riebesell 2004). Therefore, calcification can result in either reduction or even inversion of CO_2 fluxes at the ocean-atmosphere interface within the bloom area.

The natural organic surface coating on *E. huxleyi* cells (Godoi et al. 2008) facilitates the dissolution of calcite even in calcium carbonate oversaturated waters. As calcite solubility increases with decreasing temperature (Alekin 1966), the dissociation of $CaCO_3$ at depth eventually initiates the upward transport of dissociation products, thus closing the loop of carbon turnover in the ocean. The dissociation of $CaCO_3$ is especially important below the lysocline where the pressure effect dramatically increases the calcite dissolution.

E. huxleyi blooms are associated with emissions of the volatile compound dimethylsulfide (DMS) (Malin and Steinke 2004), like the blooms of some other algae (e.g., dinoflagellates and several colony-forming species, e.g., *Phaeocystis*). When emitted to the atmosphere, DMS can affect cloud formation, which is consequential for the global climate.

The present knowledge (Vogt and Liss 2010) suggests that DMS $[(H_3C)_2S]$ in seawater is produced (along with acrylate $[H_2CHCOO^-]$ and a proton) owing to extracellular cleavage of dimethylsulphoniopropionate $[(CH_2)_2 + SCH_2CH_2COO^-]$ (abbreviation DMSP) rather than direct excretion by *E. huxleyi* cells (Eq. 3):

$$\left[(CH_2)_2 + SCH_2CH_2COO^-\right](DMSP-lyase)/(\text{bacteria and algae}) \rightarrow \left[(H_3C)_2S\right] + \left[H_2CHCOO^-\right] + H^+ \quad (3)$$

The above DMSP breakdown reaction is initiated by either dimethypropiothetin dethiomethylase (DMSP-lyase) or bacteria (attached or symbiotic). The triggering mechanism of reaction (3) in the case of healthy *E. huxleyi* cell is zooplankton grazing. However, it seems that microzooplankton do not themselves convert DMSP to DSM but rather spur the activation of algal DMSP-lyase and microbial enzymic intervention. The bacterial degradation processes become the most important DMSP-lyase

activation pathway in the senescence phase of the life-cycle of *E. huxleyi* cells. At this stage of the life-cycle, viral infection is thought to play an important role as the virus lysis eventually results in liberation of the cell's content into the water, making it easy prey for bacteria (Evans et al. 2007). Alcolombri et al. (2015) have identified the DMS releasing gene in *E. huxleyi*: it proved to be Alma 1 – a tetrameric redox-sensitive enzyme belonging to the gene family common for the major phytoplankton taxa.

The physiological role of DMSP is thought to be multifaceted cell protection: osmoprotection (counteract excessive water salinity), cryo-protection (anti-freezing), and antioxidantant action (scavenging of OH^- radicals) (Vogt and Liss 2010). DMS emissions from the ocean have been found to be within 17-34TgSyr^{-1}, which accounts for about 50% of the total global sulfur entering the atmosphere annually (Lana et al. 2011).

Along with CO_2, CH_4 is one of the main greenhouse gases. There is unambiguous evidence for production of methane (CH_4) by widespread haptophytes such as Phaeocystis globosa, Chrysochromulina sp., and *E. huxleyi* (Klintzsch et al. 2019). Remarkably, this process occurs even in marine waters oversaturated with O_2, i.e., under conditions that do not favor methanogenesis. Nonetheless, a 5%-75% oversaturation of CH_4 within *E. huxleyi* bloom areas has been documented (Lenhart et al. 2016). It is conjected that CH_4 is produced by *E. huxleyi* over the entire life-cycle, including the senescence phase, so that this process is part of its normal metabolism. Indeed, the data obtained indicate that bicarbonate (taken up by the algae via autotrophic C fixation) is the principle inorganic carbon precursor of CH_4 produced in algae, while the main organic precursor of CH_4 is methionine (Met) [$C_5H_{11}NO_2S$] – a methyl group donor. Algae-derived DMSO can also act as a precursor of CH_4 in oxic seawater (Althoff et al. 2014). Cumulative (anthropogenic and natural) emissions of CH_4 are assessed at 500-600Tgyr $^{-1}$ (Lenhart et al. 2016), but the global contribution solely due to coccolithophores remains moot as other algal species, such as dinoflagellates, are also very productive in this regard.

E. huxleyi bloom CO_2-related impacts on the environment

Carbonate counter pump

Satellite-borne estimations covering the period 1998–2019 showed that *E. huxleyi* blooms in Subarctic and Arctic seas as well as in the Black Sea resulted in the release of ten to several hundreds of kilotons of inorganic carbon (PIC) into surface water in the form of $CaCO_3$. In the Barents Sea, the released PIC content varied between ~100 kt and 250-300 kt, whereas in the Bering Sea the PIC content was as high as 500 kt during two periods of exceptional activity (Kondrik et al. 2017). Although the reported estimates of annual PIC production on a global scale vary widely, they are nevertheless very high: ~ 0.4 to 1.8 PgCyr $^{-1}$ (Balch et al. 2016).

Increment of CO_2 partial pressure within blooms and in the atmospheric column over them

There is ample evidence that the release of PIC was accompanied by a significant increase in CO_2 partial pressure (ΔpCO_2) within the bloom area: between 1998 and 2016, the mean and maximum values of the ratio $\Delta pCO_2/(\Delta pCO_2)_{background}$, varied in the range ~ (20-40)%, and ~ (30-60)%, respectively. The highest numbers were registered in the Bering and Barents seas (Kondrik et al. 2018; Kondrik et al 2019).

The recent quantitative assessments of *E. huxleyi* bloom influence on surface water CO_2 partial pressure (pCO_2) showed that in the North, Norwegian, Greenland, Barents, Bering and Black seas *E. huxleyi* blooms accounted for a very significant pCO_2 enhancement (ΔpCO_2).
For the regions of prevalent coccolithophore (*E. huxleyi*) blooms in the North Atlantic, Shutler et al. (2013) found that the average reduction in the monthly air-water CO_2 flux could reach 55%, while the maximum reduction within the time period 1998–2007 was as high as 155%.

The impact of *E. huxleyi* blooms on CO_2 exchange at the air-sea surface interface was quantified from satellite OCO-2 data: the numerous remote sensing case studies over the aforementioned North Atlantic seas as well as in the Barents and Black seas proved that $(\Delta pCO_2)_{atm}$ could reach 2-3 ppm (Kondrik et al. 2019, Morozov et al. 2019). Such increments constitute ~ 0.5% of the present mean pCO_2 in the atmosphere (Dlugokencky 2016) and is comparable to the annual increase in global-mean atmospheric CO_2. These data give evidence that *E. huxleyi* blooms can significantly weaken marine carbon sinks on a global scale.

Physiological ecology, environmental impact factors

Nutrients

The canonical Redfield (1934) stoichiometric ratio (atomic ratio of carbon (C), nitrogen (N), and phosphorus (P)) in algae across the pelagic parts of the world ocean was established at 106:16:1. Using more recent data (1970–2010) this was slightly corrected to 163:22:1 (Martiny et al. 2014). Presently, the Redfield and Martiny et al. ratio is considered as a general average rather than a strict prerequisite for marine algae growth.

With regard to *E. huxleyi*, there were multiple reports that phosphorus limitation is critically important for the development of a bloom because of both an exceptionally high affinity of this alga to orthophosphate (Riegman et al. 2000; Paasche 2002) and its mixotrophic capability (Godrijan et al. 2020). *E. huxleyi* blooms do form exclusively if NO_3:PO_4 is >16, and reach their maximum at NO_3:PO_4 >25. Nevertheless, particularly high NO_3:PO_4 ratios are not indispensable for the occurrence of the massive development of this alga, as can be seen in the Barents Sea. Moreover, there are many reports of *E. huxleyi* blooms when NO_3:PO_4 was much lower than 16 (Mikaelyan et al. 2015; Silkin 2017). This might be explained by the mixotrophy of *E. huxleyi* if other sources were available for nutrition, such as organic nitrogen and phosphorus compounds. It explains the competitiveness of *E. huxleyi* in nutrient-depleted waters with regard to other co-occurring/competing algae. It is also shown that under N-depleted conditions, *E. huxleyi* susceptibility to photoactivation of photosystem (PS) II lessens (Loebl et al. 2010), which implies the ability of this alga to maintain PSII repair under high-light conditions typical of stratified surface waters.

It was shown that a phosphorus limitation does not enhance calcification (Oviedo et al. 2014), although it leads (strain specifically) to morphological changes in coccoliths and an increase in cell diameter. In phosphorus replete waters the growth rate increases, and cells and coccoliths become smaller. Conversely, a nitrogen limitation results in cell diameter decrease (Müller et al. 2008). Reportedly, phosphorus (but not nitrogen) starvation reduces the photosynthetic function of *E. huxleyi* (Silkin 2017). Unlike in N-depleted conditions, P-limitation leads to a decline in PSII functioning (Loebl et al. 2010).

The extended Redfield ratio also includes Fe as a micronutrient that can be limiting for the phytoplankton

species. The ratio should be C:16 N:1 P:0.1 Fe:0.001. As part of cytochrome and ferrodoxin molecules, Fe is an important catalytic agent in the intracellular electron transport in enzymatic systems acting in photosynthesis and respiratory processes. It has been shown to be indispensable for the growth of large-celled phytoplankton (Martin et al. 1994), DNA repair and management of reactive oxygen species accumulation (Segovia et al. 2018) despite the ample availability of macronutrients. Conversely, small-celled *E. huxleyi* are much more tolerant to Fe-limitation (Miller et al. 1991), and in combination with selective grazing (only by specific zooplankton), *E. huxleyi* is able to form uni-species blooms as it is invariably observed, e.g., in the Gulf of Alaska (Moore et al. 2012), and in the part of the Pacific Ocean known as a «high-macronutrient-low-chlorophyll» area (Muggli and Harrison 1996).

Acidification

This issue is of particular importance in light of ongoing climate change and associated enhancement of CO_2 fluxes into the ocean (Eq. 2).

As the physiological response of *E. huxleyi* to rising CO_2 is strain-specific (Lorenzo et al. 2019) and depends on other co-occurring abiotic and some biotic factors, the actual effect may be synergistic, antagonistic, or even neutral (Boyd and Hutchins 2012). Moreover, the net effect might be short-term and long-term specific (Schlüter et al. 2014). This can explain the variable and seemingly contradictory results.

There are multiple lines of evidence that ocean acidification (elevated pCO_2/reduced pH) exerts a negative effect on calcification and the cellular PIC:POC ratio in *E. huxleyi*, and it is not consequential for photosynthesis (Meyer and Riebesell 2015). At the same time some strains showed an optimum curve in response to increasing pCO_2 (Bach et al. 2011; Sett et al. 2014), no significant response (Richier et al. 2010) or increased calcification rates (Iglesias-Rodriguez et al. 2008; Fiorini et al. 2011).

Reports on photosynthesis response vary between no response (Richier et al. 2010; Fiorini et al. 2011), increase (Rokitta and Rost 2012), decrease in photosynthesis rates (Bach et al. 2011; Shi et al. 2009), and variation with an optimum curve was obtained (Gao et al. 2009). The PIC/POC ratios are reported as generally decreasing with increasing pCO_2 (Bach et al. 2011; Rokitta and Rost 2012; Shi et al. 2009; Feng et al. 2018), although some works either have not found any change (Richier et al. 2010) or observed an increase (Fiorini et al. 2011). At least in the tropical ocean, coccolithophore calcification may not be decreasing with the ongoing acidification in oligotrophic waters (Maranon et al. 2016). As according to the Maranon et al. observations, the calcification: primary production ratio did not decrease with decreasing $[HCO^-_3]/[H^+]$ (Eq. 1-2), this might be a strong indication that carbonate chemistry is not consequential with regard to calcification at the community level throughout the tropical ocean pelagic zone. In nutrient replete marine environments, CO_2 elevation may hinder *E. huxleyi* growth (Hayden 2013), but can also encourage growth (Rivero-Calle et al. 2015). Similar reports come from latitudinally varied marine environments (e.g., Scottish coastal waters (León et al. 2018)). Young et al. (2014) generalize this assertion stating that, on balance, the impact of ocean acidification is «likely low, variable between strains, and reduced by adaptation and strain selection». Bach et al. (2013) found that *E. huxleyi* growth and photosynthesis rates were sensitive to low rather than high CO_2. Comparing the concomitant influence of atmospheric CO_2 increase, water temperature, salinity, irradiance, the latter three might be even more consequential (Sett et al. 2014; Charalampopoulou et al. 2016; Feng et al. 2018). At least, water temperature strongly modulates optimum growth and calcification rates (Sett et al. 2014). However, ocean acidification might promote carbon fixation as organic matter by calcifying *E. huxleyi* (Lorenzo et al. 2019). Water temperature and irradiance rather than pCO_2 elevation are believed to be the main drivers of the observed poleward expansion of *E. huxleyi* (Winter et al. 2014), at least according to data from the Southern Ocean (Charalampopoulou et al. 2016; Smith et al. 2017; Feng et al. 2018). However, there might be other drivers, such as intensified ocean currents (Oziel et al. 2020) evoking putative changes in the foodwebs and biogechemical cycles.

Addressing *E. huxleyi* adaptation to elevated pCO_2 in water, Lohbeck et al. (2012) showed for asexual populations that the ensuing significantly higher calcification rates did not reoccur. It implies the possibility of adaptive evolution in coccolithophores, and hence the risk aversion of the whole ecosystem.

Bach et al. (2015) conjected that if *E. huxleyi* (as well as all coccolithophores) are unable to efficiently adapt to the projected increase in H^+, the calcification rate can be impeded unless this process is counteracted by elevation of oceanic HCO^-_3 due to enhanced dissolution of sedimented $CaCO_3$. But both processes are expected to take place over the forthcoming hundred thousand years: by that time the carbonate chemistry conditions might become steadily fitting for calcification. At least presently, it has been conjected based on the data from the Great Calcite Belt, that *E. huxleyi* cells, regardless of their large population sizes, may be near the limit of this species' capacity to adapt to ongoing ocean acidification (Smith et al. 2017).

Reportedly, nitrogen depletion affects *E. huxleyi* cell morphometry (size, volume, PIC production) more significantly than variations of aquatic CO_2 (Müller et al. 2012), and the sinking rate of N-limited cells seems lower than that of N-replete cells (Pantorno et al. 2013), which is essential in terms of bicarbonate pump functioning.

As in the real word, pCO_2 rise is inseparably linked with increased temperature, the collective impact of these two factors is expected to bring about a short-term decrease in cellular PIC:POC (Feng et al. 2009), and a long-term increase in this ratio (Schluter et al. 2014). This suggests that on a short-time scale (even within a few hours (Ramos et al. 2010)), this alga is able to rapidly acclimate its metabolic processes in response to changes in water acidity. After five years, the growth rates completely recovered at the upper thermal tolerance limit (~27°) and atmospheric pCO_2 = ~ 1000 µatm (as expected at the end of the present century). Assessing in the laboratory the sensitivity of *E. huxleyi* morphotypes to acidification, Müller et al. (2015) found that under future acidification scenarios the PIC:POC ratio would drop especially strongly in B/C rather than in A and A-over-calcified strains. It was also found that long-term exposure of *E. huxleyi* to elevated CO_2 (850 µatm) and temperature (~ 24°) increases calcification but not expression of the calcification-related genes (Benner et al. 2013).

However, it remains unclear whether the above results from monocultural experiments are equally valid for the natural environment where nutrient availability, stratification, light availability, and some other factors are also important. Some studies have already addressed the issue of interactive effects on *E. huxleyi* responses (Feng et al. 2018; Nissen et al. 2018; Stelmakh and Gorbunova 2019; Pozdnyakov et al. 2019). Nonetheless, in naturally acidified

waters of the Eastern South Pacific (where pH <7.8) the *E. huxleyi* community was dominated by A-over-calcified morphometric strains (von Dassow et al. 2018).

Global climate change will affect the exposure of algae to ultraviolet and photosynthetically active radiation (PAR) through changes in stratospheric ozone concentration, cloud albedo, concentrations of dissolved organic matter, and temperature-induced surface ocean stratification. However, Lorenzo et al. (2019) found that pCO_2 elevation did not significantly affect the photosynthetic sensitivity of *E. huxleyi* cells to ultraviolet (280-400 nm) and PAR radiation (400-700 nm). This might be explained by less light absorptivity of *E. huxleyi* cells under elevated pCO_2. However, exposure above a certain threshold inhibit *E. huxleyi*, because the repair rate becomes insufficient. It is notable that the photosynthetic apparatus of *E. huxleyi* shows a remarkable plasticity/acclimation faculty: this alga is able to withstand both high light conditions but at very low irradiance levels: Balch et al. (2014) report on under-ice vegetation of this alga, although they do not form a monospecific bloom in these conditions.

Environmental factors conditioning *E. huxleyi* blooms

Numerous studies found that water temperature, salinity, alkalinity/acidity, water column stratification, water movements (wind-driven vertical forcing, currents, eddies, fronts, advection), nutrients and trace metals availability, viruses infection, microzooplankton grazing, cysts seeding, water surface illumination, wind and wave driven surface water mixing, large-scale atmospheric baric formations, and air mass transport/decadal oscillations could all act as forcing factors (FFs) capable of affecting *E. huxleyi* blooms seasonally and, more importantly, interannually (Riebesell et al. 2000; Paasche 2002; Thierstein and Young 2004; Lipsen et al. 2007; Tyrrell and Young 2009; Rivero-Calle et al. 2015; Balch et al. 2016; Stelmakh and Gorbunova 2019). Against the background of longer-term changes in ocean acidification and water salinity, these factors may act both directly and through a sophisticated system of feedback mechanisms. It is therefore a challenge to disentangle the individual effects of FFs from each other. The effects of different FFs have mostly been studied individually, or for a limited number of co-acting FFs in laboratory/mesocosm conditions, as has been partly illustrated in the above section. This largely explains the reported broad ranges of FFs within which the growth of *E. huxleyi* was possible or was enhanced, potentially leading to plume formation. Very often water temperature, salinity, and CO_2 are considered as the main FFs determining the growth and extent of *E. huxleyi* blooms. Although valuable per se, such studies on a very limited number of environmental variables could not simulate the resulting impact of the entire set of FFs concomitantly acting under realistic conditions.

Notwithstanding the remarkable ability of *E. huxleyi* to grow under conditions unfavorable for algae of other taxonomic and functional groups (e.g., diatoms, flagellates, cyanobacteria), a highly irregular pattern of the registered two-decadal time-series of salinity, PIC, and ΔpCO_2 are indicative of a strong susceptibility of this alga outbursts to environmental forcing conditions (Kondrik et al. 2019; Silkin et al. 2019). Pozdnyakov et al. (2019) prioritized the FFs retrievable from two-decades of satellite data (1998–2019) from Subarctic and Arctic marine environments, viz. sea surface temperature and salinity (SST & Sal), PAR, water surface geostrophic current speed, mixed layer depth, and concentration of phytoplankton chlorophyll. Although the tested set of FFs did not explicitly include nutrient concentrations (NCs), the authors assumed that variations in the above variables indirectly account for the variations in NCs as well via such carbonate chemistry system parameters as alkalinity and basicity (Durairaj et al. 2015; Pozdnyakov et al. 2019). The representativeness of the employed FFs is supported by the fact that over the twenty years of observations the selected FFs have not failed to explain the patterns of either the areal extent or PIC content in *E. huxleyi* blooms. As expected, the prioritization results proved to be not only sea- but also time-specific: e.g., in the Barents Sea, SST was the most important FF, followed by PAR, while in the Bering Sea the sea surface salinity was the most important FF in the period 2001–2018, with PAR as a runner up, whereas SST was only in third place.

Although *E. huxleyi* is not generally considered to be a desired prey for zooplankton, nevertheless, some zooplankters can affect *E. huxleyi* blooms. In the Black Sea, up to 100% of the *Noctiluca scintillans* and *Oikopleura dioica* daily ration is constituted by *E. huxleyi* (Amelina et al. 2017). In the Barents Sea, large copepods *Metridia longa* and, to a lesser degree, *Calanus finmarchicus* are also reported as active consumers of *E. huxleyi* cells, however, their impact on the blooms was not directly assessed (Sergeeva et al. 2019). These findings fully support many of the earlier results from laboratory studies on *E. huxleyi* mortality due to grazing by copepods, including some of the earliest studies dating back to the early 1990s (Harris 1994).

Intra-annual and multi-year variations of *E. huxleyi* blooms in the current epoch of global warming

Rivero-Calle et al. (2015) conducted Random Forest statistical analysis of the in situ data from the Continuous Plankton Recorder Program executed in the North Atlantic during the last 45 years (1965–2010). They found that the occurrence of coccolithophore abundances over this time increased by more than 20%, while regional abundances in the 2000s proved to be at least ten times higher than in the 1960s. This long-term tendency was attributed to steadily increasing CO_2 and water temperature. Interannually, the observed variability was found to be modulated by the Atlantic Multidecadal Oscillation (AMO) through changes in the upward transport of nutrients, so that rising CO_2 and temperature and AMO (during positive periods) act conjointly. Nevertheless, these authors conjected that the observed growth rates might stabilize when pCO_2 reaches 500 ppm, i.e., in the really close future.

The time-series (January 2003-December 2010) obtained from satellite data (SCanning Imaging Absorption spectroMeter for Atmospheric ChartographY – SCIAMACY) for three regions in the world ocean (North Atlantic: at 53-63^{0}N, South Atlantic/eastern part of the Patagonian Shelf and South Pacific: at 38-48^{0}S) have not revealed any distinct tendency over that 8-year period, but there are appreciable interannual variations (Sadeghi et al. 2012).

Quantitative assessments of coccolithophore bloom areas (S) determined from Nimbus 7 CZCS imagery in the Subarctic North Atlantic (40-70^{0}N) and Subantarctic-Northern Antarctic (40-70^{0}S) latitudinal belts showed different patterns during 1979–1985. Whereas in the first region the bloom area declined, there was no evident trend in the second region. Extraordinarily high peaks in S were identified in 1980, 1983/1984, and 1985/1986 in the two regions, respectively (Brown and Yoder 1994).

Analyses of collated *in situ* databases from the Atlantic, Pacific, Indian, Arctic, and Southern oceans for the period 1991–2015 fail to show any clear patterns in $CaCO_3$ production (CP) distribution across the world ocean.

However, a strong relationship was established between cell abundance and CP, as well as CP surface and integrated CP (Daniels et al. 2018).

No significant tendencies in the areal coverage of coccolithophore blooms have been found from spaceborne images collected across 1997–2002 over the Black Sea, although there are large interannual variations. The Black Sea region is the second most important regarding the occurrence and extent of these algal (mostly *E. huxleyi*) blooms after the parts of the North Atlantic Ocean located above ~48^{0}N (Cokacar et al. 2004). Similarly, the surface distributions of *E. huxleyi* in the North Atlantic (35-68^{0}N) during 1998–2008 also shows large interannual variations, but no steady trend (Shutler et al. 2013). A similar result has been found from satellite observations of *E. huxleyi* blooms over Subarctic and Arctic seas for the period 1997–2013 (Kondrik et al. 2017): there was no indication of a sustained tendency in the occurrence of *E. huxleyi* blooms, but there were significant interannual variations both in the areal extent (S) (as exemplified in Fig.1 a-f) and CP. There is no tendency in variations of the integrated values of S in the time- series of blooms in either hemisphere over the period 1998–2010 (Moore et al. 2012). Kondrik et al. (2017) showed (Fig. 1) that blooms occurred annually in nearly 20 years of observations of subpolar and polar seas, but S and particulate inorganic carbon (PIC) varied between (<1 - 400) km^2 and (<1 to 250 kt) depending on the sea. Blooms within the Great Calcite Belt [~ (38-60), with the total area of 52·106 km] reportedly account for 26% of global PIC (Balch et al. 2016).

Despite the widespread lack of a tendency in bloom occurrence, *E. huxleyi* blooms in the central and especially northern parts of the Bay of Biscay displayed a distinct rise in bloom occurrence in the period 1979–2009 (Morozov et al. 2013). While there was no overall trend in *E. huxleyi* bloom occurrence in the Bering Sea, there was some interesting features of the interannual variability. There were two periods of remarkably massive blooms (in terms of both S and CP) during 1998–2001 and 2017–2019, and a significantly lower level of both S and CP in-between these periods of outbursts, which occurred in the wake of the strongest El Niño events during 1997–2019 (Lipsen et al. 2007; Pozdnyakov et al. 2020).

Intra-annual variations in S and PIC are bloom location-specific. Broadly speaking, *E. huxleyi* blooms develop in the wake of spring-time phytoplankton massive growth, which creates nutrient conditions favorable for *E. huxleyi* vegetation (Mikaelyan et al. 2015). Nonetheless, although the timing of bloom onset varies from year to year, *E. huxleyi* blooms are often reported to occur twice a year (as has been observed annually in the Black Sea since 1983 (Moncheva and Krastev 1997; Cokacar et al. 2004) or even for nearly the entire year (e.g., in the Bering Sea during 1997–2001; Kondrik et al. 2017, see Fig. 1f). Possibly they are stimulated by autumn noncalcifying phytoplankton blooming caused by intense entrainment of nutrients from below the euphotic zone (e.g., in the Black Sea), but in some other cases the respective driving mechanisms remain the subject of controversy and debate.

During the last decades, intra-annual variations in S, PIC, and the timings of bloom onset and duration are generally very significant as it is reported from a variety of marine environments, e.g., the Barents Sea (Smyth et al. 2004; Burenkov et al. 2011; Kondrik et al. 2017), Black Sea (Kopelevich et al. 2013; Mikaelyan et al. 2015; Kubryakov et al. 2019), Bay of Biscay (Morozov et al. 2013), North Atlantic (Shutler et al. 2013), Arctic Ocean (Petrenko et al. 2013), and world-wide (Brown and Yoder 1994; Moore et al. 2012; Sadeghi et al. 2012).

Future tendencies in *E. huxleyi* bloom dynamics in the warming climate

E. huxleyi have a remarkable physiological plasticity because the pan-genome allows associated transcriptional responses which assures the success of this alga in a variety of environmental conditions including those arising from nutrient limitations (Alexander et al. 2020) or acidification. However, these abilities do not imply a complete immunity of this alga to environmental changes including those resulting from ongoing climate change.

Expectedly, an increase in $_pCO_2$ is beneficial for *E. huxleyi* photosynthesis (and hence PIC production) rather than calcification as this alga has a relatively inefficient carbon concentrating mechanism. The latter responds positively to increases in HCO^-_3, and suffers from inhibition by increasing H^+ ions (Section 3). Therefore, in the forthcoming changing climate, the carbonate chemistry system would experience both detrimental and stimulating effects (Rivero-Calle et al. 2015).

Laboratory studies simulating the forthcoming climatological shifts (enhancement of ocean acidification and warming) seem strongly indicative that through evolutionary change, *E. huxleyi* is better suited to temperature adaptation than to acidification. Under combined enhanced warming and acidification, PIC production rose by 191% compared to non-adapted controls (Shutler et al. 2013).

Indeed, there is experimental evidence that *E. huxleyi* is vulnerable to frequent thermal variations, especially at elevated water temperatures expected in the future at lower latitudes (Wang et al. 2019).

Individually, climate models have large uncertainties in projected changes of the identified abiotic FFs that drive changes in *E. huxleyi*. This necessitates efforts to constrain model ensemble uncertainty, e.g., through subsampling based on the model skill in simulating historical climate. According to the selected best model ensembles (Gnatiuk et al. 2020) for scenarios of greenhouse gas concentration trajectory – RCP4.5 and RCP8.5, the main projected FFs changes in the Arctic are increasing sea surface temperature, declining sea water salinity, and reduction of short-wave solar radiation. The trends of changes in wind and current speeds are not statistically significant (~6x10^{-4} ms^{-1}yr^{-1} & ~10^{-4} ms^{-1}yr^{-1}, respectively). Simulations with a generalized coccolithophore model utilizing the input data from the Community Earth System Model Large Ensemble indicate that a 2-3° ocean temperature rise over the 21st century will entail a globally-averaged 10% increase in these species' growth (Krumhardt et al. 2017). At high latitudes, this increase is expected to proceed concomitantly with enhanced calcification. A ubiquitous doubling of oceanic pCO_2 will potentially lead to a moderate cell growth and a 25% decline in the calcification rate. Induced by warming, strengthening of surface ocean stratification may incur calcification intensification and a 25% reduction in growth because of nutrient depletion. Although such projections do not account for changes in the light limitation, *E. huxleyi* strains and co-occurring community species, a concomitant action of the above FFs will arguably result in dwindling calcification and growth rate in the majority of low to mid latitudes (but not at high latitudes) at the end of the current century (Krumhardt et al. 2017).

CONCLUDING REMARKS

Analysis of the reviewed publications suggests that all major and basic aspects of the *E. huxleyi* cell composition

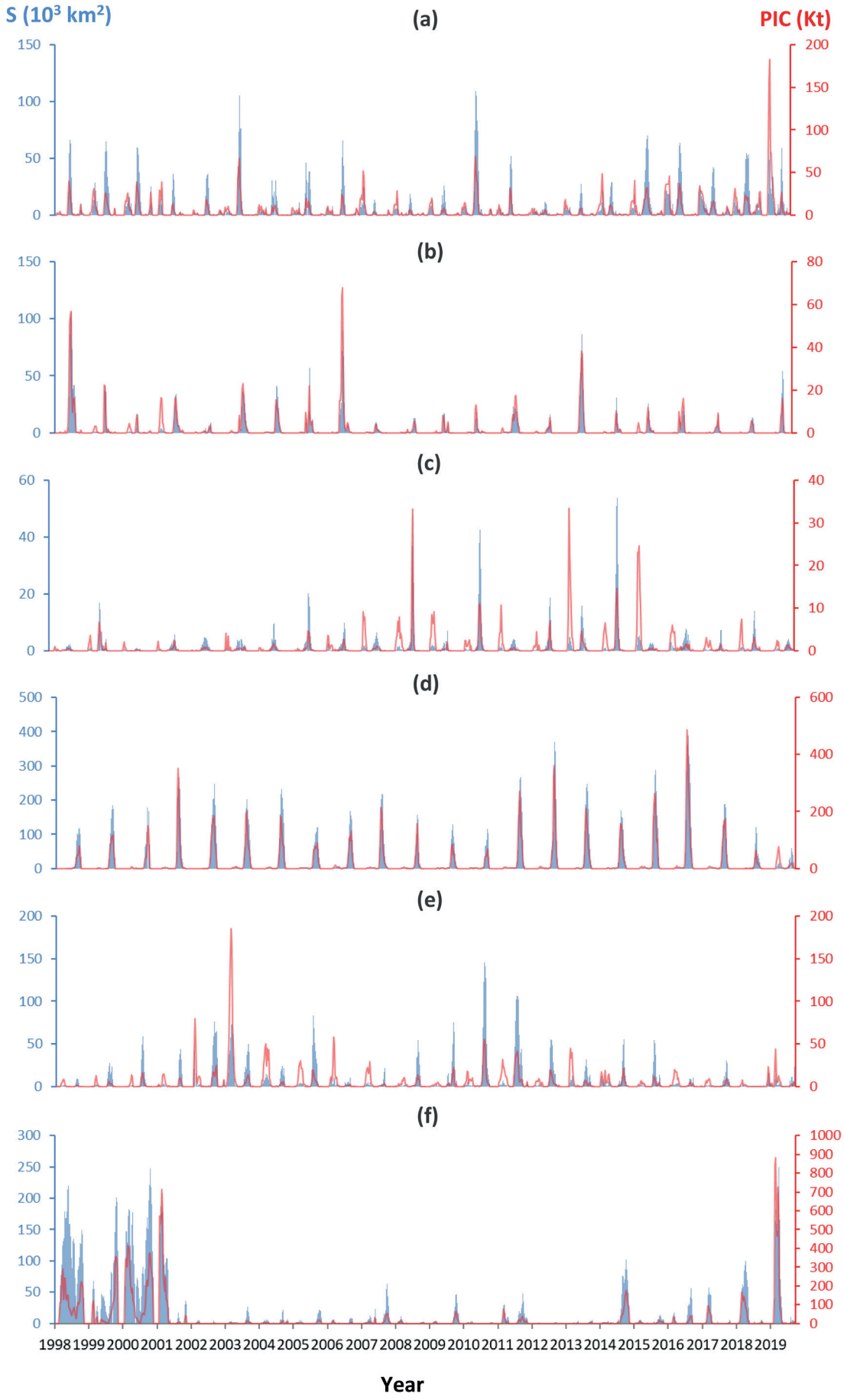

Fig. 1. Interannual variations in the occurrence of *E. huxleyi* bloom outbursts, their areal extent (blue line), and within-bloom PIC - particulate inorganic carbon content (red line) in the North (a), Norwegian (b), Greenland (c), Barents (d), and Bering (e) seas as retrieved from space observations during 1998–2019 (Kondrik et al. 2017, Pozdnyakov et al. 2020).

and functioning have been clarified to a large extent, and that indeed this alga is one of the best-studied marine organisms. At the same time, a wide range of important issues remain unexplored or insufficiently investigated. Not attempting to address all of them, we mention here only those that appear as serious obstacles to understanding and evaluating the present and future role of coccolithophores in the changing global environment.

In terms of cell morphology, there is still no insight into the causes and type of life cycle interchange between calcified diploid (2N) and non-calcified scale bearing haploid (1N) phases/forms (syngamy or meiosis?) or else between mutant naked diploid (2N) and haploid (1N) phases/forms (meiosis?). There is still no definitive prioritization of factors determining the formation and global geographic distribution of morphotypes A, B/C, overcalcified A and R forms.

With regard to genetic diversity, there is insufficient insight into how the core genome is complemented with specific genes conditioning the environmental fitness of *E. huxleyi* ecotypes to a wide range of environmental conditions, determining intricate intracellular transport routes (especially for Ca^{2+} ions), and initiation of the calcification reaction. The capacity of *E. huxleyi* to mixotrophy remains mostly conjecture, but is nevertheless a central issue in this alga nutrition depletion tolerance.

The physiological role of DMSP (as DMS precursor) in *E. huxleyi* cells and the driving factors/agents/mechanisms triggering DMSP breakdown reactions still remain obscure. Also, the organic and inorganic precursors of CH_4 produced in this alga are not sufficiently studied, particularly in conditions of calcium carbonate oversaturated waters.

A big issue is the environmental FFs affecting the formation of massive *E. huxleyi* blooms. Many FFs have been proposed, but results of investigations conducted primarily in laboratory/mesocosm conditions are of limited value because it is unclear how well they can translate to real conditions, particularly in terms of the variety of co-acting FFs. Meanwhile, the prioritization of FFs that can co-occur in real ocean conditions is of particular importance.

It is clear that due to the large extent and high intra- and interannual temporal variability of *E. huxleyi* blooms, use of satellite observations is the only means to perform statistically reliable FFs prioritization, quantification of bloom extent, release of calcite, enrichment of surface water with dissolved carbon dioxide, and trace down over long time periods the tendencies in the development of the *E. huxleyi* phenomenon and its environmental impacts. Such studies have already been conducted in individual seas, but they need to be extended to cover the entire world ocean.

Finally, in conjunction with the emerging global and regional climate models, biological models of *E. huxleyi* blooms applicable to the great variety of marine/oceanic environments are indispensable for forecasting (at least over a mid-term time-period) the forthcoming climatic and environmental role of *E. huxleyi* blooms in changing the world around us. Although the first tentative steps in this direction have been taken, much more effort is needed to develop and apply these models.

REFERENCES

Alcolombri U., Ben-Dor S., Feldmesser E., Levi Y., Tawfik D. S. and Vardi A. (2015). Identification of the algal dimethyl sulfide–releasing enzyme: A missing link in the marine sulfur cycle. Science, 348(6242), 1466-1469, DOI: 10.1126/science.aab1586.

Alekin O. (1966). Ocean chemistry. Leningrad: Gidrometizdat, 344p. (in Russian).

Alexander H., Rouco M., Sheean T. H. and Dyhrman S. T. (2020). Transcriptional response of Emiliania huxleyi under changing nutrient environments in the North Pacific Subtropical Gyre. Environmental Microbiology, 22(5), 1847-1860, DOI: 10.1111/1462-2920.14942.

Althoff F., Benzing K., Comba P., McRoberts C., Boyd D. R., Greiner S. and Keppler F. (2014). Abiotic methanogenesis from organosulphur compounds under ambient conditions. Nature Communications, 5(1), 1-9, DOI: 10.1038/ncomms5205.

Amelina A., Segeeva V., Arashkevich E., Drifts A., Louppova N. and Solovyev K. (2017). Feeding of the dominant herbivorous plankton species in the Black Sea and their role in coccolithophorid consumption. Oceanology, 57(6), 806-816, DOI: 10.1134/S000143701706011X.

Bach L.T., Riebesell U. and Schulz K. G. (2011). Distinguishing between the effects of ocean acidification and ocean carbonation in the coccolithophore Emiliania huxleyi. Limnology and Oceanography, 56(6), 2040-2050, DOI: 10.4319/lo.2011.56.6.2040.

Bach L.T., Mackinder L.C., Schulz K.G., Wheeler G., Schroeder D.C., Brownlee C. and Riebesell U. (2013). Dissecting the impact of CO2 and pH on the mechanisms of photosynthesis and calcification in the coccolithophore Emiliania huxleyi. New Phytologist, 199(1), 121-134, DOI: 10.1111/nph.12225.

Bach L.T., Riebesell U., Gutowska M.A., Federwisch L. and Schulz K.G. (2015). A unifying concept of coccolithophore sensitivity to changing carbonate chemistry embedded in an ecological framework. Progress in Oceanography, 135, 125-138, DOI: 10.1016/j.pocean.2015.04.012.

Balch W.M., Bowler B.C., Lubelczyk L.C. and Stevens M.W. (2014). Aerial extent, composition, bio-optics and biogeochemistry of a massive under-ice algal bloom in the Arctic. Deep-Sea Research II, 105, 42-58, DOI: 10.1016/j.dsr2.2014.04.001.

Balch W.M., Kilpatrick K., Holligan P.M. and Cucci T. (1993). Coccolith production and detachment by Emiliania huxleyi (Prymnesiophyceae). Journal of Phycology, 29(5), 566-575, DOI: 10.1111/j.0022-3646.1993.00566.x.

Balch W.M., Bates N.R., Lam P.J., Twining B.S., Rosengard S.Z., Bowler B.C., Drapeau D.T., Garley R., Lubelczyk L.C., Mitchell C. and Rauschenberg S. (2016). Factors regulating the Great Calcite Belt in the Southern Ocean and its biogeochemical significance. Global Biogeochemical Cycles, 30(8), 1124-1144, DOI: 10.1002/2016GB005414.

Benner I., Diner R.E., Lefebvre S.C., Li D., Komada T., Carpenter E.J. and Stillman J.H. (2013). Emiliania huxleyi increases calcification but not expression of calcification-related genes in long-term exposure to elevated temperature and pCO2. Philosophical Transactions of the Royal Society B, 368(1627), 20130049, DOI: 10.1098/rstb.2013.0049.

Boyd P.W. and Hutchins D.A. (2012). Understanding the responses of ocean biota to a complex matrix of cumulative anthropogenic change. Marine Ecology Progress Series, 470, 125-135, DOI: 10.3354/meps10121.

Brown C. and Yoder J. (1994). Coccolithophorid blooms in the Global ocean. Journal of Geophysical Research, 99(C4): 7467-7482, DOI: 10.1029/93JC02156.

Brownlee C. and Taylor A. (2004). Calcification in coccolithophores: A cellular perspective. In: H. R. Thierstein, J. R. Young, ed., Coccolithophores. Springer, Berlin, Heidelberg, 31-49, DOI: 10.1007/978-3-662-06278-4_2.

Brownlee C., Wheeler G.L. and Taylor A.R. (2015). Coccolithophore biomineralization: New questions, new answers. Seminars in Cell & Developmental Biology, 46, 11-16, DOI: 10.1016/j.semcdb.2015.10.027.

Burenkov V.I., Kopelevich O.V., Rat'kova T.N. and Sheberstov S.V. (2011). Satellite observations of coccolithophorids in the Barents Sea. Okeanologiya. 51(5), 818-826 (in Russian).

Charalampopoulou A., Poulton A.J., Bakker D.C., Lucas M.I., Stinchcombe M.C. and Tyrrell T. (2016). Environmental drivers of coccolithophore abundance and calcification across Drake Passage (Southern Ocean). Biogeosciences, 13(21), 5917-5935, DOI: 10.5194/bg-13-5917-2016.

Cokacar T., Oguz T. and Kubilay N. (2004). Satellite-detected early summer coccolithophore blooms and their interannual variability in the Black Sea. Deep-Sea Research I, 51(8), 1017-1031, DOI: 10.1016/j.dsr.2004.03.007.

Daniels C.J., Poulton A.J., Balch W.M., Marañón E., Adey T., Bowler B.C. and Tyrrell T. (2018). A global compilation of coccolithophore calcification rates. Earth System Science Data, 10(4), 1859-1876, DOI: 10.5194/essd-10-1859-2018.

Dlugokencky E. (2016). Annual Mean Carbon Dioxide Data. Earth System Research Laboratory, National Oceanic & Atmospheric Administration.

Durairaj P., Sarangi R.K., Ramalingam S., Thirunavukarassu T. and Chauhan P. (2015). Seasonal nitrate algorithms for nitrate retrieval using OCEANSAT-2 and MODIS-AQUA satellite data. Environmental Monitoring and Assessment, 187(4), 1-15, DOI: 10.1007/s10661-015-4340-x.

Evans C., Kadner S., Darroch L., Wilson W., Liss P. and Malin G. (2007). The relative significance of viral lysis and microzooplankton grazing as pathways of dimethylsulphoniopropionate (DMSP) cleavage: An Emiliania huxleyi culture study, Limnological and Oceanographic Methods, 53(3), 1036-1045, DOI: 10.4319/lo.2007.52.3.1036.

Feng Y., Hare C. E., Leblanc K., Rose J. M., Zhang Y., DiTullio G. R. and Hutchins D. A. (2009). The effects of increased pCO2 and temperature on the North Atlantic spring bloom: I. Phytoplankton community and biogeochemical response. Marine Ecology Progress Series, 388, 13-25, DOI: 10.3354/meps08133.

Feng Y., Roleda M. Y., Armstrong E., Law C. S., Boyd P. W. and Hurd C. L. (2018). Environmental controls on the elemental composition of a Southern Hemisphere strain of the coccolithophore Emiliania huxleyi. Biogeosciences, 15(2), 581-595, DOI: 10.5194/bg-15-581-2018.

Fiorini S., Middelburg J. J. and Gattuso J.-P. (2011). Testing the effects of elevated pCO2 on coccolithophores (Prymnesiophyceae): comparison between haploid and diploid life stages. Journal of Phycology, 47(6), 1281-1291, DOI: 10.1111/j.1529-8817.2011.01080.x.

Frada M. J., Bidle K. D., Probert I. and de Vargas C. (2012). In situ survey of life cycle phases of the coccolithophore Emiliania huxleyi (Haptophyta). Environmental Microbiology, 14(6), 1558-1569, DOI: 10.1111/j.1462-2920.2012.02745.x.

Gao K., Ruan Z., Villafane V. E., Gattuso J. P. and Helbling E. W. (2009). Ocean acidification exacerbates the effect of UV radiation on the calcifying phytoplankter Emiliania huxleyi. Limnology and Oceanography, 54(6), 1855-1862, DOI: 10.4319/lo.2009.54.6.1855.

Gnatiuk N., Radchenko I., Davy R., Morozov E. and Bobylev L. (2020). Simulation of factors affecting Emiliania huxleyi blooms in Arctic and sub-Arctic seas by CMIP5 climate models: model validation and selection. Biogeosciences, 17(4), 1199-1212, DOI: 10.5194/bg-17-1199-2020.

Godoi R. H. M., Aerts K., Harlay J., Kaegi R., Ro C. U., Chou L. and van Grieken R. (2008). Organic surface coating on coccolithophores Emiliania huxleyi: Its determination and implication in the marine carbon cycle. Microchemical Journal, 91(2), 266-271, DOI: 10.1016/j.microc.2008.12.009.

Godrijan J., Drapeau D. and Balch W. M. (2020). Mixotrophic uptake of organic compounds by coccolithophores. Limnology and Oceanography, 65(6), 1410-1421, DOI:10.1002/lno.11396.

Green J.C., Course P.A. and Tarran G.A. (1996). The life-cycle of Emiliania huxleyi: A brief review and a study of relative ploidy levels analysed by flow cytometry. Journal of Marine Systems, 9(1-2), 33-44, DOI: 10.1016/0924-7963(96)00014-0.

Hagino K., Bendif E.M., Young J.R., Kogame K., Probert I., Takano Y., Horiguchi T., Vargas C. and Okada H. (2011) New evidence for morphological and genetic variation in the cosmopolitan coccolithophore Emiliania huxleyi (Prymnesiophyceae) from the COX1b–ATP4 genes. Journal of Phycology, 47(5), 1164-1176, DOI: 10.1111/j.1529-8817.2011.01053.x.

Harris R. P. (2004). Zooplankton grazing on the coccolithophore Emiliania huxleyi and its role in inorganic carbon flux. Marine Biology, 119, 431-49, DOI: 10.1007/BF00347540.

Hayden L. (2013). Effects of ocean acidification and nutrient enrichment on growth of the planktonic coccolithophore Emiliania huxleyi. Available at: https://www.mbl.edu/ses [Accessed 7 February 2021].

Iglesias-Rodriguez M.D., Halloran P.R., Rickaby R.E., Hall I.R., Colmenero-Hidalgo E., Gittins J.R. and Boessenkool K.P. (2008). Phytoplankton calcification in a high-CO2 world. Science, 320 (5874), 336-340, DOI: 10.1126/science.1154122.

Iglesias-Rodriguez M.D., Schofield O.M., Batley J., Medlin L.K. and Hayes P.K. (2006). Intraspecific genetic diversity in the marine coccolithophore Emiliania huxleyi (Prymnesiophyceae): the use of microsatellite analysis in marine phytoplankton population studies. Journal of Phycology, 42(3), 526-536, DOI: 10.1111/j.1529-8817.2006.00231.x.

Johnsen S.A.L. and Bollmann J. (2020). Coccolith mass and morphology of different Emiliania huxleyi morphotypes: A critical examination using Canary Islands material. PLoS ONE, 15(3), e0230569, DOI: 10.1371/journal.pone.0230569.

Kaffes A., Thoms S., Trimborn S., Rost B., Langer G., Richter K. U. and Giordano M. (2010). Carbon and nitrogen fluxes in the marine coccolithophore Emiliania huxleyi grown under different nitrate concentrations. Journal of Experimental Marine Biology and Ecology, 393(1-2), 1-8, DOI: 10.1016/j.jembe.2010.06.004.

Klintzsch T., Langer G., Nehrke G., Wieland A., Lenhart K. and Keppler F. (2019). Methane production by three widespread marine phytoplankton species: release rates, precursor compounds and potential relevance for the environment. Biogeosciences, 16(20), 4129-4144, DOI: 10.5194/bg-16-4129-2019.

Kondrik D.V., Kazakov E.E., Pozdnyakov D.V. and Johannessen O.M. (2019). Satellite evidence for enhancement of columnal mixing ratio of atmospheric CO2 over E. huxleyi blooms. Transactions of the Karelian Research Centre of the Russian Academy of Sciences, 9, 125-135.

Kondrik D.V., Pozdnyakov D.V. and Johannessen O.M. (2018). Satellite evidence that E. huxleyi phytoplankton blooms weaken marine carbon sinks. Geophysical Research Letters, 45(2), 846-854, DOI: 10.1002/2017GL076240.

Kondrik D.V., Pozdnyakov D.V. and Pettersson L.H. (2017). Particulate inorganic carbon production within E. huxleyi blooms in subpolar and polar seas: a satellite time series study (1998-2013). International Journal of Remote Sensing, 38(22), 6179-6205, DOI: 10.1080/01431161.2017.1350304.

Kopelevich O., Burenkov V., Sheberstov S., Vazyulya S., Kravchishina M., Pautova L. and Grigoriev A. (2013). Satellite monitoring of coccolithophore blooms in the Black Sea from ocean color data. Remote Sensing of Environment, 146, 113-123, DOI: 10.1016/j.rse.2013.09.009.

Krumhardt K.M., Lovenduski N.S., Iglesias-Rodriguez M.D. and Kleypas J.A. (2017). Coccolithophore growth and calcification in a changing ocean. Progress in Oceanography, 159, 276-295, DOI: 10.1016/j.pocean.2017.10.007.

Kubryakov A. A., Mikaelyan A. S. and Stanichny S. V. (2019). Summer and winter coccolithophore blooms in the Black Sea and their impact on production of dissolved organic matter from Bio-Argo data. Journal of Marine Systems, 199, 103220, DOI: 10.1016/j.jmarsys.2019.103220.

Lana A., Bell T. G., Simó R., Vallina S. M., Ballabrera–Poy J., Kettle A. J. and Liss P. S. (2011). An updated climatology of surface dimethylsulfide concentrations and emission fluxes in the global ocean. Global Biogeochemical Cycles, 25(1), GB1004, DOI: 10.1029/2010GB003850.

Lenhart K., Klintzsch T., Langer G., Nehrke G., Bunge M., Schnell S. and Keppler F. (2016). Evidence for methane production by the marine algae Emiliania huxleyi. Biogeosciences, 13(10), 3163-3174, DOI: 10.5194/bg-13-3163-2016.

León P., Walsham P., Bresnan E., Hartman S. E., Hughes S., Mackenzie K. and Webster L. (2018). Seasonal variability of the carbonate system and coccolithophore Emiliania huxleyi at a Scottish Coastal Observatory monitoring site. Estuarine, Coastal and Shelf Science, 202, 302-314, DOI: 10.1016/j.ecss.2018.01.011.

Lipsen M.S., Crawford D.W., Gower J. and Harrison P.J. (2007). Spatial and temporal variability in coccolithophore abundance and production of PIC and POC in the NE subarctic during El Niño (1998) and La Niña (1999) and 2000. Progress in Oceanology, 75(2), 304-325, DOI: 10.1016/j.pocean.2007.08.004.

Loebl M., Cockshutt A.M., Campbell D.A. and Finkel Z.V. (2010). Physiological basis for high resistance to photoinhibition under nitrogen depletion in Emiliania huxleyi. Limnology and Oceanography, 55(5), 2150-2160, DOI: 10.4319/lo.2010.55.5.2150.

Lohbeck K.T., Riebesell U. and Reusch T.B.H. (2012). Adaptive evolution of a key phytoplankton species to ocean acidification. Nature Geosciences, 5, 346-351, DOI: 10.1038/ngeo1441.

Lorenzo M.R., Neale P.J., Sobrino C., León P., Vázquez V., Bresnan E. and Segovia M. (2019). Effects of elevated CO2 on growth, calcification, and spectral dependence of photoinhibition in the coccolithophore Emiliania huxleyi (Prymnesiophyceae). Journal of Phycology, 55(4), 775-788, DOI: 10.1111/jpy.12885.

Mackinder L., Wheeler G., Schroeder D., von Dassow P., Riebesell U. and Brownlee C. (2011). Expression of biomineralization-related ion transport genes in Emiliania huxleyi. Environmental Microbiology, 13(12), 3250-3265, DOI: 10.1111/j.1462-2920.2011.02561.x.

Malin G. and Steinke M. (2004). Dimethyl sulfide production: what is the contribution of the coccolithophores? In: H. Thierstein and J. Young, ed., Coccolithophores, Heidelberg: Springer, Berlin, Heidelberg, 127-164, DOI: 10.1007/978-3-662-06278-4_6.

Maranón E., Balch W. M., Cermeno P., González N., Sobrino C., Fernández A. and Pelejero C. (2016). Coccolithophore calcification is independent of carbonate chemistry in the tropical ocean. Limnology and Oceanology, 61(4), 1345-1357, DOI: 10.1002/lno.10295.

Martin J.H., Coale K.H., Johnson K.S., Fitzwater S.E., Gordon R.M., Tanner S.J. and Tindale N. W. (1994). Testing the iron hypothesis in ecosystems of the equatorial Pacific Ocean. Nature, 371, 123-129, DOI: 10.1038/371123a0.

Martiny A.C., Vrugt J.A. and Lomas M.W. (2014). Concentrations and ratios of particulate organic carbon, nitrogen, and phosphorus in the global ocean. Scientific Data, 1, 140048, DOI: 10.1038/sdata.2014.48.

Merico A., Tyrrell T., Lessard E.J., Oguz T., Stabeno P.J., Zeeman S.I. and Whitledge T.E. (2004). Modelling phytoplankton succession on the Bering Sea shelf: role of climate influences and trophic interactions in generating Emiliania huxleyi blooms 1997-2000. Deep Sea Research Part I: Oceanographic Research Papers, 51, 1803-1826, DOI: 10.1016/j.dsr.2004.07.003.

Meyer J. and Riebesell U. (2015). Reviews and syntheses: Responses of coccolithophores to ocean acidification: a meta-analysis. Biogeosciences, 12(6), 1671-1682, DOI: 10.5194/bg-12-1671-2015.

Mikaelyan A.S., Pautova L.A., Chasovnikov V.K., Mosharov S.A. and Silkin V.A. (2015). Alternation of diatoms and coccolithophores in the north-eastern Black Sea: a response to nutrient changes. Hydrobiologia, 755(1), 89-105, DOI: 10.1007/s10750-015-2219-z.

Miller C.B., Frost B.W., Wheeler P.A., Landry M.R., Welschmeyer N. and Powell T.M. (1991). Ecological dynamics in subarctic Pacific, a possibly iron-limited ecosystem. Limnology and Oceanology, 36(8), 1600-1615, DOI: 10.4319/lo.1991.36.8.1600.

Mohan R., Mergulhao L.P., Guptha M.V.S., Rajakumar A., Thamban M., AnilKumar N. and Ravindra R. (2008). Ecology of coccolithophores in the Indian sector of the Southern Ocean. Marine Micropaleontology, 67(1-2), 30-45, DOI: 10.1016/j.marmicro.2007.08.005.

Moncheva S. and Krastev A. (1997). Some aspects of phytoplankton long-term alterations off Bulgarian Black Sea Shelf. In: E. Ozsoy, A. Mikaelyan, ed., Sensitivity to Change: Black Sea, Baltic Sea and North Sea. Dordrecht: Springer, Dordrecht, 79-93, DOI: 10.1007/978-94-011-5758-2_7.

Moore T.S., Dowel M.D. and Franz B.A. (2012). Detection of coccolithophore blooms in ocean color imagery: A generalized approach for use with multiple sensors. Remote Sensing of Environment, 117, 249-263, DOI: 10.1016/j.rse.2011.10.001.

Morozov E.A., Kondrik D.V., Chepikova S.S. and Pozdnyakov D.V. (2019). Atmospheric columnar CO2 enhancement over E. huxleyi blooms: case studies in the North Atlantic and Arctic waters. Limnology and Oceanology Series, 3, 28-33, DOI: 10.17076/lim989.

Morozov E., Pozdnyakov D.V., Smyth T., Sychev V. and Grassl H. (2013). Space-borne study of seasonal, multi-year and decadal phytoplankton dynamics in the Bay of Biscay. International Journal of Remote Sensing, 34(4), 1297-1331, DOI: 10.1080/01431161.2012.718462.

Muggli D.L. and Harrison P.J. (1996). Effects of nitrogen source on physiology and metal nutrition of Emiliania huxleyi grown under different iron and light conditions. Marine Ecology Progress Series, 130, 255-267, DOI: 10.3354/meps130255.

Müller M.N. (2019). On the Genesis and Function of Coccolithophore Calcification. Frontiers in Marine Science, 6, 49, DOI: 10.3389/fmars.2019.00049.

Müller M.N., Antia A.N. and LaRoche J. (2008). Influence of cell cycle phase on calcification in the coccolithophore Emiliania huxleyi. Limnology and Oceanography, 53(2), 506-512, DOI: 10.4319/lo.2008.53.2.0506.

Müller M.N., Trull T.W. and Hallegraeff G.M. (2015). Differing responses of three Southern Ocean Emiliania huxleyi ecotypes to changing seawater carbonate chemistry. Marine Ecology Progress Series, 531, 81-90, DOI: 10.3354/meps11309.

Müller M.N., Beaufort L., Bernard O., Pedrotti M.L., Talec A. and Sciandra A. (2012). Influence of CO2 and nitrogen limitation on the coccolith volume of Emiliania huxleyi (Haptophyta). Biogeosciences, 9(10), 4155-4167, DOI: 10.5194/bg-9-4155-2012.

Nissen C., Vogt M., Münnich M., Gruber N. and Haumann F.A. (2018). Factors controlling coccolithophore biogeography in the Southern Ocean. Biogeosciences, 15(22), 6997-7024, DOI: 10.5194/bg-15-6997-2018.

Oviedo A.M., Langer G. and Ziveri P. (2014). Effects of phosphorus limitation on coccoliths and elemental ratios in Mediterranean strains of the coccolithophore Emiliania huxleyi. Journal of Experimental Marine Biology and Ecology, 459, 105-113, DOI: 10.1016/j.jembe.2014.04.021.

Oziel L., Baudena A., Ardyna M., Massicotte P., Randelhoff A., Sallée J. B. and Babin M. (2020). Faster Atlantic currents drive poleward expansion of temperate phytoplankton in the Arctic Ocean. Nature Communications, 11(1), 1-8, DOI: 10.1038/s41467-020-15485-5.

Paasche E. (2002). A review of the coccolithophorid Emiliania huxleyi (Prymneosiophyceae) with particular reference to growth, coccolith formation, and calcification-photosynthesis interactions. Phycologia, 40(6), 503-529, DOI: 10.2216/i0031-8884-40-6-503.1.

Pantorno A., Holland D.P., Stojkovic S. and Beardall J. (2013). Impacts of nitrogen limitation on the sinking rate of the coccolithophorid Emiliania huxleyi (Prymneosiophyceae). Phycologia, 52(3), 288-294, DOI: 10.2216/12-064.1.

Petrenko D., Pozdnyakov D., Johannessen J., Counillon F. and Sychov V. (2013). Satellite-driven multi-year trend in primary production in the Arctic Ocean. International Journal of Remote Sensing, 34(11), 3903-3937, DOI: 10.1080/01431161.2012.762698.

Poulton A.J., Young J.R., Bates N.R. and Balch W. (2011). Biometry of detached Emiliania huxleyi coccoliths along the Patagonian Shelf. Marine Ecology Progress Series, 443, 1-17, DOI: 10.3354/meps09445.

Pozdnyakov D., Chepikova S. and Kondrik D. (2020). A possible teleconnection mechanism of initiation of Emiliania huxleyi outbursts in the Bering Sea in 1998-2001 and 2018-2019. Proceedings of SPIE, 11534, 1153412, DOI: 10.1117/12.2573272.

Pozdnyakov D., Kondrik D., Kazakov E. and Chepikova S. (2019). Environmental conditions favoring coccolithophore blooms in subarctic and arctic seas: a 20-year satellite and multi-dimensional statistical study. Proceedings of SPIE, 11150, 111501W, DOI: 10.1117/12.2547868.

Raffi I., Backman J., Fornaciari E., Pälike H., Rio D., Lourens L. and Hilgen F. (2006). A review of calcareous nannofossil astrobiochronology encompassing the past 25 million years. Quaternary Science Reviews, 25(23-24), 3113-3137, DOI: 10.1016/j.quascirev.2006.07.007.

Ramos J.B., Müller M. and Riebesell U. (2010). Short-term response of the coccolithophore Emiliania huxleyi to an abrupt change in seawater carbon dioxide concentrations. Biogeosciences, 7(1), 177-186, DOI: 10.5194/bg-7-177-2010.

Read B.A., Kegel J., Klute M.J., Kuo A., Lefebvre S.C., Maumus F. and Grigoriev I.V. (2013). Pan genome of the phytoplankton Emiliania underpins its global distribution. Nature, 499(7457), 209-213, DOI: 10.1038/nature12221.

Redfield A.C. (1934). On the proportions of organic derivatives in sea water and their relation to the composition of plankton. In: James Johnstone Memorial volume. Liverpool: University Press of Liverpool, 176-192.

Richier S., Fiorini S., Kerros M.E., von Dassow P. and Gattuso J.P. (2010). Response of the calcifying coccolithophore Emiliania huxleyi to low pH/high pCO2: from physiology to molecular level. Marine Biology, 158(3), 551-560, DOI: 10.1007/s00227-010-1580-8.

Riebesell U., Zondervan I., Rost B., Tortell P.D., Zeebe R.E. and Morel F.M. (2000). Reduced calcification of marine plankton in response to increased atmospheric CO2. Nature, 407(6802), 364-367, DOI: 10.1038/35030078.

Riegman R., Stolte W., Noordeloos A.A.M. and Slezak D. (2000). Nutrient uptake and alkaline phosphatase (ec 3:1:3:1) activity of Emiliania huxleyi (Prymnesiophyceae) during growth under N and P limitation in continuous cultures. Journal of Phycology, 36(1), 87-96, DOI: 10.1046/j.1529-8817.2000.99023.x.

Rigual-Hernández A.S., Trull T.W., Flores J.A., Nodder S.D., Eriksen R., Davies D.M., Hallegraeff G.M.F., Sierro J., Patil S.M., Cortina A., Ballegeer A.M., Northcote L.C., Abrantes F. and Rufino M.M. (2020). Full annual monitoring of Subantarctic Emiliania huxleyi populations reveals highly calcified morphotypes in high-CO2 winter conditions. Scientific Reports, 10, 2594-2599, DOI: 10.1038/s41598-020-59375-8.

Rivero-Calle S., Gnanadesikan A., Del Castillo C.E., Balch W.M. and Guikema S.D. (2015). Multidecadal increase in North Atlantic coccolithophores and potential role of rising CO2. Science, 350(6267), 1533-1537, DOI: 10.1126/science.aaa8026.

Rokitta S.D. and Rost B. (2012). Effects of CO2 and their modulation by light in the life-cycle stages of the coccolithophore Emiliania huxleyi. Limnology and Oceanography, 57(2), 607-618, DOI: 10.4319/lo.2012.57.2.0607.

Rost B. and Riebesell U. (2004). Coccolithophores and the biological pump: responses to environmental changes. In: H.R. Thierstein, J.R. Young, ed., Coccolithophores: from molecular processes to global impact. Heidelberg: Springer, Berlin, Heidelberg, 99-125, DOI: 10.1007/978-3-662-06278-4_5.

Sadeghi A., Dinter T., Vountas M., Taylor B., Altenburg-Soppa M. and Bracher A. (2012). Remote sensing of coccolithophore blooms in selected oceanic regions using the PhytoDOAS method applied to hyper-spectral satellite data. Biogeosciences, 9(6), 2127-2143, DOI: 10.5194/bg-9-2127-2012.

Schlüter L., Lohbeck K.T., Gutowska M.A., Gröger J.P., Riebesell U. and Reusch T.B. (2014). Adaptation of a globally important coccolithophore to ocean warming and acidification. Nature Climate Change, 4(11), 1024-1030, DOI: 10.1038/nclimate2379.

Segovia M., Lorenzo M.R., Iñiguez C. and García-Gómez C. (2018). Physiological stress response associated with elevated CO2 and dissolved iron in a phytoplankton community dominated by the coccolithophore Emiliania huxleyi. Marine Ecology Progress Series, 586, 73-89, DOI: 10.3354/meps12389.

Sergeeva V.M., Drits A. and Flint M.V (2019). Specific features of distribution and nutrition of dominant zooplankton species under conditions of autumnal growth of coccolithophorids in the eastern Barents Sea. Oceanology, 59(5), 734-745 (in Russian), DOI: 10.31857/S0030-1574595734-745.

Sett S., Bach L.T., Schulz K.G., Koch-Klavsen S., Lebrato M. and Riebesell U. (2014). Temperature modulates coccolithophorid sensitivity of growth, photosynthesis and calcification to increasing seawater pCO2. PLoS ONE, 9(2), e88308, DOI: 10.1371/journal.pone.0088308.

Shi D., Xu Y. and Morel F. M. M. (2009). Effects of the pH/pCO2 control method on medium chemistry and phytoplankton growth. Biogeosciences, 6(7), 1199-1207, DOI: 10.5194/bg-6-1199-2009.

Shutler J.D., Land P.E., Brown C.W., Findlay H. S., Donlon C.J., Medland M. and Blackford J. C. (2013). Coccolithophore surface distributions in the North Atlantic and their modulation of the air-sea flux of CO2 from 10 years of satellite Earth observation data. Biogeosciences, 10(4), 2699-2709, DOI: 10.5194/bg-10-2699-2013.

Silkin V.A. (2017). Why coccolithophorids dominate or the physiological mechanisms of Emiliania huxleyi domination. Voprosy sovremennoy al'gologii, [online] Volume 3(15). Available at: http://algology.ru/1185 [Accessed 03.11.2020] (in Russian with English summary).

Silkin V.A., Pautova L.A., Giordano M., Chasovnikov V.K., Vostokov S.V., Podymov O.I. and Moskalenko L.V. (2019). Drivers of phytoplankton blooms in the northeastern Black Sea. Marine Pollution Bulletin, 138, 274-284, DOI: /10.1016/j.marpolbul.2018.11.042.

Smith H.E., Poulton A.J., Garley R., Hopkins J., Lubelczyk L.C., Drapeau D.T. and Balch W. M. (2017). The influence of environmental variability on the biogeography of coccolithophores and diatoms in the Great Calcite Belt. Biogeosciences, 14(21), 4905-4925, DOI: 10.5194/bg-14-4905-2017.

Smyth T.J., Tyrrell T. and Tarrant B. (2004). Time series of coccolithophore activity in the Barents Sea, from twenty years of satellite imagery. Geophysical Research Letters, 31(11), L11302, DOI: 10.1029/2004GL019735.

Stelmakh L. and Gorbunova T. (2019). Emiliania huxleyi blooms in the Black Sea: Influence of abiotic and biotic factors. Botanica, 24(2), 172-184, DOI: 10.2478/botlit-2018-0017.

Strom S. L., Barberi O., Mazur C., Bright K. and Fredrickson K. (2020). High light stress reduces dinoflagellate predation on phytoplankton through both direct and indirect responses. Aquatic Microbial Ecology, 84, 43-57, DOI: 10.3354/ame01924.

Thierstein H.R. and Young J.R. (2004). Coccolithophores: from molecular processes to global Impact. Heidelberg: Springer-Verlag Berlin Heidelberg, 565 p., DOI: 10.1007/978-3-662-06278-4.

Thierstein H.R., Geitzenauer K.R., Molfino B. and Shackleton N.J. (1977). Global synchroneity of late Quaternary coccolith datum levels: validation by oxygen isotopes. Geology, 5(7), 400-404, DOI: 10.1130/0091-7613(1977)5<400:GSOLQC>2.0.CO;2.

Tyrrell T. and Merico A. (2004). Emiliania huxleyi: bloom observations and the conditions that induce them. In: H.R. Thierstein, J.R. Young, ed., Coccolithophores, 1st ed. Heidelberg: Springer-Verlag Berlin Heidelberg, 75-97, DOI: 10.1007/978-3-662-06278-4_4.

Tyrrell T. and Young J R. (2009). Coccolithophores. In: J. H. Steele, K. K. Turekian and S.A. Thorpe, ed., Encyclopedia of Ocean Sciences. 2nd ed. San Diego: Academic Press, 3568-3576, DOI: 10.2989/16085910109503736.

Vargas C., Aubry M.-P., Probert I. and Young J. (2007). Origin and Evolution of Coccolithophores: from Coastal Hunters to Oceanic Farmers. In: G. Falkowski, A. H. Knoll, ed., Evolution of Primary Producers in the Sea. Cambridge: Academic Press, 251-285, DOI: 10.1016/B978-012370518-1/50013-8.

Vogt M. and Liss P.S. (2010). Dimethylsulfide and climate. Surface Ocean-Lower Atmospheric Processes. Geophysical Research Series, 187, 197-232, DOI: 10.1029/2008GM000790.

von Dassow P., Díaz-Rosas F., Bendif E.M., Gaitán-Espitia J. D., Mella-Flores D., Rokitta S. and Torres R. (2018). Over-calcified forms of the coccolithophore Emiliania huxleyi in high-CO2 waters are not preadapted to ocean acidification. Biogeosciences, 15(5), 1515-1534, DOI: 10.5194/bg-15-1515-2018.

von Dassow P., John U., Ogata H., Probert I., Bendif E.M., Kegel J.U. and De Vargas C. (2015). Life-cycle modification in open oceans accounts for genome variability in a cosmopolitan phytoplankton. The ISME Journal, 9(6), 1365-1377, DOI: 10.1038/ismej.2014.221.

Walker C.E., Taylor A.R., Langer G., Durak G.M., Heath S., Probert I. and Wheeler G.L. (2018). The requirement for calcification differs between ecologically important coccolithophore species. New Phytologist, 220(1), 147-162, DOI: 10.1111/nph.15272.

Wang S., Eliott S., Maltreed M. and Cameron-Smith P. (2015) Influence of explicit Phaeocystis on the global distribution of marine dimethyl sulfide. Journal of Geophysical Research, 120(11), 2158-2177, DOI: 10.1002/2015JG003017.

Wang X., Fu F., Qu P., Kling J.D., Jiang H., Gao Y. and Hutchins D. A. (2019). How will the key marine calcifier Emiliania huxleyi respond to a warmer and more thermally variable ocean? Biogeosciences, 16(22), 4393-4409, DOI: 10.5194/bg-16-4393-2019.

Winter A., Henderiks J., Beaufort L., Rickaby R.E. and Brown C.W. (2014). Poleward expansion of the coccolithophore Emiliania huxleyi. Journal of Plankton Research, 36(2), 316-325, DOI: 10.1093/plankt/fbt110.

Xu K. and Gao K. (2012). Reduced calcification decreases photoprotective capability in the coccolithophorid Emiliania huxleyi. Plant and Cell Physiology, 53(7), 1267-1274, DOI: 10.1093/pcp/pcs066.

Young J.R., Poulton A.J. and Tyrrell T. (2014). Morphology of Emiliania huxleyi coccoliths on the northwestern European shelf – is there an influence of carbonate chemistry? Biogeosciences, 11(17), 4771- 4782, DOI: 10.5194/bg-11-4771-2014.

Check for updates

CC BY

RESEARCH PAPER

EVALUATION OF LAND SUITABILITY FOR *CUNNINGHAMIA KONISHII* HAYATA (CUPRESSACEAE) PLANTING IN VIETNAM

Mai Phuong Pham[1*], Dinh Duy Vu[1], Syed Noor Muhammad Shah[2], Quoc Khanh Nguyen[1], Thanh Tuan Nguyen[3], Hanh Tong Thi[4], Van Sinh Nguyen[5]

[1]Institute of Tropical Ecology, Vietnam – Russia Tropical Centre, Hanoi, Vietnam

[2]Department of Horticulture, Faculty of Agriculture, Gomal University Dera Ismail Khan Pakistan

[3]Department of Forest Inventory and Planning, Faculty of Silviculture, Vietnam Forestry University-Dong nai Campus, Vietnam

[4]Le Quy Don Technical University, Bac Tu Liem district, Ha Noi, Vietnam

[5]Pu Hoat Nature Reserve, Que Phong district, Nghe An, Vietnam

***Corresponding author:** phamphuong911vh@gmail.com

Received: December 29th, 2020 / Accepted: May 25th, 2021 / Published: July 1st, 2021

https://DOI-10.24057/2071-9388-2020-218

ABSTRACT. The suitability of land for *C. konishii* was evaluated using the analytic hierarchy process (AHP) method, which included multiple criteria, such as elevation, soil, climate, and vegetation characteristics. 120 different sites of *C. konishii* were studied and the model approximations were verified by a confusion matrix. The subsistence of *C. konishii* was mainly affected by topographic features (elevation, slope) and soil (soil texture) conditions. 15 variables were selected for the ecological analysis and construction of the land suitability map. They were combined into four main groups for weights approximation. The weights obtained by AHP were calculated as follows: topographic features (65%), soil (21.3%), climate conditions (7.4%), and vegetation type (6.3%). The total area with the highest suitability was estimated at 4, 6, 2 and 8% of the province area in Son La, Ha Giang, Thanh Hoa, Nghe An, respectively. The suitable areas for planting were located in Mai Son, Muong La, Moc Chau, Sop Cop districts of Son La province; Hoang Su Phi, Xin Man districts of Ha Giang province; Muong Lat district of Thanh Hoa province; Que Phong, Ky Son, Tuong Duong, Con Cuong districts of Nghe An province. Nghe An province has the largest suitable area for planting. The estimated AHP accuracy was 91.6%, which indicates that the approach is reliable for forestry management. The current study will provide a ground to the local population for the selection of suitable lands, ensuring the sustainability of natural resources, sustainable use and quality forest production.

KEYWORDS: AHP, forest planting; GIS, land suitability evaluation

CITATION: Mai Phuong Pham, Dinh Duy Vu, Syed Noor Muhammad Shah, Quoc Khanh Nguyen, Thanh Tuan Nguyen, Hanh Tong Thi, Van Sinh Nguyen (2021). Evaluation of land suitability for Cunninghamia konishii Hayata (Cupressaceae) planting in Vietnam. Geography, Environment, Sustainability, Vol.14, No 2, p. 63-73 https://DOI-10.24057/2071-9388-2020-218

ACKNOWLEDGMENTS: The first author was supported by The Project «Application of geographic information method (GIS) and molecular biology for investigation, monitoring and development Cunninghamia konishii Hayata species of Vietnam» by Vietnam – Russia Tropical Centre (63 Nguyen Van Huyen street, Ha Noi, Vietnam) for 2020-2022. We are grateful to the laboratory of the Institute of Tropical Ecology of Vietnam – Russia Tropical Centre. We thank E. Sterling (New York) and K. Koy (Berkeley) for providing the map of Vietnam in Fig. 1. We appreciate Pu Hoat Nature Reserve – Nghe An province, Xuan Lien Nature Reserve – Thanh Hoa province, Xuan Nha Nature Reserve – Son La province, Hoang Su Phi protected forest – Ha Giang province for their support of the research. Special thanks to Mr Nguyen Van Manh, Mr Vi Van Tinh who have been working as forest managers at Pu Hoat Nature Reserve and some local people at Hanh Dich commune for their support of our survey.

Conflict of interests: The authors reported no potential conflict of interest.

INTRODUCTION

Cunninghamia R. Br. ex. A.Rich. is a monotypic genus of the Cupressaceae family with only one known species, namely *Cunninghamia lanceolata* (Lamb.) Hook., distributed in South-Eastern Asia (Lu et al. 1999; Chung et al. 2004). *Cunninghamia lanceolate* var. konishii was first discovered in Taiwan, it was described as *Cunninghamia konishi*i Hayata and was later also found in Vietnam, Laos and continental China (Hayata 1908; Farjon 2010; Jagel 2014). *C. konishi*i is a large tree up to 40–50 m tall with monopodial growth and diameter at breast height reaching 3-4.5 m (DBH). In Vietnam it is mainly distributed in Ha Giang, Son La, Thanh Hoa and Nghe An provinces (Phan et al. 2009; Nguyen et al. 2017; Thai et al. 2015). It can be found at elevations of 1300 – 2800 m in Taiwan (Liang 2010), 1300 – 2000 m in China, 900 – 2200 m in Laos (Averyanov 2014), 1000 – 1600 m in Vietnam (Phan et al. 2017). It grows on deep, well-drained loams or loamy sand soil, but can also be

found on weathered soils from granite or other silicate originated rocks. It requires a moderately cold and moist climate with precipitations above 4000 mm per year, and an average annual temperature of 13-19 °C but can tolerate up to 1.1-6.6 °C in some regions (Bigras 2001; Farjon 2010, Nguyen et al. 2004; Nguyen et al. 2009). The size of the natural population of *C. konishi*i in Vietnam is limited (Lu 2001; Lu et al. 2001; Nguyen 2009; Nguyen et al. 2009, 2012; Phan et al. 2013) due to its fragrance and outstanding durability in the timber industry (Cheng et al. 2012). The commercial exploitation of the species and cultivation is neglected to date (Farjon 2010). The natural population is declining due to the felling of primal forests, although some part of it is protected in nature reserves, and the species is treated as endangered (Farjon 2010; Thomas, Yang 2013; Nga et al. 2016). The species is included in the red list of IUCN threatened species and Vietnam red data book 2007 (Decree 06/2019/ND-CP of Vietnam Government). It is classified as an endangered, precious, and rare species. Therefore, the areas of distribution, ecology, natural active ingredients, phytochemicals and other possible resources of *C. konishi*i need to be explored for its conservation.

The anthropogenic pressure on natural forests is increasing every day due to the high demand for timber and leads to the reduction of forest area. To compensate for the high demand from limited resources, efficient use of land can play a significant role (Lubka 1982; Adeyoju 1983; Joyce 1981; Florence, Carron 1983). Trees can be planted and grown under different natural conditions; therefore, land evaluation is necessary. The data required to test land suitability for forest species depend on environmental parameters of exact tree species such as their soil, natural conditions and ecological requirements (FAO 1976, 1984). Olarieta et al. (2006) stated that soil factors have a major role in the growth of *Pinus radiata*. Dayawansa and Ekanayake (2003) also stated that climatic, topographic, and vegetation variables play important role in the identification of land for forest production (Dayawansa, Ekanayake 2003). Dengiz et al. (2010) estimated land suitability for forests by providing maps of suitability for each species. The researchers have also determined land potential by evaluating the ecological suitability criteria (Perpina et al. 2013). Suitability index and related criteria are determined using complex methods based on Geographic Information System (GIS) called Multi-Criteria Analysis (MCA) (Liu et al. 2007). This approach is implemented by applying a complex geographic information system (GIS) and the Analytic Hierarchy Process (AHP) for land suitability assessment through analysis of environmental parameters and provides support for species conservation (Chen et al. 2001; Draper et al. 2003). GIS can also be used in the qualitative assessment. Yüksel et al. (2001) studied the relationship between soils and land use units through the detailed soil map at Kenbag Nursery of Cankiri. The soil quality and climate are the main factors that influence productivity, among which, soil depth combined with elevation factor is the most important (Romanyà 2004). The current study was designed to evaluate the suitability of land in four provinces (Ha Giang, Son La, Thanh Hoa, Nghe An) of Vietnam for *C. konishi*i based on GIS and AHP and to optimize protected areas. The suitable lands on large scale for *C. konishi*i were mapped according to the ecological requirements including topography, climate, soil and vegetation characteristics.

MATERIALS AND METHODS

Study area

The study focuses on the provinces of Ha Giang, Son La, Thanh Hoa and Nghe An (Fig. 1), which include more than 50% of the forest area in Vietnam (Fig. 7, General Statistics Office of Vietnam 2019). Ha Giang province has a temperate monsoon climate, which is colder than in the Northeastern provinces of the country, but warmer than in the Northwestern ones. Son La province is known for its mountains characterized by a humid subtropical climate with cold and dry winters, hot and humid summers, and frequent heavy rainfalls. These areas have complex and deeply divided topography, forming many sub-climatic zones and special interzonal elements, which results in rich biodiversity and high agroforestry production.

Nghe An province is known for its tropical monsoon climate with two distinct summer and winter seasons and some climatic peculiarities. From April to August, the province is influenced by dry and hot southwest wind, while in winter the climate is cold and humid due to the northeast Pacific monsoon. Thanh Hoa province is situated in the middle of North and Central Vietnam, which is influenced by both regions including the «Laos Wind».

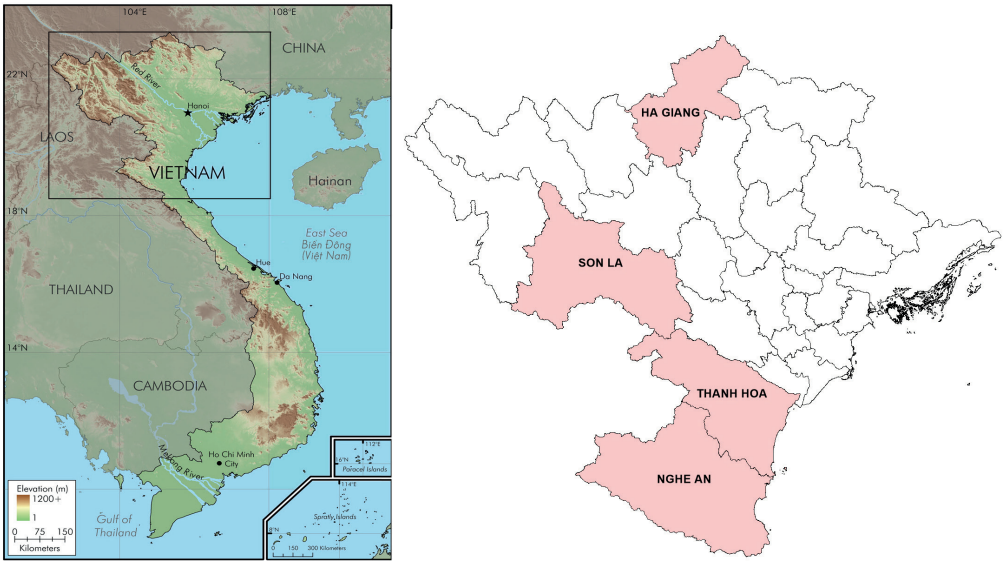

Fig. 1. Geographical location of the study areas

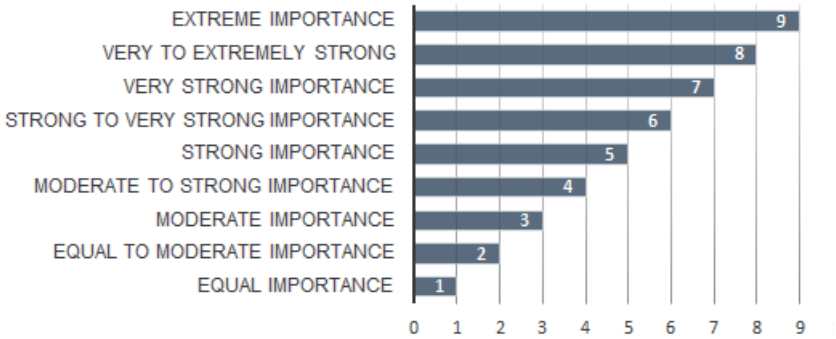

Fig. 2. The scale used for generation of the pairwise comparison matrix (Saaty 1980

Table 1. Categories of land suitability index

Categories of land suitability	Explanation	Index
Suitability index 1 (highly suitable)	Land unit is very favorable for *C. konishii* with no ecological limitations	>80
Suitability index 2 (moderately suitable)	Land unit is almost favorable for *C. konishii* with few ecological limitations	60-80
Suitability index 3 (marginally suitable)	Land unit is marginally favorable for *C. konishii* with severe ecological limitations	30-60
Suitability index N (unsuitable)	Land unit is almost unfavorable for *C. konishii* with severe ecological limitations	<30

Data collection

The distribution of *C. konishi*i was explored during July-August of 2020. The longitude and latitude of the studied 120 locations of the *C. konishi*i population were determined using a global positioning system (GPS). After that, the location data were incorporated into the geographic information system (GIS). The data on ecological factors were investigated during the field survey and determined using GIS. These factors included (1) topographic factors (elevation, slope, distance to nearest rivers and streams), (2) soil factors (soil type, texture and layer thickness), (3) general climate factors (mean diurnal and annual temperature range, annual precipitation, precipitation of the driest month and driest quarter and warmest quarter, sunshine duration of the growing month) and (4) vegetation factors (vegetation type, tree coverage). All of them were combined and considered as four main factors and 15 sub-factors (Table 2).

Table 2. Criteria for delineating land suitability of *C. konishii*

Criteria	Weight (W1)	CR	Sub- criteria	Categories				Weight (W2)	Overall weight (W1 xW2)	CR
				SI 1	SI 2	SI 3	N			
Topography	0.650	0.087	Elevation	1100-2000m	900-1100m	800-900m	<800m	0.746	0.484	0.022
			Slope	> 45^0	30-45^0	25-30^0	<25^0	0.134	0.087	
			Distance to streams	200-400m	400-600m	600-800m	> 800, <200m	0.120	0.078	
Soil	0.213		Soil type	A, Fs, Ha, Hq, Hs, Fk	Fa, Fj, Fq, Fv, Fe, Fu	Fp	Other land	0.090	0.019	0.068
			Soil texture	Loam	Sandy loam	Silty clay	Loamy sand, other soil types	0.556	0.119	
			Soil layer thickness	> 100 cm	70-100 cm	50-70 cm	<50 cm	0.354	0.075	
Climate	0.074		Mean diurnal range	6.7-8.7^0 C	5-6.6; 8.8-10^{0}C	10.1- 12^{0}C;	<4.9; >12.1^0 C	0.162	0.012	0.081
			Annual temperature range	16.7-19.70 C	14-16.7; 19.8-22^0 C	12-13.9; 22-24^{0}C	<11.9; >24.1^0 C	0.039	0.003	
			Annual precipitation	1200-1700 mm	1000-1200; 1700-2000 mm	900-1000; 2000-2100 mm	<900; >2100 mm	0.058	0.004	
			Precipitation of driest month	2-20 mm	1-2 mm	0.5-1 mm	<0.5 mm	0.199	0.015	
			Precipitation of driest quarter	> 13 mm	10-13 mm	8-10 mm	<8 mm	0.129	0.009	
			Precipitation of warmest quarter	500-1000 mm	400-500; 1000-1200 mm	300-400; 1200-1300 mm	<300; >1300 mm	0.122	0.009	
			Sunshine duration of the growing month	130-160 (hours)	100-130; 160-180 (hours)	90-100; 180-200 (hours)	<90,> 200 (hours)	0.292	0.022	

Vegetation	0.063	0.087	Vegetation type	Protection forest on mountain	Production forest on mountain	Plantation forest on mountain	Other types of vegetation	0.167	0.011	
			Tree coverage	90%	80-90%	70-80%	<70%	0.833	0.053	

A: Humus on high mountains
Fs: Red and yellow soil on clay and metamorphic rocks
Ha: Red yellow humus on acid magma rock
Hq: Light yellow humus soil on sandstone
Hs: Yellow red loam on clay
Fk: Reddish-brown soil on neutral and basic magma
Fa: Red yellow soil on acid magma rock
Fq: Light yellow soil on sandstone
Fj: Yellow red soil on metamorphic rocks
Fv: Brown red soil on limestone
Fe: Purple brown soil on purple clay
Fu: Yellow brown soil on neutral and basic magma
Fp: Yellow brown soil on ancient alluvium

Topographic factor: Digital elevation model (DEM) data with resolution 30x30m were downloaded from http://srtm.csi.cgiar.org/ and included terrain elevation for the area from 103° 14′ 14″ N to 18° 30′ 52″ N and 105° 37′ 40″ E to 23° 31′ 25.5″ E by World Geodetic System 84. The surface analysis function in Arcgis 10.0 was used to build an elevation and slope map. The data on the *C. konishii* distribution along with updated river and streams data were used to determine the distances to the nearest river. Soil data (soil type, texture and layer thickness) were collected from the Soil map of the studied provinces (with a scale of 1:100.000) as provided by the Ministry of Natural Resources and Environment (MONRE). Climatic factors: 19 bio-climate parameters with a spatial resolution of 30s (1 km2) were collected from WorldClim-Global (ver.2) and were used to gather and analyze the actual ecological requirement factors for *C. konishii*. Vegetation data: The current map of land use of the studied provinces as available up to 2020 was provided by MONRE and used for the identification of vegetation types. Vegetation coverage data were obtained from www.globalforestwatch.org and calculated per pixel cell based on the canopy cover percentage for all vegetation higher than 5m (Hansen et al 2013).

Methods

AHP hierarchical model

In this study, a focus group discussion was implemented in which the participants including experts and local people were surveyed through a questionnaire. AHP is a structured technique for organizing and analysing complex decisions based on mathematics and psychology. It was developed by Thomas Saaty and Ernest Forman in the 1970s, implemented in Expert Choice in 1983 and has been extensively studied and advanced to date. It represents an accurate approach for quantifying the weights of decision criteria. Individual experts were brought to estimate the relative magnitudes of factors through pair-wise comparison. Initial AHP questionnaire has 1 to 9 scale (Saaty 1980; Li et al. 2019; Fig. 2). Each of our respondents had to compare the relative importance of the two items under a specially designed questionnaire.

The aim was to perform the analysis of land suitability for *C. konishii* planting in Vietnam along with the parameters which have to be involved in the process including soil, climate, and topographic characteristics. The weight of such parameters was obtained through pairwise comparison and statistically analyzed. Consistency Ratio (CR) (< 10 %) was used to check the accuracy of comparisons (Saaty 2000; Malczewski 1999; Maleki 2017; Bozdağ 2016).

Land suitability analysis using the integration of GIS and AHP

The FAO guidelines recommend using the scheme of suitability classification described in the Framework for Land Evaluation. The class level was chosen to evaluate the suitability of land in its current condition. The categories were described in the following way: highly suitable; moderately suitable; marginally suitable; not suitable. The FAO guidelines do not require the use of a specific methodology for assessment but provide a framework for whichever method the user wishes to apply (FAO 1976, Dengiz 2010). To evaluate the land suitability for the planting of *C. konishii*, the data of 15 variables were classified using 4 levels (SI 1, SI 2, SI 3, N). The purpose of this work was to create 15 component maps in raster form. AHP acquired weights of the variables were applied to all the raster layers, presented in the WGS84 Zone 48N coordinate system. The suitability of land for the species was mapped through overlay (superposition) of 15 raster component maps using ArcGIS 10.0 software. Finally, the map of land suitability for *C. konishii* was obtained and classified into 4 categories (Table 1).

Validation of the method

120 different sites of *C. konishii* were studied. During the assessment, the ratio between the number of correctly predicted scores and the total number of points in the test data set was calculated. The prediction accuracy was determined from the distribution of *C. konishii* scores (species occurrence, findings) obtained during the survey, which were attributed to a highly suitable class. Confusion matrix was used to compute accuracy (ACC), true positive rate (TPR) and true negative rate (TNR) from the following equations (Cabrera 2020; Singh, Singh 2017; Table 3).

Table 3. Confusion matrix to calculate the overall accuracy (ACC)

		Actual class	
		Positive	Negative
Predicted class	Positive	TP	FP
	Negative	FN	TN
		Actual class	
		Positive	Negative
Predicted class	Positive	93	9
	Negative	2	16
		ACC= 0.91; TPR=0.98; TNR=18	
TP: true positive; TN: true negative; FP: false positive; FN: false negative			

$$ACC = \frac{TP + TN}{P + N} = \frac{TP + TN}{TP + TN + FP + FN} \quad (1)$$

$$TPR = \frac{TP}{TP + FN} \quad (2)$$

$$TNR = \frac{TN}{TN + FP} \quad (3)$$

RESULTS AND DISCUSSION

AHP and GIS analysis

The results based on the experts pairwise comparisons showed that topography (0.65) has the highest values, followed by soil (0.213), climate (0.074) and vegetation (0.063) conditions (Table 2). Among the topographic criteria, elevation is prominent while the distance from streams has the lowest values. From the total soil sub-criteria, soil texture and soil types have the highest and lowest values, respectively. Similarly, among the climatic sub-criteria, the sunshine duration of the growing season have major roles in describing the land suitability for *C. konishii*. The accuracy (ACC) was 91% for validation of the method, while true positive rate (TPR) and true negative rate (TNR) were 98% and 18%, respectively (Table 3). The consistency ratio (CR) of the matrix was 0.087 for the four main criteria. The CR of topographic, soil and climatic criteria were 0.022, 0.068, 0.081, respectively (Table 2).

We found that elevation and soil texture have a stronger impact on *C. konishii* growth compared to any other studied criteria. It was found that in Nghe An province 8% (1244 km2) of the total area was suitable for *C. konishii* planting, which is the largest potential area with a highly suitable index (73.39%) of all the provinces. The Son La and Ha Giang provinces had moderately and marginally suitable indexes covering 60% and 47% of the total area, respectively.

These results confirmed that the AHP methodology had high accuracy in the prediction of area suitability for the species. Our result also confirmed the previous studies (Huynh 2009; Lai et al 2002; Maleki et al 2017; Olarieta et al 2006), and the AHP method was found to be the best method for land suitability analysis. The elevation, shallow soil depth, steep slope, aspect trend and tough climatic conditions affect the land utilization type, which helped the local planners to reinstate the region by planting trees in proper ecological conditions (Gholizadeh 2019). Kooch and Najafi (2011) revealed the potential of an ecological zone of forest trees using soil analysis in Khanikan Forest in Iran.

In the study area, the land suitability evaluation is considered to be a vital link to the sustainability of ecosystems in terms of their productivity and environmental stability. The multi-criteria analysis has been used as an effective method as it may support the administration or decision-makers about the planning

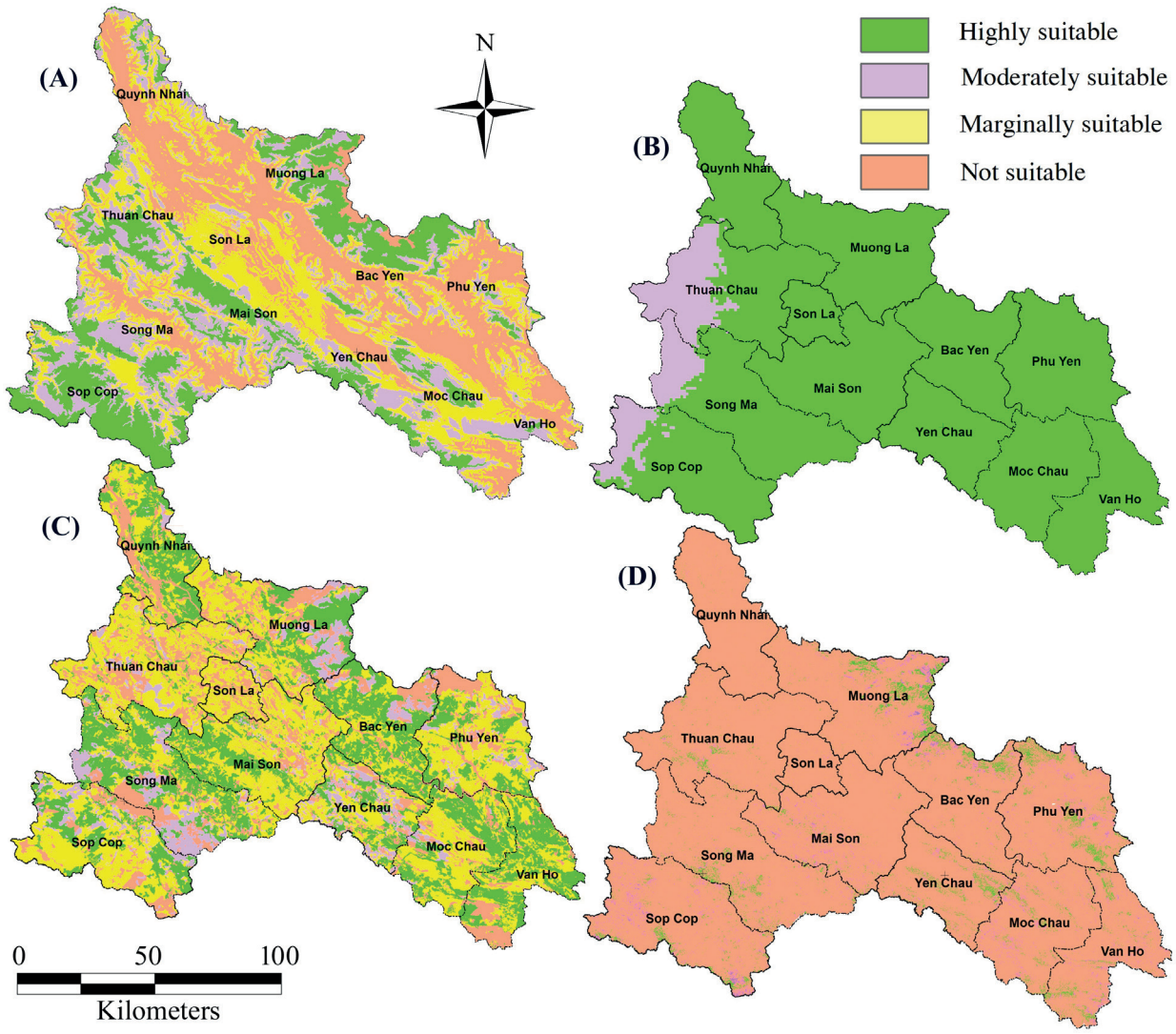

Fig. 3. Land suitability assessment for the main variables in Son La province; (A): Elevation, (B): Climate, (C): Soil; (D): Vegetation

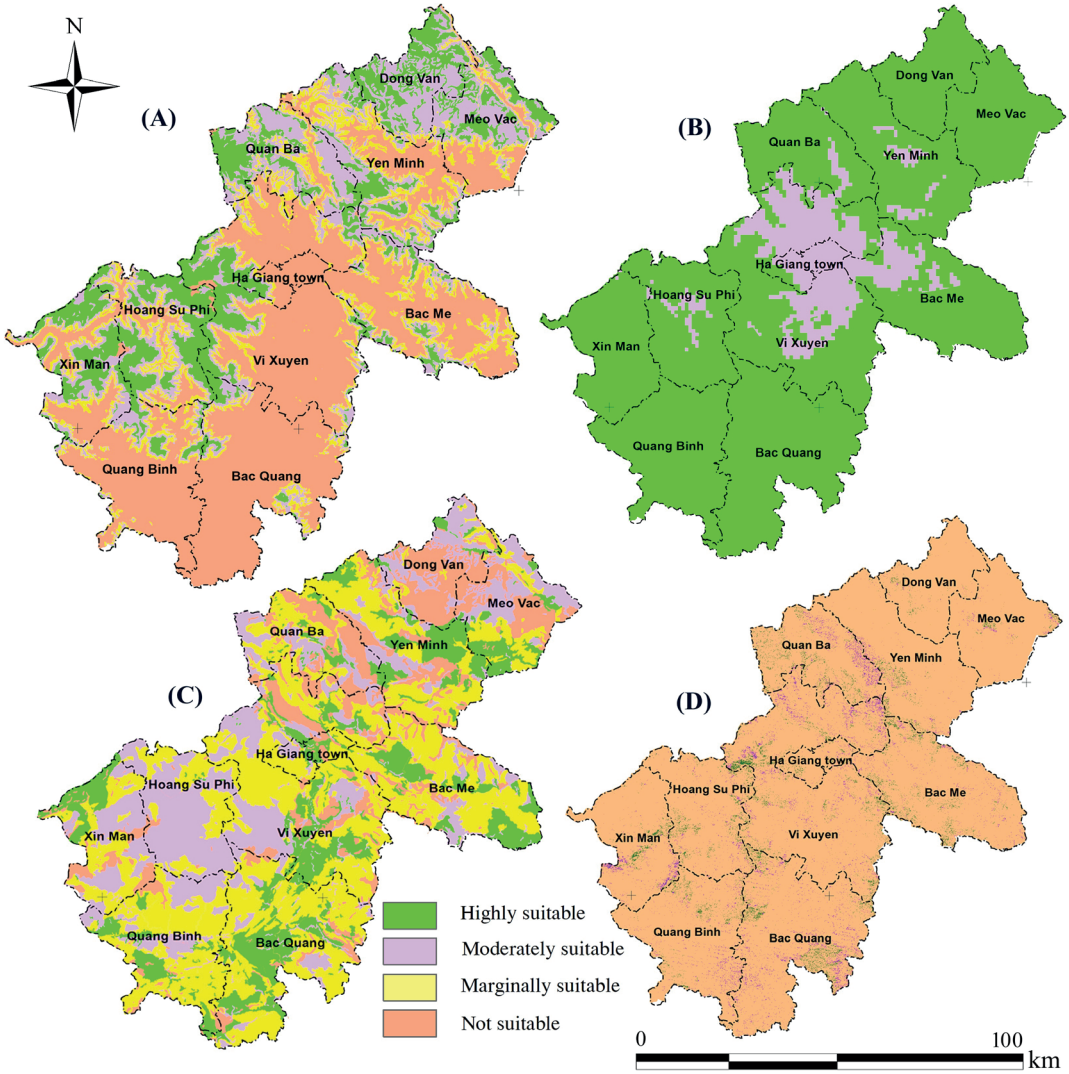

Fig. 4. Land suitability assessment for the main variables in Ha Giang province; (A): Elevation, (B): Climate, (C): Soil; (D): Vegetation

of reforestation programs. Spatial analysis methods are commonly used for land-use planning or land suitability selection studies but AHP has an advantage for decision-making compared to other proposed techniques. According to Lai et al. (2002), with AHP it is possible to measure the consistency of the decision maker's judgments.

During the study of the selected regions, elevation and climate criteria revealed that a wide range of areas is suitable to the ecological requirements of the species. Fig. 8 shows the difference among four provinces in the scuttering of land used for the regional programs of land suitability for *C. konishi*i planting. The land suitability map shows the area divided into highly suitable, moderately suitable, marginally suitable, and unsuitable class zone (Fig. 3, 4, 5, 6, 8). This subdivision had also been formerly applied in some evaluation studies for agriculture and forestry (Fao 1976; Huynh 2009; Ahmad et al. 2017a, 2017b).

Land suitability classes description

Highly suitable index (SI 1)

The highly suitable lands in Nghe An and Son La were broader than in Ha Giang and Thanh Hoa provinces, constituting about 73.39% of the total highly suitable area. The area of highly suitable class for Son La, Ha Giang, Thanh Hoa, and Nghe An comprised 4, 6, 2 and 8% of their total area, respectively (Table 4, 5). These areas are situated mainly in Mai Son, Muong La, Moc Chau, Sop Cop districts in Son La province; Hoang Su Phi, Xin Man districts in Ha Giang province; Muong Lat district in Thanh Hoa province and Que Phong, Ky Son, Tuong Duong, Con Cuong districts of Nghe An province. Based on our data, the highly suitable ecological conditions for *C. konishi*i may be described as: 1) Elevation of 1000-2000m, slope over 45° and distance to rivers/streams of 200-400m; 2) Soil condition: the presence of humus on high mountains, red and yellow clay soil and metamorphic rocks, red yellow humus on acid magma rock, light yellow humus soil on sandstone, yellow red loam on clay, reddish-brown soil on neutral and basic magma, loam soil, the thickness of soil layer of over 100 cm; 3) Climatic conditions: mean diurnal temperature range 6.7-8.7°C, annual temperature range 16.74-19.7°C; annual precipitation 1200-1700mm) precipitation of the driest month 2-20mm, precipitation of the driest quarter over 13mm, precipitation of the warmest quarter 500-1.000mm and sunshine exposition during the growing month from 130-160 hours; 4) Vegetation condition: the existence of forest protection on the mountain in the area and tree canopy coverage of 90% (Table 2).

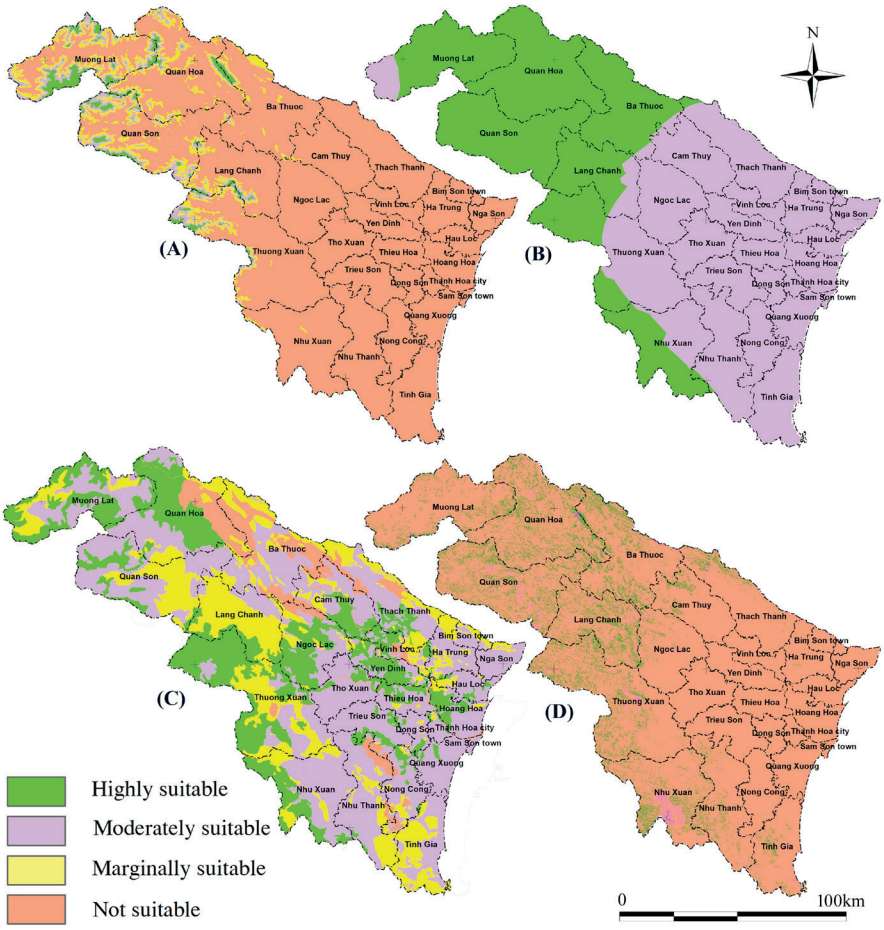

Fig. 5. Land suitability assessment for the main variables in Thanh Hoa province; (A): Elevation, (B): Climate, (C): Soil; (D): Vegetation

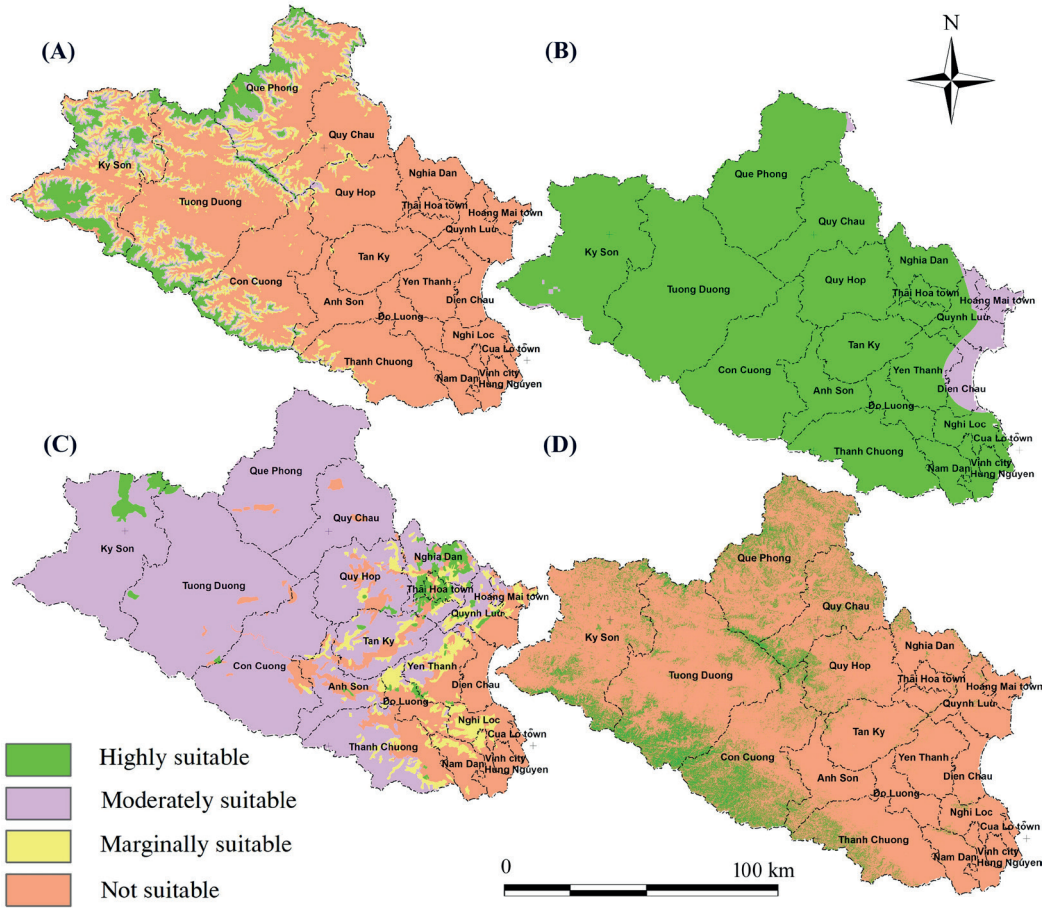

Fig. 6. Land suitability assessment for the main variables in Nghe An province; (A): Elevation, (B): Climate, (C): Soil; (D): Vegetation

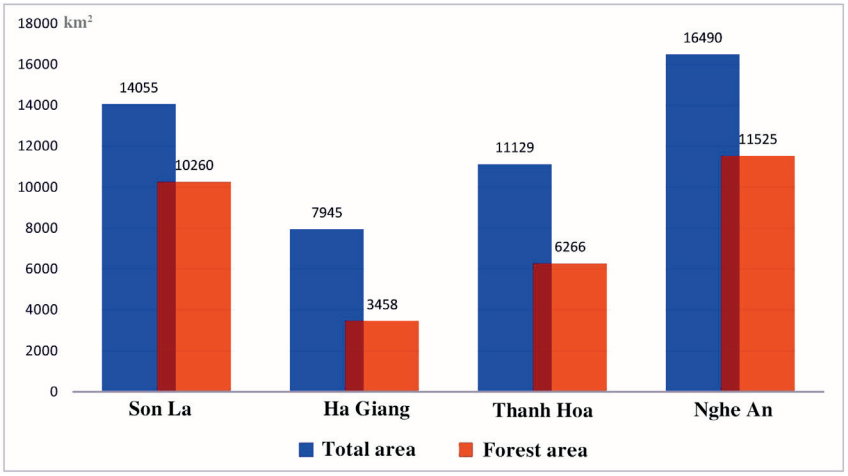

Fig. 7. Relative of total area and forest area of study provinces (km²)

Moderately suitable index (SI 2)

Moderately suitable areas in Son La and Ha Giang were more spacious than in Nghe An and Thanh Hoa province as they combine for about 65.06% of the total moderately suitable land. The ratio of moderately suitable areas for Son La, Ha Giang, Thanh Hoa, and Nghe An provinces reach 23, 25, 8 and 12% of the total province area, respectively (Table 4, 5).

Marginally suitable index (SI 3)

Marginally suitable areas in Son La and Ha Giang were larger than in Nghe An and Thanh Hoa provinces. The former two combined for about 76.89% of the total marginally suitable land. The share of marginally suitable area for Son La, Ha Giang, Thanh Hoa, and Nghe An province reaches 47, 22, 10 and 9%, respectively (Table 4, 5). These results confirmed the high potential for the *C. konishii* growth in the western part of the studied area, especially in Ha Giang, Thanh Hoa and Nghe An province. These areas are restricted from human activities but the natural conditions are generally not too favorable and forest patches are largely fragmented by socio-economic activities.

Unsuitable (N) index

The unsuitable areas for C. lanceolata in Nghe An province were larger than in other provinces. The unsuitable lands in Son La, Ha Giang, Thanh Hoa, and Nghe An province were 25, 47, 81, 72%, respectively (Table 4, 5). Although for many places the climatic conditions were found suitable, in the eastern part, especially in Ha Giang, Thanh Hoa and Nghe An province, *C. konishii* cannot realize its natural potential, probably due to too low elevations and lower slopes. These results are also in line with Phan (2017) and Nga et al. (2017a, b), who mentioned that agricultural activities, development of rural and urban residential areas, elevation and slope may act as limiting factors for the *C. konishii* planting in the zones. There may be few single trees in scattered form in these kinds of areas, but not in clusters or concentrated parcels to develop any sustainable populations.

AHP can be accurately used in unstudied areas where species presence was detected. It is quite appropriate for our case study because many populations of the species have been destroyed and left untouched. In this study, we used a mixed approach (expert-based and species distribution). 120 species locations were determined during the survey to validate the results of the AHP analysis and confirmed its results with high accuracy. In addition, it has a very wide range of other applications such as planning and choosing any kind of decision among alternatives. It also relies on judgments, meaning that if experts are from different backgrounds, the evaluation can be done easily from different aspects.

CONCLUSIONS

The current study was designed for the *C. konishii* land suitability assessment based on GIS and AHP in four provinces (Ha Giang, Son La, Thanh Hoa, Nghe An) of Vietnam. The most influential ecological variables were used as a dataset for inclusion in the matrix comparison. The AHP results showed high accuracy. It was found, that elevation and soil condition affect the *C. konishii* growth more than any other factor. In the Nghe An province, 8% (1244 km²) of the total area was found to be highly suitable for the *C. konishii* planting. It is the largest potential area with a highly suitable index (73.39%) of all the provinces. In

Table 4. Land suitability for *C. konishii* in each province

Land suitability index for *C. konishii*	Son La province (km²)	Percentage (%)	Ha Giang province (km²)	Percentage (%)	Thanh Hoa province (km²)	Percentage (%)	Nghe An province (km²)	Percentage (%)
SI 1	613	4	460	6	213	2	1244	8
SI 2	3228	23	1970	25	889	8	1902	12
SI 3	6638	47	1768	22	1060	10	1466	9
N	3576	25	3747	47	8967	81	11877	72
Total	14055	100	7945	100	11129	100	16490	100

Table 5. Distribution of area based on land suitability for *C. konishii*

Suitable index	Son La (km²)	%	Ha Giang (km²)	%	Thanh Hoa (km²)	%	Nghe An (km²)	%
Suitability area of topographic criteria								
SI 1	1666	12	1438	18	251	2	1275	8
SI 2	3288	23	1778	22	504	5	1179	7
SI 3	3660	26	959	12	717	6	1643	10
N	5441	39	3770	47	9657	87	12393	75
Suitability area of soil criteria								
SI 1	2226	16	1265	16	2731	25	491	3
SI 2	1301	9	2040	26	5138	46	12232	74
SI 3	6545	47	3282	41	2443	22	992	6
N	3983	28	1358	17	817	7	2775	17
Suitability area of climatic criteria								
SI 1	11952	85	7454	94	4734	43	15801	96
SI 2	2103	15	491	6	6395	57	689	4
Total	18038	100	9303	100	11946	100	16490	100
Suitability area of vegetation criteria								
SI 1	416	3	121	2	825	7	2088	13
SI 2	286	2	111	1	66	1		
SI 3	13353	95	7713	97	10238	92		
N							14402	87

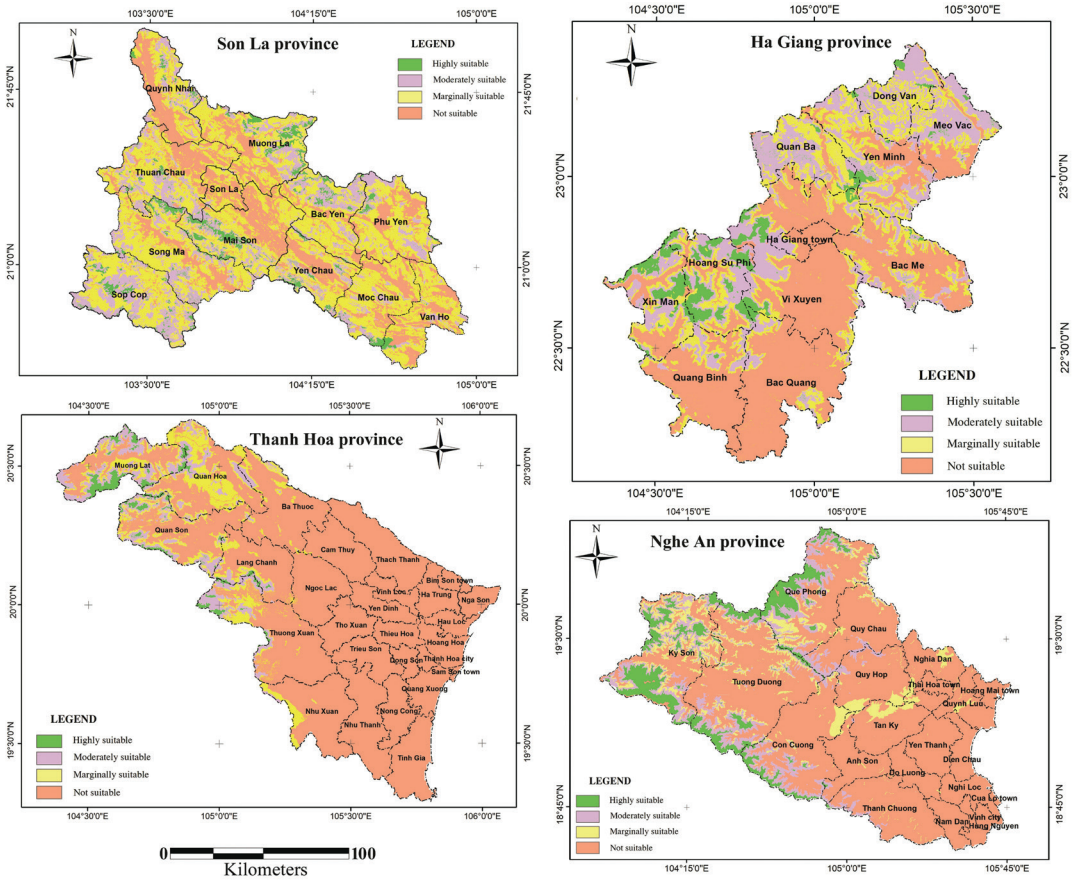

Fig. 8. Land suitability assessment map for *C. konishii* planting in Vietnam

Son La and Ha Giang provinces, the lands with moderately and marginally suitable indexes amounted to 60% and 47% of the total area, respectively.

The regional characteristics of different provinces affect the contribution of different factors. On the scale of a province, the records of environmental factors influencing the distribution of species population were not comparable with other provinces. Only data on forests and characteristics of tree layers showed variables characterizing the vegetation cover. It would be appropriate to describe the typological diversity of the vegetation for habitats of different suitability, which was not done within this study. The study will help in the development of *C. konishi*i forests on suitable land.

REFERENCES

Adeyoju S.K. (1983). Striking a balance in land-use planning. Unasylva, 35, 24-27.

Ahmad F., Goparaju L., Qayum A. (2017a). FAO guidelines and geospatial application for agroforestry suitability mapping. Case study of Ranchi, Jharkhand state of India. Agroforestry Systems, DOI: 10.1007/s10457-017-0145-y.

Ahmad F., Goparaju L., Qayum A. (2017b). Agroforestry suitability analysis based upon nutrient availability mapping. A GIS based suitability mapping. AIMS Agriculture and Food, 2(2). 201-220, DOI: 10.3934/agrfood.2017.2.201.

Averyanov L.V., Hiep N.T., Sinh K.N., Pham T.V., Lamxay V., Bounphanmy S., Lorphengsy S., Loc P.K., Lanorsavanh S., Chantthavongsa K. (2014). Gymnosperms of Laos. Nordic Journal of Botany, 32, 756-805.

Bigras F.J. and Colombo S.J. (2001). Conifer Cold Hardiness. Kluwer Academic Publishers. The Netherlands, 16-19.

Bozdağ A., Yavuz F., Günay A.S. (2016). AHP and GIS based land suitability analysis for Cihanbeyli (Turkey) County. Environmental Earth Sciences, 75(9), 813.

Cabrera J.S., Lee H.S. (2020). Flood risk assessment for Davao Oriental in the Philippines using geographic information system–based multi–criteria analysis and the maximum entropy model. Journal of Flood Risk Management, e12607.

Cheng S.S., Chung M.J., Lin C.Y., Wang Y.N., Chang S.T. (2012). Phytochemicals from Cunninghamia konishii Hayata act as antifungal agents. Journal of agricultural and food chemistry, 60(1), 124-128.

Chung J.D., Lin T.P., Tan Y.C., Lin M.Y., Hwang S.Y. (2004). Genetic diversity and biogeography of Cunninghamia konishii (Cupressaceae), an island species in Taiwan. A comparison with Cunninghamia lanceolata, a mainland species in China. Molecular Phylogenetics and Evolution, 33(3), 791-801.

Dayawansa N.D.K., Ekanayake G.K. (2003). Land suitability identification for a production forest through GIS techniques. Forestry and Biodiversity, Map India Conference, India.

Dengiz O., Gol C., Sario Lu F.E., Edi S. (2010). Parametric approach to land evaluation for forest plantation. A methodological study using GIS model. African Journal of Agricultural Research, 5(12), 1482-1496.

Decree No. 06/2019/ND-CP (2019). Management of endangered, precious and rare species of forest fauna and flora and observation of Convention on International Trade in Endangered Species of Wild Fauna and Flora.

Draper D., Rosselló-Graell A., Garcia C., Gomes C.T., Sérgio C. (2003). Application of GIS in plant conservation programmes in Portugal. Biological Conservation, 113(3), 337-349.

FAO (1976). A framework for land evaluation. Soils Bulletin 32. Food and Agriculture Organization of the United Nations, Rome, Italy. ISBN 92-5-100111-1. http.//www.fao.org/docrep/t0715e/ t0715e06.htm. Accessed November 10, 2017.

FAO (1984). Land evaluation for forestry, forestry paper 48. Rome, Italy. Food and Agriculture Organization of the United Nations.

Farjon A. (2010). A Handbook of the world's conifers, Brill Academic Publishers, Leiden, The Netherlands, 1112

Florence R.G., Carron L.T. (1983). Forest land use and environmental planning in Australia. Proc. Institute of Foresters of Australia 10th Triennial Conference, 16-21.

General Statistics Office of Vietnam (2019). Statistical Yearbook. Statistical publisher.

Gholizadeh A., Bagherzadeh, A., Keshavarzi A. (2019). Model application in evaluating land suitability for OAK and PINE forest plantations in Northeast of Iran. Geology, Ecology, and Landscapes, 1-15.

Hayata B. (1908). The Gardeners' Chronicle, ser. 3, 43, 194.

Hansen M.C., Potapov P.V., Moore R., Hancher M., Turubanova S.A., Tyukavina A., Thau D., Stehman S.V., Goetz S.J., Loveland T.R., Kommareddy A., Egorov A., Chini L., Justice C.O., and Townshend J.R.G. (2013). High-Resolution Global Maps of 21st-Century Forest Cover Change, Science 342, 850-53.

Huynh V.C. (2009). Multi-criteria soil suitability assessment for crops with GIS and AHP integrated. A case study in Huong Binh commune, Thua Thien Hue. Hue University Journal of Science, 50, 5-16.

IUCN 2020 (2020). The IUCN red list of threatened species, https.//www.iucnredlist.org.

Joyce P.M. (1981). Forest management and land use planning. Proceedings of the 17th IUFRO World Congres, Japanese IUFRO Congress Committe, Ibaraki, Division 4, 363-374.

Kooch Y., Najafi A. (2011). Ecological potential assessment of forest groups using fuzzy set theory and regression analysis of soil characteristics (case study. Khanikan Forest, Chalus, north of Iran). Journal of Wood & Forest Science and Technology, 18(1).

Lai V., Wong B.K., Cheung W. (2002). Group decision making in a multiple criteria environment; a case using the AHP in the software selection. Eur. J. Oper. Res, 137(1), 134-144.

Li R.Y.M., Chau K.W., Zeng F.F. (2019). Ranking of risks for existing and new building works. Sustainability, 11(10), 2863.

Li H.L., Keng H. (1994). Taxodiaceae – In Flora of Taiwan, 2nd ed., Taiwan. 1. 582-585.

Liang W.Y. (2010). The cutting propagation technique and afforestation experiment of Cunninghamia konishii. Subtropical Agriculture Research, 6(4), 217-221.

Liu Y., Lv X., Qin X., Guo H., Yu Y., Wang J., Mao G. (2007). An integrated GIS-based analysis system for land-use management of lake areas in urban fringe. Landsc. Urban Plan, 82. 233-246.

Lu S.Y., Chiang T.Y., Hong K.H., Hu T.W. (1999). Re-examination of the taxonomic status of Cunninghamia konishii and C. lanceolata based on the RFLPs of a chloroplast trnD-trnT spacer. Taiwan Journal of Forest Science, 14, 13-19

Lu S.Y., Peng C.I., Cheng Y.P., Hong K.H., Chiang T.Y. (2001). Chloroplast DNA phylogeography of Cunninghamia konishii (Cupressaceae), an endemic conifer of Taiwan, Genome, 44, 797-807.

Lubka L. (1982). Role of the forester in land use planning. J. For., 80, 597-601.

Maleki F., Kazemi H., Siahmarguee A., Kamkar B. (2017). Development of a land use suitability model for saffron (Crocus sativus L.) cultivation by multi-criteria evaluation and spatial analysis. Ecological Engineering, 106, 140-153.

Malczewski J. (1999). GIS and multicriteria decision analysis. New York. Wiley.

Nguyen T.H., Phan K.L., Nguyen T.D.L., Thomas P.I., Farjon A., Averyanov L., Regalado J. (2004). Vietnamese conifers. Current status and conservation studies, Fauna & Flora International, 55-56.

Nga N.T.T., Dung N.A., Chung N.T., Thai T.H., Hung N.D. (2016). The distribution and some ecological characteristics, and essential oil of Cunninghamia konishii Hayata in Pu Hoat nature reserve, Nghe An province, Vietnam. Engineering and Applied Science Research, 43, 121-124.

Olarieta J.R., Besga G., Rodríguez–Ochoa R., Aizpurua A., Usón A. (2006). Land evaluation for forestry. a study of the land requirements for growing Pinus radiata D. Don in the Basque Country, northern Spain. Soil use and management, 22(3), 238-244.

Olson D.M., Dinerstein E., Wikramanayake E.D., Burgess N.D., Powell G.V.N., Underwood E.C., D'Amico J.A., Itoua I., Strand H.E., Morrison J.C., Loucks C.J., Allnutt T.F., Ricketts T.H., Kura Y., Lamoreux J.F., Wettengel W.W., Hedao P., Kassem K.R. (2001). Terrestrial ecoregions of the world: a new map of life on Earth. Bioscience 51(11), 933-938.

Perpina C., Martinez-Llario J.C., Navarro A. (2013). Multi-criteria assessment in GIS environments for sitting biomass plants. Land Use Policy, 31, 326-335.

Phan K.L., Pham V.T., Phan K.L., Regalado J., Averyanov L.V., Maslin B. (2017). Native conifers of Vietnam – a review, Pak. J. Bot, 49(5), 2037-2068.

Phan K.L., Pham V.T., Nguyen S.K., Averyanov L.V. (2013). Conifers naturally growing in Vietnam – Updated 2013. Journal of Economy & Ecology, 45, 33-45.

Romanyà J., Vallejo V.R. (2004). Productivity of Pinus radiata plantations in Spain in response to climate and soil. Forest Ecology and Management, 195(1-2), 177-189.

Saaty T.L. (1980). The analytical hierarchy process. McGraw Hill, New York

Saaty T.L. (2000). Fundamentals of decision making and priority theory with the analytic hierarchy process. RWS Publications, Pittsburg.

Singh K.K., Singh A. (2017). Identification of flooded area from satellite images using hybrid Kohonen fuzzy C-means sigma classifier. Egyptian Journal of Remote Sensing and Space Sciences, 20. 147-155, DOI: 10.1016/J.EJRS.2016.04.003.

Thai T.H., Bazzali O., Hoi T.M., Minh D.T., Loc P.K., Nga N.T.T., Bighelli A. (2015). Chemical composition of the essential oil from Cunninghamia konishii Hayata growing wild in Vietnam. American Journal of Essential Oils and Natural Products, 2(3), 01-05.

Thomas P., Yang Y. (2013). Cunninghamia konishii. The IUCN Red List of Threatened Species.

Book V.R.D. (2007). Part II-Plants. Natural Science and Technology Publishing House, 133.

Check for updates

CC BY

RESEARCH PAPER

CHARACTERISTICS OF THE SPATIAL AND TEMPORAL DISTRIBUTION OF FIRE REGIME IN ONE OF THE MOST FIRE PRONE REGION OF THE RUSSIAN FAR EAST

Anna M. Zubareva[1]*, Vladimir A. Glagolev[1], Elena A. Grigorieva[1]
[1]Institute for Complex Analysis of Regional Problems Far Eastern Branch Russian Academy of Sciences
***Corresponding author:** anna-doroshenko@yandex.ru
Received: September 24th, 2020 / Accepted: May 25th, 2021 / Published: July 1st, 2021
https://DOI-10.24057/2071-9388-2020-159

ABSTRACT. Wildfires affect the structure and distribution of vegetation all over the globe and have their own specifics in different regions. In this study, we considered the spatial and temporal distribution of fires in the Jewish Autonomous Region (JAR), which is the most fire-prone area of the Russian Far East. Using data from the Department of Natural Resources of the Jewish Autonomous Region, fires and burned areas for more than 40 years were analyzed. The average annual number of fires is near 100, and the average area of one fire is 134 hectares, which is significantly higher compared to other regions of Russia. The largest number of fires and fires with the greatest extent took place in 1975. The intra-annual distribution of fires is bimodal and depends on the climate characteristics of the region. Mapping of burning areas showed that most of the fires occurred near settlements and along roads. The main centers of fire ignition were areas with a large number of small fires (no more than 5 hectares), located within several types of locations: (1) asphalt and dirt roads, railroads and river valleys near settlements; (2) areas of former logging that have several large burned spots of more than 300 hectares; (3) plains with a high concentration of fires over a large region; and (4) small burned spots on the mountain slopes, along the field roads and small rivers. Regions with different degree of fire exposure were identified. Sedge-reed mixed grassy meadows and Agricultural land with shaded meadows are the plant formations most prone to wildfires. At the same time, more fires were detected in Cedar-deciduous forests as well as Oak and black birch forests. The findings are useful for environmental protection agencies in planning fire management strategies, optimizing the fire services and firefighting actions.

KEYWORDS: forest fire, spatial and temporal distribution, burning, plant formations, sources of fire, pyrological characteristics, Russian Far East

CITATION: Anna M. Zubareva, Vladimir A. Glagolev, Elena A. Grigorieva (2021). Characteristics of the spatial and temporal distribution of fire regime in ONE OF the most fire prone Region Of The Russian Far East. Geography, Environment, Sustainability, Vol.14, No 2, p. 74-82 https://DOI-10.24057/2071-9388-2020-159

ACKNOWLEDGMENTS: This study was financially supported by the state budget.

Conflict of interests: The authors reported no potential conflict of interest.

INTRODUCTION

Wildfires are a significant problem worldwide, affecting all aspects of the environment, including the structure, composition and distribution of vegetation (Montz et al. 2017). Every year, up to 400,000 wildfires occur worldwide and, as a result, near 0.5% of the total forest area is damaged. The wildfire danger depends on climate indicators (Sommers et al. 2012; Dupuy et al. 2020), pyrological characteristics of vegetation (Frantz et al. 2016), anthropogenic development (Zumbrunnen et al. 2012), and landscape characteristics (Noon 2003; Díaz-Delgado et al. 2004). The burn probability has been studied in many regions all over the globe: in countries of the Mediterranean – Portugal (Goncalves and Lourenco 1990; Sofia et al. 2012), Spain (Díaz-Delgado et al. 2004), Greece (Kourmpa and Tsigdinos 2020), France, Italy (Salis et al. 2016), as well as in the USA (Radke 1995; Haiganoush et al. 2016; Parisien et al. 2012), Canada (Rogeau et al. 2016), Australia (Linacre 2018; Stephens 2014), China (Yi et al. 2016; Tian et al. 2013a), and Finland (Viegas et al. 1999; Heikinheimo 1998). Although a large number of measures to combat forest fires has been taken, they continue to play an important role in forest ecosystems (Dupuy et al. 2020).

In Russia, there are more than 30000 wildfires annually, in which 2–3 million hectares of forests are damaged. Fire destroys flora, fauna, and the natural environment as a whole, causing economic and environmental damage. In the total number of fires, the Siberian Federal District is in the first place (44% of the total number), followed by the Ural Federal District (23%). The Far East is one of the most fire-prone regions of Russia with 4% of the total number of fires and 43% of the total burned-out area in the Russian Federation; wildfires here destroy approximately 1,112,000 hectares annually, drastically changing ecosystems of the region (Forest complex… 2005).

The fire hazard in the Far Eastern regions has not been extensively studied. The papers (Sheshukov 1982; Telitsyn1988) focused mainly on the prevention and suppression of vegetation fires in Khabarovsky Krai, comparing the characteristics of wildfires in the southern and northern regions. The studies (Glagolev 2017) on wildfire hazard prediction (Kogan and Glagolev 2014; Baranovskiy et

al. 2017; Baranovskiy et al. 2017; Glagolev et al. 2018) discuss the wildfire regional scales, considering the number and area of fires within a certain unit of area. Forest protection agencies give the statistical number and size of fires for each year, determining the spatial distribution of each fire separately, without deep spatial analysis, nor separately identifying the re-burnt regions. As the importance of wood as an accessible building material has increased, large-scale studies on the Russian Far East were carried out in the 1980s. A modern detailed analysis of fire characteristics has been made for Da Hinggan Ling prefecture, located in Heilongjjiang Province, China (Tian et al. 2013b).

Fig. 1 shows that the Jewish Autonomous Region (JAR) holds one of the leading positions in the Far Eastern Federal District in terms of the relative number of wildfires and burned area per 1 million hectares (Sheshukov et al. 2009).

The purpose of this study was to provide a review and analysis of spatiotemporal and pyrological characteristics of wildfires in the Jewish Autonomous Region. Information related to the occurrence and spatial distribution of wildfires, as well as their spatial scale can provide new information, and become a scientific basis for actions to predict and reduce wildfire risk in the region.

MATERIALS AND METHODS

Study area

The Jewish Autonomous Region is located in the southern part of the Russian Far East, between the Lesser Khingan mountain range and the Amur River at latitude from 47 to 49°N and longitude from 130 to 135°E (Fig. 2). It occupies the watershed of the Bira, Bidzhan and Tunguska rivers. The area of the region is 36,600 km^2. In the west, it borders with Amur Region, and in the north, east, and south – with Upper Bureinsky and Khabarovsky Districts of Khabarovsky Krai, and the state border between Russia and China, respectively. The northwestern part of the region is occupied by the low and middle mountainous terrain of the Lesser Khingan and Bureinsky Ranges, while the southeastern part of the region is located at the flat Middle Amur lowland. The climate is considered as a moderate monsoon type (Grigorieva and de Freitas 2014). The average temperature in January ranges from -22 to -24°C, while in July it varies from +20 to +22°C; average annual precipitation ranges from 644 to 758 mm (Grigorieva and Kogan 2010). The total forestry fund land is 22,330 km^2, which covers 61% of the region.

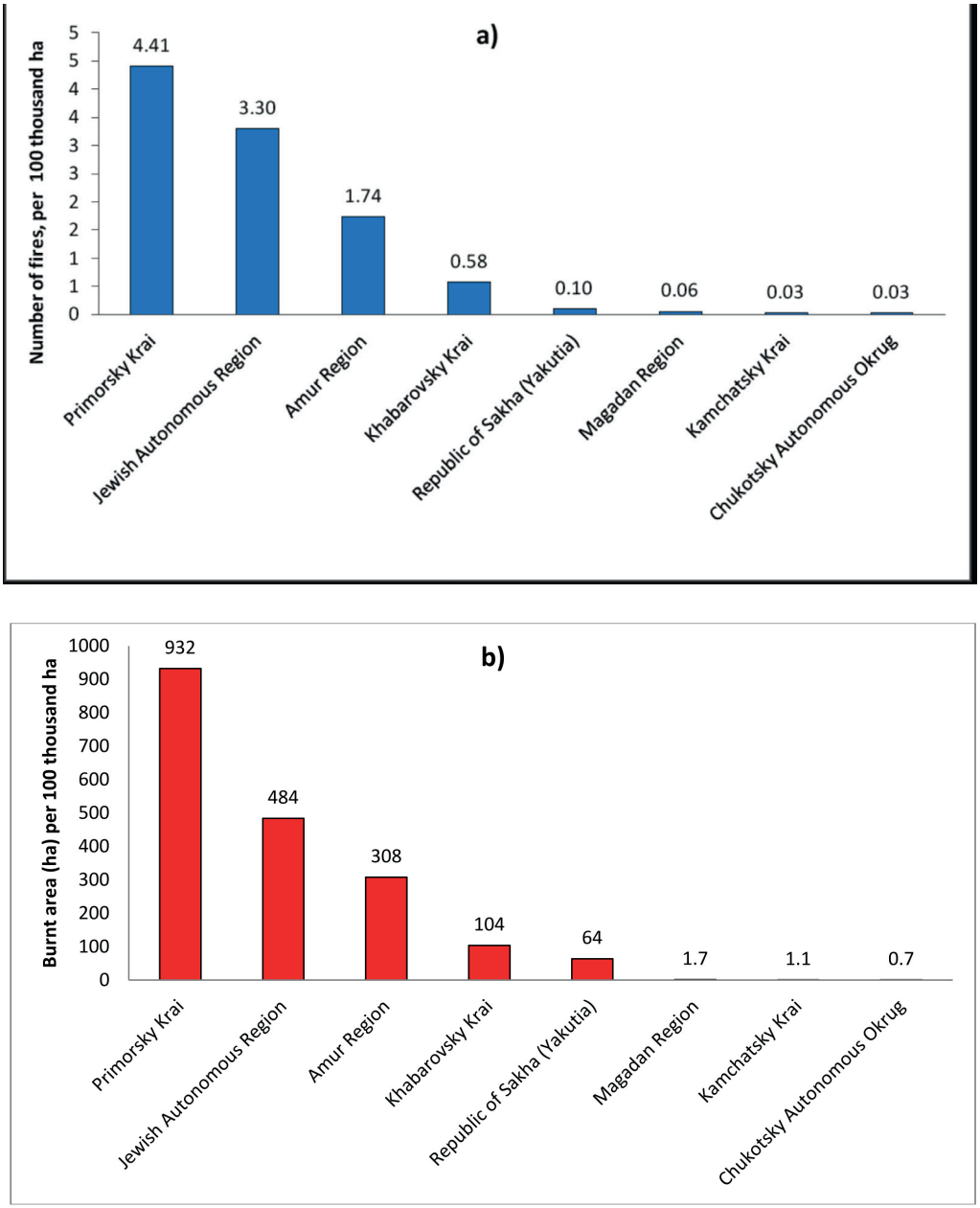

Fig. 1. Wildfires in the Far Eastern Federal District: a) number of fires; b) area covered by fires, per 100 thousand ha

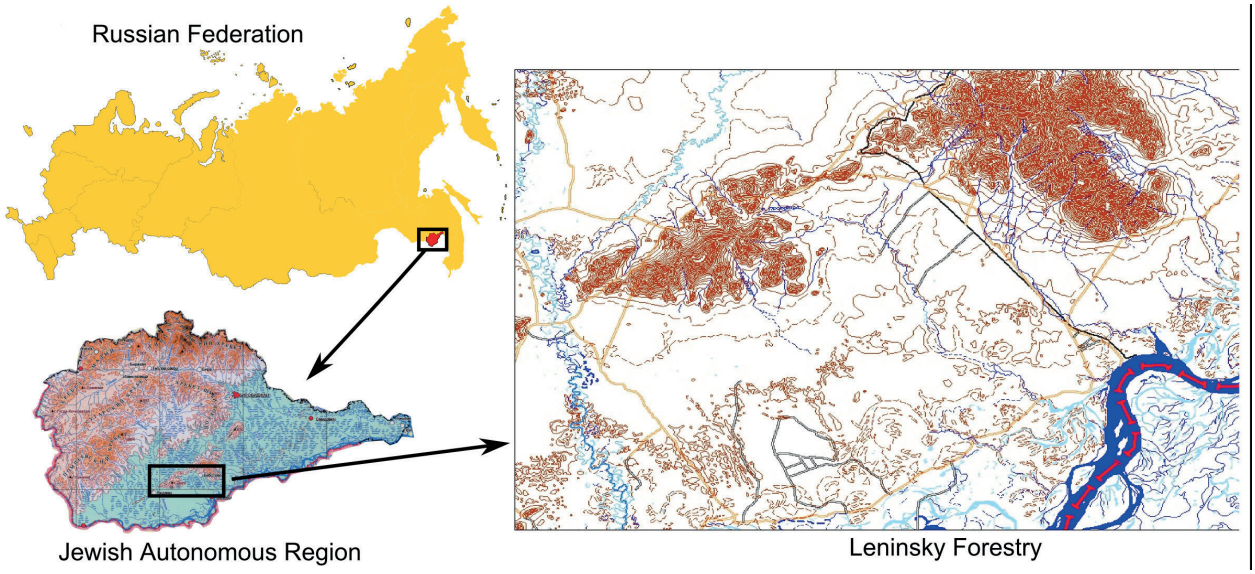

Fig. 2. Geographical location of the Jewish Autonomous Region and Leninsky Forestry unit

We selected Leninsky Forestry unit as a case study for our research on burnt areas and sources of fire. Leninsky Forestry unit is located in the southern part of the Jewish Autonomous Region, in mountainous and flat terrain. It belongs to the territory with the highest burning rate in the region. Wildfire spots here have different areas, from small (1 ha) to large (several thousand ha) ones. Most of the existing burned areas are confined to settlements and roads.

Data

We used the following data in the study: information on the number and other characteristics of wildfires from the Forestry Agency for the Jewish Autonomous Region, Ministry of Natural Resources of the Russian Federation, based on ground and aerial monitoring, for the period from 1970 to 2017. Weather data – mean air temperature and precipitation for every day – was taken from the Hydrometeorological Center of Russia (Weather of Russia 1997) and IKI RAS (Weather and detailed… 2003).

The vegetation types in the Jewish Autonomous Region were mapped by Rubtsova (2016), as shown in Fig. 3. According to the map, the main plant formations in the JAR are: thickets of cedar dwarf pine (*Pinus pumila*), ledum (*Rhododéndron*) and other alpine plants confined to the upper mountain zone; dark coniferous – fir-spruce forests (*Abieti-Piceetalia*) from Ayan spruce (Picea jezoensis) and white fir (Ābies nephrolēpis); larch-spruce and spruce-larch forests of mountains and intermountain valleys; spruce-fir and fir-spruce with cedar (*Pinus koraiensis*) and broad-leaved species; white birch (*Betula alba*) and aspen-white birch forests with conifers, broad-leaved species and derivative forests on mountain slopes; broad-leaved-spruce-cedar forests (*Quercetea mongolica*) or northern cedar forests; broadleaf mixed mixed-breed forests; forests and woodlands of Mongolian oak (*Quercus mongolica*); small-leaved forests and woodlands on plains and in river valleys, meadow and swamp vegetation (Rubtsova 2016).

Black-birch oak-larch woodlands in combination with erniks (low-growth bush forest) and willow thickets, White birch forests along with Oak and black birch forests dominate in Leninsky Forestry.

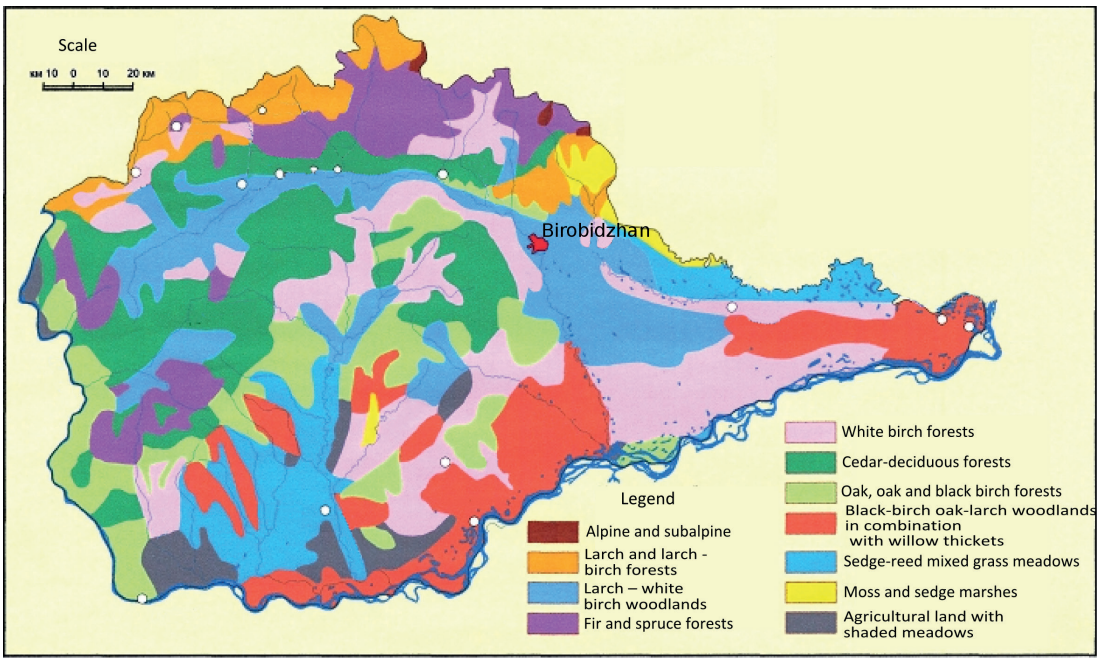

Fig. 3. Vegetation formations in the Jewish Autonomous Region (Rubtsova 2016)

Research Methodology

The methodological approach of our study with the main structural steps is presented in Figure 4.

Firstly, the position of the region in the system of pyrological zoning of Russia is determined using the classification proposed by Dichenkov (1997). Under this classification, all regions in Russia are divided into 7 classes of large fire probability, from class I (below average) with a 10% probability, to VII (the highest level) with 100% fire probability (Dichenkov 1997).

At the second step, we estimate the current efficiency of vegetation combustion looking at fire and weather statistics: the number and area of the wildfires, their spatial distribution and sources of origin, along with mean air temperature and precipitation.

Third, the structure of vegetation is considered using the map of plant formations (Rubtsova 2016). This includes calculating the area of each plant formation based on its distribution in GIS «Inventory Map of the burned areas of the Jewish Autonomous Region». GIS was created in MapInfo Professional 6.0 by researchers at the Laboratory of regional geoecological studies at ICARP FEB RAS (Doroshenko and Kogan, 2008; Zubareva 2016).

At the next step pyrological characteristics of the plant formations as the burning subject are described. The class of fire hazard of vegetation is determined using the method of Starodumov (1965). In this classification, the Far Eastern plant communities are divided into five classes according to the degree of fire danger. The I Class is characterized by a very high fire hazard, the predominance of grass-root fires throughout the fire-dangerous period, and upper fires in dry periods. Sometimes fire can occur at a low value of Nesterov's fire hazard indicator. The V Class is characterized by a very low fire hazard, with the predominance of fires only after a long drought (Starodumov1965).

Last, we applied the Combustion Index (CI) of plant formations (Sofronov and Volokitina 1990), calculated as the ratio of the number and area of fires per 100 thousand hectares (Table 1).

The data obtained as a result of a structured chain of methodological research allows us to comprehensively characterize the number, size, spatial and temporal distribution of fires, and their pyrological characteristics in the study area.

RESULTS

In the *pyrological zoning system of* the Russian Federation, the area of JAR belongs to the Ussuriysk pyrological region (Sofronov and Volokitina 1990), which is characterized by 1.7 fires per 100000 hectares. The relative fire area is 213 hectares per 100000 hectares; the Combustion Index, which indicates the number of fires divided by their total area per unit, is 6.2 (Increased grade), the average fire area is 128 hectares (Sofronov and Volokitina 1990). According to the probability of large fires, out of the existing seven classes, the region belongs to the VII Class with a 100% likelihood of annual fire occurrence (Dichenkov 1997).

Wildfire and weather statistics. Our analysis of the wildfires statistics showed that the maximum number of fires happened in 1970 and 2009, while the maximum area covered by fires was in 1976 (Fig. 5).

We mapped the burned areas in Leninsky Forestry unit as a case study based on fires data for the period from 2010 to 2017 (Fig. 6). Analysis of this map shows that most wildfires are distributed along settlements, roads and rivers. The main fire-prone locations can be divided into four types: (1) areas with a large number and small size of burners (not more than 5 hectares), located along asphalt and dirt roads, railroads and river valleys near settlements; (2) areas of former logging in the mountains that have several large burned spots of more than 300 hectares; (3)

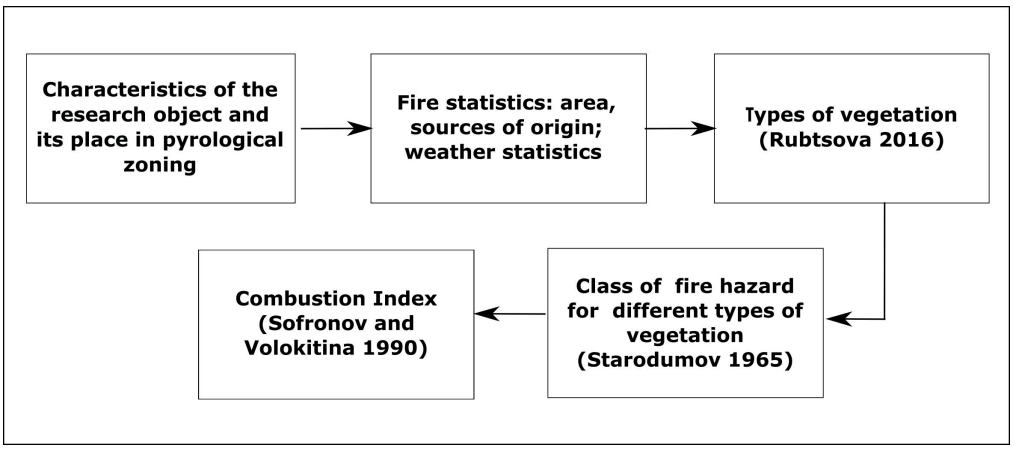

Fig. 4. Research methodology

Table 1. Assessment of the actual burning and Combustion Index (Sofronov and Volokitina 1990)

Actual burning (grades)	Combustion Index
Low (I)	< 0.7
Moderate (II)	0.8-2.5
Increased (III)	1.6-8.5
High (IV)	8.6-26.0
Very high (V)	> 26.1

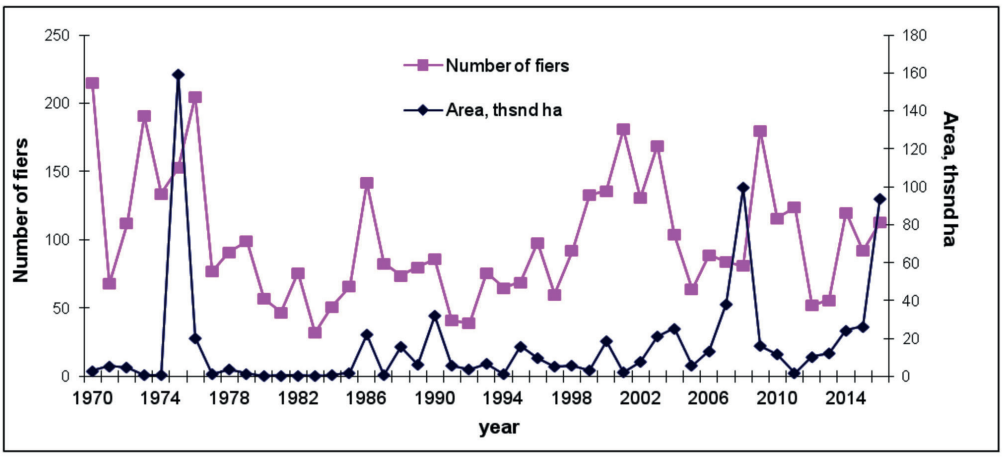

Fig. 5. The number and area of fires in the Jewish Autonomous Region, 1970–2017

plains with a high concentration of fires over a large region of more than 1000 hectares; and (4) small burned spots in mountain slopes along field roads and small rivers, where few fires are found with a small size of less than 10 hectares.

Considering the climate data in conjunction with the intra-annual fire dynamics, it is possible to determine their relationship and identify the fire hazard period within the year (Fig. 7). The largest number of fires is observed in spring. First, this period is characterized by the most favorable weather for ignition of combustible plant materials as precipitation is scarce (Grigorieva and de Freitas 2014); and second, young vegetation appears later in spring. In autumn, there are fewer wildfires and they spread less due to the relatively high precipitation.

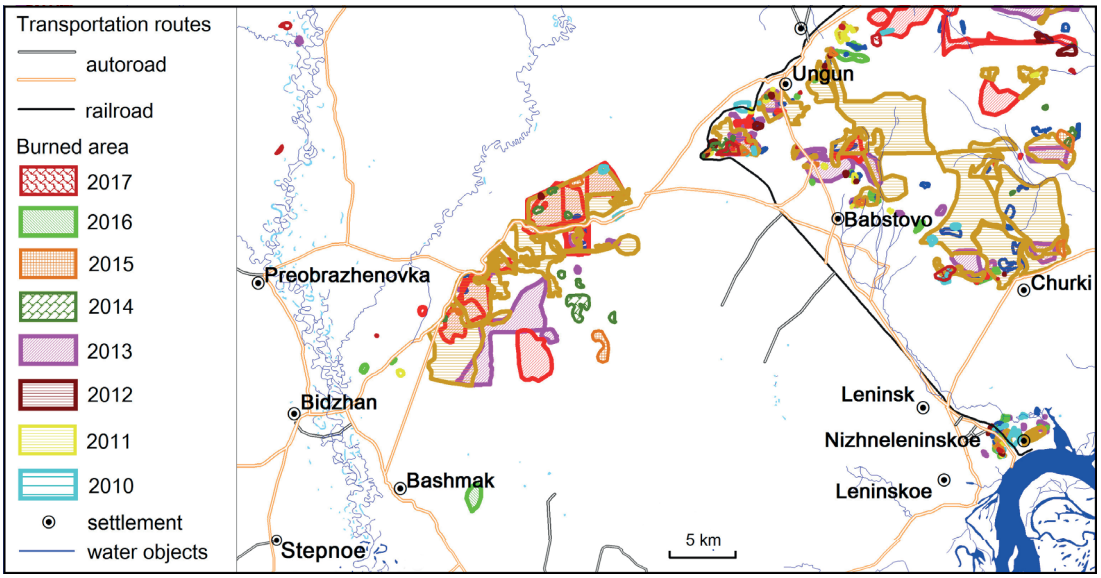

Fig. 6. Fragment «Inventory Map of the burned areas in the Jewish Autonomous Region (2010–2017)» for Leninsky Forestry unit

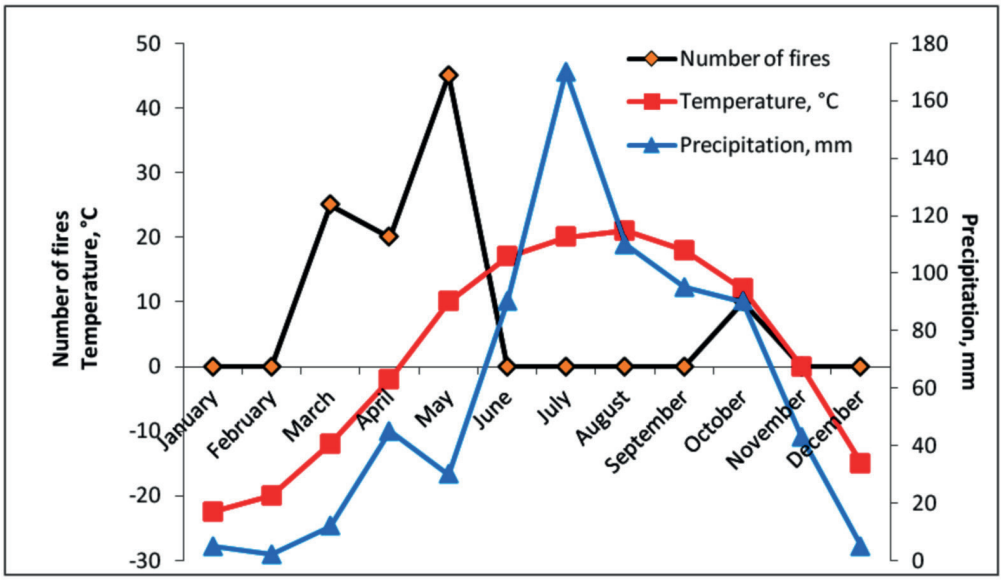

Fig. 7. The influence of climate on the intra-year dynamics of wildfires in the Jewish Autonomous Region

Based on statistical data, we show that the majority of fires are caused by human activity; however, there is also a high proportion of fires for which the source of origin is not determined (Fig. 8).

Structure of vegetation. Table 2 shows that the white birch forests are most prevalent in the region. For the most part of the region, they form a secondary vegetation type after disturbances.

The largest fire areas are found in Sedge-reed mixed-grass meadows and Black-birch oak-larch woodlands in combination with erniks (low-growth bush forest) with willow thickets.

Pyrological characteristics of the plant formations. Class of fire hazard for different types of vegetation shows that Sedge-reed mixed grassy meadows, Agricultural land with shaded meadows (I Class of fire hazard), and Cedar-deciduous forests, along with Oak and black birch forests (II Class of fire hazard) are the most fire-hazardous vegetation formations (Table 1). As a whole, they cover near 40% of the region. Moss and sedge marshes as well as Alpine and subalpine have the lowest class of fire hazard (V), covering 2% of the region (Table 1).

Combustion Index. The calculation of the Combustion Index in the plant formations per 100 thousand ha according to the method by (Sofronov and Volokitina 1990) is shown in Table 2. Cedar-deciduous forests together with Oak and black-birch forests are the most flammable. Moss and sedge swamps, Agricultural land with shady meadows and Sedge-reed mixed grasslands are the least prone to fires. The calculation of the combustion of these plant formations indicates that not always the most fire-hazardous formations are subject to the highest level of combustion. A significant number of fires are also observed in Larch and larch-birch forests (IV Class of fire hazard) and White Birch forests (III Class of fire hazard).

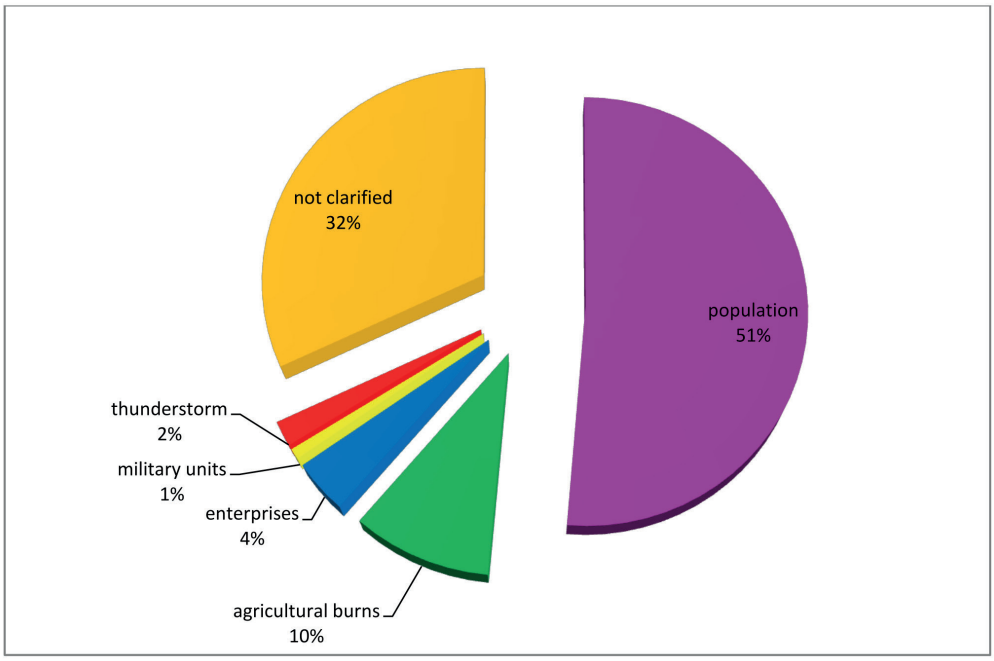

Fig. 8. Sources of fires in the Jewish Autonomous Region, 2013–2017

Table 2. Fire and fire hazard of plant formations in the Jewish Autonomous Region

№	Plant Formation	Percent of the total area, %	Vegetation fire hazard class	CI: number of fires per 100 thousand ha
1	Alpine and subalpine	0.21	V	0.00
2	Larch and larch – birch forests	6.47	IV	4.00
3	Larch – white birch woodlands	13.76	IV	2.50
4	Fir and spruce forests	9.45	III	2.19
5	White birch forests	16.16	III	3.58
6	Cedar-deciduous forests	15.37	II	5.07
7	Oak and black birch forests	12.03	II	4.39
8	Black-birch oak-larch woodlands in combination with erniks (low-growth bush forest) and willow thickets	13.28	IV	1.13
9	Sedge-reed mixed grassy meadows	7.86	I	0.88
10	Moss and sedge marshes	1.86	V	0.00
11	Agricultural land with shaded meadows	3.52	I	0.50

DISCUSSION

Spatial and temporal distribution of wildfires

Fire is a major factor in the destruction of natural landscapes. The relative influence of various pyrological factors varies across global regions. Studies of fire regimes are important for understanding fire interference and for adopting a scientific approach to fire management.

In our analysis, we found that the mean annual number of fires over the study period was near 100, which is significantly higher than in other regions of Russia. For example, Kurbatsky and Tsvetkov (1986) estimated 5 fires for Koryaksky and 33 fires for Komi-Permyatsky Autonomous Districts, 13 – for Aginsky-Buryatsky Autonomous District, 2 – for the Republic of Adygea, and others (Kurbatsky and Tsvetkov 1986). However, this is less than half of the number of fires in the neighboring province of Heilongjiang in China (Tian et al. 2013a, 2013b). The average area of a single fire in the Jewish Autonomous Region is 134 hectares. Near the border with China, province of Heilongjiang, this area is 1167 hectares (Tian et al. 2013a, 2013b).

The largest number of fires in the Jewish Autonomous Region was registered in 1970, 1973, 1975, 2001, 2005, and 2009; the wildfires had the largest area in 1976, 2009, and 2017. During these years, severe droughts were observed, and the mean precipitation during the fire hazard period did not exceed 70 mm.

The areas with the largest concentration of small fires are located in the regions of transport accessibility, which allows them to be detected and localized promptly. Areas with large fires (more than 1000 ha) are found in mountainous areas, where early localization and elimination of fires are difficult due to their remoteness and difficult communications. On plains distant from the main transport routes, fires acquire large areas because terrain features allow the ignition to spread over. This distribution of lands affected by the pyrological factor is typical for the regions of new development, which is the entire Far East of the Russian Federation in general, and the Jewish Autonomous Region, in particular.

The intra-annual distribution of fires is bimodal, which is similar to the areas of the same nature in China (Tian et al. 2013a, 2013b). Most of the forest fires occur in spring (April, May) (65%), with May having the highest rate (45%). The fire risk period in the JAR is 214 days. The high fire danger of the spring period is explained by short, snowy winters and fast melting of the snow, as well as by increasing temperature and low precipitation, which creates favorable conditions for the ignition of combustible plant materials. The second peak period of forest fires is from September to November (35%). The most fire hazardous month in autumn is October. In autumn, dried vegetation is easily ignited even when it is raining. Cedar-deciduous forests and Oak, oak and black birch forests are the plant formations most exposed to fire (Table 2).

Natural and other sources of fire ignition

The dynamics of forest fires in recent years makes it possible to identify factors contributing to the emergence of fire, the degree of influence of these factors is shown in the following sequence: 1) population; 2) forest fires; and 3) enterprises and organizations. The main source of forest fires is of anthropogenic origin, which in some years accounts for more than 90% of all fires. Therefore, it is necessary to improve the awareness of residents about the prevention of forest fires and to encourage the local population to participate in management activities and elimination of fires.

The smallest impact on the occurrence of fires in the Jewish Autonomous Region is exerted by natural sources of ignition, named as «dry thunderstorms». This is explained by the fact that the greatest thunderstorm activity falls on the less flammable pre-monsoon period when the combustion materials are sufficiently moistened.

A large number of fires with an unexplained source of origin might be associated with certain legal and practical difficulties in identifying the perpetrators of forest fires. In the forest, given the specificity of the object of burning and the absence of witnesses, it is often not possible to identify evidence that unequivocally confirms the guilt of the detainee, even at the site of the fire.

The sources of fires in forests include the activities of forest users, primarily loggers, collectors of berries, mushrooms, ferns, hay, and medicinal plants, and tourists. A significant source of fire is associated with all types of transport that cross forest tracts, since their fuel, when exposed to heat, ignites combustible plant materials. In the spring and autumn, agricultural organizations and the population deliberately burn old grass in their hayfields; these burns often turn into forest fires.

Pyrological characteristics of the plant formations and their Combustion Index

White birch forests are the most widespread plant formations. Cedar-deciduous forests and Larch – white birch woodlands cover over 45% of the Jewish Autonomous Region. The most prone to fire vegetation formations with Classes I-II of fire hazard make 40% of the area and include Cedar-deciduous forests, Oak and black-birch forests, Sedge-reed mixed grassy meadows, Agricultural land with shady meadows. The formations in which the fires are most frequent are White birch forests, Cedar-deciduous forests, Oak and black – birch forests, Larch and larch – birch forests. The area most prone to fires covers approximately 50% of the Jewish Autonomous Region. It is worth noting, that the combustion of plant formations does not always correspond to their fire hazard class. For example, a high Combustion Index is found for Larch and larch-birch forests (Class IV of fire hazard) and White birch forests (Class III). At the same time, there are practically no fires in Sedge-reed mixed grassy meadows and Agricultural land with shaded meadows – plant formations with Class I of fire hazard.

The study has some limitations, one of which is that it was based on ground and air patrol observation data only. Fires are mainly detected by air patrols (approximately 65 %). Ground fire protection services detect near 30% of fires. Satellites register no more than 5% of fires due to frequent cloudiness in the region. The reason we cannot use satellite imagery data is the large number of cloudy days observed in the study area during the fire hazard period, especially in autumn. The MODIS satellite takes low-resolution images (250 m), therefore we cannot fully detect the location of a fire and estimate its area. Satellite images do not provide an opportunity to characterize the type of fire and fully determine the damage caused to the forest fund. They can also overestimate the area of fires as they capture the heat flux that is reflected in heated soil and smoke (Bartalev et al. 2017).

CONCLUSIONS

The burning rate in the Jewish Autonomous Region was studied over the past 40 years, compared with other regions of the Russian Federation and neighboring countries (Chinese provinces). The previously compiled

«Inventory Map of Burners» was supplemented with contemporary data.

Aerial monitoring was used as the main instrument for detecting forest fires in the Jewish Autonomous Region, and this method makes it possible to find most of the fires in forest areas. The intra-annual distribution of fires has a bimodal character, which is caused by the climate characteristics, forming the conditions for the ignition of combustible plant materials.

To build an effective fire control policy for vegetation, it is necessary to know the reasons for fire occurrence. In this regard, the main cause of fires is human activity, and the main areas of ignition are within the locations of the anthropogenic load. Ignitions in these areas are frequent but small in size. The size of burnt areas increases significantly, whereas the number of burns decreases with increasing distance from the location of human impact.

In the future, in order to carry out a comprehensive pyrological zoning of the Jewish Autonomous Region, an assessment of the natural and anthropogenic fire hazard is planned. This assessment will help to identify areas with varying degrees of fire exposure and should be considered when planning the fire management strategy and optimizing the organization of the fire service.

REFERENCES

Baranovskiy N.V., Barakhnin V., Yankovich E. (2017). GIS-Technologies and mathematical simulation as tools for lightning-caused forest fire danger prediction CEUR Workshop Proceedings, 1839, 2-15, DOI: 10.1117/12.2241670.

Baranovskiy N.V., Kogan R.M., Glagolev V.A., Zubareva A.M. (2017). Grassland fire spread simulation using NDVI data. In Proc. SPIE 10466, 23rd International Symposium on Atmospheric and Ocean Optics: Atmospheric Physics, 104663B, DOI: 10.1117/12.2286782.

Bartalev S.A., Stytsenko F.V., Khvostikov S.A., Lupyan E.A. (2017). Methodology for monitoring and predicting pyrogenic forest destruction based on satellite observation data. Current Problems in Remote Sensing of the Earth from Space, 14(6), 176-193, DOI: 10.21046/2070-7401-2017-14-6-176-193.

Díaz-Delgado R., Lloret F., Pons X. (2004). Spatial patterns of fire occurrence in Catalonia, NE, Spain. Landscape Ecology 19 (7), 731-745, DOI: 10.1007/s10980-005-0183-1.

Dichenkov N.A. (1997). Assessment of the risk of large-scale forest fires. Forestry, 4, 46-48. (in Russian).

Doroshenko A.M., Kogan R.M. (2008). Analysis of the spatial distribution of forest fires on the territory of the Jewish Autonomous Region. Bulletin of the Tomsk State University, 311, 172-177 (in Russian).

Dupuy J.l., Fargeon H., Martin-StPaul N. et al. (2020). Climate change impact on future wildfire danger and activity in southern Europe: a review. Annals of Forest Science, 77, 35, DOI: 10.1007/s13595-020-00933-5.

Forest complex of the Far East of Russia: an analytical review (2005). A.S. Sheinghous (Ed.). Vladivostok, Khabarovsk, 160 (in Russian).

Frantz D., Stellmes M., Röder A., Hill J. (2016). Fire spread from MODIS burned area data: obtaining fire dynamics information for every single fire. Int. J. Wildland Fire, 25(12), 1228-1237, DOI: 10.1071/WF16003.

Glagolev V. (2017). Method foe prediction of the initiation and distribution of herbal fire. Technology of technospheric security, 4(74), 132-140 (in Russian).

Glagolev V.A., Zubareva A.M., Grigorieva E.A. (2018). Grassfire forecast at agricultural lands in Jewish Autonomous Region. Regional Problems, 21, 3(1), 93-97, DOI: 10.31433/1605-220X-2018-21-3(1)-93-97.

Goncalves Z.J., Lourenco L. (1990). Meteorological index of forest fire risk in the Portuguese mainland territory Proceedings of the international conference on forest fire research, Coimbra, 7, 1.

Grigorieva E.A., de Freitas C.R. (2014). Temporal dynamics of precipitation in an extreme mid-latitude monsoonal climate. Theor. Appl. Climatol., 116(1), 1-9, DOI:10.1007/s00704-013-0925-x.

Grigorieva E.A., Kogan R.M. (2010). Pirological characteristic of climate at the southern part of the Russian Far East. Regional Problems, 13(2), 78-81.

Heikinheimo M. (1998). Renewing the system for forest fire risk assessment at the Finnish Meteorological Institute International Forest Fire News, 18, 65-67.

Weather of Russia – weather forecast, actual weather conditions (1997). Weather archive. http: //meteo.infospace.ru [20.05.2019]

Weather and detailed weather forecast from the Hydrometeorological Center of Russia (2003). Factual data. http://meteoinfo.ru [20.05.2019]

Kogan R.M., Glagolev V.A. (2014). Features of fire-dangerous seasons in the Khabarovsk Territory and the Jewish Autonomous Region. Fundamental Research, 9(7), 1549-1553. (in Russian).

Kourmpa E., Tsigdinos S. (2020). Detection of fire-prone areas in Attica region integrating urban and transport aspect. Geography, Environment, Sustainability, 13(3), 84-89, DOI: 10.24057/2071-9388-2019-148.

Kurbatsky N.P., Tsvetkov P.A. (1986). Protection of forests from fires in areas of intensive development (for example, KATEK). Krasnoyarsk, 146. (in Russian).

Linacre E. Predicting bushfires in Australia. URL: http://www-as.uwyo.edu/~geerts/cwx/notes/chap16/oz_bush.html [Assessed on February, 05, 2021].

Montz B., Tobin G., Hagelman R. (2017). Natural hazards: explanation and integration. The Guilford press, New York, 445.

Noon E.K. (2003). A coupled model approach for assessing fire hazard at point Reyes national seashore: flam map and GIS. Proceedings of the 2nd International wildland fire ecology and fire management congress, Springs Resort.

Oliveira S.L.J., Pereira J.M.C., Carreiras J.M.B. (2012). Fire frequency analysis in Portugal (1975–2005), using Landsat-based burnt area maps. Int. J. Wildland Fire, 21 (1), 48-60, DOI: 10.1071/WF10131.

Parisien M.-A., Snetsinger S., Greenberg J.A., Nelson C.R., Schoennagel T., Dobrowski S.Z., Moritz M.A. (2012). Spatial variability in wildfire probability across the western United States. Int. J. Wildland Fire, 21(4), 313-327. DOI: 10.1071/WF11044.

Preisler H.K., Riley K.L., Stonesifer C.S., Calkin D.E., Jolly W.M. (2016). Near-term probabilistic forecast of significant wildfire events for the Western United States. Int J Wildland Fire, 25 (11), 1169-1180, DOI: 10.1071/WF16038.

Radke J. (1995). Modeling urban/wildland interface fire hazards within a geographic information system, Geographic Information Sciences, 1(1), 9-21.

Rogeau M.-P., Flannigan M.D., Hawkes B.C., Parisien M.-A., Rick A. (2016). Spatial and temporal variations of fire regimes in the Canadian Rocky Mountains and Foothills of southern Alberta. Int. J. Wildland Fire, 25(11), 1117-1130, DOI: 10.1071/WF15120.

Rubtsova T.A. (2016). Types of Vascular Plants Described from the Territory of the Jewish Autonomous Region as New to Science. Regional Problems, 19(3), 32-37 (in Russian).

Salis M., Arca B., Arianoutsou F., et al. (2016). Predicting wildfire spread and behaviour in Mediterranean landscapes. Int. J. Wildland Fire, 25(10), 1015-1032, DOI: 10.1071/WF15081.

Sheshukov M.A. (1982). Forest fire district of the Far East. Khabarovsk (in Russian).

Sheshukov M.A., Brusova E.V., Gromyko S.A., Pozdnyakova V.V. (2009). Conservation and protection of the forest. In: The current state of the forests of the Russian Far East and the prospects for their use, M.A. Sheshukov (Ed.), Khabarovsk, DalNIILKH, 470. (in Russian).

Sofronov M.A., Volokitina A.V. (1990). Pyrological zoning in the taiga zone. Novosibirsk, 205 (in Russian).

Sommers W.T., Coloff S.G., Conard S.G. (2012). Synthesis of knowledge: fire history and climate change. Final report to the Joint Fire Science Program, JFSP Project 09-02-1-09.

Starodumov A.M. (1965). Scale of fire hazard of plantings and other categories of areas for the conditions of the Far East. Khabarovsk: DalNIILKh (in Russian).

Stephens S.L., Burrows N., Buyantuyev A., Gray R.W., Keane R.E., Kubian R., Liu S., Seijo F., Shu L., Tolhurst K.G., van Wagtendonk J.W. (2014). Temperate and boreal forest mega-fires: characteristics and challenges. Frontier Ecol. Environ., 12(2), 115-122, DOI: 10.1890/120332.

Telitsyn G.P. (1988). Forest fires, their prevention and extinguishing in the Khabarovsky Krai. Khabarovsk, p. 95 (in Russian).

Tian X., Shu L., Wang M., Zhao F., Chen L. (2013a). The fire Danger and Fire Regime for the Daxing'anling Region for 1987-2010. Procedia Engineering, 62, 1023-1031, DOI: 10.1016/j.proeng.2013.08.157.

Tian X., Zhao F., Shu L., Wang M. (2013b). Distribution characteristics and the influence factors of forest fires in China. Forest. Ecol. Management, 310, 460-467, DOI: 10.1016/j.foreco.2013.08.025.

Viegas X.D., Bovio G., Ferreira A., Nosenzo A., Sol B. (1999). Comparative study of various methods of fire danger evaluation in southern Europe. Int. J. Wildland Fire, 9(4), 235-246, DOI: 10.1071/WF00015.

Yi K., Bao Y., Zhang J. (2016). Spatial distribution and temporal variability of open fire in China. Int. J. Wildland Fire, 26 (2), 122-135, DOI: 10.1071/WF15213.

Zubareva A.M. (2016). Fire rate of vegetation in the natural-territorial complexes of the Jewish Autonomous Region, In the book: Modern problems of regional development. Abstracts of the VI International Scientific Conference. Birobidzhan, ICARP FEB RAS, 18-21 (in Russian).

Zumbrunnen T., Menéndez P., Bugmann H., Conedera M., Gimmi U., Bürgi M. (2012). Human impacts on fire occurrence: a case study of hundred years of forest fires in a dry alpine valley in Switzerland. Reg. Environ. Change, 12 (4), 935-949, DOI: 10.1007/s10113-012-0307-4.

Check for updates

CC BY

RESEARCH PAPER

IDENTIFICATION OF MULTIFUNCTIONAL URBAN ACTIVITY CENTERS IN TOKYO

Vadim I. Boratinskii[1], Irina S. Tikhotskaya[1*]

[1]Lomonosov Moscow State University / Faculty of Geography, Leninskie gory, Moscow, GSP-1, 119991, Russian Federation, Faculty of Geography

***Corresponding author:** iritiro@gmail.com

Received: August 16th, 2020 / Accepted: May 25th, 2021 / Published: July 1st, 2021

https://DOI-10.24057/2071-9388-2020-136

ABSTRACT. Identification of urban activity centers is among the most important components of the urban structure study, it is necessary for reasonable planning, regulation of traffic flows and other practical measures. The purpose of this paper is to design a complex method to identify urban activity centers based on different but universal data types. In this study, we used social media data (Twitter) since it guarantees regular updates and does not rely on administrative borders and points of interest database that was considered a 'hard' representation of multifunctional urban activities. A large amount of geotagged tweets was processed by means of statistical modelling (spatial autoregression) and combined with the distribution analysis of points of interest. This allowed to identify the local centers of urban activity within 23 special wards of Tokyo more objectively and precisely than when only based on the social media data. Thereafter, delimitated centers were classified in order to define and describe their main functional and spatial characteristics. As a result of the study, railway transport was identified as the main attraction factor of the urban activity; the modern urban structure of Tokyo was identified and mapped; a new comprehensive method for identification of urban activity centers was developed and five classes of urban activity centers were defined and described.

KEYWORDS: Urban activity centers; urban structure; points of interest; social media data; Twitter, Tokyo

CITATION: Vadim I. Boratinskii, Irina S. Tikhotskaya (2021). Identification Of Multifunctional Urban Activity Centers In Tokyo. Geography, Environment, Sustainability, Vol.14, No 2, p. 83-91 https://DOI-10.24057/2071-9388-2020-136

ACKNOWLEDGMENTS: We would like to thank Timofey Samsonov (Leading Researcher, Lomonosov MSU) for advice on the spatial modelling, Prof. Toshio Omata (Former Professor, Toyo University) for assistance during fieldwork; Elena Pozdorovkina (Former UNFPA Senior Advisor) for helping with editing; and Ruslan Dokhov (Habidatum, RxD Lead) for inspiring ideas at the initial stages of the research process.

Conflict of interests: The authors reported no potential conflict of interest.

INTRODUCTION

Identification of urban structure is one of the most important tasks of Urban Geography. One of its key components is the identification of urban centers, or urban activity centers (UACs), which is necessary for urban planning, regulation of traffic flows, and other practical matters. The majority of studies aimed at identifying urban structure analyze census data, economic statistics, or employment patterns. Our work is devoted to the development of a methodology based on the use of social media data, location of points of interest (POI) and their characteristics. In this research we use the term 'urban activity centers' to refer to the areas of the city with the concentration of urban activity and points producing it, to a higher measure, in comparison to their surroundings.

This study focuses on Tokyo[1], one of the largest cities in the world by the population of the metropolitan area (Demographia 2017). Having developed over the course of several centuries, Tokyo formed a complicated socio-spatial structure: it is a polycentric urban system which consists of several urban cores interconnected by energy, human, traffic and information flows between them.

The main objective of this work is to identify and analyze the key elements of this structure – urban activity centers. This paper summarizes the stages of original research in the following sequence: development of the comprehensive methodology for identification of urban activity centers; application of the methodology to the case of Tokyo; classification of the identified centers and analysis of their qualitative and quantitative characteristics as well as their role in urban life and urban structure.

MATERIALS AND METHODS

Models and theories for identification of urban activity centers

The main aim of this study is to identify the urban structure of Tokyo by delimitation of the urban activity centers within the city boundaries. First of all we need to define what the urban activity centers are and what

[1] In this study, Tokyo means the territory within the 23 special wards of Tokyo, which is commonly understood as administrative boundaries of the city.

criteria should we use for their identification. In the second half of the 20th century these questions were on the research agenda of scholars and relevant publications. In general they interpreted urban activity centers as areas or neighborhoods characterized by an outstanding concentration of employment (e.g. number of workplaces). This kind of perception of the centers was introduced by M. Fujita and H. Ogawa in the early 1980s (Fujita, Ogawa 1982), but it has largely transformed in connection with the development of the concept of post-industrial cities. Scientists following these trends, such as B. De Goei (De Goei et al. 2010), M. Batty (Batty 2013), S.B. Pomorov and R.S. Zhukovsky (Pomorov, Zhukovsky 2015) argue that the true cores of cities are the centers of voluntary visits. In such places the facilities related to commerce, culture and recreation play the role of attraction points. They form permanent stable human flows that are even larger than in employment centers (Kotov et al. 2016).

Selection of criteria or indicators for UAC identification is certainly an important step for determining the spatial structure of a city but it is not the only one. In fact, if we identify the cores of urban activity through the actual distribution of any selected indicator in cities with a pronounced center peripheral subcenters will appear insignificant in the urban landscape. For this reason we have come up with a conceptually different approach that allows to take into account not only the size of UACs but also their distinguishing features within the local urban subsystem.

One of the most popular and sophisticated methods based on this idea in Russian Urban Studies is the «non-uniformly-zoned model of the city» (NZM) developed by A. A. Vysokovsky (Vysokovsky 2005). Basically it allows to identify commercial activity centers and the territory of their influence at different hierarchical levels. This method involves the analysis of areal units – cells of a regular or expert-selected grid instead of the pure distribution of point phenomena. The first step is to determine the general distribution of «centrality» (overall trend) in the urban space, the second is to identify the areas with the largest positive differences between the real concentration (or value) of the chosen indicator and the overall trend. The territorial units with abnormally high values are the areas with the greatest potential for attraction. They can be called local activity centers. This computational algorithm makes it possible to calculate the absolute values of the chosen indicator by the territorial units and also take into account the local importance of the sites and zones that generate commercial activity. This approach reveals the influence of the areal zones at both local and citywide levels.

The methods proposed by McMillen and McDonald consider cities as polycentric objects as well, however the centers are understood differently. To begin with, they clearly distinguish the main center, i.e. the overall core of the urban area (usually the central business district), and subcenters located around it as the main components of the urban socio-spatial structure. Subcenters represent parts of the territory with a relatively higher density of urban activity in any form (McMillen 2004) and in this sense the spatial distribution of urban activity centers is analogous to what Vysokovsky wrote about.

In his works McMillen focused on the issue of how existing employment data should eventually be processed. He developed a sophisticated method that significantly improves the objectivity urban cores identification based on the census data or economic statistics. He achieved notable progress in this area by applying non-parametric methods, such as geographically weighted regression, and semi-parametric employment density functions to identify subcenters as areas with activity density considerably higher than expected, based on the distance of these subcenters from the central business district. Logistic regression is not applicable for this task due to the asymmetric distribution of subcenters (McMillen 2001). The disadvantage of this method is that the central business district or the central point of the city should be defined at the initial stage. The crucial assumption is that the closer a certain segment is to this central point of the city, the more concentrated is its human activity. This method was widely used in the later works of McMillen, including his joint work with McDonald, (McMillen, McDonald 1997), as well as by other researchers, for example, F. Riguelle (2007).

Our definition of urban activity centers and the proposed methodology for their identification is based on the above mentioned studies of Vysokovsky and McMillen. We rely upon the Vysokovsky concept of the overall (or global) trend of centrality. Since our objective is to identify not only large concentrations of activities in the city center but also UACs that are significant at the neighborhood or ward level, we have to detect this overall trend in the urban system and eliminate it in order to identify local, smaller-scale spatial patterns of activity distribution. While Vysokovsky and his followers used moving average method, which is not very effective, for the same purpose, McMillen initiated the application of more complicated non-parametric methods. As the reader will see from the section 'Identification of urban activity centers' authors of this paper employed spatial autoregression to eliminate the issue of overall centrality trend being inspired by McMillen's findings.

Application of social media data for identifying urban activity centers

Increased availability of the Internet and, particularly, the growing use of social networks provides new opportunities for studying the spatial organization of people and interaction between people and space. The existence of social media data with spatial references opens up access to huge amounts of information describing the spatial behavior of people, their mobility and attachment to certain places. Previously social media data appeared to be actively used for political science research and marketing. Urban planners and researchers of urban space became interested in it very recently. Many scholars (Campagna 2014; Campagna et al. 2015; Evans-Cowley, Griffin 2011) have emphasized the necessity of this data for a quick response and better awareness.

The value of social media data for spatial patterns studies lies in geo-tagging, i.e. the possibility for correlating notes, photographs and web pages to geographic coordinates. Thus, researchers have an opportunity to obtain information concerning demographic, thematic, behavioral and contextual features that are temporally and spatially referenced. The main methodological problem related to the use of social media data is to generalize this heterogeneous information. Existing data analysis methods for geotagged social media datasets are developing at an impressively rapid pace. For instance, Ciuccarelli, Lupi and Simeone (2014) proposed a design of a social media data processing tool that would be user-friendly for urban planners without a technical background. Other researchers (Bingham-Hall and Tidey 2016) focused on the use of visualized social media data for enhancing the decision-making process by providing insights on local issues.

The use of social media data became of great importance in the context of the participatory planning

approach concept that implies the participation of the entire community in the process of urban management and planning. The followers of this concept argue that planning measures based on the opinion of experts or local administration are unacceptable; whereas a joint decision of the community population, experts and administration is more appropriate (Healey 1999). Such an approach does not only take into account the population interests but also allows to look at how the population interacts with the urban space. This is precisely the main intersection of our research with a participatory planning approach since this study aims to identify not the centers determined by the administration but informal UACs. In our opinion, the informal centers are the ones that play the greatest role in the life of the city's population. They do not often have names and are unknown to the residents of other parts of the city while being very important for the local community, and this could be revealed by social media data better than by almost any other source of information.

As some researchers have already shown, social media activity is more appropriate for detecting urban structure compared to other sources of big spatial data because social media activities usually take place when users encounter something new or stay in a certain location for a long time (Kaplan, Haenlein 2010). It is important that the use of this type of data allows to identify the sites with heterogeneous activity (Frias-Martinez et al. 2012), which is a key goal for us in defining UACs. The utilization of social media data as one of the indicators of urban activity is also explained by the fact that the modern population of Japan actively uses mobile communications and social media and tend to report almost about every purchase they make.

Social media data

In this study we use geotagged data from the microblogging service Twitter. This is the most popular social media platform in Japan with approximately 45 million users, which is about 35% of the country's population (TechCrunch 2018). We generated a table of original data using approximately 1 million tweets posted in 2017 covering 23 special wards of Tokyo by putting together the original data on the geographical location, timing and date of messaging. This data set makes it possible to perform the spatial-temporal analysis of the human activity in Tokyo, however, it is necessary to mention that the application of geotagged tweets, and social media data in general, has several limitations and we should take them into account while analyzing and interpreting the results. Moreover, since this data type is relatively new the theoretical background for it is not extensive and some drawbacks may still be undiscovered.

Steiger et al. (2015) outlined several limitations of social media data starting with the sampling bias related to the fact that not everyone uses social media and particularly Twitter. This bias leads to the underrepresentation of some social groups in the data and overrepresentation of the other (Heckman 1979), which is undoubtedly relevant for our case. Secondly, the coordinates of tweets may be inaccurate due to atmospheric radiation, mobile device characteristics and the effect of the surrounding environment. In addition, users may choose either to enter a specific location with precise coordinates or to keep it more general, such as city or even country. To avoid the limitations related to this bias we used only tweets with precise coordinates. Thirdly, the text of tweets may not reflect the currently happening activities at all. For instance, the tweets may refer to future or past activities. The latter can significantly affect the interpretation and the functional analysis of the data, however, it does not have any impact on the findings of this study which uses only two parameters of the tweets: time and geo-location.

Points of interest

Social media data is characterized by spatial instability and sensitivity to spontaneous events that may cause inaccuracy in the identification of spatial structure. In order to overcome this problem we used the database of POIs (points of interest) of OpenStreetMap (2017) as an additional data source. POIs are places where most social interactions occur; where people spend most of their free time. Thus, we consider the phenomenon that according to the concept of R. Oldenburg is called «third places» (Ahas et al. 2009; Cai et al. 2016; Schneider et al. 2013), which includes places different from home and work. The activities there represent a crucial part of social interactions and are certainly important for understanding the urban environment (Rosenbaum 2006).

It is necessary to mention that the POI database covers a wider range of facilities than only third places. It also includes a part of 'second places', such as schools, universities, important administrative buildings, post offices, fire departments, medical institutions. Obviously, there is urban activity at these sites as well, which is why the services provided there should not be excluded from calculations. Although many modern scholars focus on 'third places' as the generators of creative industries, grassroot democracy and special social interactions, we will try to take into account all possible points of activity to ensure completeness of the study, its better qualitative coverage, and delimitation of multifunctional centers.
Thus, the data for this study covers both 'hard' and 'soft' components of the urban environment, temporary and permanent ones. The combined use of them, with appropriate processing, will lead to complete and objective results with a much higher level of certainty.

Identification of urban activity centers

We consecutively used two data types for the identification of urban activity centers: an array of geotagged tweets and the database of POIs. The applicability of social media data for the analysis of urban activity was confirmed by the literature review presented above; however, it is hardly arguable that this data type is associated with temporal instability and sensitivity to occasional events. To address this issue we have integrated the process of identifying a second data source, i.e. points of interest. While geotagged tweets may be used to detect areas where people are concentrated during a certain period of time, POIs represent a 'hard' component of the city – commercial and public facilities that attract people. Thus, the integrated use of social media data and POIs allows to take into account both 'soft' and 'hard' spheres of the urban environment.

The process of identifying UACs included four steps starting from the calculation of the density of tweets in 23 special wards of Tokyo. Firstly, it was necessary to choose the observation units. Presumably, the administrative boundaries do not limit human activity and they may either be located in a part of one district or spread between neighboring municipalities. Therefore for analyzing the spatial distribution of tweets it was necessary to create new observation units. In addition, a new grid of observation

units to be used for further calculations was essential to avoid the modifiable areal unit problem which occurs when human activities are evaluated based on administrative boundaries (Openshaw, Taylor 1981; Openshaw, 1984). One of the widely used ways to create new observation units is to build a regular grid of polygons, commonly consisting of squares or regular hexagons. The latter geometric figure is preferable for spatial analysis since the edge effect is minimized when using hexagonal grid; they better fit with a curvature surface, and all neighbors of hexagons are identical, which is very important in this particular case (Birch 2007). Taking these benefits into account the territory slightly exceeding the area of 23 special wards of Tokyo was divided into 2328 hexagons with a radius of about 400 m, which is close to the average value of the zip code units.

After choosing the observation territorial units we calculated the density of tweets per cell of the regular hexagonal grid (Fig. 1). It is clear from this map that the overall trend of centrality (higher density in central cells and lower in peripheral) does not allow to identify concentration of tweets that is significant at a local level (local positive extrema) irrespective of whether they are situated in the central or peripheral part of the city. This is exactly what McMillen and Vysokovsky tried to address through the application of their methodologies and spatial modelling. Therefore the goal of the following stages was to clear the density map from the overall trend of centrality and to detect the maxima within the local concentration of tweets not related to the distance from the city center.

One statistical model that potentially allows to achieve these goals is spatial autoregression (SAR). This technique may predict the distribution of a given indicator taking into account spatial autocorrelation (the dependence of a value on the values in neighboring territorial units) and other independent values. Before the calculation of SAR the global Moran's Index was calculated to clarify whether autocorrelation of tweets density really exists in the studied territory. The formula for Moran's Index in the initial form developed by Moran (1950) is as follows:

$$I = \frac{\sum_{i=1}^{n}\sum_{j=1}^{n} WijZiZj}{\sum_{i=1}^{n} Z_i^2} \quad (1)$$

where n is the number of territorial cells, W is the matrix of spatial weights that demonstrates whether cells i and j are neighboring (1 if yes, 0 if no), Zi is the difference between the value of an indicator in a given cell and its average value (same for Zj in a cell j). It is a subject of debate which cells may be considered as neighboring and, in this case, applying the concept of geographical neighborhood we consider all cells with at least one common point to be neighboring. As a result, the Moran's Index slightly exceeded 0.35, while p-value was insignificantly low (2.2e-16) meaning that there is a high degree of spatial correlation of the tweets density.

The next step was to calculate the modelled number of tweets by hexagonal grid based on the global centrality trend and the values in the neighboring cells. The general formula for spatial autoregression is

$$Y = \mu + Xb + pWy \quad (2)$$

where Y is a vector of dependent and X of independent variables, W is the matrix of weights, b is regression coefficient, p is a scalar autoregressive parameter and μ refers to a vector of regression disturbances (Kelejian, Prucha 1998). P shows the extent of spatial autocorrelation, Y is the modelled value of tweets concentration, while X is the chosen explanatory value, which in this case is the distance from the geographical center of the city.

Figure 2 shows the modelled values of tweets concentration that is mathematically explained by the value of neighboring cells and distance from the city center. We introduced the distance from the city center in this model in order to make it possible to eliminate the effect of centrality at the following stage.

The third step was to calculate the difference between the real and modelled distribution of tweets to identify hexagons, the high density in which may not be explained by the overall (global centrality) or in-site (value of neighbors) trends. The aim of this stage is to highlight the local maxima of urban activity – areas where the concentration of tweets is considerably higher than in surroundings, which corresponds with our definition of urban activity centers. The map in figure 3 illustrates the results of this stage, and the local extrema of tweets concentration may be identified on it much easier than on the first map (Fig. 1).

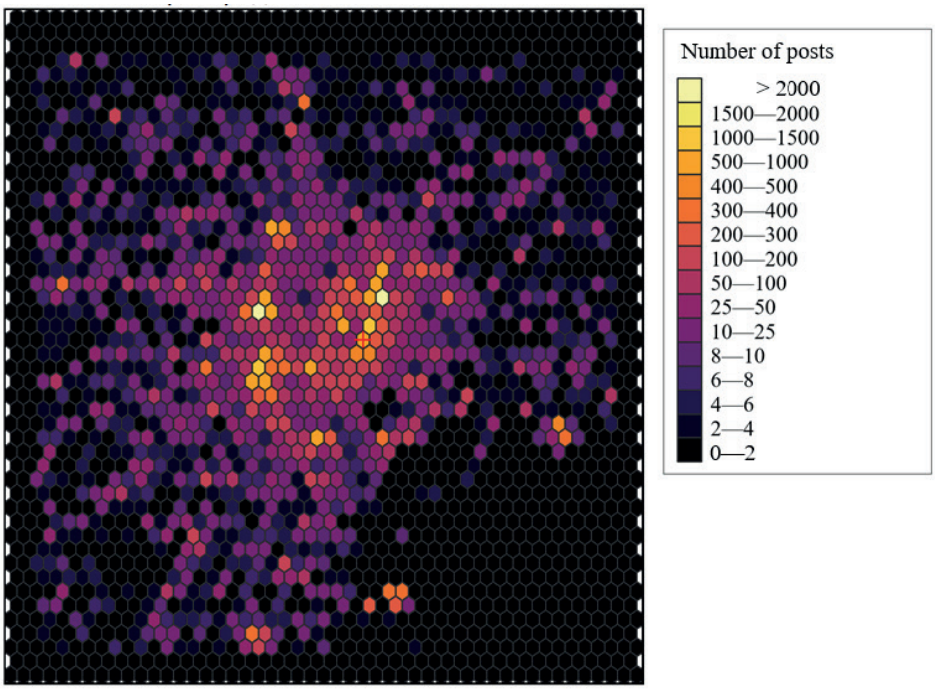

Fig. 1. The actual distribution of the posts' density

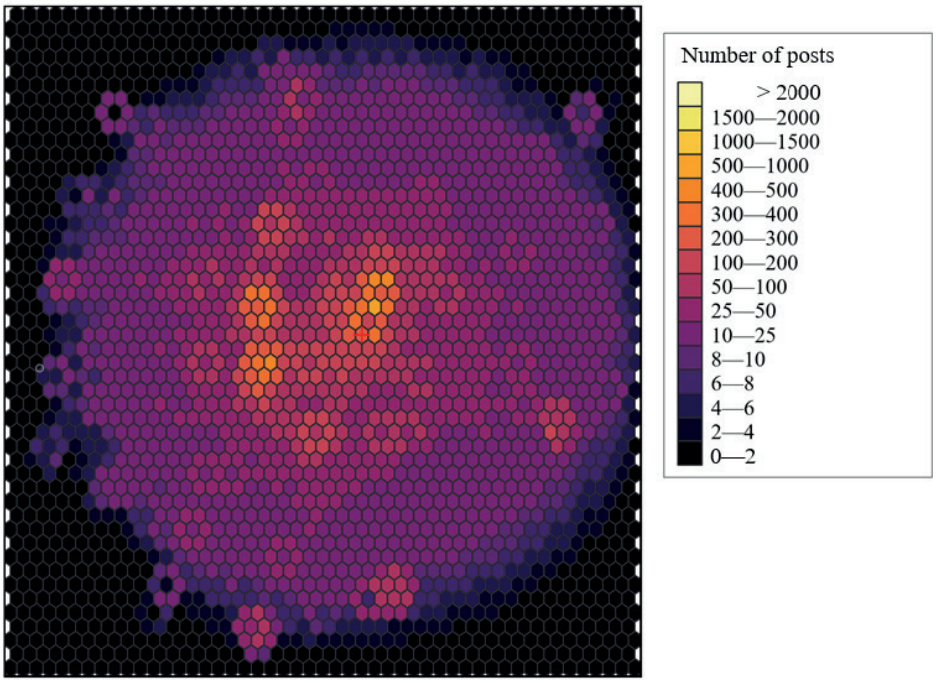

Fig. 2. The modelled distribution of posts

Finally, the last step was to delimit the borders of urban activity centers in the urban environment. It is hardly possible that UACs have an ideal form of regular hexagons due to the presence of such barriers as streets or buildings. That is why at this stage of research we utilized the POIs database supplemented by the street network of Tokyo. We ended up taking hexagons with a relatively high concentration of residual tweets (>5) as potential urban activity centers. The areas where POIs are concentrated were found and delimited manually within their territory taking into account the road network. As a result, we identified and mapped 146 urban activity centers (Fig. 5). Summarizing the identification process, we detected approximate areas of high urban activity by means of social media data analysis and after it clarified the precise location of real urban activity centers through the concentration of 'hard' objects producing those activities – points of interest.

RESULTS

Using the methodology described above we identified 146 urban activity centers within the territory of 23 special wards of Tokyo. Such a large number of objects is almost impossible to describe without applying some kind of grouping. Since some quantitative characteristics of UACs, such as the number of tweets per hexagon and the number of POIs per actual center of urban activity, were already available for calculations we decided to develop the classification of the centers based on one of these indicators. POIs seem to be a better data type for dividing UACs into subgroups according to their scale due to the fact that this data characterize the «hard» component of the city, the real content of the urban space that exists for a relatively long time. In other words, for the following qualitative and spatial analysis we classified urban activity

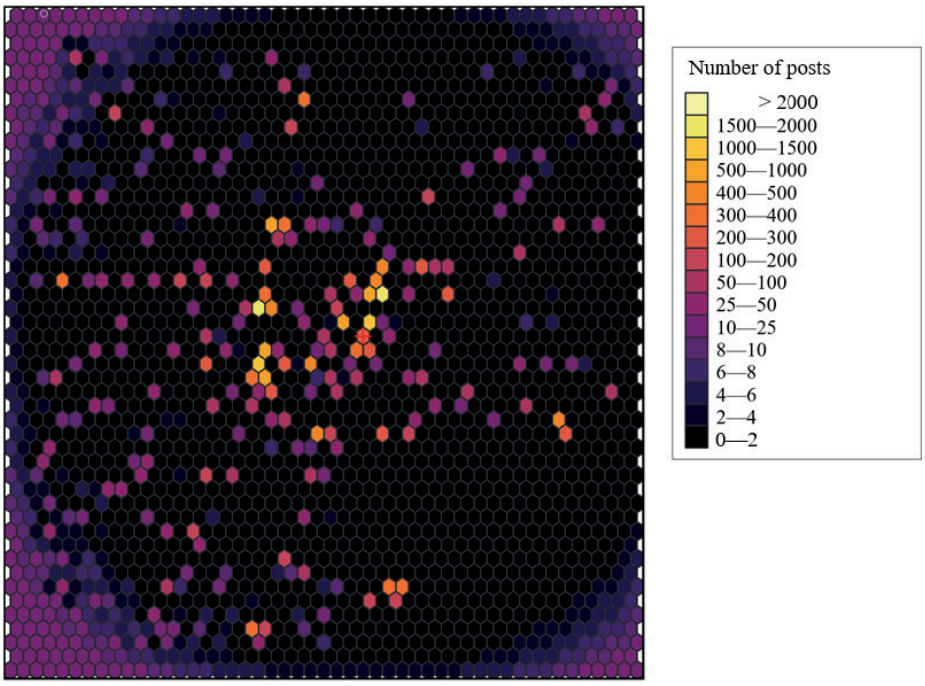

Fig. 3. Residuals of the posts density

centers according to the number of facilities attracting urban activity, or POIs because they have the potential to represent the scale and heterogeneity of centers. It is important to note that the results of this classification do not represent the final typology. The proposed classification should be looked at as a necessary step for simplification of the further analysis.

As already mentioned, POIs of Tokyo with an overall number of about 12,000 represent services covering almost all spheres of urban life: from cafes and banks to universities and car repair shops. In order to divide the centers of urban activity into classes according to the POI count we examined the distribution of this indicator by UAC (Fig. 4).

Based on the Jenks natural breaks, 5 primary groups of UACs were identified:

1. More than 99 – 7 UACs;
2. From 75 to 99 – 6 UACs;
3. From 25 to 75 – 38 UACs;
4. From 11 to 25 – 52 UACs;
5. Less than 11 – 43 UACs.

A thorough analysis of all these classes took more than 30 pages of the original text but for this article the results are presented in two tables (Table 1 and Table 2). The overall structure of the analysis was as follows: 1) identification of some basic features of the classes such as the number of centers and POIs; 2) description of the main location patterns based on a series of maps derived from figure 5; 3) investigation of the functional structure of each class and its' objects using POIs database, fieldwork experience, and additional sources (including the evaluation of the tourist attractiveness[1] of centers); 4) identification and study of the exemptions for each class.

The urban activity centers of the first class are large objects located in the central part of Tokyo. Their functional structure is characterized by diversification, often with one or two leading categories: tourist facilities, government and public services or food services. Services provided in these centers are often unique and have city-wide importance, so all the centers selected for the first class are undoubtedly tourist-attractive.

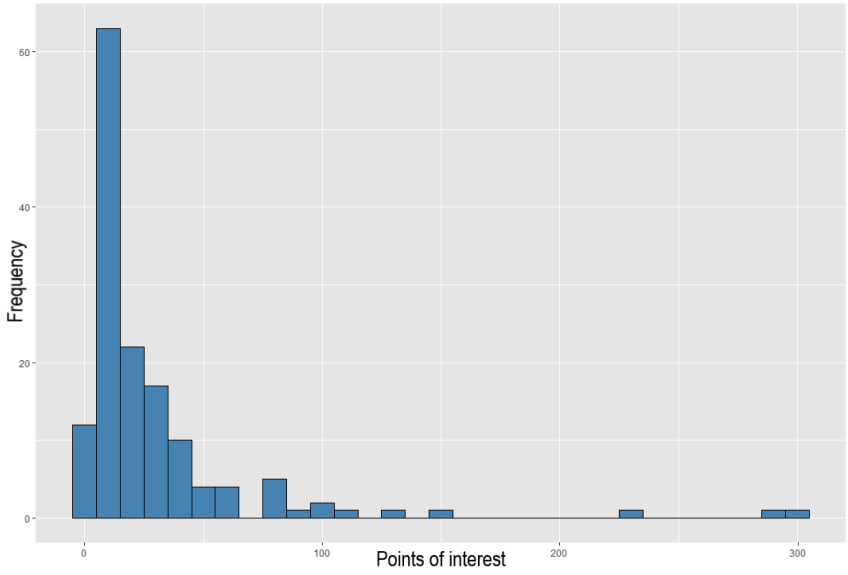

Fig. 4. Distribution of POIs by UAC

Table 1. Characteristics of the first, second and third classes of UACs

	First class	Second class	Third class	
Subclass	No	No	Upper	Lower
Number of UACs	7	6	45-75	25-45
Number of POIs	>99	75-99	38	
Location patterns	Large territory, located in the city center, mostly on the Yamanote railway line or inside it	Big territory, located on the Yamanote line or close to it, except Ogikubo (west of Suginami ward)	Located on or inside the Yamanote line except three located in the East	Located on the center-west axis
Functional structure	Significant diversification, almost all functions are present.	High diversification, the majority of functions are present, dominance of one or two sectors	Dominance of one or two sectors (strong specialization), still multifunctional	Dominance of one sector, average set of functions
Key functions	Government and public services, tourism, food service	Government and public services, food service, tourism	Eastern part of the Yamanote – government and public services, finances. Others: tourism, sports, shopping, recreation	Government and public services (high role of education in Meiji Daigaku Suginami and Meiji Daigaku Chiyoda), food service

[1]By 'tourists' hereinafter we will mean not only visitors from other cities but from other districts of Tokyo as well, emphasizing the importance and uniqueness of centers.

Interest for tourists	The highest	Very high	High	Average, high in some centers (e.g. Tokyo Tower, Ueno)
UACs	Akihabara, Mita, Shibuya, Aoyama, Ginza, Shinjuku, Takadanobaba	Ogikubo, Ikebukuro, Oji, Ebisu, Meiji-jingumae, Meiji Jingu Stadium	Asakusa, Shin-Kiba, Higashi-Ojima, Marunouchi, Toranomon, Daimon, Minami-Azabu, Okubo, Iidabashi	e.g. Roppongi, Tokyo Tower, Nihonbashi, Ueno, Yotsuya, Ueno Koen, Toyosu, Nakano

All of the second-class centers appeared to be second-level UACs both in size, scale and in the qualitative component. They are outstanding but not as significant as the leading ones. There is a wide range of services in these centers and they are characterized by high demand among both locals and tourists. For visitors from outside Ikebukuro and the centers around the Meiji Shrine are especially attractive.

The vast majority of the third-class UACs are located on the center-west axis. The largest centers of this class geographically and functionally are close to the higher classes, while the centers of the lower subclass have an average set of services that are mostly consumed by the local residents. Almost all centers in this group are located near the average-size railway stations and their emergence seems to be linked to them.

The objects of the fourth class appeared to be the clusters of organizations providing basic services for the residents of surrounding neighborhoods. There is also a high percentage of parking and other services for motorists, which is understandable as many of the centers are located in the peripheral areas, where the stations sometimes provide a starting point for moving on a private vehicle through the suburbs. Zones of increased concentration of foodservice objects are observed near the railway stations, which are the cores of these centers but their significance and share in the overall number of facilities is relatively small. Most of the group's objects lie outside the city center (the Yamanote line).

A typical fifth-class center consists of a couple of blocks where a police station, school, fire station, pharmacy, post office and railway station are located. In addition, stores and cafes are usually concentrated around the station but there are only a few of them. The fieldwork data was very useful for the description of the fifth-class centers since some of small facilities are not even included in the POIs database. Geographically, they are slightly different from the previously analyzed centers: objects of this group are concentrated in the eastern peripheral regions.

CONCLUSION

The results of the research allow us to draw several fundamental conclusions. Firstly, the methodology developed by the authors is applicable to the identification of existing urban activity centers at various scalar levels. The proposed methodology is not conceptually new, it is rather a combination and reinterpretation of Vysokovsky and McMillen ideas. However, for spatio-statistical modeling and identification of local concentrations of urban activity not related to the overall trend of centrality we used conceptually different data type. This represents the main added value of this research. Our work demonstrates that social media data that have an almost unlimited capacity for various urban studies can be used instead of census data and economic statistics in studies analogous to those conducted by McMillen and Vysokovsky. It is a crucial finding taking into account the renewability of social media data and its relevance. Comparison of the map of the

Table 2. Characteristics of fourth and fifth classes of UACs

	Fourth class		Fifth class	
Subclasses	Exceptions	Regulars	Exceptions	Regulars
Number of UACs	4	48	3	40
Number of POIs	11-25		<11	
Location patterns	In the city center (inside the Yamanote line or close to it)	On the periphery or semi-periphery (mostly in the western half of the city)	Mostly small, concentrated in the eastern and southern periphery of Tokyo (e.g. Edogawa, Katsushika, and Adachi). A few of centers are located on or inside the Yamanote line	
Functional structure	Diversified structure, equal distribution of sectors	A few functional sectors are presented (from 1 to 3 mostly)	Diversified for Odaiba, one or two dominant sectors for others	Very low diversification, a few sectors with a small number of POIs
Key functions	Food service facilities, stores, reduced presence of hotels and tourism	Basic services for locals: schools, kindergartens, post offices, banks, shops	Odaiba: trade, leisure, food service, and tourism; Haneda: airport; Tokyo Skytree: tourism, shops	Only basic functions for locals (police station, school, kindergarten, fire station, pharmacy, post office, shops and railway station)
Interest for tourists	Relatively high	Below average	Very high	Insignificant
UACs	Sengoku, Akasaka-Mitsuke, Tsukiji, Suitengumae	e.g. Narimasu, Futakotamagawa, Oidzumi-gakuen	Odaiba, Haneda Airport and Tokyo Skytree	e.g. Tabata, Kitami, Akatsuka, Yanaka, Kiba, Kasai, Tamagawa

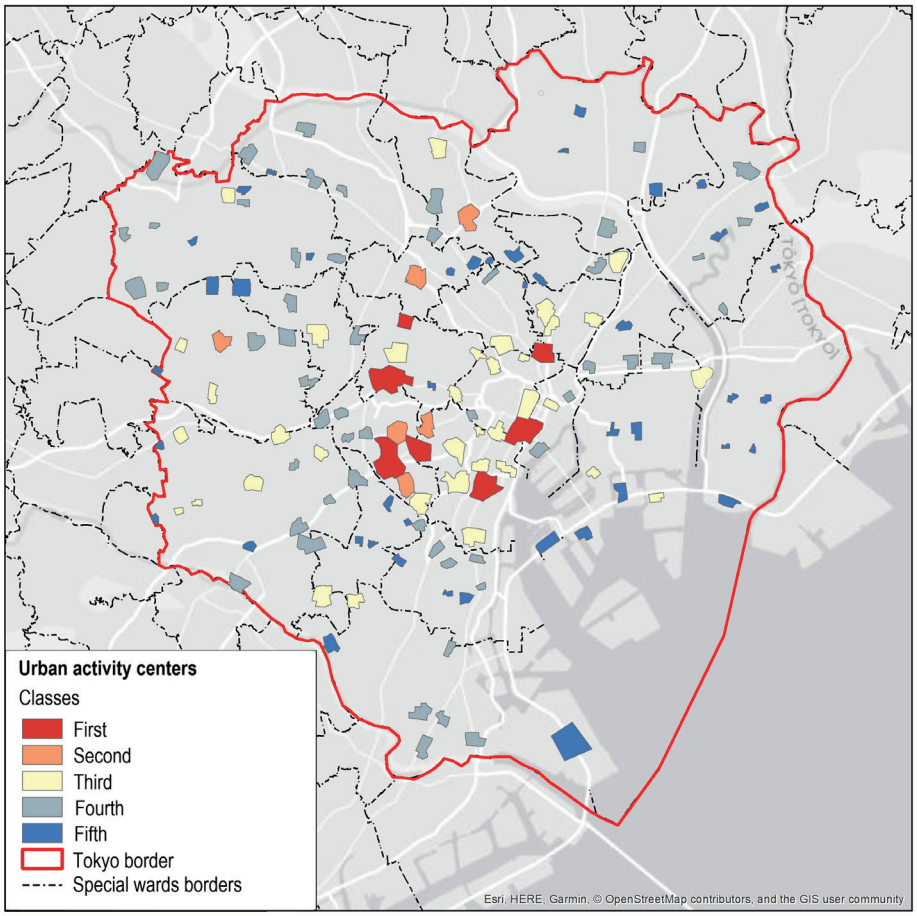

Fig. 5. Classes of UACs in Tokyo

delimitated UACs with the results of field studies, studies of other scholars and a priori knowledge of the urban structure of Tokyo confirm the accuracy of localization of these centers. Consequently, this study once again demonstrates the applicability of big social media data (with appropriate processing using mathematical modelling and adequate interpretation) for studying urban space.

We can summarize the main characteristics of the subject of this study – centers of urban activity and the urban structure of Tokyo. In general Tokyo has a radial-ring spatial structure: the first ring of UACs is located around the Imperial Palace and the second – along the Yamanote railway line, which plays a key role in the city's life. Peripheral radiuses of UACs are situated along railway lines of the corresponding directions in almost every sector of the city.

One could observe certain spatial differences when dividing the peripheral parts of the city into sectors. For example, the western sector is characterized by the highest activity density; it contains a large number of high-class diversified UACs, while in the eastern sector objects of the fourth and fifth classes prevail. This is probably because Tokyo prefecture extends to the west of the center, which promotes closer ties and as a result, the western part of the city is more heterogeneous, even at a long distance from the center, while in eastern Tokyo the suburban area is located much closer to the city center. Finally, using the classification of UACs certain relations were identified between their quantitative (number of POIs) and qualitative characteristics. They include functional features and geographic location that may lead to further comparative studies of sectoral differences within Tokyo and to enhancing currently existing models of functional zoning of the city. In addition, the applicability of this work is evident for more practical purposes such as transportation management, community building and urban planning.

REFERENCES

Ahas R. et al. (2009). Modelling home and work locations of populations using passive mobile positioning data. In: Gartner and Rehrl (eds.), Location-Based Services and Tele-cartography II, Springer, Berlin, 301-315.

Anselin L. (1995). Local indicators of spatial association-LISA. Geogr. Anal. 27(2), 93-115.

Batty M. (2013). The New Science of Cities, MIT Press, Cambridge, MA.

Bingham-Hall J. & Tidey J. (2016). Visualizing social medias impact on local communities. Visual Communication, 15(3), 317-328, DOI: 10.1177/1470357216645710.

Birch C. et al. (2007). Rectangular and hexagonal grids used for observation, experiment, and simulation in ecology. Ecological Modelling, 206, 3-4, 347-359.

Cai J., Huang B., Song Y. (2016). Using multi-source geospatial big data to identify the structure of polycentric cities. Remote Sensing of Environment, 202, 210-221, DOI: 10.1016/j.rse.2017.06.039.

Campagna M. (2014) The Geographic Turn in Social Media: Opportunities for Spatial Planning and Geodesign. In: Murgante B. et al. (eds) Computational Science and Its Applications – ICCSA 2014. ICCSA. Lecture Notes in Computer Science, 8580. Springer, Cham/

Campagna M., Floris R., Massa P., Girsheva A., Ivanov K. (2015). The role of social media geographic information (SMGI) in spatial planning. In S. Geertman, J. Ferreira, Jr., R. Goodspeed et al. (Eds.), Planning support systems and smart cities: Lecture notes in geoinformation and cartography (41-60). Basel: Springer International Publishing Switzerland, DOI: 10.1007/978-3-319-18368-8_3.

Ciuccarelli P., Lupi G., Simeone L. (2014). Visualizing the data city: Social media as a source of knowledge for urban planning and management. Heidelberg: Springer, DOI: 10.1007/978-3-319-02195-9/

De Goei, B., Burger, M.J., Van Oort, F.G., Kitson, M. (2010). Functional Polycentrism and Urban Network Development in the Greater South East, United Kingdom: Evidence from Commuting Patterns, 1981–2001. Regional Studies, 44(9), 1149-1170, DOI: 10.1080/00343400903365102.

Demographia World Urban Areas (2018). 14th Annual Edition (PDF), archived from the original (PDF) on 3 May 2018. https://web.archive.org/web/20180503021711/http://www.demographia.com/db-worldua.pdf. [Accessed 14 march 2019].

Evans-Cowley J.S., & Griffin G.P. (2011). Micro-participation: The role of microblogging in planning. Social Science Research Network, DOI: 10.2139/ssrn.1760522/

Frias-Martinez V., Soto V., Hohwald H., & Frias-Martinez E. (2012). Characterizing Urban Landscapes Using Geolocated Tweets. 2012 International Conference on Privacy, Security, Risk and Trust and 2012 International Confernece on Social Computing.

Fujita M., Ogawa H. (1982). Multiple equilibria and structural transition of non-monocentric urban configurations. Regional Science and Urban Economics, 12(2), 161-196, DOI: 10.1016/0166-0462(82)90031-X.

Healey P. (1999). Institutionalist analysis, communicative planning, and shaping places. Journal of Planning Education and Research, 19, 111-121.

Heckman J. J. (1979). Sample selection bias as a specification error. The Econometric Society Stable, 47(1), 153-161.

JR Higashi Nihon Kaisha Yōran (東日本会社要覧) (2017)/ (JR East Company Directory for 2016-2017). URL: https://www.jreast.co.jp/youran/pdf/2016-2017/jre_youran_all.pdf. (24.03.2019) (in Japanese).

Kaplan A.M., Haenlein M. (2010). Users of the world, unite! The challenges and opportunities of social media, Bus. Horiz.

Kelejian H.H., & Prucha I.R. (1998). The Journal of Real Estate Finance and Economics, 17(1), 99-121.

Kotov E., et al. (2016). Moscow: a course for polycentricity: Summary of proceedings for the Moscow, Urban Forum Graduate School of Urbanism, Moscow (In Russian).

McMillen D.P. (2001). Nonparametric employment subcenter identification. Journal of Urban Economics, 50(3), 448-473.

McMillen D.P. (2004). Employment densities, spatial autocorrelation, and subcenters in large metropolitan areas. Journal of Regional Science, 44(2), 225-244, DOI: 10.1111/j.0022-4146.2004.00335.x.

McMillen D.P., McDonald J.F. (1997). A nonparametric analysis of employment density in a polycentric city. Journal of Regional Science, 37(4), 591-612, DOI: 10.1111/0022-4146.00071.

Openshaw S. (1984). The Modifiable Areal Unit Problem, GeoBooks, Norwich, U.K.

Openshaw S., Taylor P.J. (1981). The modifiable areal unit problem in Quantitative Geography. In N. Wringley and R. J. Bennett, (eds.), Routledge, London, U.K., 60-70.

OpenStreetMap (2017). Retrieved December 24, 2017. URL: https://www.openstreetmap.org/search?query=tokyo#map=17/35.70059/139.77445.

Pomorov S.B., Zhukovsky R.S. (2015). Retrospective of the development of urban polycentrism and theoretical ideas about it. Teoriya arhitektury (Architecture Theory), 52 (In Russian).

Riguelle F., Thomas I., Verhetsel A. (2007). Measuring urban polycentrism: a European case study and its implications. Journal of Economic Geography, 7(2), 193-215, DOI: 10.1093/jeg/lbl025.

Rosenbaum MS. (2006). Exploring the social supportive role of third places in consumers lives. Journal of Service Research, 9(1), 59-72, DOI: 10.1177/1094670506289530.

Schneider C.M., Belik V., Couronné T., Smoreda Z., and González M.C. (2013). Unravelling daily human mobility motifs. Journal of the Royal Society Interface, 10(84), DOI: 10.1098/rsif.2013.0246.

Steiger E., Westerholt R., Resch B., & Zipf A. (2015). Twitter as an indicator for whereabouts of people? Correlating Twitter with UK census data. Computers, Environment and Urban Systems, 54, 255-265.

TechCrunch (2018). Twitter data reported in Dec 2018. Retrieved from. https://jp.techcrunch.com/2018/12/26/twitter-2/

Tokyo Metro official website (2019). URL: https://www.tokyometro.jp/en/subwaymap/ (23.03.2019).

Train-media.net (2017). Tokyo Railway Performance Report 2017. URL: http://www.train-media.net/report/index.html (24.03.2019).

Vysokovsky A.A. (2005). Land use and development rules: design guide. The experience of introducing legal zoning in Kyrgyzstan, Ega-Basma, Bishkek (In Russian).

Check for updates

CC BY

RESEARCH PAPER

CLIMATE CHANGE IMPACT ON RENEWABLE ENERGY RESOURCES IN THE ARAB WORLD BASED ON JACOBSON'S ROADMAP OF RENEWABLE WIND, WATER, AND SUNLIGHT (WWS) 2050

Waleed Abbas[1], Ahmed Hassan[2] and Hossam Ismael[3*]

[1]Department of geography & GIS, faculty of Arts, Ain Shams University, Egypt.

[2]Ministry of education, Kuwait.

[3]Department of geography & GIS, faculty of Arts, New Valley University, Egypt.

***Corresponding author:** hosam.ismael@artnv.au.edu.eg

Received: August 6th, 2020 / Accepted: May 25th, 2021 / Published: July 1st, 2021

https://DOI-10.24057/2071-9388-2020-133

ABSTRACT. Most Arab countries are part of the Sunbelt where solar insolation is among the highest in the world (as high as 9.5 kWh/m^2 per day). At the same time, Arab countries have a high-risk of climate change. Of the 19 countries that set new temperature high in 2010, five were Arab countries. Temperature in Kuwait reached 54.3 °C in 2019. The aims of this study were fourfold: to discuss the current situation of renewable energy in the Arab countries, to analyses the regional patterns of climate change, to secure a certain amount of the future energy needs by establishing the suitability map for renewable energy exploitation, and to assess the Jacobson's «world plan»,100% Clean and Renewable Wind, Water, and Sunlight (WWS) All-Sector Energy Roadmaps for Arab Countries according to climate change impacts 2050. To achieve these aims, the current study depended on climatic data from web-based WorldClim utility and the global climate model ECHAM5-MPIOM that downscaled by the regional climate model RegCM and CORDEX domain. A site suitability map has been developed using the Geographic Information System (GIS). We analyzed the results based on the IPCC A2 scenario for the periods 2011–2040 and 2041–2070. We found that transforming Arab countries to a 100% WWS system as suggested by Jacobson et al. (2016) will reduce the end-user demand in 2050 by about 32%. This difference can be attributed to the conversion of fossil fuel combustions to a more efficient sustainable renewable energy.

KEYWORDS: Sustainable Development; Renewable energy; Climate change impacts; suitability map

CITATION: Waleed Abbas, Ahmed Hassan and Hossam Ismael (2021). Climate Change Impact On Renewable Energy Resources In The Arab World Based On Jacobson's Roadmap Of Renewable Wind, Water, And Sunlight (Wws) 2050. Geography, Environment, Sustainability, Vol.14, No 2, p. 92-104 https://DOI-10.24057/2071-9388-2020-133

Conflict of interests: The authors reported no potential conflict of interest.

INTRODUCTION

The Arab countries are expected to be strongly affected by climate change, enhancing the already hot and dry climatic conditions. Furthermore, the region of limited water resources, renewable energy, and high population growth like the Arab world; a recent climate change may increase the frequency and severity of climate extremes related to the future of renewable energy (Sanchez et al. 2004; Giorgi and Lionello 2008; Önol and Semazzi 2009; Lelieveld et al. 2012; Almazroui 2013: Önol et al. 2014; Ozturk et al. 2015; Seneviratne et al. 2016).

Economically, The Arab world is one of the most extreme uneven regions in the world. The yearly Gross Domestic Product (GDP) per capita in the oil-rich Arab countries is the highest (more than US$20,000 in the Arab Gulf countries), while it is very low (only US$1400) in countries like Morocco and Yemen (World Bank 2016). In consequence, adaptive capacity and vulnerability to climate change hazards vary tremendously within the region (Katharina et al. 2017).

Inherently, the Arab countries have been endowed with plentiful natural energy resources wealth. The region holds about half of oil reserves and a quarter of natural gas reserves in the world. It controls almost a third of oil production and 14% of natural gas production. When renewable energy resources and climate change are considered in the same context, the analysis usually focuses on the impacts that renewables might have on mitigation of or adaptation to climate change, with the aim to reduce emissions of greenhouse gases (GHGs) list (World Bank 2016& 2017).

Climatic variability over the next century is projected to increase, and the Arab countries may experience unprecedented weather extremes (World Bank 2016, 2017). In this connection, climate models are the only tools that enable understanding of how climate will change in the future. However, model predictions are only approximations about the future state of the climate system (Pasicko et al. 2012). The integration between global climate models (GCMs) and regional climate models (RCMs) is necessary to make climate predictions more reliable and applicable in the current study.

Previous studies

A synthesis of the literature on climate change impacts of renewable energy show that the Arab countries region is highly affected by present and future climate change, and the region emerges as one of the hot spots for worsening extreme heat, fossil fuels into force under climate change. as a result, this has a great impact on the future of energy resources and drives the dependence on renewable energy resources available in the Arab world (Evans 2009, 2010).

Önol and Semazzi (2009) concluded that increasing concentrations of carbon dioxide in the region will exacerbate the crisis. While Lelieveld et al (2012) clarified that the region's commitment to long-term contracts to export oil and natural gas complicates leaves these countries vulnerable to the risks of climate change.

Almazroui (2013, 2019) concluded the necessity of getting used to climate models to predict future climate changes, with reference to the necessity of relying on climate models domain that were specially created for the countries of MENA region. Önol et al (2014) and Ozturk et al (2015) agreed on the importance of using renewable energy resources available in the countries of the region in order to avoid the repercussions of climate change impacts.

In the Arab countries, previous studies of climatic variability have focused mainly on the analysis of air temperature (El Kenawy et al. 2009; Almazouri et al. 2012) and precipitation (Nazemosadat & Cordery 2000; Raziei et al. 2012; El Kenawy et al. 2014; Deng et al. 2015). The spatiotemporal variability of climate has been described as being driven by the atmospheric–oceanic circulation in many areas across the Middle East and North Africa (MENA) region (Nazemosadat & Cordery 2000; Rahimzadeh et al. 20l09; Raziei et al. 2013; El Kenawy et al. 2010 & 2014). This is of great importance when considering that the climate of the Arab region is transitional, with both midlatitude and subtropical configurations influencing the region. More attention is required to assess climate variability impacts within the Arab countries, for example on renewable energy prospects.

Overall, the motivation behind the topic of this research relies on the following three observations: Firstly, Arab countries currently are doing very poorly from a renewable energy perspective. Secondly, they have all the necessary environmental factors to have the potential to have a robust renewable energy sector. Lastly, Arab countries can greatly benefit from making the transition to relying on renewable energy. This research relied on Jacobson's plan for Arab countries in the World Plan proposal—Jacobson et al. (2016) and it has been proved that the roadmap can be doable.

STUDY AREA

The Arab countries consist of 22 states in Africa and Asia, cover a vast area of 14 million Km^2, geographically, The Arab world extends from the tip-east in the Arabian Gulf to the Atlantic Ocean in the tip-west, and from the mountains of Syria and Lebanon until the tropical plateau of Somalia.

The Arab countries mainly have a transversal extent, where it roughly extends 77 Longitude, excluding distant detached Comoros. Given the world geodetic coordinate system 1984 (WGS-84), the Arab land spreads between longitudes 17°06'7.5"W - 59°50'52.4"E, and between latitudes 12°22'59.4"S - 37°23'1.0"E. The Arab lands are mostly ruled by hot arid (BWh) and semi-arid (BSh) climates in Koppen classification (Kottek M. et al. 2006). So, it forms the largest desert realm in the world, The warm climate with hot summers (CSa) dominates minor territories in Northwest Africa and northern fringes of Iraq, Syria and Lebanon. Only the Comoros characterized by an equatorial climate of fully humid (Af) and monsoonal (Am) (Figure 1). In the current research, data and analysis are presented in three sub-regions as defined in the Arab Human Development Reports (2010, 2014& 2018): (1). The Middle East and North Africa (MENA), namely, Mauritania, Morocco, Algeria, Tunisia, Libya, Egypt, Palestinian, Jordan, Lebanon, Iraq, Syria, and Yemen (2) The Gulf Cooperation Council (GCC), including Saudi Arabia, the United Arab Emirates, Kuwait, Oman, Bahrain, and Qatar, (3) the sub-Saharan countries, namely, Sudan, Somalia, Djibouti, and Comoros. These sub-regions are strongly linked to geographic connectivity, climatic zoning, socio-economic aspects, natural resources, vulnerability patterns to climate change, and development status.

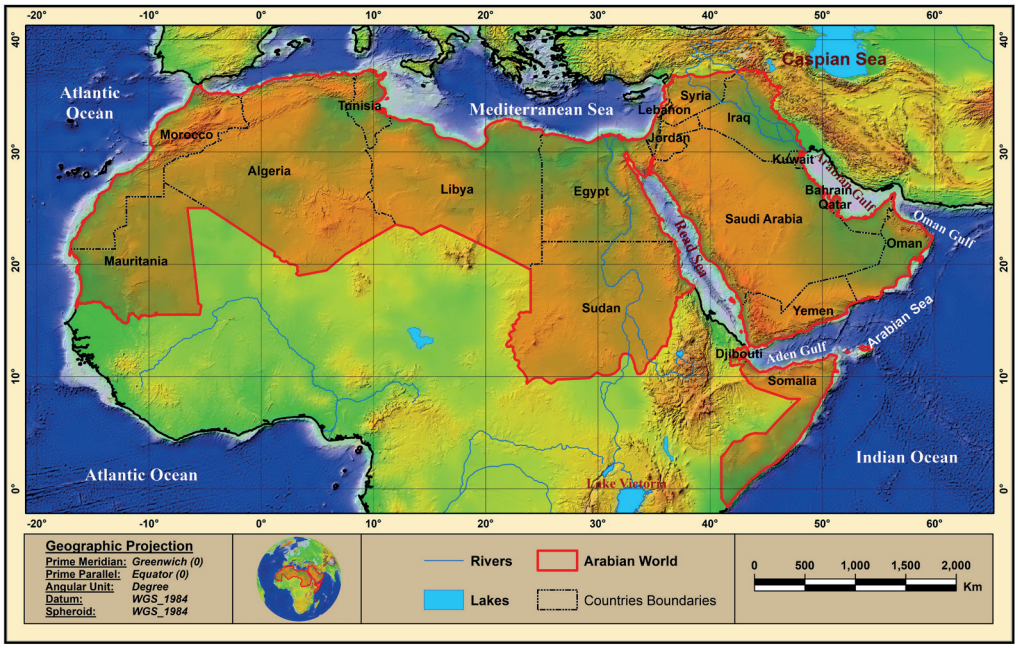

Fig. 1. The geographical location of the Arab countries

The main questions of this study were:

• Does the Arab countries in urgent need to use renewable energy sources to mitigate the impacts of climate change?
• Does Jacobson's plan (WWS) 2050 provide Arab countries with the ideal opportunity to replace fossil fuels with renewable energy available in all Arab countries?

DATA AND METHODOLOGY

In order to answer the research questions and to assess climate change impacts on renewable energy resources in the Arab countries several data references are analyzed in the data and methodology section:
1) Tracking SDG 7: Energy Progress Report 2019, Arab Region .
2) Climatic data from WorldClim—Global Climate Data .
3) Regional Climate Model (RegCM).
4) Ensemble results of CMIP5 model for two Representative Concentration Pathways (RCPs), RCP2.6 and RCP8.5, adopted by the IPCC for its fifth Assessment Report (IPCC 2013).
5) Road map of 100% Wind, Water and Sunlight (WWS).

These sources include an updated statistical data from the energy progress report 2019 and a road map of (WWS). Also, the methodology depended on data extracted from satellite images, and climate data extracted from climate models such as; RegCM and CMIP5. The methodology and tools used in the current study are most suitable for answering our research questions because it achieved integration between all aspects of the data on which the research is based.

RESULT AND DISCUSSION

The current situation of renewable energy in the Arab countries

Only 18% of the Arab region's renewable energy consumption is accounted for by electricity generation. Egypt, Morocco, and Sudan are high consumers of renewable energy for electricity generation in 2016, together they account for over 80% of the Arab world region are total. Table 1 illustrates that with around 13% of total renewable energy consumption, hydropower remains the most important renewable energy source in the Arab region after solid biofuel.

Solar radiation is the most abundant and widely accessible in the desert, but the least tapped form of energy in Arab countries. The world's hot deserts cover around 36 Million km^2 (UNEP 2012) of the earth's land surface with about 14 Million km^2 in the Arab region, around 39% of the global available hot desert. The solar radiation falling on the Arab desert area is estimated at 88,219 TWh per day (assuming annual irradiation of 2300 kWh per m^2 per year) which is a vast amount.

In addition, solar-powered mini-grids have gained increased traction in a number of different settings, from Egypt's comparably large Masdar Siwa Project (2015) and benban solar park in Aswan (2017), and mini-grids on islands, as in the United Arab Emirates islands of Al Hayl and Al Jarnain (both since 2015) (International Energy Agency 2018).

Interestingly, while Arab countries are behind on its renewable energy production, with less than 7% of its energy produced by renewable (solar and wind) energy, Arab countries are actually ranked first in the world in solar water heating collector capacity per capita. This further illustrates Arab countries' renewable energy resources availability and potential (Figure 2 and 3).

Table 1. Renewable energy consumption in the Arabian countries (World Bank 2014

Country	Solar	Wind	Hydro	Total (TJ)	% of Total Consumption
Morocco	1889	6942	5906	69683	2
Mauritania	0	0	0	13103	33
Algeria	0	0	691	902	0
Tunisia	758	1458	161	40093	12
Libya	0	0	6332	6332	2
Egypt	0	4040	42950	11950	6
Sudan	1015	6	174	6747	3
Yemen	0	0	0	2372	1
Oman	0	0	0	0	0
UAE	937	0	0	3309	0
Qatar	0	0	0	0	0
Bahrain	0	0	0	0	0
Kuwait	0	0	0	0	0
Iraq	6368	0	6851	7894	3
KSA	5	0	0	285	0
Palestine	0	0	0	0	0
Jordan	1015	6	174	6747	3
Lebanon	0	0	627	8091	3
Syrian	2650	0	7832	6770	11

On the other hand, the solar power consumption increased markedly from very low initial rates: up 55% across the region during the 2000s and 20% over the period 2012–2016, especially in the GCC economies. GCC members Saudi Arabia and the United Arab Emirates have set consecutive world low-price records for utility-scale solar PV and CSP in 2016 and 2017, making solar PV cost-competitive with every other fuel on the market. Now, wind park stations in Aswan (Egypt), Morocco, and Jordan have been manufacturing extremely competitive electricity. Increased use of distributed generation, for use by both off and on-grid market segments, adds significantly to deployment in recent years.

The wind is another resource available for Arab countries to generate clean energy. Research to date suggests that it be unlikely that multi-year annual mean wind speeds will change by more than a maximum of ±25% over most of the Arab countries during the present century, while research covering North Africa and the Middle East suggest that multi-year annual mean wind power densities will likely remain within ±50% of current values (Figure 4).

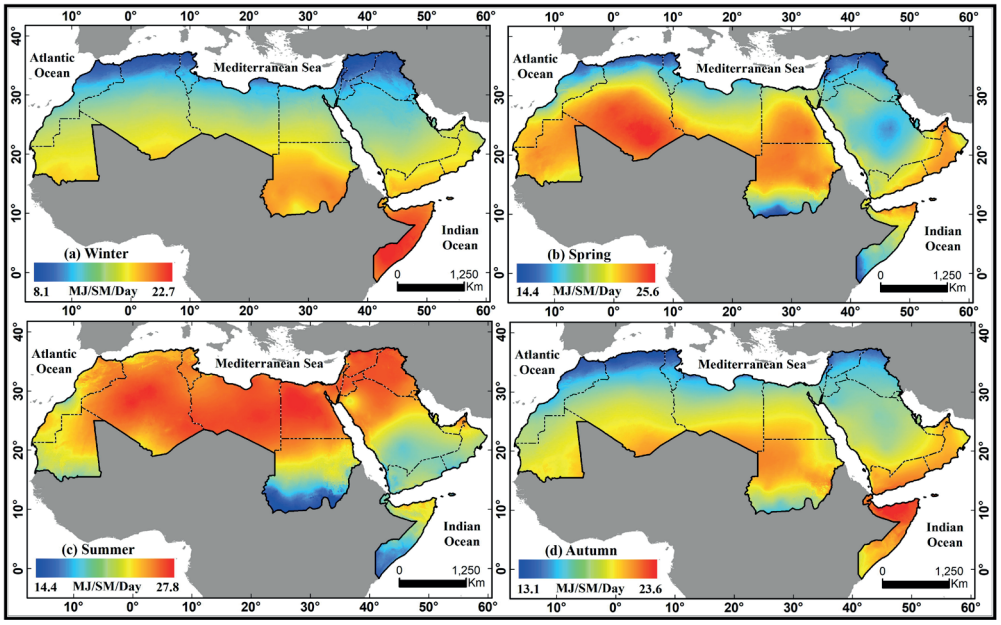

Fig. 2. Seasonal solar radiation variations in the Arab countries

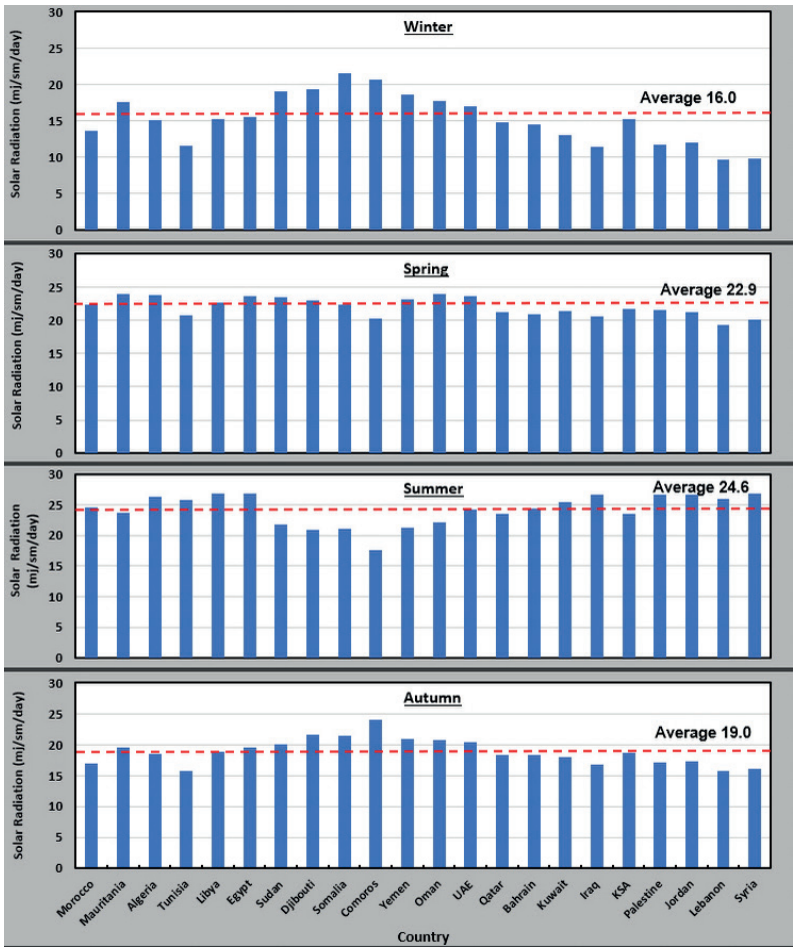

Fig. 3. Seasonal averages of insolation (mj m^{-2} day^{-1}) in the Arab countries

To illustrate this further, wind energy is considered local, in the sense that it is available in locations where the wind speed structure has specific characteristics. It is located in main sites in the Arab world that contain (Gulf of Aqaba) in Jordan, Tunisia, and Algeria (the Mediterranean coastal plain), Sudan (the Red Sea coastline), Oman (Indian Ocean coastline), Egypt (the Red Sea coastline and the Gulf of Suez Coast), Morocco and Mauritania (the Atlantic coastline), Yemen, and some locations in the Arabian Gulf Coast (Figure 4).

Egypt, Morocco, and Sudan together account for over two-thirds of the Arab region's renewable energy consumption (UN ESCWA, 2016d). Wind energy in the Arab region has reached 2400 MW in 2016. Installed capacities are concentrated in Egypt, Morocco, and Tunisia. The power of renewable energy generated from wind power plants represents around 0.35% of the total electricity generated in the Arab countries (ibid, 2016d).

(Figure 5) indicates that the annual wind speed at 100 meters above ground level (AGL) in Arab countries area is about 18 m/s and the annual capacity factor at that height, assuming 123 MW turbines with 126-meter rotor diameter, is about 0.3. When compared to other countries, Arab countries annual wind speeds and capacities are very high. Arab countries have the highest annual wind speeds and capacities when compared to other locations; the region has in most locations high enough wind speeds to generate electricity using wind energy.

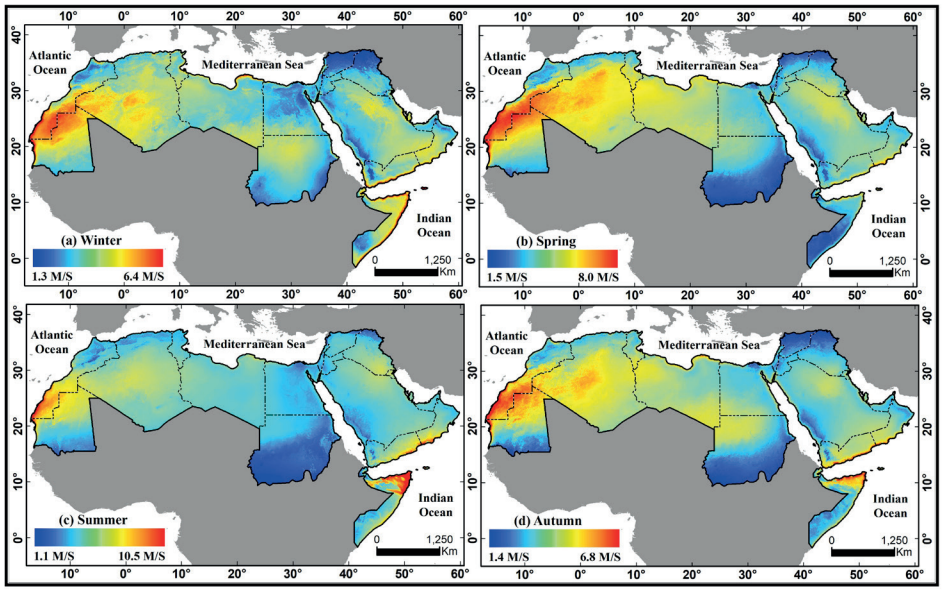

Fig. 4. Seasonal wind speed variations in the Arab countries

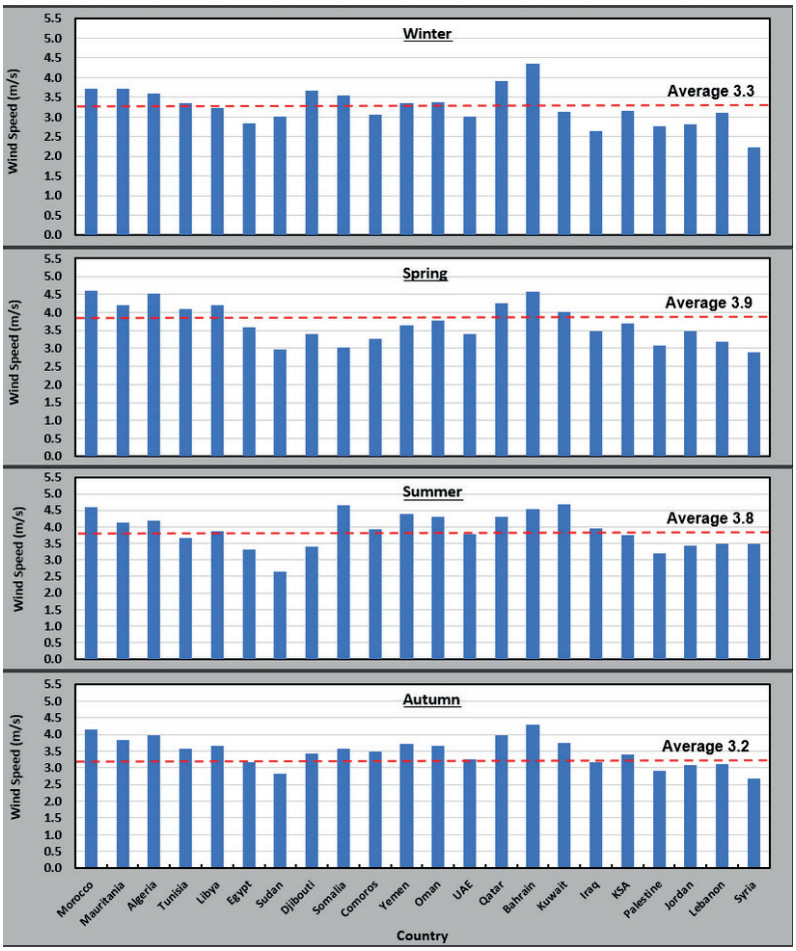

Fig. 5. Seasonal averages of the wind speed in the Arab countries (ms^{-1})

In sub-regional terms, renewable energy consumption is screwed in the Arab LDCs, followed by Arab countries in North Africa, with smaller quantities consumed in the Arab countries in Mashreq and almost none in the GCC economies where, despite the recent great value of solar power, renewable energies continue to account for relatively small amounts of the region's power mix (Figure 6).

A few Arab countries account for practically all the Arab region's newly used renewables-powered electricity-generation capability. The capacity addenda in renewable energy in the Arab world from the period 2012–2015 came from Egypt (with some 700 MW new capacities installed from 2012 to 2015). Morocco (with some 547 MW new capacity installed during 2013 to 2014) and the UAE (113 MW new generation capacity primarily from CSP) (Table 4).

In the coming decade, both countries aim to significantly increase their renewable energy-generation capacity further: Egypt to a total of 3.200 MW, Morocco to a total of 2,000 MW installed wind and 2,000 MW solar capacity by 2022 (around 42% of total generation capacity), to be doubled by 2030 (to account for 52% of total generation capacity); and Dubai to 5,000 MW, or 25% of electricity generation by 2030 in the UAE.

It can also be noticed that other countries in the region have even considerable renewable energy plans, with the elevated capacity targets currently in Saudi Arabia, aiming for 9,500 MW renewable energy by 2030; Egypt with total capacity targets of 12,500 MW (wind and solar power), or 25% of total electricity by 2022 (World Bank 2017a).

It could be observed, both wind and solar power grew significantly over the tracking period 2012–2016. New regional wind-power-generation capacity increased by around 670 MW in 2013 and 2014, driven primarily by large-scale projects in Morocco (542 MW over a period of two years) and to a lesser extent Egypt (60 MW) and Tunisia (60 MW). Moreover, between 2012 and 2014, the Arab region combined added some 50 MW of solar PV and over 100 MW of CSP capacities, with significantly more capacity additions since 2015 (Figure 6).

Regional Patterns of Climate Change

Temperatures and Heat Extremes

(Figure 7) illustrates a multi-model mean temperature anomaly for RCP2.6 and RCP8.5 by the Potsdam Institute for Climate change Impact Research and Climate Analytics, 2014, for the months of June-July-August for the Arab countries. The results detect that warming of about 0.2° per decade has been spotted in the region from 1961 to 1990, and an even faster rate since then, which is a match with an increase in frequency in temperature extremes. Climatically, the strongest warming is projected to take place close to the Mediterranean coastal plain. The impacts not only in the coastline areas, but also in the inland of Algeria, Libya, and large parts of Egypt, warming by 3 °C in a 2 °C world scenario is predicted by 2100. In a 4 °C world scenario, the mean summer air temperatures are forecasted to be up to 8 °C warmer in abundant areas of Algeria, KSA, and Iraq by 2100. By the end of the century, in a 2 °C world scenario, unusual heat extreme waves in temperatures will occur in about 33% of summer months almost everywhere in the Arab countries.

This means that on average one of the summer months each year will override temperatures warmer than four standard deviations beyond the baseline average. Unusual heat extreme waves, however, will reside preponderantly in a 2 °C world, unless in some isolated coastal regions overall the Mediterranean coasts of Tunisia, Egypt, Yemen, Djibouti, and Oman. Here these events are projected to be relatively rare in a 2 °C world scenario but are notwithstanding expected to occur in 5–10 percent of summer months.

Whereas the increase in the frequency of heat extremes is expected to level off by mid-century in a 2 °C world, in a 4 °C world scenario it will continue increasing to the end of the century. In a 4 °C world scenario, 80% of summer months are projected to be hotter than five degrees (unprecedented heat extremes) by 2100, and about 65% are projected to be hotter than five degrees during the 2071–2099 period.

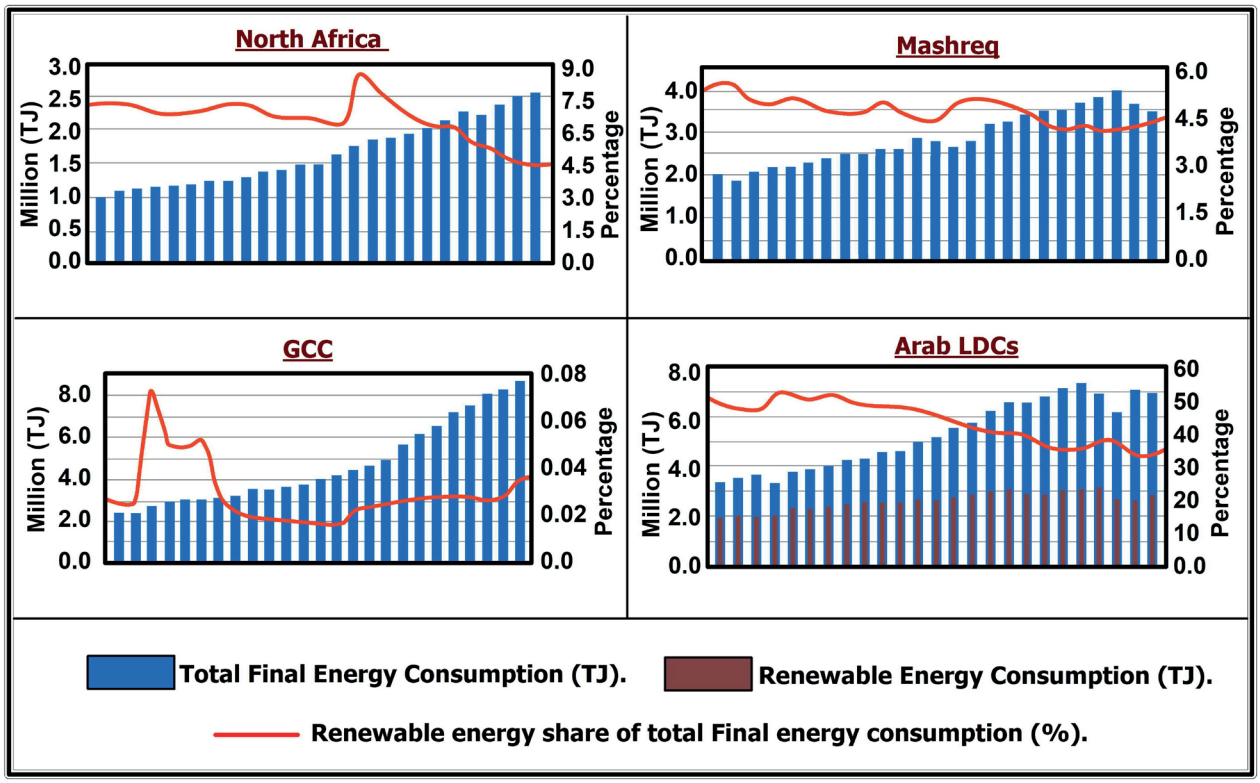

Fig. 6. World Bank determination of renewable energy share in energy consumption 2017 in the Arab subregion

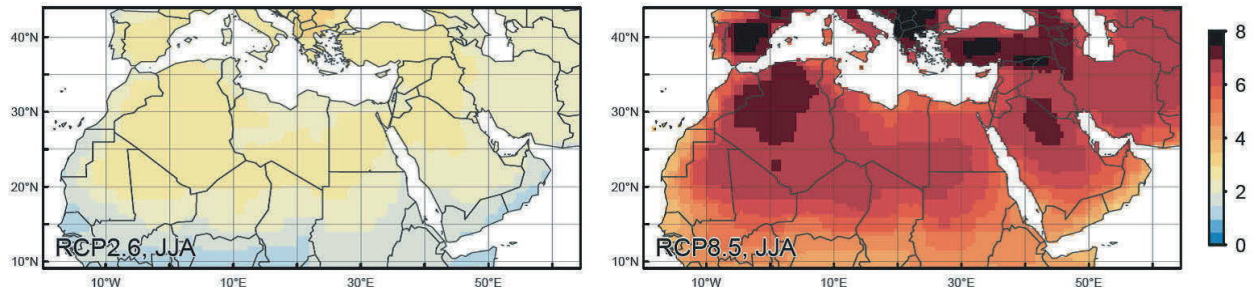

Fig. 7. Deviations from the mean temperature for the summer months according to models RCP2.6 and RCP8.5 (After Word Bank 2014)

Projected Temperature Changes

The projected increase in temperatures during the northern summer (June, July, and August) over the Arab countries is shown in Figure 9 for both the 2 °C and 4 °C world scenario. The multi-model means warming by 2100 is about 2.5 °C in a 2 °C world, and about 7.5 °C in a 4 °C world, which is substantially more than the global mean land warming. Under the low-emission scenario (i.e., a 2 °C world), summer temperatures in the Arab countries peak by 2040 at about 2.5 °C above the 1951–1981 baseline and remain at this level until the end of the century. In a 4 °C world scenario, the warming continues almost linearly beyond 2040, reaching about 7.5 °C above the 1951–1981 baseline by 2100 (Figure 8).

Climatically, the strongest warming is projected to take venue close to the Mediterranean coastal plain. Also, inland in Algeria, Libya, Tunisia, and large parts of Egypt, regions warm by 3 °C in a 2 °C world. In a 4 °C world, mean summer temperatures in 2071–2099 are expected to be up to 8 °C warmer in parts of Algeria and 6 °C, 7 °C warmer in Egypt and Libya respectively. Warming over the Arabian Gulf region (i.e., below about 29° 47 N in Figure 9) is more moderate (3 °C in a 2 °C world and 6 °C in a 4 °C world), which is likely related to an increase in precipitation.

In a 4 °C world, the prospect density functions of monthly temperatures (correlating with the year-to-year variability of monthly temperatures) shift by six standard deviations toward warmer conditions across all regions in the Arab world, from the Sahara to the Arabian Peninsula to the eastern Mediterranean coast. Such a large move beholds that summer temperature will move to a new climatic regime by the end of the 21st century. Such a dramatic change would be avoided in a 2 °C world; even then, however, a substantial shift is expected (i.e., by about 2–4 standard deviations).

By using five GCMs indicate we find that by the end of the century, in a 2 °C world scenario, 3 unusual heat extremes will occur in about thirty-five percent of summer months almost everywhere in the Arab countries' region (Figure 9, top). This reveals that on average one of the summer months June, July, and August each year will be an unusually hot month. Five unprecedented heat extremes (Figure 9, bottom) happen much less frequently with a return period of several thousand years. 5-peak heat extremes, however, will remain broadly missing in a 2 °C world scenario, predictable for in some secluded coastal regions including the Mediterranean coasts of Egypt, Libya, and in Yemen, Djibouti and Oman (Figure 8, lower right panel). In a 4 °C world scenario, about 65% of summer months are predicted to be distributing as 5-peak heat extremes by 2071–2099 in the Arab countries. Whereas the increase in the frequency of heat extremes is predictable to standard off by mid-century with 2 °C global warming, with 4 °C global warming it will continue increasing to the end of the century.

CMIP5 model results

J. Lelieveld et al. (2016) applied results from an ensemble of 26 models that have been interpolated to a common spatial resolution of 2.5 degrees, about 280 km at the 0° latitude (Equator). Evaluate the CMIP5 model results for the reference period, based on observations compiled in the gridded datasets of the Climate Research Unit (CRU, version 3.22), and test the level of consistency of the climate model projections we performed robustness calculations as proposed in (Figure 9). The figure presents the projected changes in near-surface temperature, for the mid- and end-century periods and the RCP 4.5 and 8.5 scenarios.

(Figure 9) shows that the level of robustness is high, especially for the summer warming, and is highest for

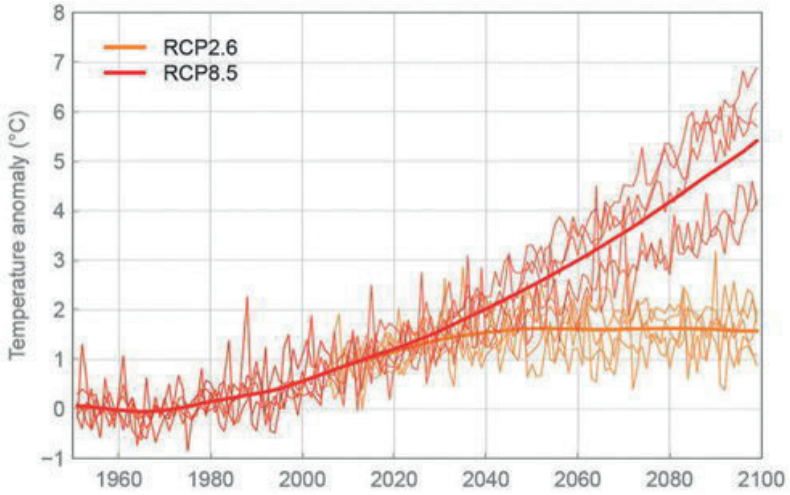

Fig. 8. Interannual temperature projections for MENA land area compared to the baseline (1951–1980)

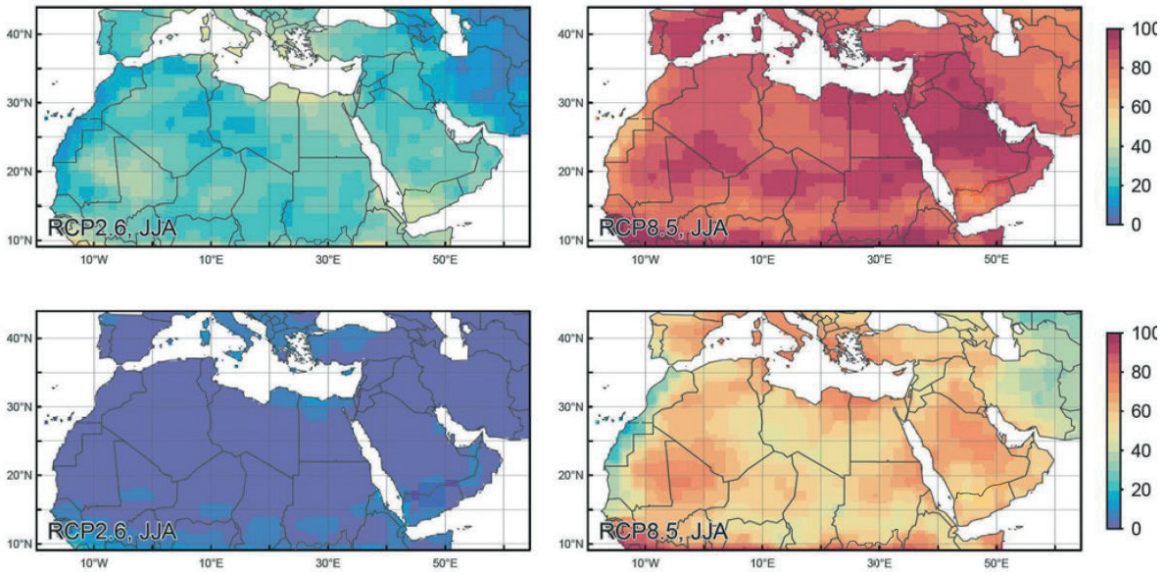

Fig. 9. The percentage of the mean temperature of the summer months (2071-2099)compare with the standard deviation of the reference climate in (1951-1980) based on scenarios RCP2.6 and RCP8.5 according to Word Bank (2014)

the end-of-century projections, special for the RCP8.5 scenario, reference overall agreement among the models. According to IPCC (2013) global mean warming is projected to reach about 2 °C around 2050, i.e., a bit less for the RCP4.5 and a bit higher than 2 °C for the RCP8.5 scenario.

Also, the deep inspection of the (Figure 10) reveals that the 2 °C approximately synchronizes with the mid-century warming in the Arab countries during winter in the RCP4.5 scenario, albeit that IPCC (2013) relates to pre-industrial times while (Figure.10) illustrates to the 1986–2005 period. It also explains that the quantity of heating during the summer is around twice that through the winter. According to the RCP8.5 scenario, by the end of the century, large parts of the Arab countries in summer are projected to experience a temperature increase in excess of 6 °C relative to 1986–2005. Furthermore, the figure shows that climate warming in the Arab countries is stronger than in equatorial Africa, where hydrological feedback through cloud formation limit the increase of temperature at the surface (Lelieveld J. et al. 2016).

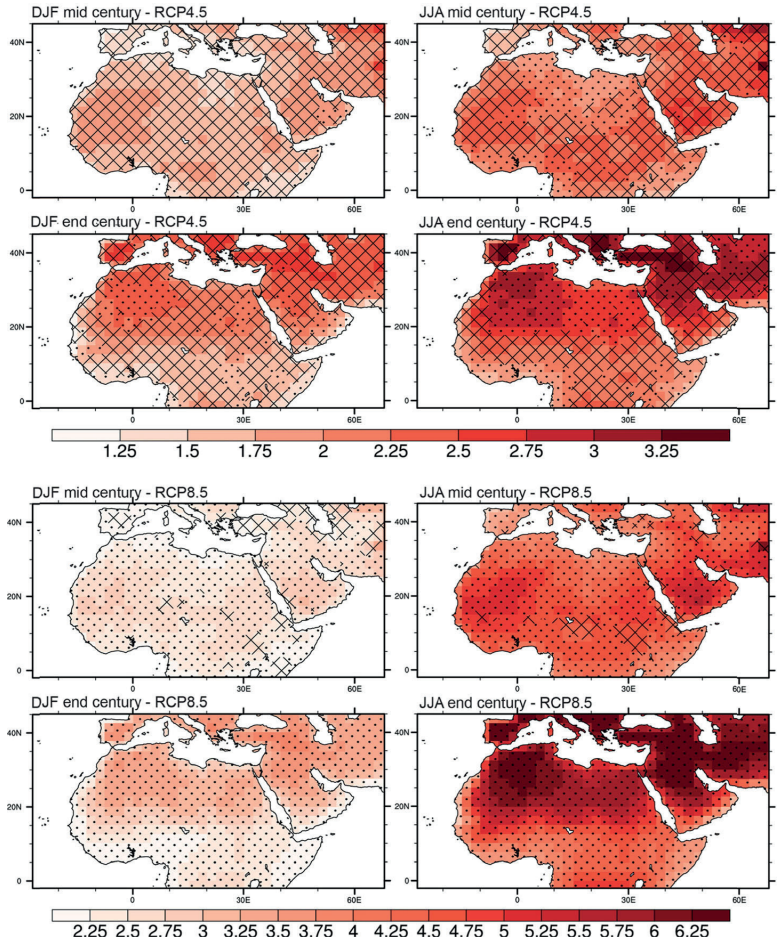

Fig. 10. The robustness of Multi-model means for the change in near-surface temperature in winter and summer months according to the RCP4.5 and RCP8.5 scenarios (After J. Lelieveld et al. 2016)

Suitability Map for renewable energy exploitation

The intensive introduction of power generation from renewable energy sources, like solar radiation, wind, and water, as a replacement to traditional power plants depending on ecology-contaminated fossil fuels, requires a punctual and comprehensive database about the current potentials of clean power in the Arab territories. One of the main aims of the research is to provide a definite suitability map of power generation potentials from renewable energy sources in the Arab world. This map could be a guideline and framework for the Arabian policymaker, who are elaborating development plans to exploit natural resources in the Arabian countries.

Producing such a map is based basically on the wide-range capabilities of GIS multi-criterion analysis, and feasibly can offer organized priorities of high-to-low promising regions containing clean energy possibilities. We utilized the spatial distribution of the wind and solar radiation (insolation) in each season as a total of eight parameters to GIS model. The data were normalized to a common scale of 0–1, and then were combined through GIS overlay techniques to produce the suitability map of power generation priorities from physical sources of energy (Figure.11). The Arabian lands are divided into ten zones of suitability according to seasonal possibilities of power generation from wind speed and solar radiation, as quantitatively described in tables 2 & 3.

The first suitable zone (Zone 1) indicates areas of the highest renewable energy potentials from both wind speed and solar radiation. Seasonal wind speed in the zone is the largest among the Arabian lands, where it reaches 5.5, 5.8, 8.2, and 5.7 m s^{-1} in winter, spring, summer, and autumn respectively, in Table 1. It also receives high seasonal insolation of (18.9, 24.0, 24.3, and 21.1 MJ m^{-2} day^{-1}) respectively.

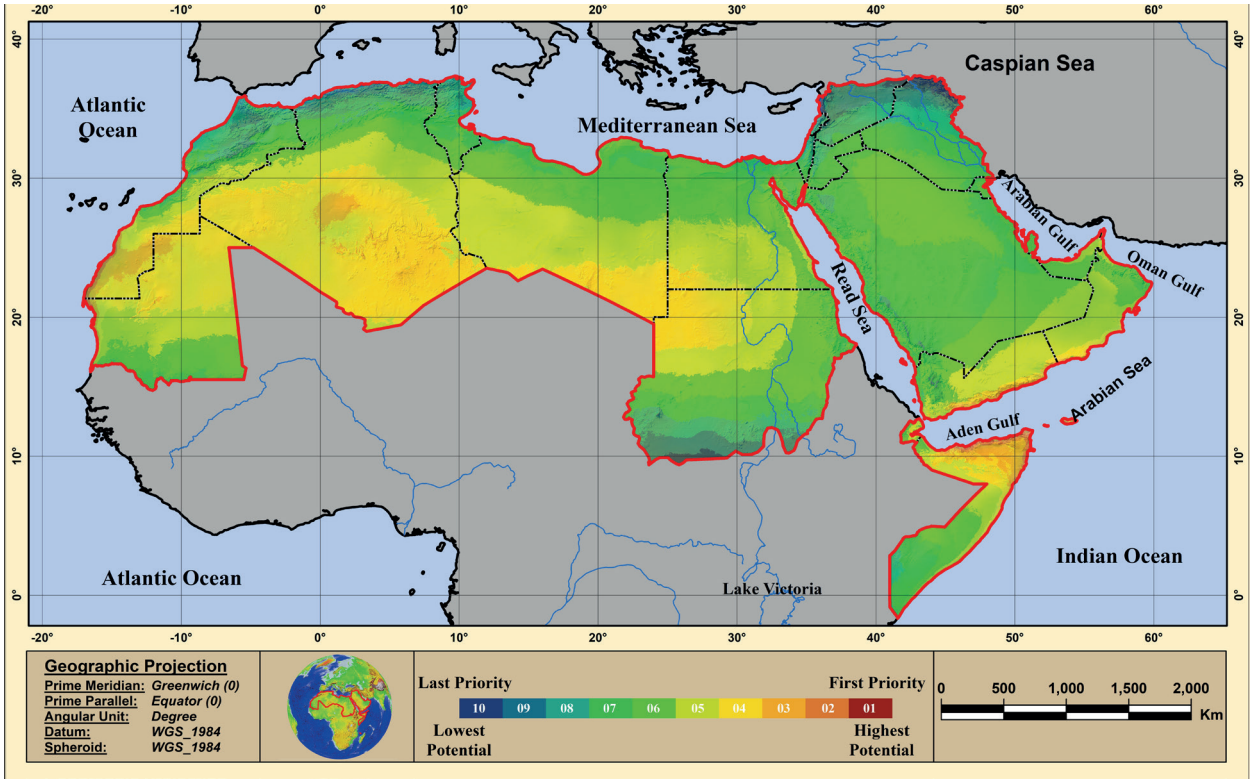

Fig. 11. Suitability map zones of renewable energy potentials and exploitation priorities in the Arab countries

Table 2. Suitability zones characteristics of renewable energy potentials and exploitation priorities in the Arab countries

Suitability Zones	Area (1000 Km^2)	Wind Speed potentials (m s^{-1})				Solar Radiation potentials (mj m^{-2} day^{-1})			
		Win.	Spr.	Sum.	Aut.	Win.	Spr.	Sum.	Aut.
1 (Best)	10.7	5.5	5.8	8.2	5.7	18.9	24.0	24.3	21.1
2	40.3	4.9	5.2	7.4	5.0	18.9	23.9	24.2	21.1
3	263.4	4.3	4.9	5.9	4.3	17.7	24.1	24.7	20.1
4	2418.5	3.8	4.5	4.4	3.7	17.2	24.4	25.7	19.9
5	2687.0	3.3	4.0	3.9	3.3	16.9	23.6	25.0	19.7
6	2987.5	3.1	3.7	3.6	3.0	15.7	22.6	24.5	18.9
7	1962.9	2.9	3.4	3.4	2.7	15.1	21.7	23.6	18.3
8	710.59	2.8	3.1	3.1	2.5	13.4	20.9	23.5	16.7
9	372.2	2.4	2.7	2.8	2.1	12.9	20.1	22.8	16.1
10 (Worst)	70.0	2.1	2.3	2.4	1.8	12.3	19.0	23.2	15.9

So, the zone should be considered as a first priority of exploitation when preparing development plans. However, the first suitable zone has a limited area of 10700 km^2 (accounts for 0.1% of the Arab lands) and extends only in Morocco, Mauritania, Somalia, and Yemen. Suitability map, Fig.1, shows that the spatial distribution of the zone exclusively related to the coastal lands overlooking the Atlantic Ocean in Morocco and Mauritania, and the Indian Ocean in Somalia and Yemen.

The second suitable zone also has a confined space, where it only occupies 0.35% (approximated to 40300 Km^2). It exists in the same four countries embracing the first zone, besides Oman, and closely related to spatial locations of the first zone. Average wind speeds in the zone are the second largest after the first zone, where they are (4.9, 5.2, 7.4, and 5.0 m s^{-1}) in winter, spring, summer and autumn respectively. Seasonal averages of incident solar radiation on the area are about 18.9, 23.9, 24.2, and 21.1 MJ m^{-2} day^{-1} respectively.

Mitigation of the potential climate change hazards

A 100% WWS framework in each country will eliminate such hazards in the Arab countries, as they represent the region with the richest renewable energy resources in the world. The range of the 2050 social cost of carbon from recent papers is $500 (282–1,063)/metric tonne-CO_2 in 2013 dollars (Jacobson et al. 2015a).

The value ranges of climate-change benefits as a result of switching to WWS in the Arab countries, attributed to in-country emissions reduction in 2050 (between 20 and 657 billion dollars) for Sudan and Saudi Arabia, respectively. In addition, the values of climate-change benefits for (Egypt, Iraq, Qatar, and Libya) are (287.01, 155.34, 110.62, and 80.01 billion dollars) respectively based on the middle estimate. While The value ranges of Per-person climate-change benefits in Arab countries as a result of switching to WWS, attributed to emissions reduction in-country in 2050 ($/person/year) (between 651 and $43,229/person/Year) for Sudan and Qatar, respectively. In addition, the value of per-person climate-change benefits for (Kuwait, Bahrain, Saudi Arabia, and Oman) are (32,974, 17,083, 16,336, and $13,865/person/Year) respectively based on the middle estimate.

On the other hand, the value ranges of total air-pollution-reduction benefits in 2050 (billion 2013-$) as a result of switching to WWS in the Arab countries, attributed to emissions reduction in country in 2050 (between 6 and 243 billion dollars) for Qatar and Egypt, respectively. In addition, the values of total air-pollution-reduction benefits in 2050 (billion 2013-$) for (Sudan, Saudi Arabia, Iraq, and Oman) are (236, 102, 103, and 78 billion dollars) respectively based on the middle estimate (Jacobson et al, 2019).

While The value ranges of Per-person air-pollution-reduction benefits in Arab countries as a result of switching

Table 3. The matrix suitability zones of renewable energy potential in the Arab countries

No	Country	Suitability Zones Area (1000 Km^2)									
		1	2	3	4	5	6	7	8	9	10
	Morocco	3.9	11.2	71.7	126.4	91.4	87.2	91.1	124.2	24.2	-----
	Maurita.	0.4	3.4	29.3	383.6	235	222.2	42.1	0.9	-----	-----
	Algeria	-----	-----	66.6	1188.1	414.4	152.4	109.4	111.4	63.1	0.2
	Tunisia	-----	-----	-----	-----	3.7	45.6	55.3	41.8	13.4	-----
	Libya	-----	-----	-----	231.1	662.9	473.4	89.6	3.8	-----	-----
	Egypt	-----	-----	-----	63.6	377.7	375.9	84.9	7.3	-----	-----
	Sudan	-----	-----	-----	266.7	292.3	424.9	253.6	177.5	127.4	24.2
	Djibouti	-----	-----	-----	4.4	9.9	8.3	1.7	-----	-----	-----
	Somalia	6	24.8	72	78.1	115.4	116.5	105	22.7	-----	-----
	Comoros	-----	-----	-----	-----	1.3	1.9	0.1	-----	-----	-----
	Yemen	0.4	0.8	18	43.5	191.9	88.3	29.7	3.6	0.1	-----
	Oman	-----	0.1	5.8	29.9	165.4	69.6	10.6	-----	-----	-----
	UAE	-----	-----	-----	3.1	23.1	42.5	-----	-----	-----	-----
	Qatar	-----	-----	-----	-----	2.9	9.1	0.6	-----	-----	-----
	Bahrain	-----	-----	-----	-----	0.5	0.4	-----	-----	-----	-----
	Kuwait	-----	-----	-----	-----	0.5	10.6	7.7	-----	-----	-----
	Iraq	-----	-----	-----	-----	-----	89.6	157.4	86.4	50.2	31.3
	KSA	-----	-----	-----	-----	98.7	765	833.5	21.7	-----	-----
	Palestine	-----	-----	-----	-----	-----	1.5	16.5	10.5	3.1	-----
	Jordan	-----	-----	-----	-----	-----	2.57	66.1	18.7	0.7	-----
	Lebanon	-----	-----	-----	-----	-----	-----	0.1	7.7	2.5	0.2
	Syria	-----	-----	-----	-----	-----	-----	7.9	72.4	87.5	14.1

to WWS, attributed to emissions reduction in-country in 2050 ($/person-year) (between 649 and $13,306/person-Year) for Libya and Oman, respectively. In addition, the value of Per-person air-pollution-reduction benefits for (Bahrain, Kuwait, Iraq, and Egypt) are (3,58, 2,83, 1,82, and $1.76/person-Year) respectively based on the middle estimate (Jacobson et al, 2019).

Replacing fossil fuels with WWS technologies is expected to generate a total reduction of end-use demand by 60% relative to a BAU scenario. These projections are based on expected Arab countries' population growth by 32.5% (between 2017 and 2050). Jacobson et al. (2016, 2017) project that Arab countries' population will grow from 407.5 million in 2016 to 646 million in 2050.

Arab countries' reduction of end-use demand in 2050 is projected to be 51.2% due to electrification of end uses 6% due to changes in upstream energy use, and 11.8% due to additional efficiency measures. Some of the Arab country's efficiency gains due to the electrification of and use in the WWS scenario is projected to be influenced mainly by efficiency in the transportation and industrial sectors (32% and 43%, respectively).

There are many benefits of using renewable energy sources for Arab countries. At the job creation level, the average job opportunity that will be available about 149,000. For example, Saudi Arabia will have more than half a million job opportunities. Arab countries will benefit by reducing energy demand by up to 60%. Moreover, Arab countries will reap the health and financial benefits, especially in health cost savings per year, which will be 6.63% of each country GDP.

CONCLUSION

The current research was concluded that most of the Arab countries have done a lot of harsh measures to reduce the negative effects of climate change, and the most important of these measures is to seriously search for renewable energy sources.

The current research adopted Jacobson's et al. (2016) «world plan»,'100% Renewable Wind, Water, and Sunlight (WWS), and it was validated by assessing the potential renewable energy in Arab countries' WWS, while taking into account the Arab world's unique topography, climate conditions, economic, environmental impacts, and regulation settings.

Based on the estimated 2050 power demand, Arab country's 2050 energy mixes as suggested by Jacobson et al. (2016, 2017) are 65.5% solar, 22.8% wind, and less than 0.05% hydro and geothermal. When broken down into specific technologies, the energy mix is as follows: residential rooftop PV system 17.2%, commercial and governmental rooftop PV 9.1%, utility-scale PV 32.4%, CSP plant 14.5%, onshore wind 11.7%, and offshore wind 14.2%. The current research concluded that the appropriate areas that are technically and practically suitable for installing wind farms are mainly in most Arab countries; about 65% of the area that was found practically suitable for wild winds in the Arab countries particularly in North Africa, in addition to the Empty Quarter Desert in the Kingdom of Saudi Arabia. Thus, Arab countries have enough area that complies with technical limitations for WWS 2050 all-purpose energy demand is generated with onshore wind.

The appropriate areas differed technically and practically suitable for installing offshore marine wind turbines mainly vary in the Arab countries. As the lowest percentage reached about 1% of the area of Iraq, while the percentage reached about 27% in Lebanon, followed by the State of Oman with a rate of 14.5%, then Egypt and Morocco with a rate of 10.8, 10.5 Respectively.

The practical potential of offshore wind reached an average of 10% of the total area of the Arab countries, PV on the scale of facilities concentrated solar energy and photovoltaic energy on the residential and commercial surface by at least 37% is higher than the total plate capacity required for each resource, with less dependence in the form of Great for land and sea winds. This analysis confirms that the Arab countries have enough wind and solar resources to meet their energy demand in 2050 when taking technical constraints into account and when calculating environmental and regulatory restrictions.

The technical capabilities of the Arab countries were confirmed for both wind and solar technologies are greater or like the total capacity of the nameplate required to provide the entire request of Arab countries in 2050 for all purposes of energy.

It has been verified that the practical potential of onshore wind, utility-scale PV and CSP, and residential and commercial PV energy on the commercial and residential surface is greater than or similar to the total panel capacity required to provide the demand of Arab countries for 2050 all-purpose energy according to Jacobson's proposal.

Transforming Arab countries to a 100% WWS system as suggested by Jacobson et al. (2016) will reduce the end-use demand in 2050 by about 32%. This difference can be attributed to the conversion of fossil fuel combustions to a more efficient electrified system. All sectors will be electrified as suggested by Jacobson et al. (2016): Short distance ground transportation will be electrified with battery electric vehicles (BEVs) and hydrogen fuel cell vehicles (HFCVs) (hydrogen will be produced by electrolysis from WWS electricity), long-distance ground transportation will use BEVs with fast charging or battery swapping, heavy-duty ground transportation will use BEV-HFCV hybrids and ships, aircraft, and long-distance flights will use hydrogen-energy storage.

Despite the current research being dedicated to the analysis of the assessment of climate change impacts on renewable energy sources in the Arab World, the economic, social, and institutional factors must be considered in future researches.

REFERENCES

Almazroui M. (2012). Dynamical downscaling of rainfall and temperature over the Arabian Peninsula using RegCM4. Clim. Res. 52, 49-62, DOI: 10.3354/cr01073.

Almazroui M. (2016). RegCM4 in climate simulation over CORDEX-MENA/Arab domain: selection of suitable domain, convection and land-surface schemes. Int. J. Climatol, 36, 236-251, DOI: 10.1002/joc.4340 [Accessed January 2019].

Almazroui M., Islam M.N., Al-Khalaf A.K., Saeed F. (2015). Best convective parametrization scheme within RegCM4 to downscale CMIP5 multi-model data for the CORDEX-MENA/Arab domain. Theor. Appl. Climatol, 124, 807-823.

Almazroui M., Islam M.N., Alkhalaf A.K., Saeed F., Dambul R., Rahman M.A. (2016). Simulation of temperature and precipitation climatology for the CORDEX-MENA/ Arab domain using RegCM4. Arab. J. Geosci. 9 (1), 1-13.

Andrade C., Corte Real J. (2014). Spatial distribution of climate change indices in the Iberian Peninsula. ICNAAM-2014. AIP Conf Proc 1648: 1

Arab Union of Electricity (2016b). Statistical Bulletin 2016. Available at https://www.irena.org/-/media/Files/IRENA/Agency/Publication/2016/IRENA_Arab_Region_Overview_2016.pdf [accessed March 2019].

Arab Monetary Fund (2019). Database available at https:// www.amf.org.ae/en/arabic_economic_database [accessed January 2020].

Arnold T. (2019). Saudi's PIF invests more than $1 billion in electric carmaker Lucid Motors. Reuters, 17 September 2018. Available at https://www.reuters.com/article/us-saudiinvestment- auto/saudis-pif-invests-more-than-1-billion-inlucid- motors-idUSKCN1LX1IG.

Baltas E. (2007). bIpatial distribution of climatic indices in northern Greece. Meteorol Appl 14: 69–78

Beck Thorsten. (2011). Finance and Oil: Is Therea Resource Curse in Financial Development?, In Beyond the Curse: Policies to Harness the Power of Natural Resources, edited by Rabah. Arezki, Thorvaldur Gylfason and Amadou Sy. Washington, DC: International Monetary Fund.

Centre for Environment and Development for the Arab Region and Europe (2016). Fuel Economy Policies & Labeling for New Cars:Improving Fuel Efficiency and CO2 Emissions in Egypt. Available at http://pharos.cedare.org/wp-content/ uploads/2017/01/Handout-Fuel-Economy-for-Cars_Policy_ Brief_EGYPT-GFEI.pdf

Collins W.D., Ramaswamy V., Schwarzkopf M.D., Sun Y., Portmann R.W., Fu Q., Casanova S.E.B., Dufresne J.-L., Fillmore D.W., Forster P.M.D., Galin V.Y., Gohar L.K., Ingram W.J., Kratz D.P., Lefebvre M.-P. et al. (2006). Radiative forcing by well-mixed greenhouse gases: Estimates from climate models in the Intergovernmental Panel on Climate Change (IPCC) Fourth Assessment Report (AR4). J. Geophys. Res., 111, D14317, DOI:10.1029/2005JD006713.

Coumou D., Robinson A. and Rahmstorf S. (2013). Global increase in record-breaking monthly-mean temperatures Clim. Change, 118, 771-82.

Croitoru A., Piticar A., Imbroane A.M., Burada D.C. (2013). Spatio temporal distribution of aridity indices based on temperature and precipitation in the extra-Carpathian regions of Romania. Theor Appl Climatol 112: 597-607.

Deng L., McCabe M.F., Stenchikov G., Evans J.P., Kucera P.A. (2015). Simulation of flash-flood-producing storm events in Saudi Arabia using the weather research and forecasting model. J Hydrometeorol, 16, 615-630.

Donat M.G. et al. (2014). Changes in extreme temperature and precipitation in the Arab region: long-term trends and variability related to ENSO and NAO. Int J Climatol, 34, 581-592.

El Kenawy A., Lopez-Moreno J., Vicente-Serrano S., MekldM (2009). Temperature trends in Libya over the second half of the 20th century. Theor Appl Climatol, 98, 1-8.

El Kenawy A., Lopez-Moreno J., Vicente-Serrano S., Abdelal M. (2010). Temperature variability along the Mediterranean and its links to large-scale atmospheric circulation (1957–2006), Bull Egypt Geog Soc, 83, 121-140.

El Kenawy A., McCabe M.F., Stenchikov G., Raj J. (2014). Multi-decadal classification of synoptic weather types, observed trends and links to rainfall characteristics over Saudi Arabia. Front Environ Sci, 2, 37.

Grell G.A., Dudhia J., & Stauffer D.R. (1994). A Description of the Fifth Generation Penn State/NCAR Mesoscale Model (MM5). Boulder: National Center for Atmospheric Research.

Giorgi F., Lionello P. (2008). Climate change projections for the Mediterranean region. Glob. Planet. Chang. 63(2), 90-104.

Giorgi F., Jones C., Asrar G.R. (2009). Addressing climate information needs at the regional level: the CORDEX framework. In: World Meteorological Organization (WMO) Bulletin, 58(3), 175.

International Renewable Energy Agency (2019a). Renewable Energy Market Analysis: GCC (2019). Abu Dhabi. https://www.irena.org/publications/2019/Jan/Renewable-Energy-Market- Analysis-GCC-2019 [Accessed January 2020].

International Renewable Energy Agency (2019b). Renewable Capacity Statistics 2019. Abu Dhabi. Available at https://www.irena.org/publications/2019/Mar/Renewable-Capacity- Statistics-2019 [Accessed January 2020].

IPCC (2013a). In: Stocker T.F., Qin D., Plattner G.-K., Tignor M., Allen S.K., Boschung J., Nauels A., Xia Y., Bex V., Midgley P.M. (Eds.), Climate Change 2013: The Physical Science Basis. Contribution of Working Group I to the Fifth Assessment Report of the Intergovernmental Panel on Climate Change. Cambridge University Press, Cambridge. https://www.ipcc.ch/report/ar5/wg1/ [Accessed March 2019].

IPCC (2013b). Annex I: atlas of global and regional climate projections. In: van Oldenborgh, G.J., Collins, M., Arblaster, J., Christensen, J.H., Marotzke, J., Power, S.B., Rummukainen, M., Zhou, T. (Eds.), Climate Change 2013: The Physical Science Basis. Contribution of Working Group I to the Fifth Assessment Report of the Intergovernmental Panel on Climate Change. Cambridge University Press, Cambridge, United Kingdom and New York, NY, USA (Stocker TF, Qin D, Plattner GK). https://www.ipcc.ch/site/assets/uploads/2018/02/WG1AR5_AnnexI_FINAL-1.pdf [Accessed January 2019].

IPCC (2018). An IPCC Special Report on the impacts of global warming of 1.5°C above pre-industrial levels and related global greenhouse gas emission pathways, in the context of strengthening the global response to the threat of climate change, sustainable development, and efforts to eradicate poverty, IPCC, Switzerland, 2018.https://www.ipcc.ch/site/assets/uploads/sites/2/2019/06/SR15_Full_Report_High_Res.pdf [Accessed January 2019].

Kottek M., Grieser J., Beck C., Rudolf B. and Rubel F. (2006) World Map of the Köppen-Geiger climate classification updated, Meteorologische Zeitschrift, 15(3), 259-263.

Laprise R., Hernandez-Diaz L., Tete K., et al. (2013). Climate projections over CORDEX Africa domain using the fifth-generation Canadian regional climate model (CRCM5). Clim. Dyn. 41, 3219e3246, DOI: 10.1007/s00382-012-1651-2.

Lelieveld J., Hadjinicolaou P., Kostopoulou E., et al. (2012). Climate change and impacts in the eastern mediterranean and the Middle East. Climatic Change 114, 667e687, DOI: 10.1007/s10584-012-0418-4.

Lelieveld J., Proestos Y., Hadjinicolaou P., et al. (2016). Strongly increasing heat extremes in the Middle East and North Africa (MENA) in the 21st century. Climatic Change, 137, 245e260, DOI: 10.1007/s10584-016-1665-6.

Mitchell T.D., Jones P.D. (2005). An improved method of constructing a database of monthly climate observations and associated high-resolution grids. Int. J. Climatol. 25(6), 693e712, DOI: 10.1002/joc.1181.

Nazemosadat M.J., Cordery I. (2000). On the relationships between ENSO and autumn rainfall in Iran. Int J Climatol, 20, 47-61.

Önol B and Semazzi FHM. (2009). Regionalization of climate change simulations over the Eastern Mediterranean. J Clim, 22, 1944-1961.

Önol B., Bozkurt D., Turuncoglu U.U., Sen O.L., Dalfes H.N. (2014). Evaluation of the twenty-first century RCM simulations driven by multiple GCMs over the Eastern Mediterranean-Black Sea region. Clim Dyn, 42, 1949-1965.

Pasicko, Robert et al. (2012). Assessment of climate change impacts on energy generation from renewable sources in Croatia, Renewable Energy 46 (2012) 224e231 (The rest of the authors' names).

Seneviratne S.I., Nicholls N., Easterling D., Goodess C.M., Kanae S., Kossin J., Luo Y., Marengo J., McInnes K., Rahimi M., Reichstein M., Sorteberg A., Vera C., Zhang X. (2016). Changes in climate extremes and their impacts on the natural physical environment. In: Field CB, Barros V, Stocker TF, Qin D, Dokken DJ, Ebi KL, Mastrandrea MD, Mach KJ, Plattner G-K, Midgley PM, Allen SK, Tignor M, Midgley PM (eds) Managing the risks of extreme events and disasters to advance climate change adaptation. A special report of working groups I and II of the intergovernmental panel on climate change (IPCC), Cambridge: Cambridge University Press, 109-230.

Sillmann J., Kharin V.V., Zwiers F.W., Zhang X., and Bronaugh D. (2013). Climate extreme indices in the CMIP5 multi-model ensemble. Part 2: Future projections, J. Geophys. Res., (pp. 109–230), DOI: 10.1002/jgrd.50188.

Somot S., Sevault F., Déqué M., Crépon M. (2008). 21st century climate change scenario for the Mediterranean using a coupled atmosphere–ocean regional climate model. Glob. Planet. Chang, 63(2), 112-126.

UNEP (2015). Climate Change in the Arab Region. Regional Coordination Mechanism (RCM) Issues Brief for the Arab Sustainable Development Report. Available at http://css.escwa.org.lb/SDPD/3572/Goal13.pdf [Accessed March 2019].

UN ESCWA (2015e). Survey of Economic and Social Development in the Arab Region 2014–2015. Available at https://www.unescwa.org/publications/survey-economic-and-social development- arab-region-2014-2015 [Accessed March 2019].

UN ESCWA (2016d). Arab Governance Report II: Governance and Institutional Transformations in Conflict-affected Arab Countries. Available at https://www.unescwa.org/publications/arabgovernance- Report-2016. [Accessed March 2020].

World Bank (2014). Turn Down the Heat: Confronting the New Climate Normal. Washington, DC: World Bank. License: Creative Commons Attribution—Non Commercial—No Derivatives 3.0 IGO (CC BY-NC-ND 3.0 IGO). http://documents1.worldbank.org/curated/en/317301468242098870/pdf/927040v20WP00O0ull0Report000English.pdf [Accessed January 2020].

World Bank (2016a). Delivering Energy Efficiency in the Middle East and North Africa. International Bank for Reconstruction and Development, Washington DC, USA. Available at https://openknowledge.worldbank.org/ bitstream/handle/10986/25295/109023-WPP148222- PUBLIC-DeliveringEEinMENAMayEN. pdf?sequence=1&isAllowed=y [A ccessed April 2020].

World Bank (2017). Health, Nutrition and Population Statistics Database. Available at http://data.worldbank.org/data-catalog/healthnutrition- and-population-statistics [Accessed March 2020].

Zittis G., Hadjinicolaou P. (2017). The effect of radiation parameterization schemes on surface temperature in regional climate simulations over the MENA-CORDEX domain. Int. J. Climatol, 37(10), 3847-3862.

ges.rgo.ru/jour/

ISSN 2542-1565 (Online)